

Magnetoencephalography and neuropathological studies of autism spectrum disorders and the comorbidity with epilepsy

David Antoine Menassa

University College

Michaelmas Term 2013

A thesis submitted in fulfillment of the requirements for the degree of Doctor of Philosophy to the University of Oxford

'The formulation of a problem is often more essential than its solution which may be merely a matter of mathematical or experimental skill'. Albert Einstein

This thesis is dedicated to Johnny, Douglas, Marilyne, Pascale, Christelle, Nina and Tony.

This dissertation is the result of my own work and includes nothing, which is the outcome of work done in collaboration except where specifically indicated in the text. It does not exceed 50000 words in length excluding tables, figures, footnotes, bibliography and appendices.

Magnetoencephalography and neuropathological studies of autism spectrum disorders and the comorbidity with epilepsy

David Antoine Menassa, University College

Abstract

Autism spectrum disorders (ASD) are neurodevelopmental disorders with multiple neurobiological aetiologies, which could be genetic, structural, metabolic or immune-mediated. ASDs are diagnosed with deficits in social communication and restricted and repetitive behaviours, and are associated with sensorial atypicalities. 30% of cases have co-existing epilepsy. A series of *in vitro*, *in vivo* and post-mortem investigations were undertaken to examine sensory atypicalities in ASD.

In vitro characterisation of hippocampal neuronal cultures using immunofluorescence demonstrated the presence of multiple cell types including neurons, astrocytes and microglia. The distribution of ion channels of the *Shaker* family and tumour necrosis factor α receptors in astrocytes and neurons were identified but not explored further.

Neuroanatomical and neuropathological investigations of primary olfactory cortex, using post-mortem stereology, demonstrated a specific increase in glial cell densities in layer II, which was negatively associated with age in ASD. Increases in glia were also associated with symptom severity and often co-localised with the presence of corpora amylacea in layer I. Qualitative analysis of the olfactory tubercle demonstrated that corpora amylacea did not extend to this neighbouring region of the primary olfactory cortex in ASD. These changes were independent of co-existing epilepsy and not observed in epilepsy without ASD. Preliminary pilot studies of the hippocampus provided a stereological sampling strategy to quantify cell densities in future investigations of this area in ASD.

Neurophysiological investigations using collected magnetoencephalography data demonstrated diminished occipital gamma oscillatory synchrony in ASD in a visual time perception task. This did not always predict behavioural outcome but was specific to ASD and could not be explained simply in terms of changes in task performance. Moreover, changes in oscillatory synchrony were associated with symptom severity.

These observations in primary sensory domains in post-mortem tissue and in patients suggest possible novel mechanisms in ASD and extend knowledge of the neurobiological bases of these disorders.

Acknowlegements

This dissertation would have not been possible were it not for the support of many people. First, I would like to thank my magnetoencephalography supervisor, Dr. Sven Braeutigam, for his close supervision of this part of my work, for his teaching, general guidance, support, and inspiration. I would also like to thank my neuroanatomy supervisor, Dr. Steven Chance for his supervision of this part of the thesis, for his help, academic and financial support of this work as well as his insightful comments. I am indebted to Dr. Christine Falter who, with Dr. Braeutigam, granted me permission to use MEG-recordings they had collected with Dr. Sarah Carrington and Professor Anthony Bailey: this has been an important turning point in my DPhil as I would have otherwise missed out on a fascinating field of functional neuroscience, which I intend to pursue in my career as a junior academic. Thank you both for this, it has been a great pleasure working with you. I am grateful to Professor Angela Vincent for her supervision of the *in vitro* work in this thesis, for her advice and inspiration, and for contributing generously to my Clarendon scholarship to support my DPhil project.

I would like to thank Professor Margaret Esiri, Consultant Neuropathologist at the John Radcliffe, for supporting my neuropathology work, for being a source of great inspiration, for her insightful comments and for being generous with her time and proofreading parts of this thesis. I would also like to thank Dr. Thomas Berney, Consultant Psychiatrist at the Brain Bank for Autism, who has been extremely helpful and prompt in providing clinical reports, behavioural tests, and general advice. Thank you for the extensive Skype communications and for your comments regarding the clinical element of this work.

I wish to thank my examiners, Dr. Francis Szele and Professor Gina Rippon for their helpful comments that have greatly contributed to the improvement of this thesis.

I wish to also thank all the participants and donors who were part of this study.

I would also like to thank Ms. Carolyn Sloan for her great support with tissue processing, cutting and staining. It would have taken me forever to cut over 300 thick sections: Carolyn, were it not for your assistance, I would still be cutting sections! I thank Ms. Lai San Hong, not only for being a true friend, but also for teaching me about R-statistics, multivariate statistics and regressions and for inspiring me to learn more about robust methods to examine my data.

I thank the Clarendon Fund, the Department of Clinical Neurology, the University Hardship Fund and University College for funding my studies. My thanks also go to the Saïd Foundation and the Physiological Society for supporting my attendance at, and presentations to, various conferences.

I also thank both the Oxford Human Brain Activity Centre (OHBA) and the Nuffield Department of Clinical Neuroscience for acting as host departments during this DPhil.

I thank all the many friends and academic colleagues who have contributed to this DPhil, sometimes without knowing it: each and every one of you has inspired me or supported me in one-way or another. My thanks go to: Dr. Lindy Castell, Dr. Andrew Gregory, Dr. Damineh Morsali, Halim Shebaya, Sally Harte, Professor Uwe Ackermann, Dr. Andrew Murray, Dr. Gabriele De Luca, Professor Nicola Ragge, Professor Peter Jezzard, Dr. David Holcman, Bahar Saba, Istvan Adorjan, Rebecca McKavanagh, Mathura Ravishankar, Maren Brünjes, Simon Baptist, Raed Joundi, Mark Ebden, Tanja Brenner, Aude Fauvel, Lily Soucy, Antoine Panaioti, Rhiannon Alexander, Daan Beekers, Karim Honein, Johannes Lang, Elizabeth and Mike Dunmore, Vincent La Rochelle, Rina Soloveitchik, Yasmine El Masri, Rima Majed,

Max Sloan, Marie Philipps, Maya and Joseph Barhouche, Nony and Cocy, Louis Atallah, Arunesh Mittal, Brianna Doherty, Anna-Magdalena Elsner, Tom Walker and Janis Carter.

Finally, my heartfelt thanks go to Douglas Crockett, who has been incredibly supportive during the course of this DPhil, in particular tolerating the occasional crisis of confidence and giving calm advice, which helped me to regain perspective! My family have also supported me unstintingly - my parents, Nina and Tony, my sisters, Pascale, Christelle and Marilyne and my brother Johnny: if it were not for all of you, life would mean far less than it does now. Thank you all for being wonderful, I love you so much.

Table of Contents

Chapter 1 General introduction

1.1 Autism spectrum disorders: brief history and classification 1

1.2 Diagnosis and assessment 3

1.3 Epidemiology 4

1.4 Aetiology 5

1.5 Neurobiological basis of ASD 6

1.5.1 Incidence of epilepsy 6

1.5.2 Neuropathological and neuroanatomical findings in ASD 7

1.5.3 Neuroimmune findings in ASD 8

1.5.4 Neurophysiological findings in ASD 10

1.6 The notion of superior performance in ASD 11

1.7 Sensory atypicalities in ASD 12

1.8 The balance between excitation and inhibition in ASD 13

1.8.1 Evidence from the incidence of epilepsy 13

1.8.2 Evidence from minicolumnar spacing in ASD 14

1.8.3 Evidence from studies on GABA-ergic dysfunction in ASD 14

1.8.4 Evidence from neuroimaging studies 14

1.8.5 Evidence from sensory atypicalities 15

1.9 Rationale and aims of the thesis 15

Chapter 2 Autoimmunity, cytokines, ion channels and neuronal excitability

2.1 Introduction 17

2.2 Aims and hypothesis 20

2.3 Methods 21

2.3.1 Hippocampal cell cultures 21

2.3.2 Characterization of cell types in hippocampal cultures 22

2.3.4 Optimizations of hippocampal cultures for immunocytochemistry 22

2.3.5 Cell counting 23

2.3.6 Immunocytochemistry of Kv1 channels in hippocampal neurons 23

2.3.7 Homogeneous cortical astroglial cell cultures 24

2.4 Results

2.4.1 Types of cells in Po cultures 26

2.4.2 Kv1 channel localizations in GABA-ergic neurons 28
2.4.3 TNFα receptor expression in astrocytes and neurons 30
2.5 Discussion 32

Chapter 3 The piriform cortex in ASD and epilepsy
3.1 Definition 34
3.2 Anatomy of the piriform cortex 35
3.3 Cytoarchitecture 33
3.4 Afferents and efferents of the piriform cortex 39
3.5 Roles of the piriform cortex 40
3.6 Summary 41
3.7 The piriform cortex in ASD and epilepsy 41
3.7.1 Olfactory dysfunction in ASD 42
3.7.2 Olfactory dysfunction in epilepsy 42

Chapter 4 Post-mortem stereology of the piriform cortex in ASD and epilepsy
4.1 Rationale, aims and hypothesis 45
4.2 Methodology 46
4.2.1 Case selection 46
4.2.2 Confirmation of ASD diagnosis 49
4.2.2.1 Autism diagnostic interview revised (ADI-R) 49
4.2.2.2 Social communication questionnaire (SCQ) 50
4.2.2.3 Social responsiveness scale 2nd edition (SRS-2) 50
4.2.2.4 Intellectual disability (ID) using ICD-10 50
4.2.3 Clinical profiles of selected cases 51
4.2.3.1 Clinical profiles of ASD cases 51
4.2.3.2 Clinical profiles of ASD co-morbid with epilepsy cases 52
4.2.3.3 Clinical profiles of epilepsy cases 53
4.2.3.4 Cases without ASD or epilepsy 54
4.2.4 Anatomy and choice of area for neurohistological sampling 54
4.2.5 Neurohistological sampling 56
4.2.6 Embedding 57
4.2.7 Histological sections and Nissl-staining 58
4.2.8 Cell density studies 58

4.2.8.1 Systematic random sampling using Axiovision 61
4.2.8.2 Reliability and accuracy 67
4.2.8.3 Assessment of strengths of stereological quantifications 72
4.2.9 Statistical analyses 76
4.3 Results 82
4.3.1 Reliability of the measurements 82
4.3.2 Accuracy 83
4.3.3 Effects and interactions of rmANOVA 83
4.3.3.1 Effects of diagnosis, layer, cell-type and storage time 87
4.3.3.2 Storage-by-cell-type interaction 88
4.3.3.3 Layer-by-cell-type interaction 88
4.3.4 Confounding factors 89
4.3.4.1 Bivariate correlations between age and density 89
4.3.4.2 Bivariate correlations between brain weight and density 91
4.3.5 Mean differences in cell density between diagnostic groups 91
4.3.5.1 Glial cell densities in layers II and III 92
4.3.5.2 Pyramidal cell densities in layers II and III 92
4.3.5.3 Non-pyramidal cell densities in layers II and III 93
4.3.5.4 Neuronal cell densities in layers II and III 94
4.3.5.5 Summary of mean cell densities and the GCE 95
4.3.6 Power of the study 96
4.3.7 Association between cell densities and symptom severity in ASD 97
4.4 Discussion 98

Chapter 5 Neuropathology of the piriform cortex in ASD and epilepsy
5.1 Rationale, aims and hypothesis 103
5.2 Methods 104
5.3 Results 106
5.3.1 Pathological findings 106
5.3.2 Corpora amylacea differences between diagnostic groups 108
5.3.3 Association of corpora amylacea with glial cell densities in ASD 109
5.4 Discussion 111

Chapter 6 Neuropathology of neighbouring regions of the PiC: the olfactory tubercle and the hippocampus in ASD and epilepsy.

6.1 The olfactory tubercle 113
6.1.1 Introduction 113
6.1.2 Methods 116
6.1.3 Results 118
6.1.4 Discussion 126
6.2 The hippocampus pilot studies in ASD 128
6.2.1 Introduction 128
6.2.2 Methods 130
6.2.2.1 Neurohistological sampling & hippocampal anatomy 130
6.2.2.2 Pilot stereological studies 132
6.2.3 Conclusions of the pilot study 136

Chapter 7 Magnetoencephalography studies of autism spectrum disorders

7.1 Magnetoencephalography: An overview 138
7.1.1Artefact correction 140
7.1.2 Source localization 140
7.1.3 Analytical tools 141
7.1.4 Clinical applications in ASD 143
7.2 Roles of gamma oscillations 143
7.2.1 Evoked and induced gamma responses 144
7.2.2 Roles of gamma in visual processing 145
7.2.3 Cellular mechanisms of gamma and the E/I balance 147
7.2.4 Summary 149
7.3 Gamma oscillations in ASD: a review of the MEG and EEG literature 149
7.3.1 Evidence of gamma anomalies in resting-state paradigms 150
7.3.2 Evidence of gamma anomalies in response to visual stimuli 151
7.3.3 Gamma anomalies in response to language and auditory stimuli 154
7.3.4 Evidence of gamma anomalies in relation to the E/I balance 155

Chapter 8 Gamma oscillations in perceptual simultaneity in ASD: time-frequency analyses of magnetoencephalographic recordings

8.1 Rationale and hypothesis 157

8.2. Methodology 161

8.2.1 Participants 161

8.2.2 Experimental paradigm and design 163

8.2.3 Data acquisition 164

8.2.4 Event related fields 165

8.2.5 Principal variance components of evoked responses 166

8.2.6 Time-frequency analyses 169

8.2.7 Choice of gamma range (30-80 Hz) 172

8.2.8 Strengths and weaknesses of MEG analyses 172

8.2.9 Summary of analyses 173

8.3 Results 175

8.3.1 Behavioural results 175

8.3.2 Time-frequency planes and analyses 176

8.3.2.1 ANOVA interaction between group and condition 177

8.3.2.2 ANOVA main effect of group 178

8.3.2.3 ANOVA main effect of condition 179

8.3.2.4 Post-hoc analyses of main ANOVA interaction 181

8.3.2.5 Mann-Whitney U for between group differences for different conditions 183

8.3.2.6 Within-group comparisons between conditions 185

8.3.2.7 ANOVA interaction within the TD group 187

8.3.2.8 Evoked γ-phase-locking (50-80 ms/50-80 Hz) 190

8.3.2.9 Evoked γ-phase-locking (20-40 ms/70-80Hz) 195

8.3.3 Phase locking correlations with symptom severity 198

8.3.3.1 (50-80 ms/50-80 Hz) t/f range 198

8.3.3.2 (20-40 ms/70-80 Hz) t/f range 201

8.3.4 Validity and robustness of findings 203

8.3.4.1 Increasing the scale of main ANOVA-interaction 203

8.3.4.2 Taking a larger evoked gamma time interval 204

8.3.4.3 Mapping evoked gamma in TD&ASD in both conditions 205

8.3.4.4 Excluding TDs who performed well on task 207

8.3.5 The LONG condition 208
8.3.6 Other evoked phase locking differences in SHORT condition 210
8.3.6.1 Gamma differences in the SHORT condition 210
8.3.6.2 Lower frequencies in the SHORT condition 211
8.4 Discussion 213

Chapter 9 Final discussion and conclusion 220

Appendix 230

Bibliography 247

List of Abbreviations

AD: autistic disorder

ADI-R: autism diagnostic interview revised

ADOS-G: autism diagnostic observation schedule generic

AMPAR: α-amino-3-hydroxy-5-methyl-4-isoxazolepropionic acid receptor

ANOVA: analysis of variance

aPiC: anterior piriform cortex

AS: Asperger's syndrome

ASD: autism spectrum disorder

ASD+E: autism co-morbid with epilepsy

ATP: autism tissue programme

BA: Brodmann area

Ca: caudate

CA: corpora amylacea

CA1 and CA4: cornu ammonis 1 and 4

CE: coefficient of error

CL: claustrum

CNTNAP2: contactin-associated protein-like 2

CR: calretinin

DLPFC: dorsolateral prefrontal cortex

DSM-IV: diagnostic statistical manual of mental disorders

E: epilepsy

E/I: excitation and inhibition

EC: entorhinal cortex

EEG: electroencephalography

En: endopiriform nucleus

Ent: entorhinal area

Es: entorhinal sulcus

ERF: event-related fields

ERP: event-related potentials

fMRI: functional magnetic resonance imaging

fPiC: frontal piriform cortex

GABA: gamma-aminobutyric acid

GAD: glutamic acid decarboxylase

GAT-1: GABA-1 transporter

GCE: group coefficient of error

GC: glial cells

GCD: glial cell density

HFA: high-functioning autism

HLA: human leukocyte antigen

ICC: intra-class correlation coefficient

ICD-10: international classification of diseases

ID: intellectual disability

IL-1: interleukin 1

IQ: intellectual quotient

LOT: lateral olfactory tract

MEG: magnetoencephalography

Magnetic resonance spectroscopy: MRS

NC: neuronal cells

NCD: neuronal cell density

NF-κβ: nuclear factor kappa-light-chain-enhancer of activated B cells

NICHD: Eunice Kennedy Shriver National Institute of Child Health and Human Development

NMDAR: N-methyl D-Aspartate receptor

NPC: non-pyramidal cells

NPCD: non-pyramidal cell density

Olf: olfactory tract

PAC: phase-amplitude coupling

PC: pyramidal cells

PCD: pyramidal cell density

PDD: pervasive development disorders

PDD-NOS: pervasive development disorder-not otherwise specified

PET: positron emission tomography

PiC: piriform cortex

pPiC: posterior piriform cortex

PiT: temporal piriform cortex

PLF: phase-locking factor

PMI: post-mortem interval

Pu: putamen

PV: parvalbumin

rmANOVA: repeated measures analyses of variance

RRB: repetitive and restricted behaviours domain

rTMS: repetitive transcranial magnetic stimulation

SCI: social communication interaction domain

SCQ: social communication questionnaire

SHANK3: SH3 and multiple ankyrin repeat domains 3

SQUID: super-conducting quantum interference device

SRS-2: social responsiveness scale

T/f: time-frequency

TD: typically-developing

TLE: temporal lobe epilepsy

TNF-α: tumor necrosis factor alpha

TSC1: tuberous sclerosis complex 1 protein (hamartin)

TSC2: tuberous sclerosis complex 2 protein (tuberin)

Tu: tubercle

TWOBC: Thomas Willis Oxford Brain Collection

VCl: ventral claustrum

VGLUT1/2: vesicular glutamate transporters 1 and 2

WASI: Welscher abbreviated scale of intelligence

List of figures

Figure 1.1 New DSM-V diagnostic categories of ASD 3

Figure 2.1 Cell types in culture 26

Figure 2.2 Astrocytes and neurons in culture from division days 10-21 27

Figure 2.3 Mean number of neurons to astrocytes per counting frame 28

Figure 2.4 Dendritic and somatic expression of Kv1.1 29

Figure 2.5 Somato-dendritic expressions of Kv1.2 and 1.3 29

Figure 2.6 Somatic expression of Kv1.4 29

Figure 2.7 Kv1.6 expression is non-specific to neurons 30

Figure 2.8 TNFα receptors 1 and 2 in GFAP astrocytes and GABA neurons 31

Figure 3.1 Coronal slice of primary olfactory areas in the human brain 36

Figure 3.2 Types of cells in the piriform cortex 39

Figure 4.1 Antero-posterior mapping of the PiC in Nissl stain coronal sections 55

Figure 4.2 Coronal neurohistological sampling of the PiC 56

Figure 4.3 Morphological identification of cell types 60

Figure 4.4 Cytoarchitecture of the PiC and anatomical boundaries 61

Figure 4.5 The counting box 63

Figure 4.6 Scatterplot of point thicknesses 64

Figure 4.7 Number of counting boxes for a representative density 66

Figure 4.8 Normogram of predicted CE based on the shape of the area of interest 74

Figure 4.9 Summary of methodology 75

Figure 4.10 Normality validations 77

Figure 4.11 Summary of statistical analysis 81

Figure 4.12 Box-plot example of CE on cell counts 84

Figure 4.13 Box-plot example of CE on cell densities 85

Figure 4.14 Correlations between age and pyramidal cell densities in layer II 90

Figure 4.15 Correlations between age and glial cell densities in layer II 90

Figure 4.16 Mean glial cell densities in layers II and III 92

Figure 4.17 Mean pyramidal cell densities in layers II and III 93

Figure 4.18 Mean non-pyramidal cell densities in layers II and III 94

Figure 4.19 Mean neuronal cell densities in layers II and III 95

Figure 4.20 Post-hoc power of glial cell density measurements 96

Figure 4.21 Associations between cell densities and symptom severity 97

Figure 5.1 Morphology of glial cells and corpora amylacea 105

Figure 5.2 Qualitative layer II changes of the PiC in selected cases 106

Figure 5.3 Mean corpora amylacea differences between diagnostic groups 108

Figure 5.4 Corpora amylacea deposits in ASD compared with TD 109

Figure 5.5 Gliosis associated with corpora amylacea levels 110

Figure 6.1 Trilamination of the tubercle 119

Figure 6.2 Variability in cell clusters 120

Figure 6.3 Cell densities in layer II of the tubercle 121

Figure 6.4 Ca deposits in the tubercle in autism 122

Figure 6.5 Glial cells in the tubercle 123

Figure 6.6 Satellitosis in an autism and epilepsy case 124

Figure 6.7 Sampling of the hippocampus 131

Figure 6.8 Cell morphologies in hippocampal subfields 133

Figure 7.1 MEG measurements 139

Figure 7.2 Evoked and induced gamma 144

Figure 8.1 Event-related fields in perceptual simultaneity 158

Figure 8.2 Correlation between performance difference and latency difference 159

Figure 8.3 Visual paradigm of perceptual simultaneity 164

Figure 8.4 Signal variance between TD and ASD in the simultaneous condition 167

Figure 8.5 Signal variance between TD and ASD in the short condition 168

Figure 8.6 Gabor wavelet convolution of the signal 169

Figure 8.7 Summary of analysis 173

Figure 8.8 Mean percentages of simultaneous responses 176

Figure 8.9 Interaction between group and condition 178

Figure 8.10 Main effect of group 179

Figure 8.11 Main effect of condition 180

Figure 8.12 Between-group differences in the simultaneous condition 182

Figure 8.13 Between-group differences in the short condition 183

Figure 8.14 Between-group differences in different conditions (1) 184

Figure 8.15 Between-group differences in different conditions (2) 185

Figure 8.16 Within-TD differences between SHORT and SIM conditions 186

Figure 8.17 Within-ASD differences between SHORT and SIM conditions 187

Figure 8.18 Identification of time-frequency intervals of interest 188

Figure 8.19 Within-TD group and condition effects 190

Figure 8.20 Between-group differences in the SIM condition in t/f interval of interest 191

Figure 8.21 Between-group differences in the SHORT condition in t/f interval of interest 193

Figure 8.22 Mean phase locking between TD and ASD in SHORT and SIM conditions 194

Figure 8.23 Mean phase locking between conditions in ASD and TD 195

Figure 8.24 Between-group differences in the higher gamma range in the SIM condition 196

Figure 8.25 Between-group differences in the higher gamma range in the SHORT condition 197

Figure 8.26 Mean phase locking differences in the higher gamma range in the SHORT condition between TD and ASD 198

Figure 8.27 Correlations between gamma phase locking and severity scores in first t/f interval 200

Figure 8.28 Correlations between gamma phase locking and severity scores in the second t/f interval 202

Figure 8.29 Increased scale of ANOVA interaction 203

Figure 8.30 Inclusion of larger t/f interval of significance 204

Figure 8.31 Strength of the association between symptom severity and gamma 205

Figure 8.32 Individual gamma phase locking averages at higher latencies 206

Figure 8.33 Exclusion of top TD performers in SHORT condition 207

Figure 8.34 LONG condition between ASD and TD 209

Figure 8.35 Gamma differences in SHORT condition at later latencies 211

Figure 8.36 Beta differences in the SHORT condition 212

List of tables

Table 1.1 Cytokine effects on ion channel expression in hippocampal cultures 18

Table 4.1 Demographics of cases 47

Table 4.2 Causes of death 48

Table 4.3 Behavioural scores for ASD cases 51

Table 4.4 Intellectual disability scores of ASD cases 52

Table 4.5 Behavioural test scores for ASD+E cases 52

Table 4.6 Intellectual disability scores of ASD+E cases 53

Table 4.7 Seizure histories of ASD+E cases 53

Table 4.8 Example of calculation of Gundersen and Jensen variables 71

Table 4.9 Intra-rater reliability of layer II cell densities 82

Table 4.10 Inter-rater reliability of layer II cell densities 82

Table 4.11 Intra-rater reliability of layer III cell densities 83

Table 4.12 Inter-rater reliability of layer III cell densities 83

Table 4.13 Coefficients of error in layer II 86

Table 4.14 Coefficients of error in layer III 86

Table 4.15 Layer II cell densities and group CE 95

Table 4.16 Layer III cell densities and group CE 95

Table 5.1 Pathological findings of the piriform cortex 107

Table 5.2 Corpora amylacea across all diagnostic groups 110

Table 6.1 Demographics of tubercle cases 117

Table 6.2 Pathological findings of the olfactory tubercle 125

Table 6.3 CA1 neuronal cell density 135

Table 6.4 CA1 glial cell density 136

Table 8.1 Demographics and diagnostic scores of ASD and TD subjects 162

Table 8.2 Time and frequency uncertainties 171

Table 8.3 Percentage of simultaneous responses with standard deviations 176

Table 8.4 Dispersion of ADOS-G domain scores 201

Chapter 1 General introduction

1.1 Autism spectrum disorders (ASD): a brief history and classification

In 1943, Leo Kanner, a paediatrician at Johns Hopkins, published the first clinical descriptions of early childhood autism in a group of eight children who shared an inability to form affective contact with people, who were happiest when alone and who showed repetitive actions such as spinning toys for a long period of time oblivious to all else (Kanner 1968). One year later, Hans Asperger (1944), an Austrian paediatrician published his findings on highly intelligent children with superior abilities to the general population (e.g. mathematical abilities). These children shared symptoms of difficulties in social integration but had no delays in acquiring speech in contrast with the cohort that Kanner described who had speech development delays (Etchepareborda, Diaz-Lucero et al. 2007). Between 1950-1960, there were no consistent definitions of autism and it was viewed as an early presentation of childhood schizophrenia with emotional disturbances (Baker 2013). In the 1970s, and for the first time, autism became associated with mental retardation thereby suggesting a biological basis for the disorder (Baker 2013). Wing et al (1981) described the clinical profiles of 34 individuals who resembled strongly Asperger's descriptions many years earlier. Wing (1981) also suggested that Asperger's descriptions as well as hers were associated with early childhood autism and are part of a wider group of conditions. In 1994, the diagnostic statistical manual of mental disorders (DSM-IV) included both autistic disorder (AD) and Asperger's syndrome (AS)[1] as relatively distinct clinical groups falling under the general category of

[1]AS and high-functioning autism (HFA) were considered distinct clinical subtypes of PDDs largely differentiated based on the history of language delay according to the DSM-IV-TR. Gilchrist et al (2001) showed that an early childhood diagnosis of AS showed similar behavioural characteristics into adulthood as HFA and other studies have shown that HFA and AS might be the same syndrome. Under the new DSM-V, there is no qualitative distinction between HFA and AS.

autism, a neurodevelopmental prototypical disorder with impairments in the development of social interaction, communication and imagination (Gilchrist, Green et al. 2001, Giles 2013). According to the DSM-IV-TR (text version), both AD and AS fall under the umbrella of pervasive developmental disorders (PDDs) alongside Rett's syndrome, childhood disintegrative disorder and PDD-not otherwise specified (PDD-NOS) (American Psychiatric Association Task Force on DSM-IV 2000). Affected PDD individuals share a common triad of behavioural manifestations demonstrated by impairments in reciprocal social interaction and communication (verbal and non-verbal) as well as having restricted interests and showing stereotypy (American Psychiatric Association Task Force on DSM-IV 2000). The new DSM-V published in May 2013 replaced clinical subtypes of PDDs with a single diagnostic dimension of autism spectrum disorders (ASDs). With the removal of categorical diagnoses, ASD diagnosis with the new DSM-V has become along a continuum of severity. ASDs are now diagnosed based on deficits in the social communication interaction domain (SCI) and restricted and repetitive behaviours (RRB) domain, which resulted from the merging of the previously distinct DSM-IV social interaction and communication domains into one diagnostic domain (Buxbaum and Baron-Cohen 2013, Grzadzinski, Huerta et al. 2013). The DSM-V has also introduced in the RRB domain a diagnostic criterion of unusual sensory responses in line with up to 90% incidence of sensorial anomalies in ASD children in vision, olfaction and audition (Leekam, Nieto et al. 2007) and up to 50% if combined with the adult population (Ben-Sasson, Hen et al. 2009). In view of the large heterogeneity in the ASD phenotype, Grzadzinski et al (2013) suggest that ASD researchers increase the specificity of the diagnostic criteria by reporting the cognitive abilities, the level and type of intellectual disability, the existing psychiatric and neurological co-morbidities,

the degree of language impairments and the pattern of onset (see figure 1.1 below) (Grzadzinski, Huerta et al. 2013).

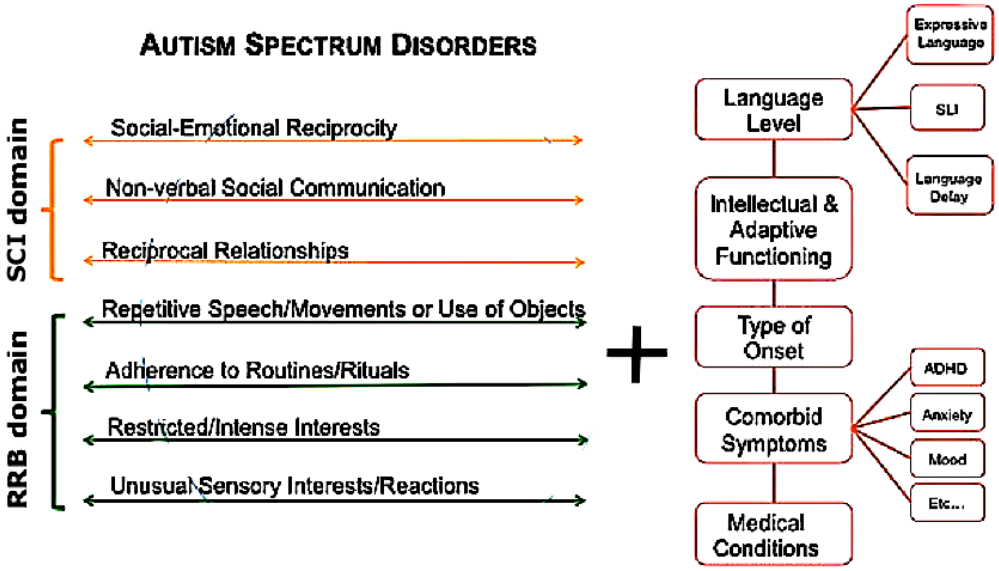


Figure 1.1 New DSM-V diagnostic categories of ASD. This figure has been modified from (Grzadzinski, Huerta et al. 2013) and shows the diagnostic criteria in the RRB and SCI domains. Additionally, researchers and clinicians on ASD are called to assess the language level, the type of onset and any co-morbidity or underlying medical condition to increase the specificity of the diagnostic criteria. *ADHD*: attention-deficit hyperactivity disorder; *RRB:* restricted and repetitive behaviour domain; *SCI:* social communication domain; *SLI*: specific language impairment.

1.2 Diagnosis and assessment

Typically, parents express concern when their 15-18 month-old child fails to develop or lose spoken language (McConachie, Le Couteur et al. 2005), lacks joint attention (Charman 1997), or does not respond to his/her own name (Baranek 1999). The age of early pre-school diagnosis of ASD in the UK is between 4-5 years (Caronna, Milunsky et al. 2008) even though symptoms might appear much earlier than the age of 3 (Allely, Gillberg et al. 2013). Early brain overgrowth associated with a clinical

diagnosis of macrocephaly in ASD between the ages of 6-14 months seemed to be a robust and specific feature of ASD (Courchesne, Carper et al. 2003) until it was called into question very recently by Raznahan et al (2013) who found that this overgrowth was not specific and could be found also in the typically-developing population (Raznahan, Wallace et al. 2013).

In early childhood, a diagnosis of ASD means that symptoms must be present in 2 areas of deficits in the RRB domain and all deficit areas in the SCI domain according to the new DSM-V. Diagnostic assessments to confirm the diagnosis of ASD are still based on the previous DSM-IV triad of impairments. Screening tools include the autism diagnostic interview revised (ADI-R) (Lord, Rutter et al. 1994), which is an interview and questionnaire with the parent/care-taker assessing impairments in three domains and the autism diagnostic observation schedule generic (ADOS-G) (Lord, Risi et al. 2000), which is an interview and questionnaire with the patient also assessing impairments in three domains. In conjunction with a full assessment of language and speech delays, co-morbidities, family history, intellectual disability (ID) levels according to the international classification of diseases (ICD-10) mental retardation guidelines and the cut-off scores from the ADI-R and ADOS-G, an ASD diagnosis is made (Roth and Rezaie 2011). Note that in this thesis, all of the described cases and diagnostic assessments used (ADI-R, ADOS-G) adhere to the DSM-IV criteria for autism and distinct clinical subtypes are reported (AS, AD, HFA) based on the medical history provided by the consultant psychiatrist.

1.3 Epidemiology

Epidemiological studies on ASDs show a prevalence of 1:100 UK and US school-aged children (Baird, Simonoff et al. 2006, Weintraub 2011). The prevalence is the same for adults in England (Brugha, McManus et al. 2011). Between 1991 and 1997,

a 556% increase in the paediatric prevalence of ASD was reported compared to the 1980s (Muhle, Trentacoste et al. 2004). Initially, epidemiological studies linked the surge in ASD prevalence to immunisations with the measles-mumps-rubella vaccine (DeStefano and Chen 2001). However, subsequent evidence found that environmental factors in fact accounted for very few ASD cases (Rutter 2005). The increase in ASD diagnosis is therefore most likely due to the increase in awareness regarding ASDs in the general population, as well as the usage of systematic standardised screenings of total populations that may be more sensitive than previously (Rutter 2005).

1.4 Aetiology

ASDs are largely hereditary with genetic factors contributing to the aetiology of more than 50% of cases (Gadad, Hewitson et al. 2013). Recurrence rates within the same family are between 10-18% (Ritvo, Jorde et al. 1989, Constantino, Zhang et al. 2010) and twin studies show a 95% concordance of ASD in monozygotic twins and 24% in dizygotic twins (Ritvo, Freeman et al. 1985). There are more than 400 susceptibility genes associated with ASDs many of them thought to be related to synaptic mechanisms, and many arise from *de novo* mutations associated with the fragile-X mental retardation protein (Voineagu, Wang et al. 2011, Iossifov, Ronemus et al. 2012). Candidate gene studies in animal models show that synaptic SHANK3 (Herbert 2011) and CNTNAP2 (Strauss, Puffenberger et al. 2006) variants are ASD risk genes; tuberous sclerosis associated variants TSC1 and TSC2 are also ASD risk genes thought to underlie abnormalities in neuronal migration, growth and differentiation (Numis, Major et al. 2011); and finally, channelopathies affecting subunits of NMDAR and voltage-gated sodium channels are also thought to be ASD risk genes underlying balanced inhibitory and excitatory neurotransmission (O'Roak, Vives et al. 2012).

1.5 The neurobiological basis of ASD

In this section, I briefly review the incidence of epilepsy in ASD as well as the neuropathology, neuroimmune and neurophysiology literature on ASD. These reviews are not meant to be exhaustive but highlight the general consensus in each subfield. The neuropathology and neurophysiology of ASD relative to the research question and structure of interest are discussed in more detail in later chapters.

1.5.1 Incidence of epilepsy

The incidence of a clinical diagnosis of epilepsy in children with ASDs is between 30 and 47% (Carod, Prats et al. 1995, Billstedt, Gillberg et al. 2005, Munoz-Yunta, Palau-Baduell et al. 2008), the rate of epilepsy being highest in ASDs who have severe intellectual disabilities. Regardless of intellectual quotient (IQ), incidence of epilepsy is higher in autism than in non-autism severe mental retardation (Steffenburg, Gillberg et al. 1996). Milder forms of ASD with normal IQ such as AS have lower rates of epilepsy (5-15%) (Danielsson, Gillberg et al. 2005). Irrespective of the severity of ASDs, the prevalence of a clinical diagnosis of epilepsy is between 10-20% overall (Roth and Rezaie 2011). Electrophysiological recordings using electroencephalography (EEG) and magnetoencephalography (MEG) in sleep and wakefulness on children with ASD show that irrespective of severity, 60-80% of patients on average show on-going sharp spike epileptiform activity in the perisylvian areas (Lewine, Andrews et al. 1999, Chez, Chang et al. 2006, Munoz-Yunta, Ortiz et al. 2008). Thus, epilepsy and epileptiform activity are associated strongly with ASDs though the direction of causality between ASD and epilepsy is not yet established. Interestingly, and with early onset epilepsy, autism and cognitive impairment seem to develop subsequently suggesting possibly causality (Engel and International League

Against 2001). Further work is needed to determine why ASD individuals have a lower threshold for epilepsy compared with controls.

1.5.2 Neuropathological and neuroanatomical findings in ASD

The most consistent neuroanatomical finding in ASD is reduced minicolumnar (basic functional units of the neocortex) spacing in layer III of the human dorsolateral prefrontal cortex (DLPFC) (Casanova, Buxhoeveden et al. 2003). Casanova et al (2002) showed that neuronal density increased in 14 ASD cases with mental retardation possibly as a result of decreased intercolumnar spacing. Courchesne et al (2011) reported increased neuronal density in layer III of the prefrontal cortex associated with a 17.6% increase in brain weight in ASD (Courchesne, Mouton et al. 2011). Purkinje cell loss, decrease in cell number and size in the cerebellum are consistent findings in ASD (Bailey, Luthert et al. 1998, Fatemi, Halt et al. 2002, Whitney, Kemper et al. 2008). Limbic system studies report a 12% decrease of neuronal numbers in the amygdala with no changes in cell size or volume, though a 14% amygdala volume enlargement in 3 to 5 year-old ASD individuals has been reported (Schumann and Amaral 2006). Hippocampal studies on ASD show an increase in cell-packing density and a decrease in neuronal size in the Cornu Ammonis 1 (CA1) region (Kemper and Bauman 1993). Hippocampal volume has been reported to be larger on the right side in ASD (Amaral, Schumann et al. 2008). Reductions in neuronal densities layer III and neuronal numbers in layers III, V, and VI have been reported in the fusiform gyrus in ASD and no changes in primary visual cortex (van Kooten, Palmen et al. 2008). Thus, brain development in ASD is altered. Courchesne et al have noted that differences in brain anatomy between ASD and typically-developing individuals (TD) might be evident at certain ages and not others, suggesting that the timing of brain development for certain structures in the brain to

be of primordial importance for ASD diagnosis in the very early stages (Courchesne and Pierce 2005).

The neuropathology of many areas of the brain remains under investigated in ASD. For example, olfactory processing in autism has received much attention recently. Higher-order olfactory processing takes place in a structure called the piriform cortex (PiC) (Howard, Plailly et al. 2009). Many studies have shown impairments in olfactory identification in ASD (Gottfried, Smith et al. 2004, Howard, Plailly et al. 2009, Galle, Courchesne et al. 2013), yet very few studies have investigated the neuropathology of the PiC cortex in ASD in human post-mortem tissue.

1.5.3 Neuroimmune findings in ASD

There is general support that the immune system might be involved in ASD pathophysiology. Cytokine studies report increased pro-inflammatory TNFα and IL-1β cytokines in the cerebrospinal fluid of patients with ASD (Angelidou, Asadi et al. 2012). An increase in pro-inflammatory cytokine concentrations is usually characteristic of an inflammatory state. Cytokines are released by immune cells of both the innate and adaptive immune responses such as macrophages, natural killer cells and lymphocytes in the periphery. In the central nervous system, microglia and astrocytes release most of the pro- and anti- inflammatory cytokines and therefore mediate brain neuroinflammatory processes (Meme, Calvo et al. 2006, Ota, Zanetti et al. 2013). The rise in cytokine levels is characterized by two phases of clinical importance: an early phase whereby local activation of microglia accounts for the initial increase in pro-inflammatory cytokine release and a late phase 12-24 hrs after injury whereby microglial IL-1 release activates local astrocytes resulting in further inflammatory cytokine release (Phelps and Korneva 2008). Activated microglia have also phagocytic functions like macrophages and therefore act as antigen-presenting

cells (Mack, Vanderlugt-Castaneda et al. 2003), whilst activated astrocytes contribute to local glial scarring following inflammation in a process called astrocytic gliosis that might affect neuronal survival and compromise blood-brain barrier integrity (Ota, Zanetti et al. 2013). Therefore, the rise in central pro-inflammatory cytokines presumably reflects underlying microglial and astrocytic activations in ASD. Neuropathological post-mortem studies have begun to assess astrocytes and microglia in ASD and one recent study found that astrocytes are denser and smaller in the frontal cortex in ASD (Cao, Yin et al. 2012). Qualitative studies have reported gliosis co-occurring with a reduction in Purkinje cell numbers in the cerebellum (Bailey, Luthert et al. 1998) and no astrogliosis in neocortical structures, the cerebellum and the hippocampus in infantile ASD (Kemper and Bauman 1998). A recent study found increased microglial cell densities in ASD in fronto-insular cortex, visual cortex and prefrontal cortex compared with TDs (Morgan, Chana et al. 2010, Tetreault, Hakeem et al. 2012). Increased microglia and astrocyte NF-κβ (marker of inflammation and pro-inflammatory cytokine release) extranuclear translocation, relative to neurons, has been reported in orbitofrontal cortex in ASD (Young, Campbell et al. 2011). Interestingly, a recent study tagged microglia with a [^{11}C](R) PK-11195 radiotracer in young men with ASD. Microglial activation was highest in the cerebellum but also sizable in other areas such as the fusiform gyrus and the orbitofrontal cortices (Suzuki, Sugihara et al. 2013). Thus, both microglia and astrocytes are implicated in inflammatory processes in ASD. However, the causes and timing of inflammatory insults mediated by glial cells remain unclear.

The involvement of the immune system in ASD pathophysiology is also indicated by studies showing the presence of anti-fetal brain antibodies in the plasma of mothers of ASD children (Braunschweig, Ashwood et al. 2008); increased incidence of maternal

infection during pregnancy in mothers of ASD children (Zerbo, Qian et al. 2013); a higher incidence of autoimmune disorders in ASD (Valicenti-McDermott, McVicar et al. 2006); and the strong genetic linkage between ASD and markers of the immune system such as linkage with HLA haplotypes (A2) and alleles of the complement protein C4 (Saxena, Ramdas et al. 2012).

1.5.4 Neurophysiological findings in ASD

Electrophysiological recordings using EEG and MEG in ASD generally suggest that ASD is associated with altered neuronal connectivity (Rippon, Brock et al. 2007). The benefit of EEG/MEG to other imaging modalities is the high temporal resolution that they provide that is of the order of the millisecond (see chapter 7 for more details). In recent years, the extraction of the time-frequency content of EEG/MEG signals and its relationship to human cognition has gained interest. Neuronal assemblies firing in response to a sensory stimulus synchronize their activity to an oscillatory mode. Depending on the stimulus and therefore the type of central processing required, local oscillatory synchrony can occur within the same area or long-range synchrony between several areas (Tallon-Baudry 2003). Alterations in the frequency content of MEG/EEG recordings therefore might provide us with clues about local and long-range connectivity. The gamma frequency range above 30 Hz is suggested to play a role in visual cognition and the grouping of an object into a coherent percept (Tallon-Baudry and Bertrand 1999). Gamma-band abnormalities in ASD have been investigated though most of the evidence is on local processes. ASD individuals show increased parietal induced gamma-band activities or decreased evoked gamma occipitally in response to illusory contours such as the Kanisza triangle stimuli (Brown, Gruber et al. 2005, Stroganova, Orekhova et al. 2012). Studies using Gabor Patches or image identification tasks usually show a decrease in evoked and induced

gamma-band activity occipitally (Bailey, Braeutigam et al. 2005, Milne, Scope et al. 2009, Snijders, Milivojevic et al. 2013). In response to auditory and language stimuli, evoked and induced gamma-band activity are sometimes increased frontally or decreased temporally (Braeutigam, Swithenby et al. 2008, Rojas, Teale et al. 2011, McFadden, Hepburn et al. 2012). Oscillatory synchrony is also altered in ASD in lower frequencies notably the alpha (8-12 Hz) (Khan, Gramfort et al. 2013) and the beta ranges (15-25 Hz) (Cornew, Roberts et al. 2012). Thus, oscillatory synchrony in the gamma-range mainly is altered in ASD in response to visual, auditory and language stimuli. Though other frequencies are gaining interest, we only focus in this thesis on the gamma-range. The use of MEG to investigate gamma-band alterations in ASD is gaining more interest and studies on ASD using this technology are still relatively few.

1.6 The notion of the superiority in performance in ASD

Superior performance of ASD individuals in some psychophysical tests has gained interest in recent years. For example, individuals show a local bias in visual perception and visuo-spatial construction: they perform well on the embedded figures task where a hidden shape has to be found in a picture (Baron-Cohen, Jolliffe et al. 1997) and also the block design task where individuals construct a pattern from painted blocks (Shah and Frith 1983, Dakin and Frith 2005). Superior visuo-perceptual processing under certain conditions has been linked to several cognitive theories particularly the weak central coherence theory incepted by Uta Frith that postulates that central to autism is a high degree of local processing and attention to detail. This confers a better ability to process parts but a general inability to process context or the whole (Gestalt) thereby explaining why affected individuals might perform superiorly in perceptual tasks (Happe and Frith 2006). Though weak central

coherence theory might predict why ASD individuals might locally process visual information better than typically developing controls, a number of studies involving the Navon hierarchical figures paradigm challenged this view. Individuals were asked to process the local or global level of a figure and in fact, global processing was no different between the TD and ASD group even though local processing was still superior in ASD (Love, Rouder et al. 1999, Plaisted, Swettenham et al. 1999). Furthermore, and in more able adolescents and adults with ASDs, superior processing in a block design task was not universal to all autism subjects with less than 45% of ASDs doing better on the task (Caron, Mottron et al. 2006). Other cognitive accounts have been also advanced to explain superior performance such as reduced generalization theory (Burack 2001) and enhanced perceptual functioning theory (Mottron, Dawson et al. 2006) though discussion of these theories is beyond the scope of this thesis. Much remains to be done to investigate further the neural correlates underlying these superior abilities.

1.7 Sensory atypicalities in ASD

Sensory atypicalities in ASD have been documented in the visual, olfactory, gustatory and auditory domains and are usually translated by either a hyper-responsiveness (for e.g. avoidance of places or people because of how they smell) or a hypo-responsiveness (an unawareness of the unpleasantness of an odour) (Kern, Trivedi et al. 2007). Hypo-responsiveness seems typical of toddlers and younger children whilst hyper-responsiveness is more prevalent in the adult population (Tuchman and Rapin 2006). Interestingly, sensory abnormalities seem to relate to ASD severity in the young and not the adult population (Kern, Trivedi et al. 2007). A recent study has shown that restricted and repetitive behaviours are more present in children who

showed increased sensory responsiveness (Riby, Janes et al. 2013). This suggests a possible link between sensory atypicalities and symptomatology.

1.8 The balance between excitation and inhibition in ASD

The imbalance between excitation and inhibition (E/I) may be at the core of ASD pathophysiology. Hussman (2001) previously suggested that the lack of GABA-mediated inhibition in the ASD brain might result in the over-stimulation of glutamate specialized neurons and a possible loss of sensory gating (Hussman 2001). He supports this hypothesis based on two observations: the first is that $GABA_A$ receptor pathology is common in many cases of autism and second, that excessive stimulation of non-NMDA glutamate receptors and disinhibition of GABA-ergic influence, generate autism-like pathology in experimental animal models of autism (Hussman 2001). In accordance with Hussman's hypothesis, Rubenstein et al (2003) suggested that in ASD, the imbalance between excitation and inhibition contributed to disrupted connectivity therefore accounting for the various sensorial and perceptual deficits encountered in ASD cases (Rubenstein and Merzenich 2003).

1.8.1 Evidence from the incidence of epilepsy

The high incidence of epilepsy and epileptiform activity in ASD individuals discussed previously is possibly the strongest argument for a possible imbalance between excitation and inhibition being at the core of ASD pathophysiology. Interestingly, and as even milder former of ASD such as AS show epileptiform activity in EEG recordings, it may be suggested that this imbalance is not only characteristic of more severe forms of ASD.

1.8.2 Evidence from minicolumnar spacing in ASD

The neuropil space between minicolumns is usually where glia and interneuronal connections develop thereby regulating the excitability of the milieu. Both increased neuronal numbers in ASD (Courchesne, Mouton et al. 2011) and decreased intercolumnar spacing might suggest an imbalance between E/I in ASD (Casanova, Buxhoeveden et al. 2003).

1.8.3 Evidence from neuropathological studies on GABA-ergic dysfunction in ASD

Post-mortem studies support the notion that there is a dysfunction of the GABA/glutamate system in ASD. Studies on post-mortem tissue have reported decreases in glutamic acid decarboxylase (GAD) protein levels (Gadad, Hewitson et al. 2013), abnormalities in glutamate levels either through changes in AMPA and NMDA receptor expression (mRNA and protein), changes in vesicular glutamate transporters VGLUT1 and VGLUT2 in frontal and temporal lobe regions in the hippocampus, amygdala and cerebellum (Amaral, Schumann et al. 2008, Gadad, Hewitson et al. 2013, Parellada, Penzol et al. 2013). Thus, the chemical balance between excitation and inhibition in ASD also seems altered in the post-mortem brain.

1.8.4 Evidence from neuroimaging studies

Neuroimaging studies have addressed the chemical balance between excitation and inhibition in ASD by measuring GABA/glutamate and other metabolite levels in cortical areas. There is evidence of decreased cortical GABA in the frontal lobe, motor and auditory areas in three magnetic resonance spectroscopy studies on children with ASD, (Harada, Taki et al. 2011, Gaetz, Bloy et al. 2013, Rojas, Singel et al. 2013). Furthermore, gamma abnormalities reported in autism might yet be another marker for an imbalance between excitation and inhibition in ASD specifically

because they have been shown to reflect the synchrony of inhibitory neuronal populations in the cortex (Sohal, Zhang et al. 2009). Thus both spectroscopy and electrophysiology studies might be suggestive of an imbalance between excitation and inhibition in autism.

1.8.5 Evidence from sensory atypicalities

Recent studies have demonstrated that atypical cortical dynamics based on the push and pull model of excitation and inhibition (binocular rivalry) in the visual system highly predicted autism symptomatology (Robertson, Kravitz et al. 2013). This also suggests a link between sensory atypicalities and the E/I balance.

1.9 Aims of the thesis

Many factors could contribute to altering the excitability of cortical networks, which could underlie the pathogenesis of ASDs. Initially, neuroimmune factors such as the effects of cytokines and autoantibodies on specific ion channels and their roles in altering neuronal networks in rodent postnatal hippocampal neuronal cultures were explored. It was hypothesized that inflammatory cytokines would decrease the expression of specific ion channels such as the voltage-gated postassium channels (VGKCs) and the $GABA_A$ receptors that regulate neuronal excitability. However, the opportunity to work with human subjects and human tissue arose and the *in vitro* work was not explored further. The preliminary work from these rodent cultures is briefly presented here and the main work in this thesis examines the neuropathology, neuroanatomy and neurophysiology of ASDs in greater detail.

As reviewed above, ASD is a heterogeneous disorder that is characterized by anomalies in various sensory domains including olfaction, touch and vision. The high incidence of epilepsy in autism, altered minicolumnar structure, altered resting

oscillatory activity and altered cortical GABA-ergic inhibition in sensory areas are neurobiological correlates that might account for this heightened sensitivity to respond to mild sensory stimuli (Schaaf, Toth-Cohen et al. 2011). Thus, differences in basic sensory processing areas and sensory anomalies might be suggestive of an imbalance between excitation and inhibition in cortical circuits and that this might be predictive of autism symptomatology.

This thesis explores sensory anatomy and neuropathology of olfactory areas in post-mortem tissue from consenting ASD and epilepsy donors. It also addresses sensory physiology in the visual domain in consenting ASD adults using collected MEG recordings with an emphasis on the neural correlates that might underlie superior performance. Furthermore, the imbalance between cortical E/I might underlie neuroanatomical and neurophysiological differences observed in these two sensory domains. Anatomical and physiological data could not be collected from the same sensory modality as insufficient tissue was accessible for the visual area and olfactory MEG data were not available for analyses.

Chapter 2 Autoimmunity, cytokines, ion channels and neuronal excitability

2.1 Introduction

Cytokines are immune-cell signaling molecules with many biological roles. In 1991, the first line of evidence of the neuromodulatory effects of cytokines emerged, and IL-1β, a proinflammatory cytokine, was suggested to affect neuronal ion channel activity via an interaction with the $GABA_A$ receptor (Miller, Galpern et al. 1991). Tumour necrosis factor α (TNFα), another inflammatory cytokine, and interleukin 1β (IL-1β) have also been shown to alter ion channel conductance, and both inhibitory and excitatory post-synaptic currents through the VGKCs, the voltage gated calcium channels (VGCCs), the $GABA_A$ receptors and the NMDA receptors (Schafers and Sorkin 2008). Inflammatory cytokines are also able to modify channel subunits via the activation of enzymatic cascades such as kinase-mediated cascades. For example, IL-1β during hyperthermia and fever may exert genomic effects via MAP-kinase and NF-κβ signalling pathways, and modify gene expression. They may therefore indirectly alter neuronal excitability (Bender and Baram 2007).

The VGKCs and the $GABA_A$ receptors are ion channels expressed in mammalian neurons that play a role in regulating neuronal excitability. These are ion channels expressed in mammalian neurons. Whereas the main function of $GABA_A$ receptors is to depress neuronal excitability (Sigel and Steinmann 2012, Miller and Aricescu 2014), the main function of Kv1s is to repolarize the membrane potential after depolarization. The Kv1s are a good example of channels widely expressed in the mammalian brain and spinal cord and are otherwise known as *Shaker*-type channels. Structurally, $GABA_A$ receptors are postsynaptic GABA-gated pentameric channels made up from 2α, 2β and 1γ subunits surrounding a central ion-selective chloride

channel. The VGKCs however are formed of an α-subunit with six or seven transmembrane segments and a single pore region. Functional channels are formed of tetrameric associations of different subunits (Benarroch 2009).

Table 1.1 Cytokine effects on ion channel expression in hippocampal cultures

Cytokine	Cell population	Receptors Affected	Reference
TNFα	Rat hippocampal neurons	• ↑AMPA (↑GluR1; ↓GluR2 subunits) • ↓ $GABA_A$ (β2/3)	(Stellwagen, Beattie et al. 2005) (Beattie, Hermann et al. 2002)
IL-1β	Rat hippocampal neurons	• ↓AMPA (↓GluR1) • NMDA (NR1); no change	(Lai, Swayze et al. 2006)
IL-6	Rat hippocampal neurons	• ↓mGluR (2/3 dimer) • ↓AMPA (↓GluR2) • NMDA (NR1); no change • ↓L-type VGCC	(Vereyken, Bajova et al. 2007)

A summary of the effects of TNFα, IL-1β and IL-6, all multifunctional cytokine, on ion channel subunits. The affected subunits are indicated in parentheses. *AMPA:* α-amino-3-hydroxy-5-methyl-4-isoxazolepropionic acid; *mGluR*: metabotropic glutamate receptors; *NMDA*: N-methyl-D-aspartate; *VGCC:* voltage-gated calcium channels.

Clinically, patients with brain inflammation conditions such as autoimmune encephalitis, which are autoantibody-mediated, have a pre-existing systemic viral infection in which cytokines would be clearly involved. These patients have antibodies against the VGKC-complex and the $GABA_A$ receptors (Vincent, Bien et al. 2011, Irani, Gelfand et al. 2014, Petit-Pedrol, Armangue et al. 2014). Whether the autoantibodies are pathogenic *per se*, or whether they are merely a marker coinciding with a separate disease process are questions that have been the focus of study.

Antibodies mediate their pathogenicity in several ways but the most common mechanisms are internalisation of their antigenic target, activation of the lytic complement cascade or directly interference with ion channel function (discussed in (Diamond, Huerta et al. 2009) in more detail). Irrespective of their pathogenic mechanism, the first step always involves binding of the antibody to the antigen: an important paradigm, therefore, is that autoantibodies against cell surface receptors are more likely to be pathogenic than autoantibodies against intracellular antigenic targets (Vincent, Bien et al. 2011, Lancaster and Dalmau 2012).

Pathogenic autoantibody binding to synaptic cell surface or structural proteins of ion channels also has implications for neuronal excitability in the CNS. This would be supported by the cessation of seizures, when immunotherapy suppresses autoantibody titres. Autoantibodies have been linked with hyperexcitability in the case of the VGKC-complexes, $GABA_B$, and glycine receptors (Irani, Bera et al. 2010, Lancaster, Lai et al. 2010, Carvajal-Gonzalez, Leite et al. 2014). 30-40% of neurons in the CNS use GABA as their neurotransmitter and inhibitory effects are predominantly mediated via the $GABA_A$ receptors.

Local pathological inflammation may also contribute to excitability *in vivo*. A localised immune response, with the subsequent release of cytokines particularly TNFα and IL-1β could impact onto the local neuronal signalling pathways: activated microglia and reactive astrocytes can alter the balance between excitation and inhibition in the milieu (Pannasch, Freche et al. 2014). Finally, blood-brain barrier integrity could also be affected through cytokine-activated receptors on endothelial cells, leading to a further recruitment of immune cells to the CNS.

2.2 Aims and hypothesis

Do cytokines influence neuronal excitability directly and do they alter ion channel activity? Pro-inflammatory cytokines have regulatory effects on the gene expression of VGKCs and $GABA_A$ receptors (Schafers and Sorkin 2008) (see also table 1.1). The interactions between autoantibodies against the Kv1s and the $GABA_A$ receptors and inflammatory cytokines are unknown. The aims here were to explore in neuronal cultures the interaction between cytokines, VGKCs and $GABA_A$ receptors and the possible implications on neuronal excitability. Neurons would be incubated in the presence of TNFα and IL-1β and the expression of VGKCs and $GABA_A$ receptors quantified by immunofluorescence. It was hypothesized that inflammatory cytokines would decrease VGKC and $GABA_A$ receptor expression *in vitro*. The interactions between cytokines and autoantibodies could be explored subsequently.

2.3 Methods

The methods consisted first of optimizations of a cell culture model that is usually used to test the binding of autoantibodies to neurons. Therefore, its suitability for cytokine responses needed to be established first. Subsequent to the characterisation of the cultures, the expression of various Kv1 channels as well as TNF receptors was determined in both neurons and glia using immunocytochemistry. All antibodies were from Santa Cruz, Dallas, Texas.

2.3.1 Hippocampal cell cultures

Rat hippocampal cell cultures were grown from hippocampi isolated from P_o pup brains within an hour from death of the pups, which were killed according to schedule 1 methods. The brains were left on ice until dissection. All dissection tools were autoclaved and sterilized beforehand. Hippocampi were kept in a solution of ice-cold filter sterilized HBSS solution during the dissection. Isolated hippocampi were incubated in a 10 mL solution of HBSS-Trypsin at 37°C for 25 minutes. After the hippocampi had settled to the bottom of the tube, the HBSS-T solution was discarded and replaced with 10 mL of MEM medium. The hippocampi were then triturated and centrifuged at RT at 1000g for 5 minutes. Subsequently, the supernatant was discarded and the cells were triturated and homogenized. Cells were counted using a haemocytometer and diluted at 1:20 in a PBS-Trypan blue solution and plated at 80000 cells per coverslip on 24-well plates with poly-lysine-L-coated coverslips and stored at 37°C in a 5% CO2 incubator overnight. The following day, 50% of the medium was changed to an enhanced filter-sterilized neurobasal medium with L-glutamine, FCS (10%), and a bottle of B-27 supplement. Half of the medium was changed every two to three days. The cells were grown for a period of 10 to 21 days.

Cytosine arabinoside was used at a final concentration of 5 μM to curb glial growth two days after plating.

2.3.2 Characterization of cell types in hippocampal cultures

As cytokine responses are best tested in relatively homogeneous cell populations (Phelps and Korneva 2008, Vezzani, Ravizza et al. 2008), a partial characterization of hippocampal cell cultures was undertaken to determine the percentage of astroglia:neurons *in vitro*. Using immunofluorescence, cultures were stained for the glial fibrillary acidic (GFAP) with an anti-GFAP rabbit antibody at 1:1000 to visualize astrocytes. A mouse anti-microtubular protein 2 (MAP2) antibody at 1:1000 was used to visualize neurons. For non-reactive microglia, anti-CD11b (mouse) was used at 1:200, oligodendrocytes with anti-CNP-ase (mouse) at 1:500 and interneurons with anti-parvalbumin at 1:1000 (rabbit). The secondary antibodies were Alexa-fluor 488 (anti-mouse) or Alexa-Fluor 568 (anti-rabbit).

2.3.3 Optimizations of hippocampal cultures for immunocytochemistry

Based on previous experiments, cells in culture were fully differentiated by 10 days from hippocampal isolation from the P_0 brains and plating *in vitro.* Cells were stained for GFAP and MAP2 at division days 10, 12, 14, 17, 19 and 21 in order to determine when it would be best for neurons to be stained using immunocytochemistry. Cells were fixed with 3% formaldehyde for 15 min and washed 3 times with PBS. Subsequently, cells were permeabilized with 1.5% Triton-X-100 for another 15 min, and then incubated with the following primary antibodies diluted in PBS-T and in 5% goat serum at 4°C on shaker in the cold room overnight [anti-GFAP (rabbit) at 1:1000 for astrocytes and anti-MAP2 (mouse) at 1:1000 for neurons]. Cells were washed

three times (5 min x3) with PBS at RT and secondary antibodies were added at 1:1000 in PBS-T and 5% goat serum. The secondary antibodies were Alexa-Fluor 488 (anti-mouse), and Alexa Fluor 568 (anti-rabbit). Incubation was for 45 minutes on the shaker at 4°C. Cells were subsequently washed (5 min x 3) with PBS. Coverslips were mounted on microscope slides with DAKO/1:100 (DAPI) mounting medium to visualize nuclei. Slides were covered in aluminium foil and stored at 4°C to dry and viewed with an immunofluorescence microscope a couple of hours later. Photos were taken using a canon-camera X43/E687 attached to the immunofluorescence microscope. Excitations for immunofluoescence were at λ = 488 nm (green colour) and λ = 568 nm (red colour).

2.3.4 Cell counting

GFAP cells and MAP2+ cells were counted from a total of 9 coverslips at each division days 10, 12, 14, 17, 19 and 21 in a systematic randomized fashion. Immunofluorescent photos were taken at 10X magnification and 1mm x 1mm counting grids were placed on each photo and both neurons and astrocytes were counted usually with usually a minimum of 80 cells counted overall. Results were quantified using SPSS.

2.3.5 Immunocytochemistry of Kv1 channels in hippocampal neurons

Division day 13 hippocampal cultures were incubated with primary antibodies against the subunits of the Kv1 channels with the following dilutions (Kv1.1 at 1:1000/ Kv 1.2 at 1:1000/ Kv1.3 at 1:500/ Kv1.4 at 1:1000/ and Kv1.6 at 1:500). The cells were fixed and permeabilized as above to visualize channel subunits. For Kv1.1, the antibody targeted the extracellular part of the channel. Live cells were incubated with

the primary antibody for one hour at RT in PBS and 5% goat serum prior to fixing and permeabilisation. For Kv1.2, Kv1.3, Kv1.4, and Kv1.6, incubation was done overnight with primary antibodies in PBS in 5% goat serum at 4°C on shaker. The following day, cells were washed three times in PBS. Anti-mouse secondary antibodies were added for 45 minutes at RT. Inhibitory neurons were visualized using anti-GABA (rabbit) at a 1:1000 dilution. DAPI stained nuclei.

2.3.6 Immunocytochemistry to identify TNFαR in astrocytes and neurons

Both glia and neurons express TNFα receptors (Phelps and Korneva 2008). TNFα mediates its effects via two receptors: TNFαR1, which is also known as the 'death' receptor because it orients the cell toward the apoptotic route by activating caspases whilst TNFαR2-mediated effects are considered neuroprotective (Phelps and Korneva 2008).A similar protocol as that used to identify the Kv1 channel subunits was used to identify the TNF-R1 and TNF-R2 receptors in astrocytes and neurons. Commercial antibodies were against the intracellular epitope, so fixing and permeabilisation were done before the incubation with the primary antibodies. Anti-TNF-R1 was a rabbit IgG used at a 1:500 dilution, whilst anti-TNFR2 was a goat IgG used at 1:1000. Corresponding Alexa-Fluor anti-rabbit or anti-goat were used secondary antibodies at 1:1000 dilutions.

2.3.7 Homogeneous cortical astroglial cell cultures

Rat P0 pups were killed according to schedule 1 methods, and brains were left on ice until dissection. All dissection tools were autoclaved and sterilized beforehand. The cortices were isolated within a half-hour for an 8 lot of brains. The cortices were kept in a solution of ice-cold filter sterilized HBSS solution during the dissection. After the

dissection, the isolated cortices were incubated in a 10 mL solution of HBSS-Trypsin at 37 degrees for 25 minutes. After they have settled to the bottom of the tube, the HBSS-T solution was discarded and replaced with 10 mL of MEM medium. The cortices were then triturated and centrifuged at RT at 1000g for 5 minutes. Subsequently, the supernatant was discarded and the cells were triturated and homogenized. Cells were counted using a haemocytometer and diluted 1 in 20 in a PBS-Trypan blue solution. Then, the cells were plated at 50000 cells per coverslip on 24-well plates with PLL-coated coverslips and stored at 37 degrees in a 5 % CO2 incubator. The following day, the medium was changed completely to an enriched glial medium, and half the medium changed every two to three days. The cells were grown for a period of 10 days, and were sub-cultured to improve purity. Cells for subculture were treated with Trypsin-EDTA to eliminate any contaminating microglia. Immunocytochemistry was similar to the protocol for visualising GFAP astrocytes in hippocampal cultures.

2.4 Results

2.4.1 Types of cells in P_0 cultures

Hippocampal cell cultures from rat P_0 pup brains were not predominantly neuronal. In addition to pyramidal and non-pyramidal neurons, the somas and dendrites of which were positive for MAP2, GFAP astrocytes constituted the more predominant cell type in the cultures. Astrocyte:neuron ratio was about 1:1 at division days 10 and 12. By division day 14, astrocyte:neuron ratio was about 3:1. Mean neuronal numbers decreased compared to astrocytes until there were very few neurons left by division day 21. Cultures also contained few CD11b microglia and CNP-ase oligodendrocytes. Non-pyramidal neurons were mostly GABA-ergic and PV (see figures 2.1 and 2.2).

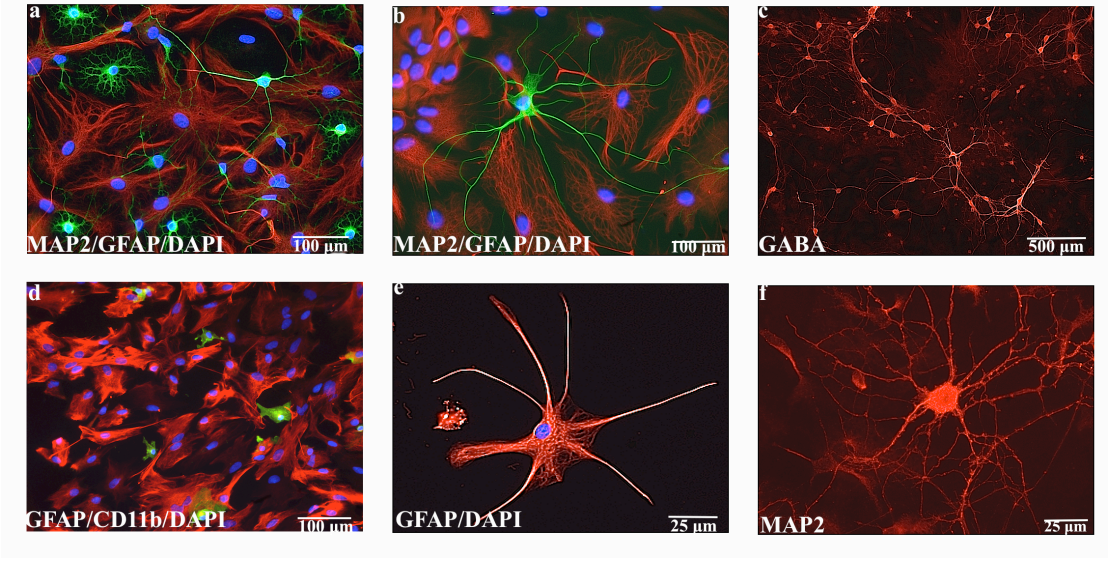


Figure 2.1 Cell types in culture. The variety of different cell types present in hippocampal neuronal cultures are shown above: GFAP astrocytes in red and MAP2 neurons in green with a DAPI nuclear stain in blue (a) & (b); GABA-ergic neurons in culture (c); GFAP astrocytes in red and CD11b microglia in green (d); characteristic star-shaped GFAP astroglial cell *in vitro* (e) and a multipolar MAP2 neuron in red (f).

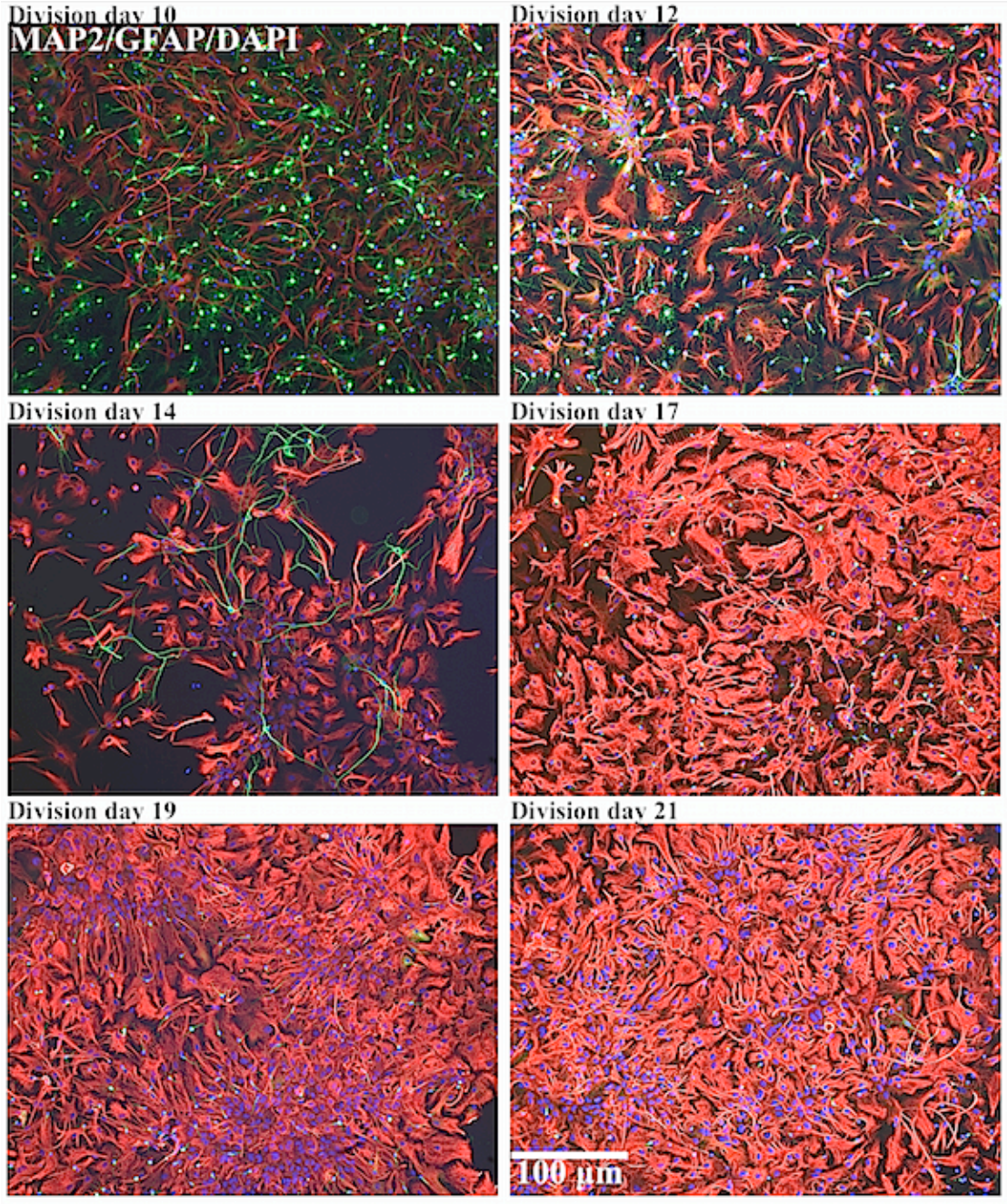


Figure 2.2 Astrocytes and neurons in culture from division days 10-21.

GFAP astrocytes are in red whilst MAP2 neurons are in green and DAPI stain in blue. Immunofluorescence of astrocytes and neurons shows rapid proliferation of astrocytes from division day 12 through to 21. Neurons are best developed on a bed of astrocytes as in division day 14.

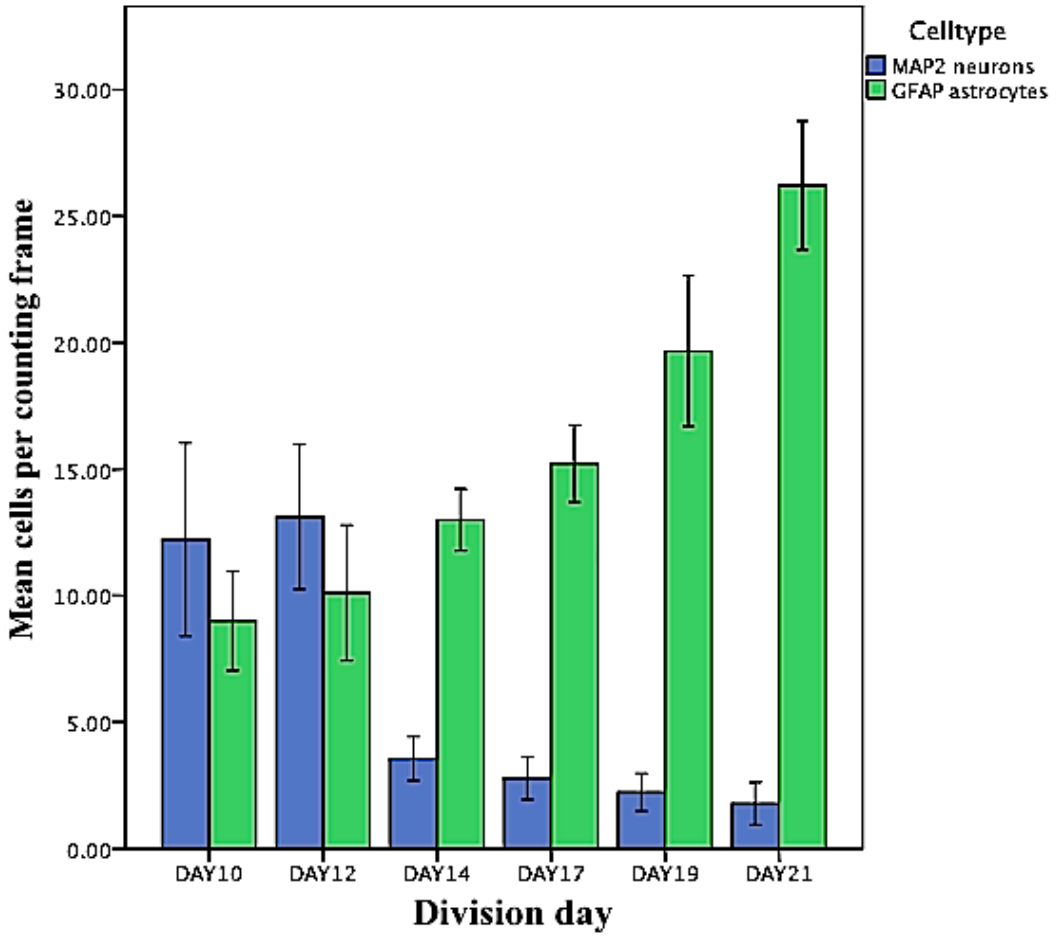


Figure 2.3 Mean number of astrocytes to neurons per counting frame.

From division day 14, astrocytes outnumber neurons *in vitro*.

2.4.2 Kv1 channel localizations in GABA-ergic neurons

Co-expression of Kv1.3, Kv1.4 and Kv1.6 subunits, with GABA immuno-labeling to define GABA-ergic neurons, was mostly somatic whilst Kv1.1 and Kv1.2 were both somatic and dendritic (see figures 2.4, 2.5, 2.6, 2.7). Axonal staining was also visible for Kv1.2 channel. Kv1.3 and Kv1.6 stains were not neuron-specific as there was binding to other cell types in the cultures.

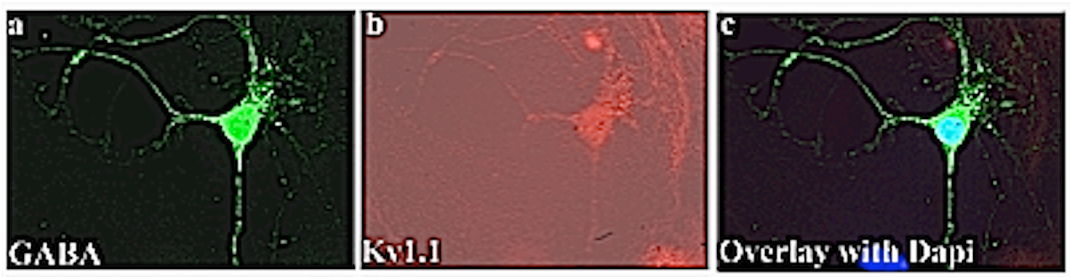


Figure 2.4 Dendritic and somatic expression of Kv1.1.

GABA neuron in (a), Kv1.1 in red in (b). Merge is in (c) with nuclear stain in blue.

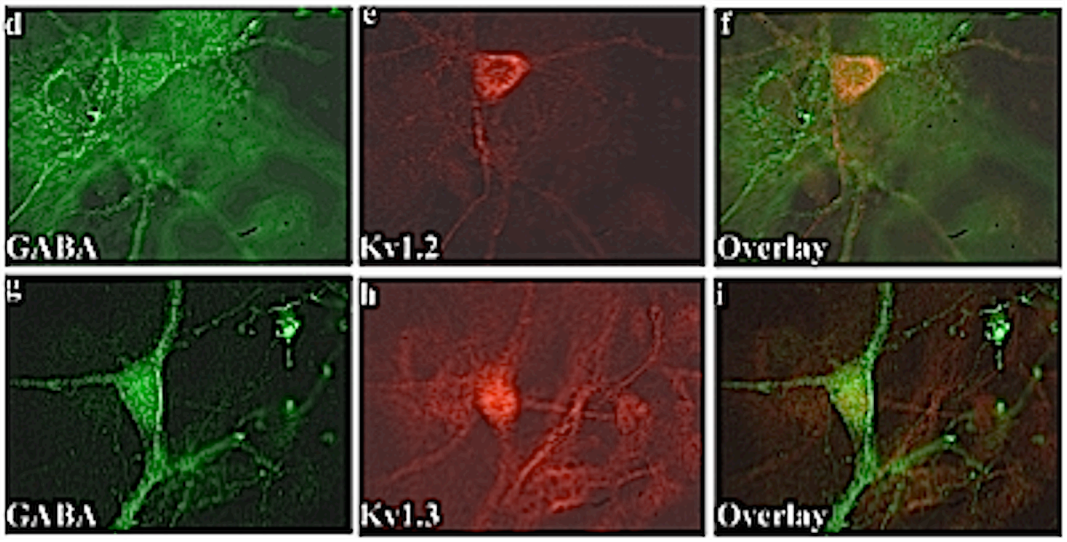


Figure 2.5 Somato-dendritic expressions of Kv1.2 and 1.3.

GABA-neuron in (d) and (g), Kv1.2 and 1.3 in red in (e) and (h). Merges are in (f) and (i).

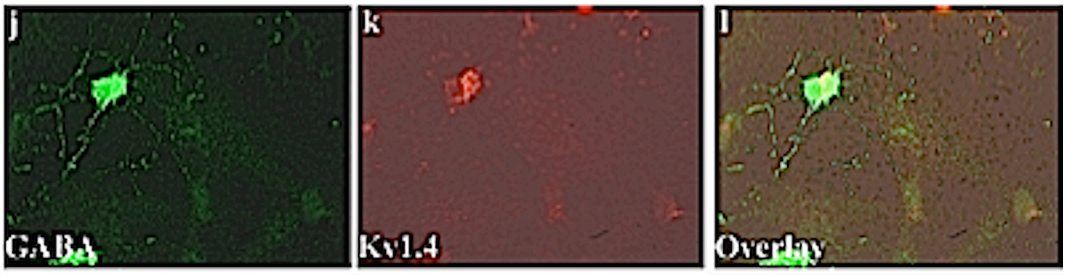


Figure 2.6 Somatic expression of Kv1.4.

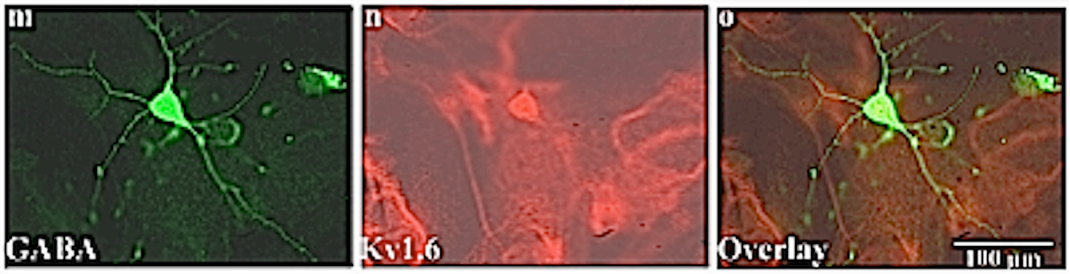


Figure 2.7 Kv1.6 expression is not specific to neurons. This figure shows that Kv1.6 expression was also present in other cell types and not only neurons. Note the non-specific red staining in the cultures.

2.4.3 TNFα receptor expression in astrocytes and neurons

TNFR2 (s) were localized to the cell body and processes of astrocytes in culture whilst TNFR1 (s) were localized in the processes in both astrocytes and neurons (see figure 2.8).

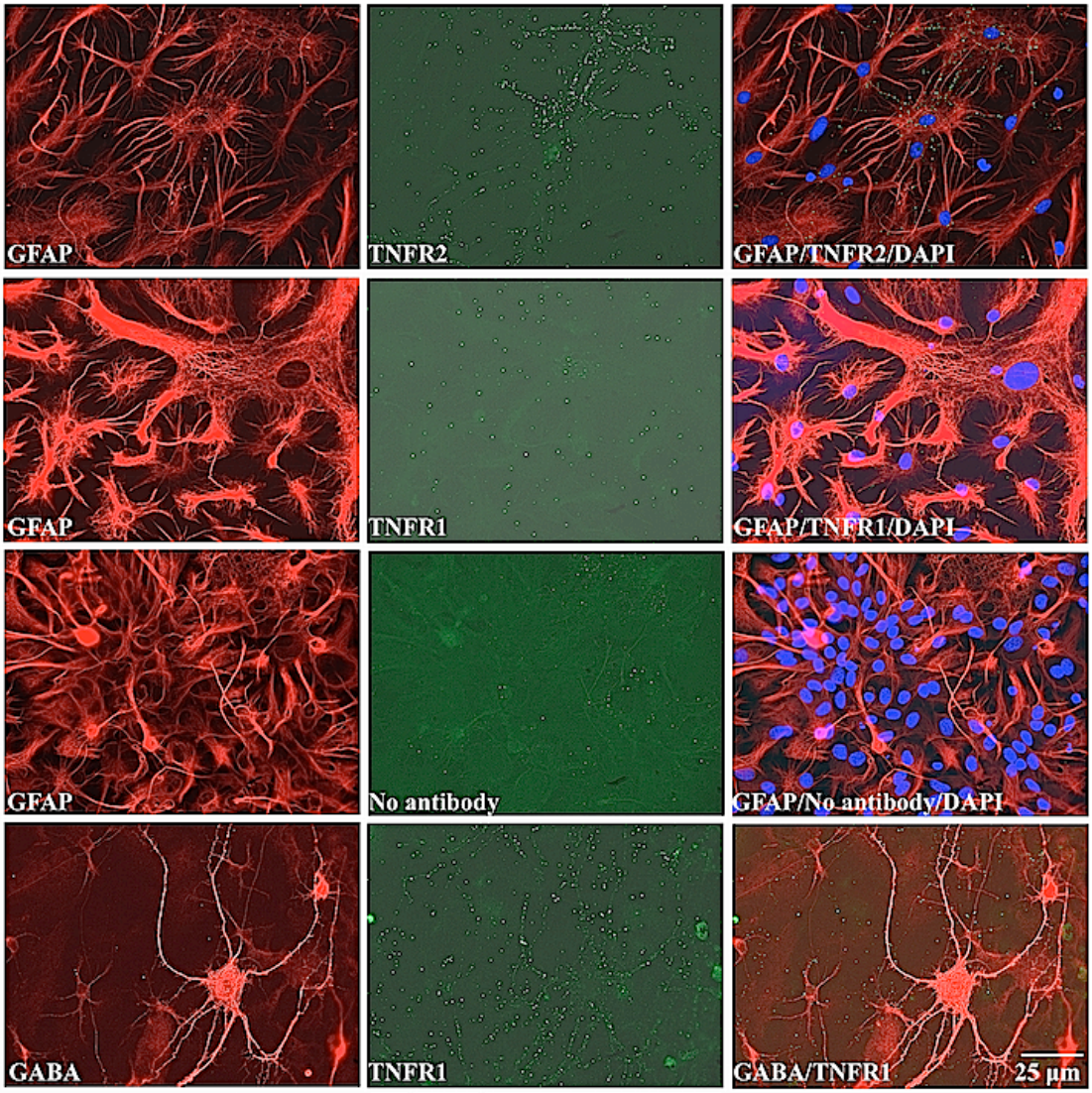


Figure 2.8 TNFα receptors 1 and 2 in GFAP astrocytes and GABA neurons. Green is the TNF receptor stain, red is GFAP astrocytes and right column is the merge between the nuclear stain (blue), GFAP and TNF receptor.

2.5 Discussion

Inhibitory neurons play an essential role in the control of neuronal excitability. This preliminary work established hippocampal neurons in culture, and began to characterise the expression of VGKC Kv1 and GABA in the cells. The neurons were distributed on a bed of astrocytes and other glial cells, and the ratios of neurons to glial cells were quantified at different time points in order to establish the most suitable time for study.

Many studies have shown that highly purified neuronal cultures may be obtained from hippocampi isolated from embryonic rat brains at days 15 through to 18 (E15-18) (Kaech and Banker 2006), but astroglia were the predominant cell type in the P_0 cultures apart from the neurons, and exceeded the neurons by day 12. Because astrocytes support neuronal metabolism and indirectly affect the excitability of the neuronal milieu, their presence *in vitro* is crucial for the development of healthy neurons. Indeed useful co-culture systems have been described whereby postnatal mouse hippocampal neurons were grown suspended above a feeder layer of astrocytes (Jones, Cook et al. 2012). In the P_0 cultures here, neurons *in vitro* looked healthiest with extensive dendrites and connections to the underlying astrocyte bed by division day 14. This was determined to be the optimal day for performing immunocytochemical experiments on the neurons. Beyond this date, cultures were no longer suitable for staining and astrocytes proliferated at a far quicker rate and asphyxiated the neurons.

The localization of Kv1 channels was consistent with descriptions in the literature: most of the Kv1s are somatodendritic and some such as Kv1.2 also show axonal localisation (Monaghan, Trimmer et al. 2001, Benarroch 2009). The non-homogeneity of postnatal hippocampal cultures makes them unsuitable for study of cytokine

responses. Glia are sources of cytokines and both neurons and glia express TNFR receptors (Vezzani, Ravizza et al. 2008). Both microglia and astrocytes also express some Kv1 channels similarly to postnatal neurons in culture such as Kv1.3 and Kv1.5 (Beeton and Chandy 2005). Therefore, though the effects of inflammatory cytokines may be quantifiable in neurons, perhaps co-culturing neurons with astroglia, would constitute a more suitable model to study interactions between both cell types and also quantify responses in the presence/absence of patient sera and the cytokine of interest. Following these pilot studies, the next step would have been to use VGKC and $GABA_A$ receptor antibody positive sera from patients with epilepsy to screen for TNFα and IL-1β cytokines. However, this would require freezing of the sample within 30 min from collection mainly because cytokines have very short half-life, and obtaining fresh frozen sera from patients for cytokine measurements proved difficult. Subsequently, astrocyte-neuron co-cultures would make a suitable cell model to study the effects of anti-VGKC and anti-$GABA_A$ antibodies on these cultures in the presence of inflammatory cytokines and quantifications by qPCR would be the subsequent step.

In conclusion, the use of rodent cell cultures would be very useful for understanding disease processes at a cellular level, and could have been adapted for further investigations. However, the possibility of working with human tissue offered an opportunity to investigate disease processes more directly related to the clinical phenotype in humans, particularly in the context of autism spectrum disorders. Therefore, though it was greatly beneficial to work within the Vincent group, interests in the human condition were pursued within the department of neuropathology and the subsequent work was carried out on post-mortem samples from consenting donors who had autism and epilepsy during life.

Chapter 3 The piriform cortex in ASD and epilepsy

In this part, an under investigated area of paleocortex involved in olfactory processing was examined in post-mortem human tissue. This area is introduced below followed by a review of the literature in autism and epilepsy.

3.1 Definition

The PiC is a trilaminar paleocortical structure located at the medial junction of the frontal and temporal lobes at the level of the entorhinal sulcus. The PiC is a much older structure than the neocortex and has been demonstrated to play a central role in higher order olfactory processing particularly in relation to odour perception (Gottfried 2010). Historically, the PiC has been described in histological studies on rodents and primates as a 'pear-shaped' structure and this nomenclature still resides in the modern literature even though the shape of the PiC bears no resemblance to the pear but has rather a –s-, –c- or even –w- shape in mammalian species (Paxinos 1990). Confusingly, the term PiC is also sometimes used interchangeably with the term 'primary olfactory cortex'[2] (Gastaut 1961, Powell, Cowan et al. 1965), which encompasses many anatomical areas implicated in olfactory processing such as the amygdala, the olfactory tubercle and the rostral entorhinal cortex (Pigache and SpringerLink (Online service) 1970). Brodmann located the PiC to the most rostral part of the parahippocampal gyrus or presubicular areas (Brodmann 1909) and Brodmann's Area 27 (BA27) has remained conventionally in use by neuroanatomists when referring to the PiC even though this might cause confusion as BA27 is

[2]Powell et al (1965) considered the PiC as primary olfactory cortex based on their studies of rat olfactory bulb. This is probably in reference to the piriform lobe rather than the piriform cortex as we define it today. Gastaut et al (1961) kept primary olfactory cortex and PiC as separate entities. In today's nomenclature, the PiC is one structure within the primary olfactory cortical areas that include the amygdala, rostral entorhinal, anterior olfactory nucleus and olfactory tubercle.

sometimes called the hippocampal area[3]. To avoid confusion and throughout this text, primary olfactory cortex as a term is employed to designate all olfactory processing areas as mentioned above including the PiC.

The PiC area is also used as a term instead of BA27. In this section, the detailed anatomy and cytoarchitecture of the PiC are described as well as its main roles in olfactory processing.

3.2 Anatomy of the PiC

The human PiC is situated along the lateral olfactory tract on the caudolateral aspect of the orbitofrontal cortex at the level of the entorhinal sulcus. It then continues onto the dorsomedial aspect of the temporal lobe. The rostral limit of the PiC is where it passes into the anterior olfactory nucleus and the transition occurs where the olfactory peduncle is attached to the cerebral hemisphere (Pigache and SpringerLink (Online service) 1970). The PiC is bound laterally by the rhinal fissure (anterior and posterior), medially by the fissura rhinalis arcuata that separates it from the olfactory tubercle, the amygdala fissure that separates it from the amygdala nuclei and the claustral cleft (capsula externa) that separates it from the claustrum, which continues ventrally to the PiC to form the endopiriform nucleus (Paxinos 1990). Caudally, the PiC passes eventually into the entorhinal cortex (EC) (Paxinos 1990). The PiC is further divided into anterior (aPiC) and posterior (pPiC) portions based on anatomical, physiological and functional differences (Bekkers and Suzuki 2013). The distinct roles of these two areas are described in the section on roles of the PiC.

[3] BA27 is referred to in the literature as the parahippocampal area or hippocampal neocortex. Sylvius' neuroanatomical reference considers BA27 as the hippocampal area and Harvard's brain atlas defines BA27 as the pre-subicular area. These are potentially confusing definitions mainly particularly when it comes to sampling the PiC from human tissue. In fact, the closer we get to the hippocampus, the only remaining subset of the PiC is temporal and represents the end of the structure (see methodology).

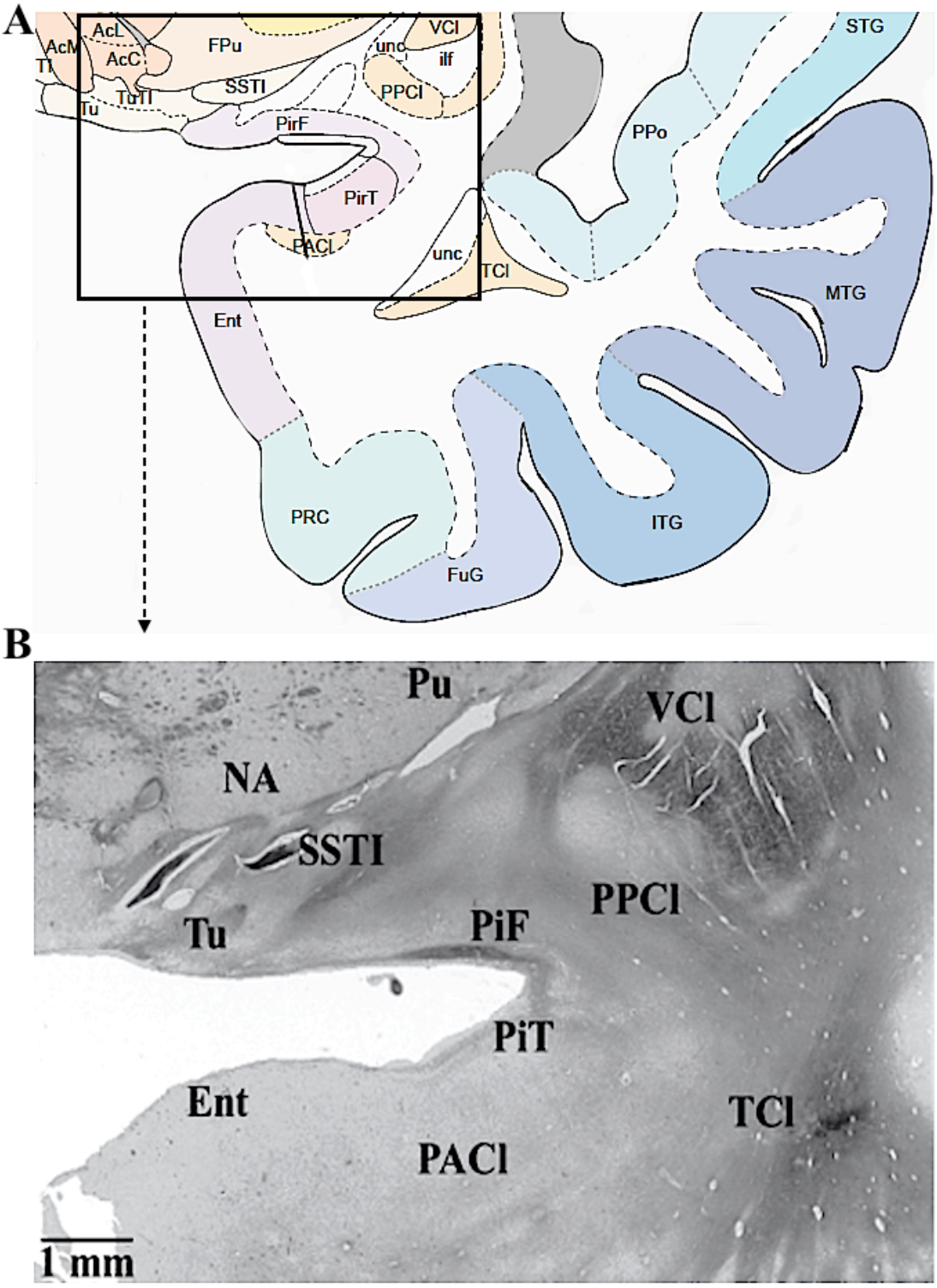


Figure 3.1 Coronal slice of primary olfactory areas in the human brain.

(A) This shows the temporal lobe and frontal lobe of the right hemisphere at the junction where the piriform is located in the coronal plane. (B) This shows a magnified and simplified view of the piriform area in its frontal (*PiF*) and temporal

(*PiT*) parts surrounded by various anatomical structures. The photo was modified from (Mai, Voss et al. 2008). *AcC:* central accumbens, *AcL*: lateral accumbens, *AcM:* middle accumbens, *Ent:* entorhinal cortex, *FPu:* fundus of putamen, *FuG*: fusiform gyrus, *Ilf:* inferior longitudinal fasciculus, *ITG:* infernal temporal gyrus, *MTG*: middle temporal gyrus, *NA:* nucleus accumbens, *PACl*: preamygdalar claustrum, *PPCl:* prepiriform claustrum, *PPo*: planum polare, *PRC:* perirhinal cortex*, Pu:* putamen, *SSTI*: substriatal terminal island, *STG*: superior temporal gyrus, *TCl:* temporal claustrum, *TI:* terminal island, *Tu:* olfactory tubercle, *TuTI:* tubercle terminal island, *Unc*: uncinate fasciculus, *VCl:* ventral claustrum.

3.3 Cytoarchitecture

Some of earliest descriptions of the cytoarchitecture of the mammalian PiC can be traced to studies on cats (Cajal 1955) and rodents (O'Leary 1937). Price (1973) studied the primate PiC and he broadly described, consistent with the findings of his peers from studies on mammalian PiC, that three layers characterize this structure (Paxinos 1990, Nieuwenhuys, Huijzen et al. 2008, Economo and Triarhou 2009). A superficial and sparse molecular layer I that only has very few neurons, a very dense cellular layer II that has moderately large pyramidal cells and a thick layer III that is characterized by larger perikarya belonging to pyramidal cells. Unfortunately, there are not many accounts on the different cell types in the human PiC, to the author's knowledge, and the closest thorough descriptions are from rodent PiC (rat and mouse) by Suzuki et al (Suzuki and Bekkers 2007, Suzuki, Bekkers et al. 2010, Suzuki, Bekkers et al. 2010). Suzuki reported that layer I mostly consists of GABA-ergic interneurons known as horizontal cells that are positive for calretinin (CR), which receive excitatory input from the lateral olfactory tract and provide feedforward

inhibition onto principal cell dendrites (Suzuki and Bekkers 2007). In layer I also, globular neurogliaform GABA-ergic cells with thin dendrites that ramify locally have been described (Suzuki and Bekkers 2007). In Layer II, moderately large glutamatergic pyramidal cells are the main input cells of the PiC together with GABA-ergic parvalbumin positive (PV) and/or CR multipolar interneurons (40% of total interneurons) with long spiny dendrites that exert perisomatic feedback inhibition onto layer II pyramidal cells (Nieuwenhuys, Huijzen et al. 2008, Bekkers and Suzuki 2013). Layer III mostly consists of large multipolar or small globular GABA-ergic interneurons that are positive for PV and/or positive for CR and large deep pyramidal cells (Bekkers and Suzuki 2013). Finally, layers II and III can also contain GABA-ergic bitufted basket cells with vertically oriented dendrites spanning several layers which are hypothesized to provide feed-forward and feedback persiomatic inhibition of layer II neurons (Suzuki and Bekkers 2007). Little evidence exists regarding the type of glial cells in layers of the PiC. In a study on the rat pilocarpine model of temporal lobe epilepsy, the only glial cell types studied to date in the PiC were glial fibrillary acidic protein (GFAP) reactive astrocytes and microglial cells positive for Cd11b (Eidt, Kendall et al. 2004).

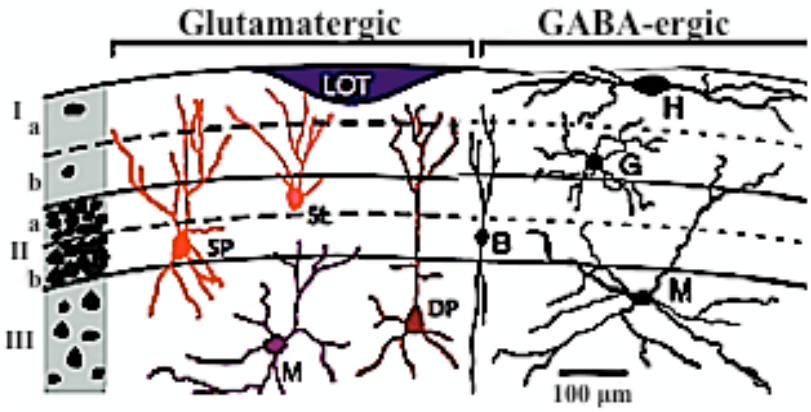


Figure 3.2 Types of cells in the piriform cortex.

This figure is modified from Suzuki et al (2013) (Bekkers and Suzuki 2013) and shows the various neuronal morphologies in layers I, II and III of mouse PiC. Black coloured cells represent different inhibitory interneuronal populations that are primarily GABA-ergic, whilst glutamatergic cells are in alternative colours. (a,b) represent the most superficial as opposed to deeper parts of layers I and II, a distinction that has not been made in this study. *B*: bitufted cell, *DP*: deep pyramidal, *G*: neurogliaform cell, *H:* horizontal cell, *MS & M*: multipolar cells *SL*: semi-lunar cell, *SP*: superficial pyramidal cell.

3.4 Afferents and Efferents of the PiC

The superficial layer I of the PiC receives the majority of sensory afferents (monosynaptic) from bulbar mitral cell axonal projections via the lateral olfactory tract and olfactory processing is believed to occur at the level of pyramidal neurons in layers II and III though it is unclear whether the different neuronal types perform different functions (Gottfried 2010). The deeper part of layer I contains associative inputs from other primary olfactory areas. Most of layer I afferents terminate in the aPiC whilst most of the associative input terminates in the pPiC. The efferent circuitry of the PiC includes all areas that have direct afferents from the olfactory bulb such as

orbitofrontal cortex (Gottfried 2010, Bekkers and Suzuki 2013). Furthermore, projections to the insular cortex, putamen and hippocampus have also been suggested (Economo and Triarhou 2009). Johnson et al (2000) described the associative function of the PiC and they showed that some PiC pyramidal neurons projected into more than one limbic area via long-range axonal arbours (Johnson, Illig et al. 2000).

3.5 Roles of the PiC

The PiC plays a role in relaying olfactory information and in odour object perception. Odour discrimination tasks and odour detection threshold tasks are usually used to assess lower-order processing in the olfactory domain, whilst higher-order processing is investigated by using olfactory identification tasks. Human fMRI studies and electrophysiological rodent studies found that the aPiC and the pPiC code odours differently (Gottfried, Deichmann et al. 2002, Gottfried, Smith et al. 2004). Gottfried et al (2010) suggested that the anatomical connectivities of the aPiC and pPiC also give us clues as to their functional roles: the aPiC receives primary sensory afferents from the olfactory bulb and therefore might be better suited to represent elemental features of an odour, whilst the pPiC acts as associative cortex whereby its connections with the limbic cortices make it better suited to represent odour perceptual quality (Gottfried 2010). Based on mammalian experiments, the aPiC seems to encode olfactory background segmentation or the identification of a novel odour against a background of older odours whilst the pPiC seems to encode olfactory categorization and discrimination, which are associated with long-term episodic memory and learning (Gottfried, O'Doherty et al. 2002, Gottfried, Smith et al. 2004).

3.6 Summary

The PiC is central to olfactory processing. The elucidation of the PiC's anatomical connectivity and cytoarchitecture is largely based on rodent and much more rarely primate post-mortem samples. More importantly, it is not clear whether the described literature is always relevant to humans particularly as the size of the PiC and olfactory areas in rodents is much larger than it is in humans. In contrast, many studies on human controls or patient groups using functional magnetic resonance imaging (fMRI) in conjunction with animal electrophysiological studies have led to the elucidation of the functional roles of the PiC in olfactory discrimination, categorization and identification. However, we still lack studies on human control and patient post-mortem tissue to examine the detailed anatomy of this area, in an attempt to understand the underlying cell population distributions that might help us relate olfactory structure to function particularly in the context of pathology. In this next part, the existing post-mortem literature and to some extent the imaging literature on the PiC in the context of ASD and epilepsy are reviewed.

3.7 The piriform cortex in ASD and epilepsy

Olfactory function and olfactory processing in the PiC are generally underinvestigated in ASD specifically but also more broadly in neuropsychiatric disorders. According to Schleckmann (2013), even if we combine studies on both children and adult samples, the number of functional olfactory studies in ASD still remains low (Schecklmann, Schwenck et al. 2013). Even more rare are anatomical olfactory studies in ASD particularly as the PiC is epileptogenic (Laufs, Richardson et al. 2011, Laufs 2012) and 30% of ASD cases are co-morbid with epilepsy (Bolton, Carcani-Rathwell et al.).

In the section below, what we know on the PiC in olfactory dysfunction in both ASD and epilepsy is briefly reviewed.

3.7.1 Olfactory dysfunction in ASD

In ASD, decreased olfactory identification (Suzuki, Critchley et al. 2003, Bennetto, Kuschner et al. 2007, May, Brewer et al. 2011) in children and adults in ASD (AS, HFA) is the general consensus though one study found a decrease in olfactory sensitivity (Dudova, Vodicka et al. 2011) and another study found a decrease in olfactory discrimination (Schecklmann, Schwenck et al. 2013). Interestingly, and as olfactory identification usually requires higher-order processing in the pPiC and is generally associated with a good verbal ability, the observed reduction usually correlates highly with speech delays in ASD cases. Very little is known about cytoarchitectural changes in the PiC area associated with ASD. In a recent study on haplo-insufficient +/- reeler mice, layer II pyramidal cells and PV interneurons in the PiC were decreased alongside oxytocin-insufficiency and mice demonstrated impairments in social interaction, suggesting that the PiC area might be affected in ASD (Liu, Pappas et al. 2005). Therefore, further studies on human tissue are needed to investigate PiC cytoarchitecture in ASD.

3.7.2 Olfactory dysfunction in epilepsy

There are generally more studies suggesting impaired olfactory function particularly in temporal lobe epilepsy where unpleasant olfactory auras have been reported since the early 20th century in human patients, and have been shown to correlate with post-mortem gliosis in the piriform area (Paxinos 1990). These auras precede complex partial seizures where uncinate fits are generated by the PiC subsequently. Further

evidence between epilepsy and olfactory dysfunction comes from a patient who underwent bilateral temporal resection; odour detection thresholds were maintained but not judgements of perceptual similarity between pairs of odours (West and Doty 1995). The involvement of the PiC in seizure activity has been recently described in a paper by Laufs et al (2011) where seizure activity was detected in the frontal PiC ipsilaterally to the cortical focus in focal epilepsy patients, and this correlated with haemodynamic increases in the area measured by simultaneous EEG/fMRI as well as reduced $GABA_A$ receptor binding measured by [^{11}C] flumanezil positron emission tomography (PET) scans (Laufs, Richardson et al. 2011). In fact, mouse studies show that the aPiC area seems to receive less GABA-ergic inhibitory input onto anterior pyramidal cells making it more prone to seizure generation than the pPiC (Loscher, Lehmann et al. 1998). Very few studies on human patients have examined changes in the PiC in post-mortem tissue. A post-mortem study by Fujikawa et al (2000) showed qualitatively that neuronal loss and severe gliosis were exhibited in the periamygdaloid PiC area in all three layers following death by status epilepticus in 3 patients (Fujikawa, Itabashi et al. 2000). To the author's knowledge, all other cytoarchitectural differences of the PiC reported in epilepsy are from animal models of experimental epilepsy.

The area tempestas (dorsal endopiriform nucleus) of the PiC has long been established as a trigger epileptic zone in the kainate, pilocarpine, bicuculline and rat kindling models (Loscher and Ebert 1996). PiC brain slices from kindled adult rats show a decrease in $GABA_A$-receptor-mediated inhibition of pyramidal cells in layer II of the PiC at the very early stages of epileptogenesis (Loscher, Lehmann et al. 1998). A study on the bicuculline rat model showed that ictal discharges in the PiC originated in the aPiC, although it is not clear why and how seizure propagation is

generalised (Ebert, Wlaz et al. 2000). Kainate and pilocarpine epilepsy model studies report decreases in GABA-ergic neurons in layer II of the central PiC and severe obliteration of that layer only a few hours after injection of the inducing agent (Loscher and Ebert 1996). Interestingly, subpopulations of GABA-ergic neurons seem to have increased mRNA glutamate carboxylase isoenzymes, which are suggested to be upregulated to help control the hyperexcitability of pyramidal cells (Freichel, Potschka et al. 2006). Thus, animal studies of experimental epilepsy suggest that the PiC has a role in seizure generation and that the cytoarchitecture of the pPiC makes it less prone to seizures than the aPiC.

Chapter 4 Post-mortem stereology of the piriform cortex in ASD and epilepsy

4.1 Rationale, aims and hypothesis.

The PiC area is affected in autism and epilepsy. To the author's knowledge, there are no studies that have investigated changes in the cytoarchitecture of the PiC in post-mortem tissue from patients with autism. The PiC area is prone to seizures and 30% of individuals with ASD have a clinical diagnosis of epilepsy. Therefore, it is unclear whether the type of pathology affects the distribution of cell populations in layers II and III of the PiC. This might imply an altered balance between E/I in the PiC and possibly account for olfactory anomalies encountered in patients with ASD and epilepsy.

Pyramidal, non-pyramidal and glial cell densities in layers II and III of the PiC were quantified using systematic random sampling based on stereological concepts in 39 post-mortem cases, of which 11 had a confirmed diagnosis of ASD, 11 were confirmed as epilepsy cases, 6 were confirmed as ASD co-morbid with epilepsy cases and 11 typically-developing control cases.

It was hypothesised that neuronal populations in layers II and III of the PiC would be decreased in ASD, ASD co-morbid with epilepsy (ASD+E) and epilepsy (E) cases. It was also hypothesised that glial cell densities would be increased in ASD and epilepsy and that this effect might be worse in the ASD + E group.

4.2 Methodology

The entire methodology is summarized in a diagram in figure 4.9.

4.2.1 Case selection

11 TD, 11 idiopathic/chronic epilepsy, 11 ASD with no neurological co-morbidity and six ASD+E cases were selected based on the author's assessment of full medical history (when available) from the clinical notes. The diagnosis of ASD was confirmed by Dr. T. Berney (consultant psychiatrist for the Thomas Willis Oxford Brain Collection (TWOBC), Newcastle, UK) in 12/17 cases using cut-off scores of the Autism Diagnostic Schedule Revised (ADI-R) (see table 4.2). One case was confirmed in the USA and four cases were identified as ASD from clinical notes. Intellectual disability (ID) was assessed in 14/17 autism cases using ICD-10 guidelines (five with severe ID; one with moderate ID; four with mild ID; four with no ID; three n/k). Post-mortem reports were available for all cases. The Autism Tissue Programme (ATP) and the TWOBC ethics committees granted ethical approval for this study. Cases were age-matched. Patient data and diagnosis are presented in table one. (For cause of death, see table 4.2).

Table 4.1 Demographics of cases								
Subjects	**ASD**		**Chronic E**		**ASD + E**		**Comparison TD**	
	7M:4F		7M:4F		5M:1F		5M:6F	
	Mean	**SD**	**Mean**	**SD**	**Mean**	**SD**	**Mean**	**SD**
Age at death (years)	30.09	14.87	36.45	17.5	25.67	9.58	34.18	25.56
Post-mortem interval (hours)	65.14	38.59	49.01	28.72	72.5	29.42	35.01	19.48
Storage time in formalin (years)	5.27	4.11	19.09	9.61	5.17	5.96	14.59	9.28
Mean fixed brain weight (grams)	1486.4	279.33	1439.27	129.07	1452.17	250.32	1447	124.09
Hemisphere	9L:2R		8L:3R		4L:2R		8L:2R:1n/k*	
Brain bank of origin								
Harvard	0		0		1		1	
NICHD	0		0		0		2	
TWOBC	11		11		5		9	
Total Number	11		11		6		11	

Demographics of ASD, chronic epilepsy, ASD co-morbid with epilepsy and TD subjects shown as means (SD) for age at death in years, the post-mortem interval in hours, storage time of tissue in formalin prior to sampling for processing in years and the fixed brain weight post-fixative in grams. A parametric one-way analysis of variance (ANOVA) shows no significant differences between groups for age ($F=0.520$, $df=3$, $p=0.672$), PMI ($F=2.7$, $df=3$, $p=0.063$), and brain weight ($F=0.102$, $df=3$, $p=0.962$). However, storage duration was significantly different between groups ($F=7.69$, $df=3$, $p<0.0001$) with the TD and chronic epilepsy samples having spent a significantly ($p<0.05$) longer time in formalin compared with the ASD and ASD+E groups. **n/k*: hemisphere not known for one case. M: male; F: female; L: left; R: right; NICHD: Eunice Kennedy Shriver National Institute of Child Health and Human Development.

Table 4.2 Causes of death

Diagnosis	Gender	Age	Cause of Death
TD	F	9	Asphyxia
TD	F	21	Acute cardiac failure
TD	F	26	n/k
TD	F	34	No structural cause identified
TD	F	49	Stroke
TD	F	82	n/k
TD	M	5	Drowning
TD	M	13	Structural heart anomalies in COD
TD	M	19	Peritonitis
TD	M	45	Pulmonary oedema
TD	M	73	n/k
Autism suspected	F	32	Breast carcinoma
Autism	F	44	Asphyxia
Autism	F	45	Non-Hodgkins lymphoma
Autism	F	49	Hyponatremia
Autism, ADHD and Tourette syndrome	M	14	Asphyxia
Autism	M	14	Suicide
Autism with mild ID	M	16	Glioblastoma
Autism suspected	M	18	Carbon monoxide poisoning
Autism	M	22	Pulmonary haemorrhage
Autism	M	25	Heart failure
Autism	M	52	Pulmonary embolism
Autism, mosaic duplication chromosome 3 and epilepsy	F	29	Acute right cerebral infarction
Autism and chronic epilepsy	M	9	Seizure
Autism and epilepsy	M	23	SUDEP*
Autism and epilepsy	M	24	Epilepsy due to SUDEP
Autism and epilepsy	M	33	Epilepsy
Autism and epilepsy	M	36	Vomit aspiration due to seizure
Autism, mosaic duplication chromosome 3 and epilepsy	F	29	Acute right cerebral infarction
Chronic epilepsy	F	16	Vomit aspiration due to seizure
Chronic epilepsy	F	38	Hypoxia secondary to seizure
Idiopathic epilepsy	F	52	Cardiac arrest
Idiopathic epilepsy	F	54	Epilepsy, ischaemic heart disease
Idiopathic epilepsy	M	7	Seizure associated with epilepsy
Chronic epilepsy with mental retardation	M	23	Epileptic seizure and pneumonia
Chronic epilepsy	M	25	Epileptic seizure
Chronic epilepsy	M	32	Status epilepticus
Idiopathic epilepsy	M	42	Grand-mal seizure
Chronic epilepsy with mental retardation	M	49	Respiratory obstruction; seizure
Chronic epilepsy	M	63	Ventricular arrhythmia
Chronic epilepsy	F	16	Vomit aspiration due to seizure

TD: typically developing; M: male; F: female; SUDEP: sudden unexplained death in epilepsy; n/k: not known. Age is given in years ascending order within diagnosis x gender groups

4.2.2 Confirmation of ASD diagnosis

Dr. T. Berney using clinical records confirmed diagnosis of ASD and, where possible, a diagnostic interview with the parents of the subject was conducted, which was based on the ADI-R. The parents also completed the SRS-2 and the SCQ. He also classified the subject's intellectual ability according to the ICD-10 categories for mental retardation. Below is a description of the screening instruments first.

4.2.2.1 Autism Diagnostic Interview Revised (ADI-R)

The ADI-R (Lord, Rutter et al. 1994) is a semi-structured, 93-item interview of an informant who is well acquainted with the subject, both as an adult and in early childhood. It is designed to take a developmental history and focuses on the presentation in early childhood as well as the current state. Its purpose is to establish a diagnosis of ASD, excluding items that are not immediately relevant, and it focuses on symptoms across the three main diagnostic domains for ICD-10: qualitative abnormalities in social interaction (e.g. emotional sharing, peer relationships, and a sharing of interests, etc.); communication (e.g. delayed or idiosyncratic speech, limited conversation, etc.); and restricted repetitive and stereotyped patterns of behaviour, interests and activities which include, for example, routines and unusual sensory interests. Each symptom is allocated a grade that can be used in a well-tested diagnostic algorithm. Designed as a research tool, it is internationally recognized and frequently referred to as the Gold Standard. The clinician scores the symptoms according to the informant's description using a 4-point scale in which 0=absent behaviour, 1=probably abnormal behaviour but not diagnostic, 2=definitely symptomatic of ASD, 3= severely symptomatic. To meet the ICD-10/DSM-IV

criteria, summed scores must meet or exceed specified thresholds in all three domains of communication.

4.2.2.2 Social Communication Questionnaire (SCQ)

The SCQ (Rutter, Bailey et al. 2003) is a 40-item questionnaire based on the ADI-R and, like that instrument, to be completed by an informant. The 2-point scale can be summed to give notional rating of severity for autism.

4.2.2.3 Social Responsiveness Scale 2nd edition (SRS-2)

The SRS-2 (Constantino and Gruber 2005, Constantino 2012) is a 65-item questionnaire asking about characteristic symptomatology over the previous 6 months. Each item is scored from 0 (`never true') to 3 (`almost always true') and the summed total ranges from 0 to 195. The SRS-2 assesses autistic behaviour in 5 treatment subscales: social awareness, social cognition, social communication, autistic mannerisms and social motivation. A total score is then calculated and generally the cut-off score of 75 in the total T-score is used to distinguish between children with ASD and TD (Constantino & Gruber (2005) p.38 (Constantino and Gruber 2005)). SRS scores are strongly correlated with ADI-R domain scores (r=0.65-0.77; (Constantino, Davis et al. 2003). SRS-2 is used to support the diagnosis of ASD but not as a main diagnostic tool and assesses behaviour in agreement with the RRB and SCI subscales of the DSM-V.

4.2.2.4 Intellectual disability (ID)

The degree of intellectual disability was assessed as defined by ICD-10 definitions (World Health Organization. and ebrary Inc. 1992), which categorizes people as

having no ID, mild ID, moderate ID, severe ID, and profound ID, based on the subject's overall functional ability.

4.2.3 Clinical profiles of selected cases

Clinical profiles of post-mortem cases are discussed below.

4.2.3.1 Clinical profiles of ASD cases

7 male and 4 female patients diagnosed with ASD with their symptoms meeting the ADI-R, SCQ and SRS-2 for autism. Three cases were diagnosed as ASD from the clinical notes but no severity scores were provided because the families were unavailable. 5 subjects were of normal ability, 2 had mild ID, 1 had severe ID and the level of ID was unknown in three cases.

Table 4.3 Behavioural test scores for ASD cases

Behavioural test	Summed Scores (SD)	Diagnostic threshold
ADI-R-social interaction	21 (6)	10
ADI-R-verbal communication	19 (5)	8
ADI-R-restricted repetitive behaviour	6 (3)	3
SRS-2 total raw score	128 (37)	75
SCQ	25 (7)	15

ASD cases with mean scores of the SRS-2, SCQ and ADI-R domains.

Table 4.4 Intellectual disability scores for ASD cases		
ASD identifier	**Level of ID**	**ICD-10**
07-09-	No ID*	--
151-08	Severe ID	n/k
167-08	Severe ID	F-72
99-1071	n/k	n/k
162-05	Mild ID	F-70
92-1014	n/k	n/k
56-10	No ID	--
72-11	Mild ID	F-70
90-09	No ID	--
27-11-	No ID	--
27-12-	Mild ID	--

*No ID = no Intellectual disability, n/k = not known

4.2.3.2 Clinical profiles of ASD +E cases

Of the subjects for whom the area under study was available, only six (5 male and 1 female) had epilepsy with their ASD. Of these, one subject did not have detailed assessment but a diagnosis made from clinical records.

Table 4.5 Behavioural test scores for ASD+E cases		
Behavioural test	**Summed scores (SD)**	**Diagnostic threshold**
ADI-R social interaction	24 (2)	10
ADI-R-verbal communication	15 (5)	8
ADI-R-restricted repetitive behaviour	7 (2)	3
SRS-2 total raw score	121 (21)	75
SCQ	24 (5)	15

ASD+E cases with mean scores of the SRS-2, SCQ and ADI-R domains.

Seizure type, age of onset and medication history are summarized below.

Table 4.6 Intellectual disability scores of ASD + E cases

ASD + E identifier	Level of ID	ICD-10
B4925	Severe ID	F-72
98-1174	Severe ID	F-72
36-12	Severe ID	F-72
121-11	Moderate ID	F-71
26-11	Mild ID	F70
55-13	n/k	n/k

n/k = not known

Table 4.7 Seizure histories of ASD+E cases

ASD+E identifier	Age of onset (yrs)	Seizure type
B4925	3	Generalized tonic clonic
98-1174	3	Generalized tonic clonic, absence
36-12	18	Myoclonic, generalized tonic clonic
121-11	24	Generalized tonic clonic
26-11-	15	Generalized tonic clonic, complex partial absences
55-13	n/k	n/k

In terms of medication history, individuals with ASD+E were on classic anti-epileptic drugs (lamotrigine, phenytoin, sodium valproate, carbamazepine, levetiracetam), and psychotropics (risperdal, ritalin, sertraline, clonidine). AEDs and psychotropics were often administered together from age of onset.

4.2.3.3 Clinical profiles of epilepsy cases

Epilepsy cases chosen for this study were older than the ASD cases and full clinical profiles were not available for most. However, they did not have a psychiatric

diagnosis and only three subjects had a significant ID (one had mild ID, two had severe ID). They were on anti-epileptic drugs until they died. One case had gone into status epilepticus before death.

4.2.3.4 Cases without ASD or E

TD cases identified in this study had no history of epilepsy, ASD or any psychiatric diagnosis based on the information available in their clinical notes and post-mortem histology reports. Exclusion criteria also included any underlying pathology such as brain cancer and severe damage to the fronto-temporal areas.

4.2.4 Anatomy and choice of area for neurohistological sampling

Using the previously described delineations, 10 μm sections were cut using a microtome at room temperature (RT) with a spacing of 200 μm and stained with cresyl violet (0.1%) (see Appendix A). Every 10^{th} section (from a total of 120) was stained. To observe the characteristic s-shape, the PiC was sampled from the anterior side of the coronal slice containing the anterior hippocampus. Cytoarchitectonic boundaries were determined as follows: dorsal and medial limits of the PiC were identified by a cell-free layer below the claustral complexes. The ventral limit was identified where layer III fuses with the periamygdaloid area. Layer III was contained within those limits. Layer II was identified as a very dense layer in the shape of a –w- or an –s. Layer I was identified as the cell-sparse region between layer II and the pial surface. All histological photos were taken using the Aperio slide scanner from Leica biosystems.

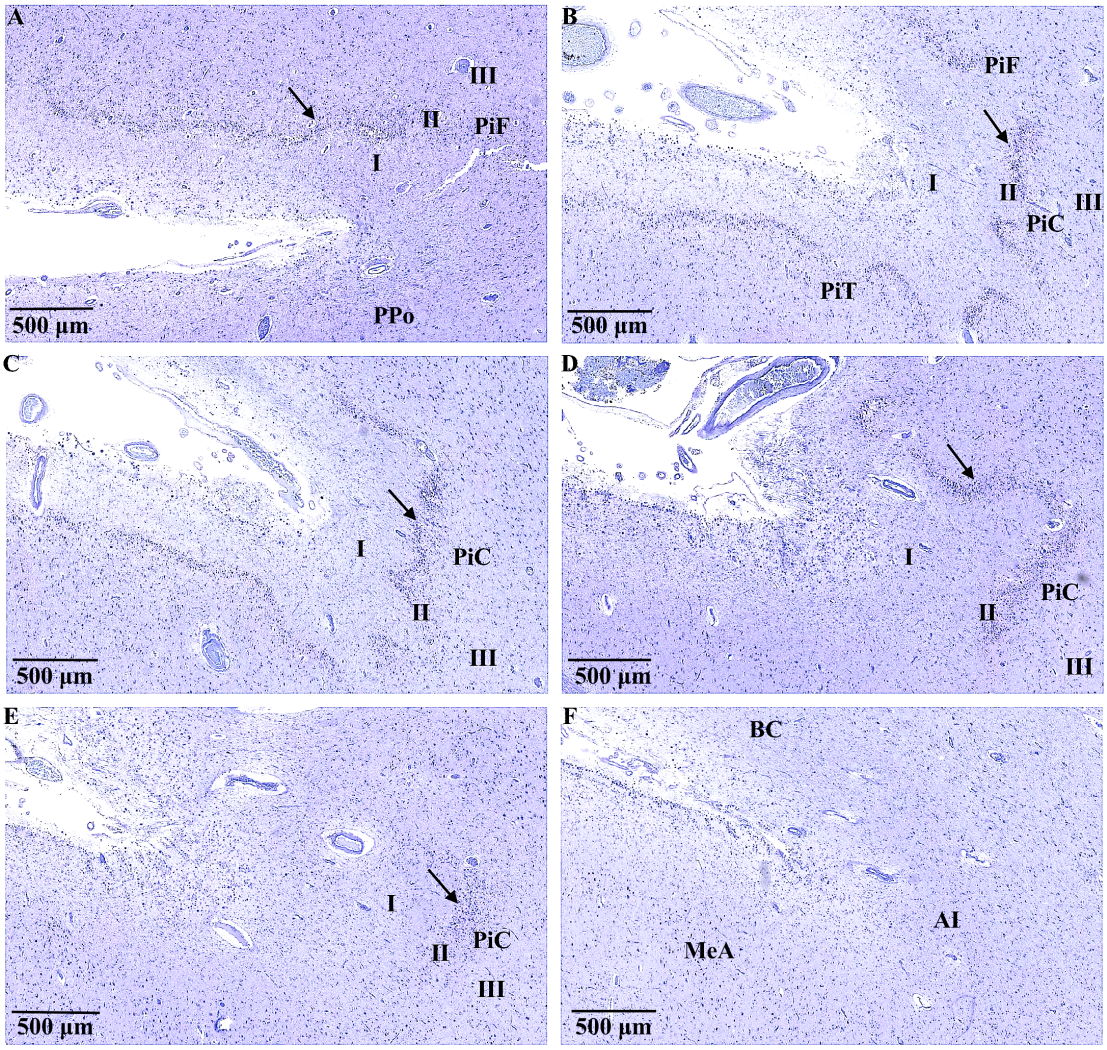


Figure 4.1 Antero-posterior mapping of the PiC in Nissl-stained coronal sections

This shows antero-posterior mapping of the piriform cortex with (A) being the most anterior coronal slice and (F) being the most posterior. The arrows point to the dense second layer of the PiC. In (A), the frontal PiC (*PiF*) is visible bound ventrally by the planum polare (*PPo*). In (B) and (C), the characteristic W-shape of the PiC is visible with its frontal part and its temporal part (*PiT*). In (D) and (E), the structure starts disappearing and the *PiT* portion of it remains visible until it disappears completely in (F). *AI*: amygdaloid island; *BC*: basal nucleus, compact part; *MeA*: medial amygdaloid nucleus. I, II and III represent the layers of the PiC. Top of each figure is dorsal and left is medial.

4.2.5 Neurohistological sampling

The neurohistological sampling of the PiC for the majority of cases (n=36) was conducted in the UK Oxford brain bank (see table 4.1). Additional cases were provided via the ATP from the Harvard Brain Bank (n=2) and the NICHD brain bank (n=2). 5 mm-thick coronal slices were made at the start of the fronto-temporal junction through the entire length of the temporal lobe and 2 cm x 2 cm x 2 cm blocks of the PiC were sampled from the anterior aspect of the coronal slice containing the anterior hippocampus (see figure 4.2). All blocks were photographed and marked on their anterior side to allow cutting from along the antero-posterior axis.

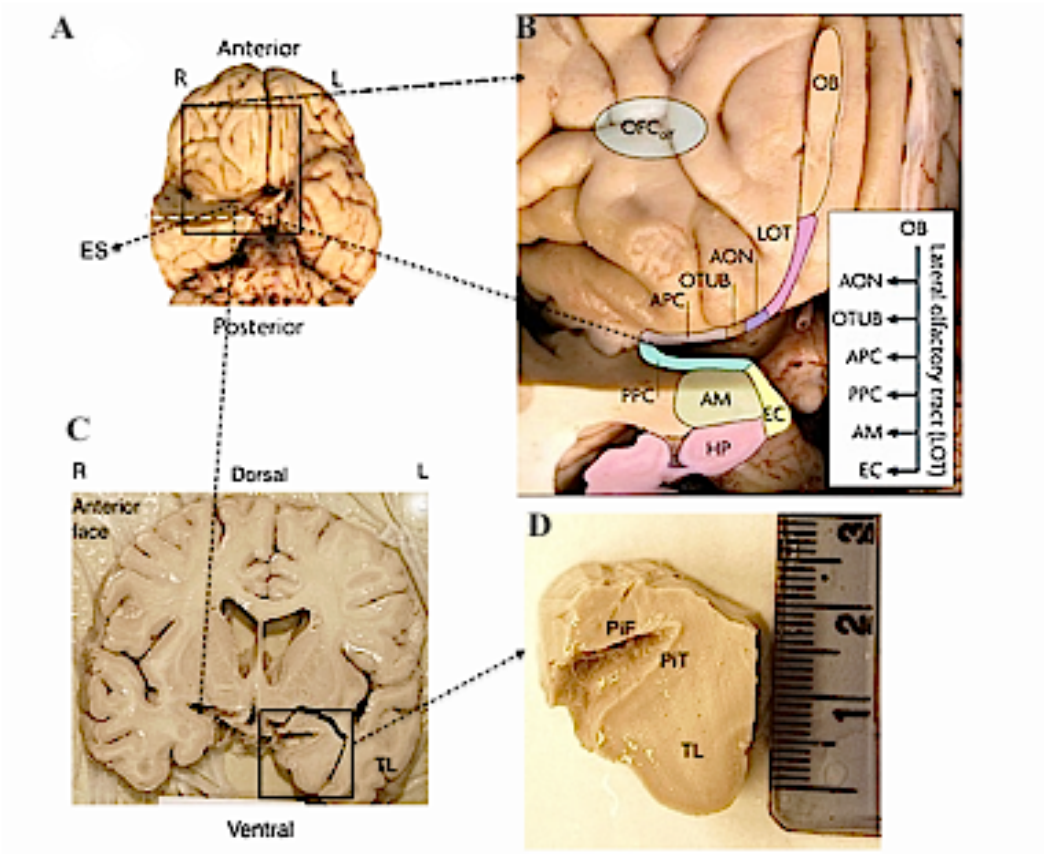


Figure 4.2 Coronal neurohistological sampling of the PiC. This figure represents the sampling procedure of the PiC. (A) & (B) in the top panel have been modified

from and with permission from (Gottfried 2010): (A) shows the location of the entorhinal sulcus (ES) at the fronto-temporal junction of a ventral view of the human brain; (B) shows the location of the *aPiC* (*APC* here) and *pPiC* (*PPC* here) along the lateral olfactory tract (*LOT*) as well as other structures adjacent to it. *AM*: amygdala*; AON*: Anterior olfactory nucleus; *EC*: entorhinal cortex; *HP*: anterior hippocampus; *OB*: olfactory bulb; *OFC*: orbitofrontal cortex; *OTUB*: olfactory tubercle. Bottom panel shows neurohistological sampling of the PiC in the selected cases for the study: (C) shows coronal sampling of the left PiC from the anterior face of the coronal slice containing the anterior hippocampus; (D) shows the sampled left PiC block with the approximate location of the frontal piriform (*PiF*) and the temporal part *(PiT)*. *TL* represents the temporal lobe. The orientation of the tissue in (D) is the same as in (C).

4.2.6 Embedding

Paraffin is known to preserve cell morphology in post-mortem tissue, limit the guard zone problem and restrict collapse in the z-axis as cited by many stereologists (Ward, Rosen et al. 2008, von Bartheld 2012). Therefore, it was the material of choice in this study. 2 cm x 2 cm x 2 cm blocks were paraffin-embedded. They were either processed automatically by the apparatus or hand-processed. Decision on the type of processing depended on whether brain tissue had been exposed to fomblin oil, which is used when the brain is MRI scanned and which can cause the processing apparatus to break.

4.2.7 Histological sections and Nissl-staining

Five 25-µm thick sections per case were cut at room temperature using a microtome. The spacing distance between sections was set at 200 µm from anterior to posterior.

This distance was decided as optimal based on both boundaries of the structure seen by anatomical mapping of the area in conjunction with how much tissue was available. Sections were then stained for the Nissl-substance using cresyl-violet (0.1%) and exposed to the reagent for a maximum for 3 minutes (see Appendix A for protocol). All sections were coded and identifiers were hidden from the experimenter and only revealed upon completion of the study to group the data. The author of this work and the laboratory technician performed the histological sectioning and the staining.

4.2.8 Cell density studies

Cells were counted in layers II and III of the PiC based on their morphology and their corresponding densities were calculated according to equation 1.

$$N_T = \sum_{i=1}^{k} N_i = \sum_{i=1}^{k} \frac{n}{A_{z_i}} \tag{1}$$

where

N_T signifies the total density per cell type per layer and is the sum of point densities N_i per case in 5 sections.

N_i is calculated by summing the total number of cells -*n*- per cell type at a specific location of the section divided by the area of the counting box -*A*- multiplied by the measured thickness at the point location in the section.

Glial, pyramidal and non-pyramidal cells were recognized based on their morphology. Nuclear DNA and ribosomal RNA are the main anionic structures in cells. Cresyl-violet is a cationic dye that binds these entities according to their prevalence in

mammalian cells thereby revealing detailed morphology of the cell body and cytoplasm (Esiri and Oppenheimer 1996). The morphological characteristics for counting the cells are briefly described below. Anatomical boundaries in the Nissl-stained PiC are described in figure 4.4.

Pyramidal cells

Pyramidal cells are rich in nuclear DNA and ribosomal RNA. The nucleolus is hence usually prominent and very darkly stained. The nuclear membrane is well defined and homogeneously stained, though staining is lighter than that of the nucleolus. Cells have generally a strong apical smooth dendrite that is well outlined. Pyramidal cells can be encountered in both layers II and III of the PiC. The orientation of the apical dendrite in layer II is towards layer I and in layer III, it is towards layer II. The spines are sometimes visible. The cell body is pyramidal and clearly visible, but with much lighter staining. The cells are usually large in size (15-20 μm in diameter). Sometimes and as a function of the level of hypoxia in the tissue, shape is preserved though nuclei might be shrunken and the cell size would be much smaller. In layer II and III, pyramidal cells can be superficial or deep (Esiri and Oppenheimer 1996).

Non-pyramidal cells

Non-pyramidal cells contain nuclear DNA but little cytoplasmic ribosomal RNA compared with pyramidal cells. Therefore, the staining will be slightly lighter for the nucleus and the cell body may not be visible. The cell body is non-pyramidal in shape. They can be aspiny. Non-pyramidal cells encountered in layer II can be large and multipolar, they can be bitufted, gliaform or semi-lunar (Esiri and Oppenheimer 1996).

Glial cells

Glial cells often have an invisible cytoplasm except for a faint halo sometimes or a haze. They may have one visible nucleus but can also be binucleated in the case of reactive astrocytosis (Garman 2011). The cell outline is sometimes indistinct. They rarely contain an easily visible nucleolus and are much smaller in size than neuronal cells (2-5 µm in diameter). Glial cells are spread across layers I, II and III of the PiC (Esiri and Oppenheimer 1996).

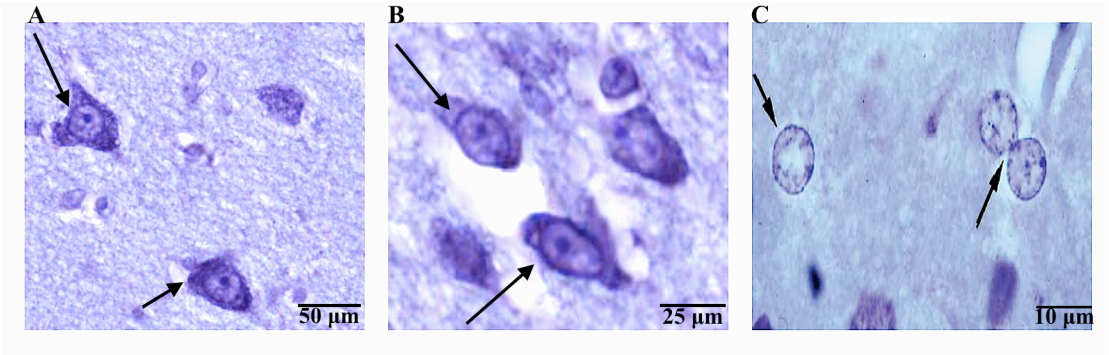


Figure 4.3 Morphological identification of cell types

Based on the pattern of cresyl-violet staining of the Nissl-granules, one can identify different neuronal cell types morphologically such as (A) pyramidal cells and (B) non-pyramidal cells but also (C) astroglial cells. In (C), figure was modified from (Garman 2011).

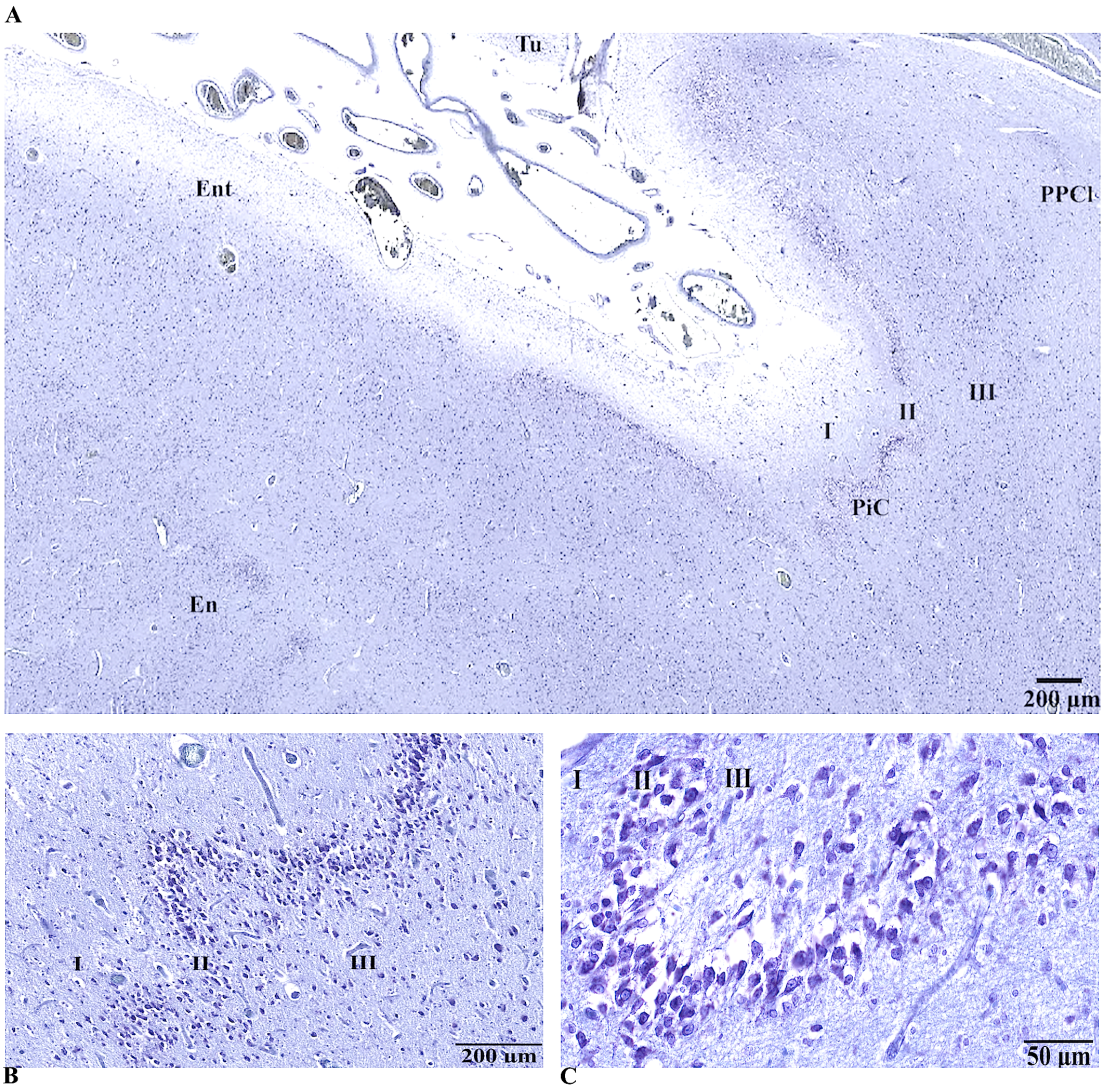


Figure 4.4 Cytoarchitecture of the PiC and anatomical boundaries

This figure shows Nissl-staining of the PiC in (A) with the characteristic trilamination (I, II and III). High-magnification photos in (B) and (C) show the dense second layer formed mostly of pyramidal and non-pyramidal cells. Top of every figure is dorsal and left is medial. *En*: endopiriform nucleus; *Ent:* entorhinal cortex; *PiC*: piriform cortex, *PPCl:* prepiriform claustrum, *Tu*: olfactory tubercle.

4.2.8.1 Systematic random sampling using Axiovision

All counts were performed using the stereology module of image analyses system Axiovision (version 4.8.1, 2010, Zeiss company, Bicester, England). The optical

fractionator allows the estimation of object number from a region of interest (ROI) and was used in this study to calculate cell numbers. Briefly, the stereology module of Axiovision allows us to first identify the ROI at 2X magnification, select it according to precise anatomical landmarks, and count cells within a pre-defined counting box known as a probe. At every probe destination, a point thickness is measured. The stage is programmed manually to move in the x and y directions from one probe to the next in a systematic random manner until all probes have been covered and all thicknesses have been recorded. The distances in the x and y directions are kept constant for all measurements within the same layer. The z-depth is also pre-set across all experiments and cells are counted within this depth. The top and bottom of the sections are set at every probe. Finally, cell numbers are extracted, grouped according to cell type and densities are calculated as specified in equation (1). In the section below, the parameters of the experiment are discussed.

The counting box

For cells in layer II of the PiC, the counting grid was calibrated at 95 μm x 95 μm. For layer III, the counting grid was calibrated at 120 μm x 95 μm. The counts were done on a microscope with a high numerical aperture (NA = 1.4). Layer II is a thin and dense layer and the distance between the probes was set to 150 μm in the x-direction and 120 μm in the y-direction beginning from a random position. Layer III is a sparse layer and the probe distance was set to 400 μm in both the x and y directions beginning from a random start position. The total number of counting boxes over 5 sections that would be representative of the cell densities of all three cell populations in layer II was 35 counting boxes and for layer III, it was 40 counting boxes. The justification for this is in the pilot studies below.

Counting rules

Cells were counted at 60X magnification. The red lines below are exclusion lines so cells falling within these lines are not counted and the green lines below are inclusion lines and the cells falling within them are counted.

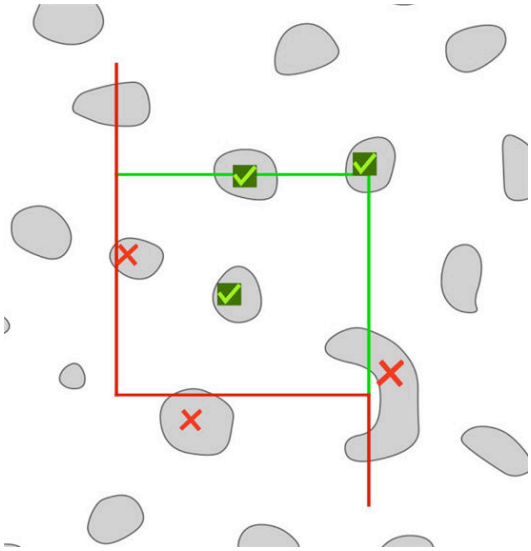


Figure 4.5 The counting box. The figure above shows cell-counting rules per counting box. Grey shapes represent cells. Figure is courtesy of MBF bioscience (bioscience 2013).

Choice of z-depth

Paraffin-embedded tissue shrinks as a result of processing. The distribution of particles in the z-axis in sections is hence affected. However, many authors have demonstrated that in paraffin sections, the final section thickness varies little compared to the nominal section thickness (von Bartheld 2002, Ward, Rosen et al. 2008, von Bartheld 2012). Furthermore, the z-axis collapse is not as dramatic as it is in cryosections for example. For this study, the z-depth was set to 20 µm based on an estimated theoretical collapse of 20% of the nominal thickness of 25 µm. Guard zones

were set at the top and the bottom of the sections (mean guard zone dimension across all sections: 6.5 μm (8.89)). The mean real thickness of the sections was assessed in all cases (200 sections x 2 layers) and was equal to 16.31 ± 3.07 (μm).

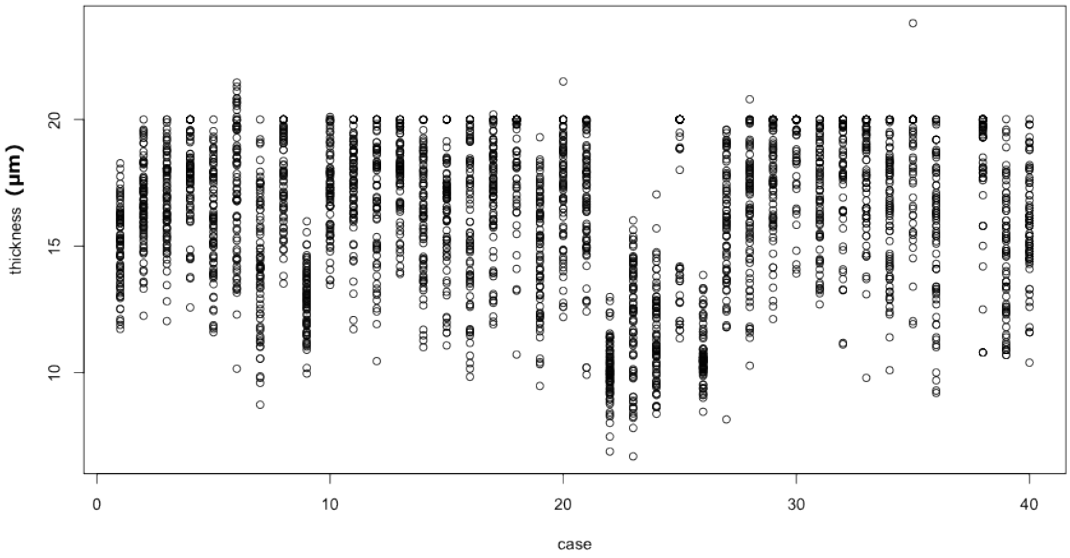


Figure 4.6 Scatterplot of point thicknesses. These thicknesses were measured per counting box per case and variability within each case and across all 39 cases is demonstrated above.

Therefore, for comparison with reports from the literature that limited z-depth to 12 μm, I compared cell densities from a subset of cases (n = 5) using a restricted z-depth of 12 μm. As predicted, the lower z-height did not affect density measurements in both layers II and III and all measurements varied on average by less than 10% from the primary measurements acquired using a mean 20 μm z-depth (see Appendix F).

Anatomical delineation

Cytoarchitectonic boundaries were determined as follows: dorsal and medial limits of the PiC were identified by a cell-free layer below the claustral complexes. The

ventral limit was identified where layer III fuses with the periamygdaloid area. Layer III was contained within those limits. Layer II was identified as a very dense layer in the shape of a –w- or an –s. Layer I was identified as the cell-sparse region between layer II and the pial surface.

Choice of number of counting boxes

As a pilot study, it was important to establish the minimum number of counting boxes required so that the calculated cell densities are representatives of the real density in layers II and III. For this purpose, 5 cases to which the experimenter was blind were chosen to carry out this pilot study. In layer II, 5, 10, 15, 25 and 35 counting boxes were used to count all cell types in the ROI. In layer III, 15, 30, 45, 60 and 75 counting boxes were used to count all cell types in the ROI. The z-height was 20 μm and the area of the counting box for layer II was 95 μm x 95 μm and layer III, 120 μm x 95 μm as previously defined. For layer II, counting a minimum of 35 counting boxes per case per cell population would represent the true density. For layer III, counting a minimum of 40 counting boxes per case per cell population would represent the true density.

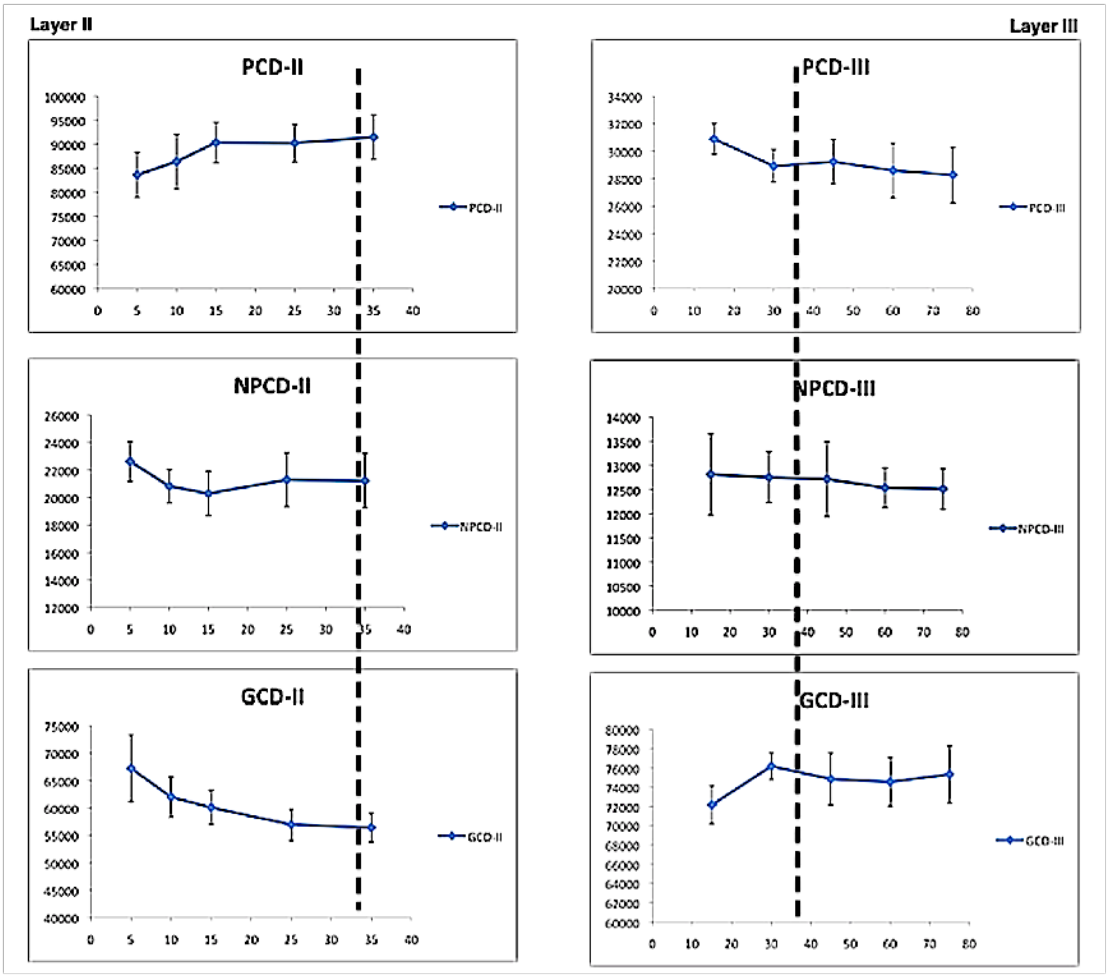


Figure 4.7 Number of counting boxes for a representative density. This figure shows the mean density on the y-axis (cells/cubic mm) as a function of the number of counting boxes (the x-axis) used for n = 5 cases. Cell densities for layer II plateau at 25 counting boxes for all cell types. For layer III, densities plateau at 30 counting boxes. The black line represents an approximate cut-off point for the minimum number of counting boxes used in this study to calculate a representative value of true density per case and layer (layer II: 35; layer III: 40).

Sampling strategy

Sampling was carried out in a systematic random manner. For layer II, glial, pyramidal and non-pyramidal cells were counted in 35 randomly placed counting

frames over 5 sections per case (7 counting frames per section). In line with stereological guidelines, this resulted in at least 100 cells of each type being counted per case. For layer III, 40 counting frames were randomly placed in the selected ROI and cells were counted by cell-type in 8 frames/section. Unidentifiable cells were less than 5% of the total of counted cells. Finally, glial, pyramidal, non-pyramidal and total neuronal densities were calculated. The time required to extract cell numbers and calculate all cell densities in one case in both layers was about 5 hrs on average.

4.2.8.2 Reliability and accuracy.

Reliability of the protocol was assessed by measuring intra- and inter-rater reliabilities. The correlation coefficient (ICC) was calculated in SPSS. The Gundersen-Jensen estimator was used to calculate the coefficient of error (CE) on a case-by-case basis (5 sections per case) and then averaged to yield a group CE per cell population number per layer (Gundersen and Jensen 1987).

Intra-rater variability The intra-class correlation coefficient (ICC_1) was used to measure absolute agreement between measurements in 8 cases in both layers. The ICC_1 represents the ratio of the variance between subjects to the sum of error and subject variances. The closer the ICC_1 tends to 1, the higher the reliability (Burton, Conway et al. 2000). Intra-rater reliability measurements are reported in the results section. Equation of the ICC_1 is reported below.

$$ICC = \frac{\sigma_s^2}{\sigma_s^2 + \sigma_r^2 + \sigma_e^2} \quad (2)$$

where

σ_s^2 is subject variability.

σ_r^2 is variability in repetition.

σ_e^2 is measurement error.

Inter-rater variability

This was measured using the ICC_2 for absolute agreement of measurements between raters. Average measures of the ICC_2 are reported in 5 cases in both layers in the results section. Professor M. Esiri acted as rater number 2 and performed all these measurements. Equation of the ICC is reported below.

$$ICC = \frac{\sigma_s^2}{\sigma_s^2 + \sigma_e^2} \quad (3)$$

Accuracy

The CE for individual estimates of cell density and cell number as described by Gundersen and Jensen and West and Gundersen was calculated for each case (Gundersen and Jensen 1987, West 2012, West 2013). The CE is an index of the covariability of measures made from a particular layer across the slices and thus is a measure of accuracy (West 2013). Mean values were calculated for each measurement for each subject group (ASD, TD, ASD + E and E). Relative variance percentage of each measure accounted for by true inter-individual variance was

estimated. In addition, the group coefficient of error (SEM/mean) was calculated. The group coefficient of error gives an estimate of the accuracy of the estimate of the mean calculated for each subject group. The lower the value of the CE, the more accurate the measure of the mean (Walker, Highley et al. 2002).

CE on cell counts

The estimator examines how well a sequence of counts approximates the smooth outline of the true distribution of cells and how closely the estimate might be representative of the true value (Gundersen and Jensen 1987, West 2012).

$$CE(\sum_{i=1}^{5} Q_i^-) = \sqrt{\frac{[3(A - S^2) - 4B + C]}{\alpha \sum_{i=1}^{5} Q_i^-}} \quad (4)$$

where:

A is the sum of the squares of counts obtained from all individual sections of the sample:

$$A = \sum_{i=1}^{5} (Q_i^- x Q_i^-) \quad (5)$$

B is the sum of the products of the count in section i with the count in the subsequent section $i+1$ for all the sections in the sample:

$$B = \sum_{i=1}^{4} (Q_i^- x Q_{i+1}^-) \quad (6)$$

C is the sum of products of the count in section i with the count in section $i+2$ for all the sections in the sample:

$$C = \sum_{i=1}^{3} (Q_i^- x Q_{i+2}^-) \quad (7)$$

S^2 is the variance introduced by local errors for point counting and in this case is calculated by the following:

$$S^2 = \sum_{i=1}^{5} Q_i^- \tag{8}$$

α is a smoothness factor that describes the distribution of the areas of the sections along the sectioning axis (West 2012). This factor is sensitive to sharp changes in the counts and tends to have a value of 240 for smooth data and 12 for irregular data. Based on the count profiles of the sections, the data is assumed to be smooth and the smoothness factor used here is 240 (Gundersen and Jensen 1987, West 2012).

The variability of the sampling method is measured by accounting for intra-sectional and inter-sectional variability.

$$VAR_{total} = Var_{(SRS)} + S^2$$
$$where \tag{9}$$
$$Var_{(SRS)} = \frac{3(A - S^2) - 4B + C}{a}$$

To calculate the CE based on Gundersen's formula, cell counts are assumed to follow a Poisson distribution. The basic characteristic of a Poisson distribution in counting data is that the sum of counts is equal to variance S^2. In that respect, counts per cell population per layer and per group were tested for a Poisson trend using a Chi-squared goodness of fit test whereby the null-hypothesis was rejected for $p<0.05$ (see Appendix D).

To illustrate the calculation of the CE of one case using the above, an example is included below.

Example of glial cell counts on layer II of case 1 (B4925) in the ASD + E epilepsy group to calculate the CE based on Gundersen & Jensen's equation.

Table 4.8 Example of calculation of Gundersen and Jensen variables

Section number	Gundersen and Jensen variables			
	Q_i^-	*A*	*B*	*C*
1	82	6724	6560	6084
2	80	6400	4960	5520
3	62	3844	4278	4092
4	69	4761	4554	0
5	66	4356	0	0
Σ over all sections	359	26085	20352	15696

Example of glial cell counts on layer II of case 1 (B4925) in the ASD + E epilepsy group to calculate the CE based on Gundersen & Jensen's equation (see below for continuation).

$$Var_{(SRS)} = \frac{3(26805 - 359) - 4(20352) + 15696}{240} = 47.775$$

$$Var_{total} = 47.775 + 359 = 406.775$$

$$CE(\sum_{i=1}^{5} Q_i^-) = \frac{\sqrt{406.775}}{359} = 0.056$$

CE on cell densities

To assess the precision of density estimates, the coefficient of error for these measurements was calculated on a case-by-case basis as follows. The standard deviation accounted for the dispersion between mean sectional densities per case as opposed to the sum of count data. The grand mean μ was calculated from 5 section means and included in the formula below to calculate an individual CE. A group CE (GCE) was calculated as the SEM of the all cell densities per group, layer and cell-

type divided by the mean density for the whole group. This gives an estimate of the accuracy of the mean for each subject group. The lower the GCE, the more precise the mean and typically GCE values < 0.10.

$$CE(\sum_{i=1}^{5} Q_i^-) = \frac{SD}{\mu_{sample} x \sqrt{n}} \quad (10)$$

where

SD represents the standard deviation between the sum of counts of 5 sections

μ_{sample} represents the mean of counts obtained from 5 sections

n represents the total number of sections (5 in this case)

4.2.8.3 Assessment of strength of stereological quantifications

Section thickness, heterogeneity of cell distribution and the shape of the quantified region were all accounted for in this protocol as follows.

Section thickness

The minimum recommended section thickness for stereological quantifications is 20 μm and post-processing tissue that is between 12-30 μm thick is considered suitable (von Bartheld 2002, Ward, Rosen et al. 2008, von Bartheld 2012). In this study, the initial starting thickness was 25 μm, which is superior to the minimum recommended thickness. Additionally, the real section thickness post-processing was assessed in all cases and was consistent with the above guidelines (average thickness of all sections in all cases = 16.31 ± 3.07 (μm).

Heterogeneity of cell distributions in the piriform

Stereological theory assumes that objects are arranged randomly. In practice, whilst glia are spatially arranged randomly, neurons are not (Benes and Lange 2001). The

heterogeneity of cell distributions was accounted for in this protocol. To the author's knowledge, paleocortex cell distributions have not been examined at the same level of detail as the neocortical matrix. Layer II was dense in neurons but very thin whilst layer III was thick and less dense. The choice of the number of counting boxes per layer and the distance between the probes in the x and y directions took into account the spatial arrangement of cells in the PiC. For layer II, probes were placed closer to each other in the x and y directions than they were for layer III. In all cases, systematic random sampling was followed. Pilot studies showed that using 35 probes for layer II and 40 probes for layer III in the specified x and y directions provided a good estimate of the numerical density.

Shape and sphericity of the ROI

A normogram from (Gundersen and Jensen 1987) was used to approximate the shape of the PiC. Although this normogram is usually used for volume estimations, it is an appropriate tool to estimate the sampling density required for cell counting. In line with stereological guidelines and the normogram, at least 100 cells of each cell type were counted per case in at least 35 randomly distributed counting frames in each layer to achieve a coefficient of error of less than 0.1 in serial sections based on the shape of the PiC (see figure 4.8).

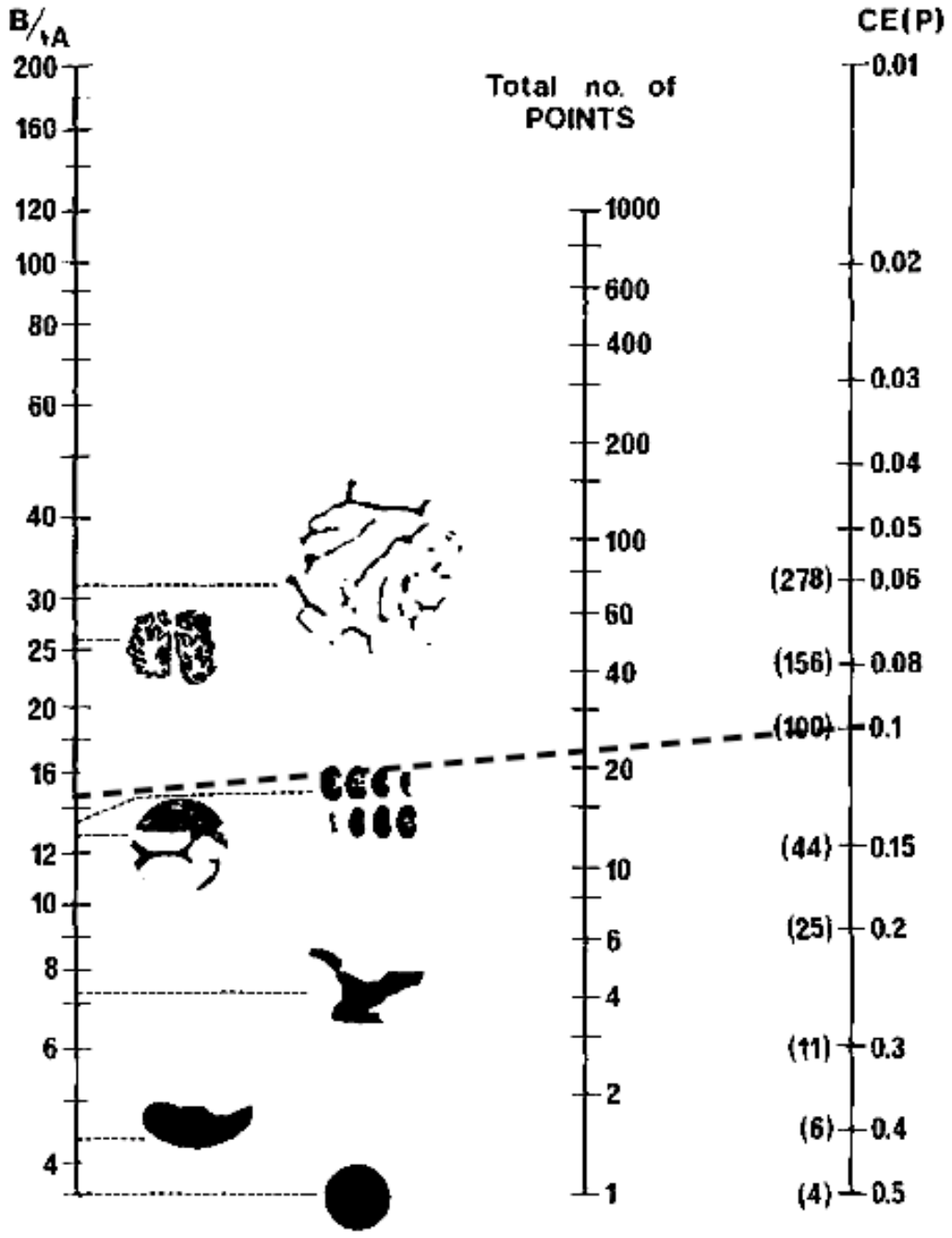


Figure 4.8 Normogram of predicted CE based on the shape of the area of interest. The overall shape of the PiC expressed as B/A with B being the total boundary length and A being the total area is between 12 and 16. The lattice would be randomly positioned and orientated. The dotted line connecting CE and B/A in this case demonstrates that at least 20 points (P)/frames need be counted (middle axis) to result in a CE<0.1 based on PiC shape (Gundersen and Jensen 1987).

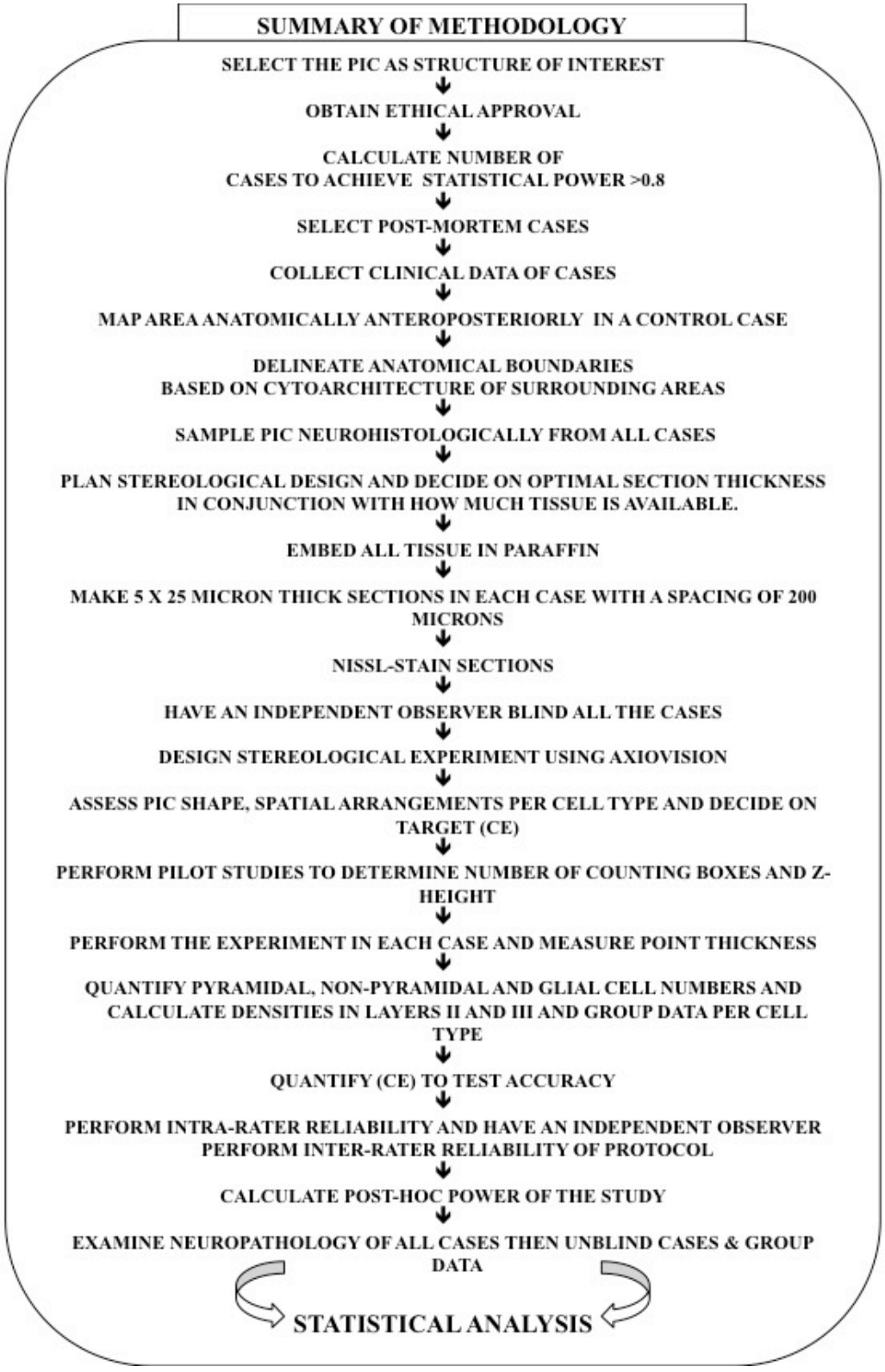


Figure 4.9 Summary of methodology. This diagram summarizes the workflow from selecting the PiC as an area of interest to sampling and quantifying cell densities before all data are grouped prior to applying the general linear model.

4.2.9 Statistical analyses

An overview of statistical methods is included in figure 4.11. A 2 x 3 x 4 repeated measures ANOVA (rmANOVA) was used to analyze density measurements. This test is routinely used in stereological studies (Highley, Walker et al. 2002, Walker, Highley et al. 2002) and is appropriate when different measures of the dependent variable are extracted from the same case (Field, Field et al. 2012). The 2 x 3 x 4 model included layer (2 levels) and cell-type (3 levels: non-pyramidal cells, pyramidal cells, glia) as within-subject factors and diagnosis (4 levels) as a between-subject factor. In order to preserve degrees of freedom when performing comparisons, the total number of comparisons was limited guided by assessment of demographic variables. Additional demographic variables were assessed for differences between groups. Brain weight and age did not differ between groups; however, storage duration of tissue in formalin was significantly different between groups ($F=7.69$, $df=3$, $p<0.0001$) (due to shorter duration in the ASD cases) and was therefore included in an analysis of covariance (repeated measures ANCOVA). The ANCOVA included layer and cell-type as within subject factors and diagnosis between subjects with fixation time as a covariate.

The assumptions to apply rmANOVA have been met as specified below:

1.The dependent variable –density- is continuous.

2.Normality Density measurements must follow a Gaussian distribution to satisfy the assumption of normality to apply the general linear model. This was assessed at group level by layer and cell-type and across groups by layer and cell-type. Histogram of frequencies, quantile-quantile (q-q)[4,1] plots and the detrended[4,2] qq-plots (see figure

[4,1] The q-q plot is a graphical representation of data quantiles from our measurements against a theoretical normal distribution. If data are normally distributed, one would typically see the data points aligned perfectly along the line y = x.

4.10) (Field, Field et al. 2012)were traced and analyzed to assess normality at group level and across groups. The Shapiro-Wilk statistic tested whether data points were significantly different from a normal distribution for all groupings. All measurements at group level and across groups followed Gaussian distributions with $p > 0.05$ according to the Shapiro-Wilk statistic (see Appendix B).

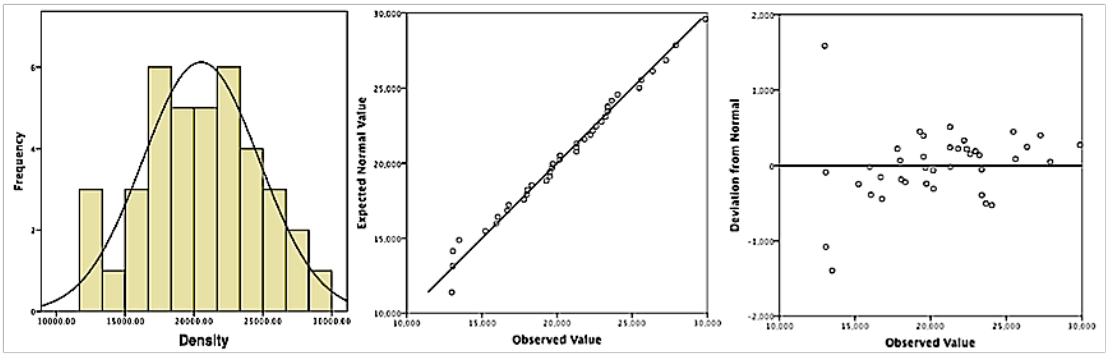


Figure 4.10 Normality validations. This represents the distribution of non-pyramidal cell densities across groups for layer II. Left graph represents the histogram of frequencies as a function of non-pyramidal cell density (μ= 20503.66 cells/cubic mm; SD = 4236.26, N =39). The bell-shape curve is superimposed onto the histogram for reference and the distribution is normal. Middle graph shows the normal q-q plot of the non-pyramidal cell population across groups in layer II and measurements are aligned along the equation y = x. Right graph shows the detrended q-q plot where non-pyramidal cell densities cluster horizontally around zero with no pattern and 3 values that seem out of range. The Shapiro-Wilk p-value here is 0.76.

3.Homoscedasticity is the second assumption to use the GLM. The Brown-Forsythe test for homogeneity of variances was used here. The Brown-Forsythe assesses the

[4,2] The detrended q-q plot shows the differences between our measured and expected values of a normal distribution. Data points should cluster in a horizontal band around zero with no pattern if distribution is normal.

equality of variance by measuring absolute deviations from group medians and was suggested to have higher statistical power than the Levene test though the Levene and Box's M test applied to this data were in agreement with the Brown-Forsythe. Data were grouped as in *normality* section and passed the Brown-Forsythe test with $p>0.05$ suggesting homogeneity of variance across all comparisons (see Appendix C). Where appropriate, summarized results of Box's and Levene's are included in the results section for reference.

4.Sphericity is the final assumption to apply rmANOVA. This is an additional step to verify equality of variances in a repeated-measures design. In this study, this assumption was violated when Mauchly's test for sphericity was applied to our data suggesting inequality of variances. This was corrected for by using the Greenhouse-Geisser ($\varepsilon<0.75$) and Huyn-Feldt ($\varepsilon>0.75$) corrections as appropriate and summaries of the Mauchly statistic were included in the results section for reference.

Post-hoc analyses using simple one-way ANOVA to test differences between means across groups followed by the appropriate Bonferroni corrections were applied subsequently in SPSS.

Correlation analyses

Pearson bivariate correlation analyses were performed to examine relationships between age and cell density, brain weight and cell density, within layer and between layer cell-type correlations. To avoid multiple testing, data were combined into rmANOVAs wherever possible. When appropriate, a conservative Bonferroni correction was applied to correct for multiple comparisons.

Bivariate Pearson's correlation analyses were performed to correlate measured neuronal and glial densities of both layers II and III of the PiC with severity. This was

to test the relationship between the density per cell type and layer and the severity of the disorder in autism. Spearman's rank-order correlations to test associations between two variables when one of them had a narrow range of numbers: this is characteristic of semi-quantitative approaches where mild, moderate and severe for example are associated with numbers 1, 2, and 3. Some of the cases did not have severity scores and as a result, the total case numbers decreased. Correlations here were not corrected for multiple comparisons.

Power analyses

Power of the study was estimated by calculating the probability of not obtaining a type II error (Field, Field et al. 2012). Simplistically, power of a study is equal to 1-β where β is the probability of making a type II error. The post-hoc power of this study was calculated by using G*power analysis software (version 3.1).

Supplementary statistics: linear regression

As an additional investigation of the effects of diagnosis, gender, hemisphere, brain weight, post-mortem interval, age, layer and cell-type on the obtained densities, a multiple 2-way linear regression model was also designed though this did not contribute to the main analyses in the end. The outcome or dependent variable was the density; diagnosis, hemisphere, age, gender, brain weight, post-mortem interval, cell-type and layer were the predictors or independent variables. The goodness of fit of the model was assessed by calculating the coefficient of determination ($\boldsymbol{R^2}$) and investigating the residuals versus fitted graph that should be centered around 0 and with no specific trend. The equation for the multiple regression was as follows:

$$y = \beta_0 + \beta_1 x_1 + \ldots + \beta_n x_n + \varepsilon$$

Density ~ (cell type + layer + diagnosis + brain-weight + gender + hemisphere + post-mortem interval + age)^2

After much verification, the linear model did not predict accurately the actual density measurements (see appendix I). Therefore, rmANOVA analyses were performed instead. Linear regression models in R-software were designed with the expert advice and help of Ms. Lai San Hong, MRC statistician at the University of Oxford clinical trials unit.

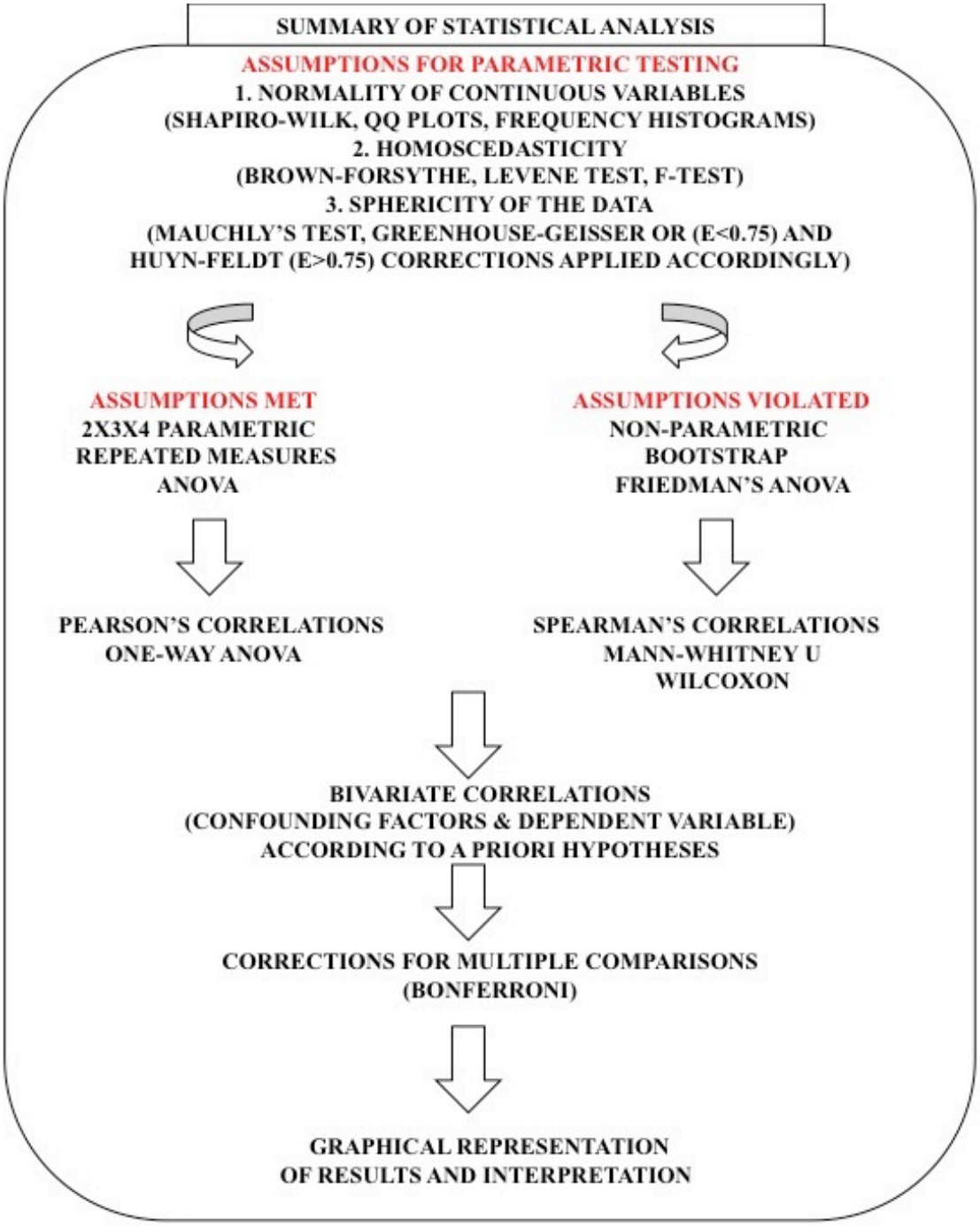


Figure 4.11 Summary of statistical analysis. This figure summarises the workflow for applying the general linear model (repeated measures ANOVA in this case) on stereological data. Interactions are followed by the corresponding correlations and testing of means.

4.3 Results

4.3.1 Reliability of the measurements

This study had good intra-rater reliability (group ICC_1 per layer and cell-type > 0.65). Best reliability was achieved for glial cell densities (GCD) in layers II and III with the least variability between 1st and 2nd measurements in both layers.

Table 4.9 Intra-rater reliability of layer II cell densities

Case No.	Layer II Cell Densities					
	PCD-1	**PCD-2**	**NPCD-1**	**NPCD-2**	**GCD-1**	**GCD-2**
1	122744.78	121215.97	27431.24	27080.03	77956.27	76195.92
2	90268.18	72513.88	20793.46	27080.03	39873.69	31278.24
9	100379.36	99757.38	23489.03	20315.71	46799.22	34046.15
17	100447.48	85275.1	15627.39	18783.99	56455.51	65093.71
22	160447.44	124396.67	25544.74	25784.31	102893.71	80631.24
3	91977.19	94787.2	16787.19	19342.94	52128.22	61543.23
10	98354.65	87237.62	22386.47	27538.26	79077.37	73283.28
13	133982.26	124397.32	20196.26	18729.65	46809.84	42356.18
IntraCC		***0.77***		***0.66***		***0.86***

This table represents repeats of measurements of densities of pyramidal cells (PCD), non-pyramidal cells (NPCD), and glial cells (GCD) in layer II of the PiC performed by the same rater. (1) This represents the first measurement and (2) the second one. Single measures of the group ICC are reported here.

Table 4.10 Inter-rater reliability of layer II cell densities.

Case No.	Layer II Cell Densities					
	PCD-1	**PCD-2**	**NPCD-1**	**NPCD-2**	**GCD-1**	**GCD-2**
33	61694.64	31840.6	15235.44	17204.44	65488.64	76680.25
13	133982.3	60399.93	20196.26	27071.84	46809.8	54612.25
10	98354.65	39513.5	22386.47	38556.41	79077.4	90356.66
3	91977.19	22308.96	16787.19	29823.44	52128.22	33015.31
17	100447.5	22308.96	15627.39	8906.22	56455.55	66376.84
InterCC		***0.232***		***0.528***		***0.857***

This represents repeats of measurements as calculated by two different raters in layer II for GCD, PCD and NPCD.

Inter-rater reliability was good for GCD and non-pyramidal cell densities (NPCD) in layers II and III but was lower for pyramidal cell density (PCD) measurements. The highest ICC_2 reported was for GCD in layer II (ICC_2=0.857) and NPCD in layer III (ICC_2=0.792).

Table 4.11 Intra-rater reliability of layer III cell densities.

Case No.	Layer III Cell Densities					
	PCD-1	**PCD-2**	**NPCD-1**	**NPCD-2**	**GCD-1**	**GCD-2**
1	22984.84	29277.87	13850.01	10318.55	93684.41	96713.92
2	18425.17	20865.81	9151.16	9417.47	52812.79	46722.79
9	24779.38	24997.43	12938.9	11703.83	77130.91	79660.08
17	20052.25	21328.99	13506.76	12771.66	79885.25	76258.84
22	29329.82	28980.12	16350.78	13982.37	122222.03	115450.76
3	27620.08	25120.9	11629.75	10031	74626.95	72292.59
10	34629.1	34535.81	13611.62	12676.01	83317.69	91171.06
13	26280.35	27491.58	13241.07	13041.62	73222.29	67906.84
IntraCC		***0.86***		***0.65***		***0.97***

This table represents repeats of measurements of densities of PCD, GCD and NPCD in layer III of the PiC performed by the same rater

Table 4.12 Inter-rater reliability of layer III cell densities.

Case No.	Layer III Cell Densities					
	PCD-1	**PCD-2**	**NPCD-1**	**NPCD-2**	**GCD-1**	**GCD-2**
33	22422.82	15028.24	9657.82	9616.16	72152.03	62981.13
13	26280.35	20694.37	13241.07	12500.14	73222.29	55303.22
10	34629.1	22559.75	13611.62	13417.05	83317.69	80264.22
3	27620.08	24736.86	11629.75	7746.4	83317.69	62981.13
17	20052.25	25241.21	13506.76	12697.65	79885.25	83861.09
InterCC		***0.218***		***0.792***		***0.481***

This represents repeats of measurements as calculated by two different raters in layer III for GCD, PCD and NPCD.

4.3.2 Accuracy

Individual CE values on cell counts are reported in detail in appendix G. The mean CEs for pyramidal, glial and non-pyramidal cell counts fell below 0.10 indicating a high degree of accuracy of measurements. Means and ranges are presented in tables 13 and 14. Mean CE values for non-pyramidal cell measurements however tended to be slightly higher and averaged 0.11, values sometimes reaching 0.14. An example box-plot is illustrated in figure 4.12.

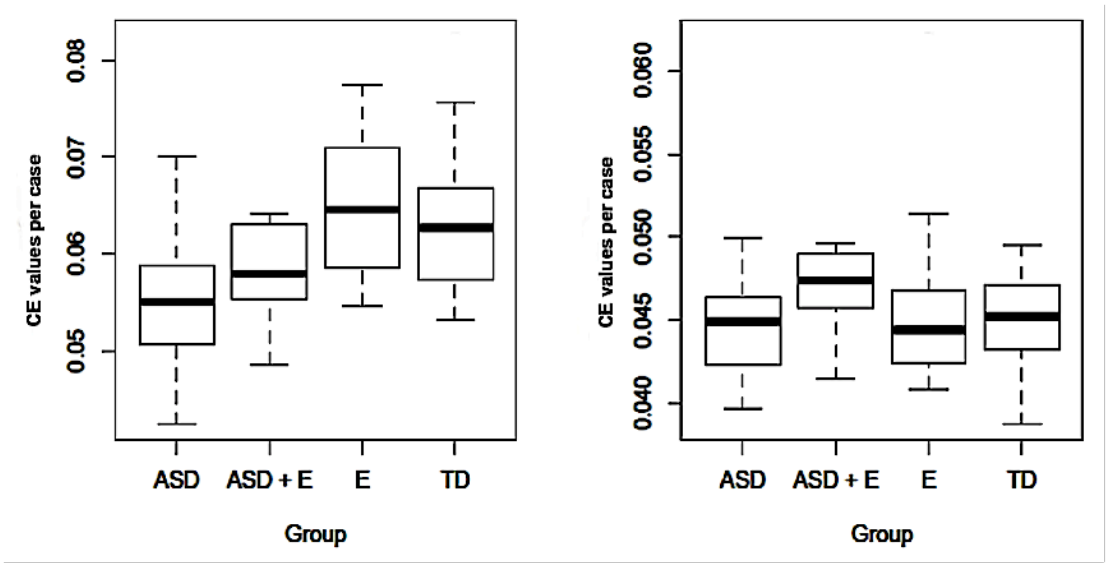


Figure 4.12 Box-plot example of CE of cell counts. The box-plots above show the distribution of values of the CE according to group in layer II for glial cell counts (left) and neuronal cell counts (right). Left figure shows that 75% of CE values for glial cell counts across groups fell below 0.07. Right figure shows that 75% of CE values fell below 0.05 across groups for neuronal cell counts in layer II.

Individual CE values on cell densities are reported in detail in appendix H. Mean CEs for pyramidal cells (PC), non-pyramidal cells (NPC), glial cells (GC) and neuronal cells (NC) densities fell below 0.10 indicating a high degree of accuracy for density measurements. Means and ranges are presented in tables 4.13 and 4.14.

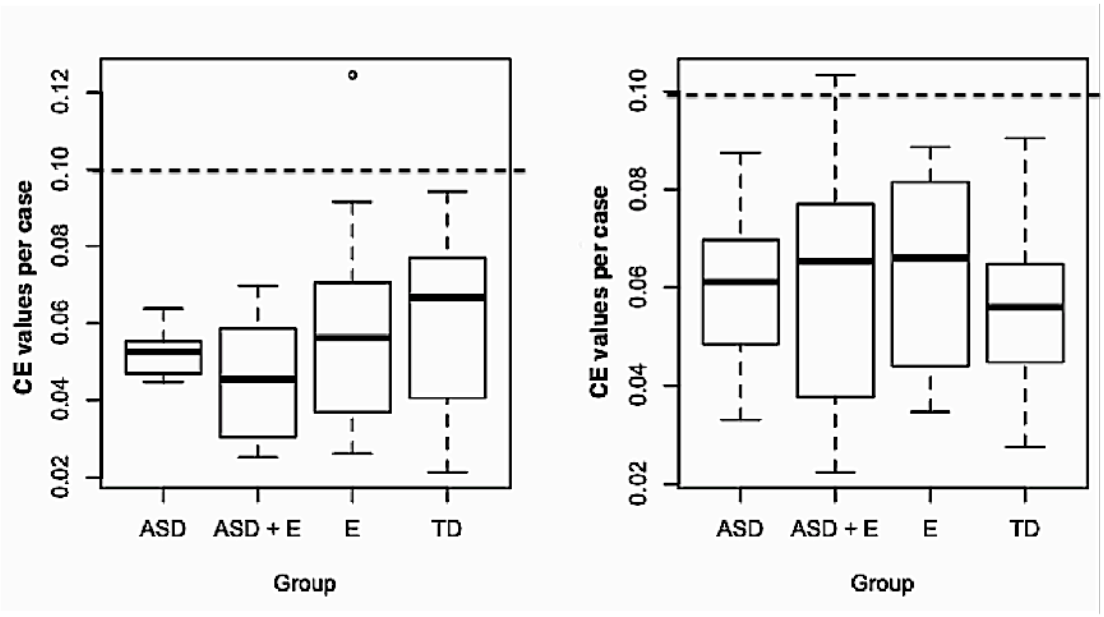


Figure 4.13 Box-plot example of CE of cell densities. The box-plots above show the distribution of values of the CE around the median (thick black line in each box) according to group in layer III for glial cell densities (left) and neuronal cell densities (right). Dotted line indicates the 0.10 cut-off point for the CE. Left figure shows that 75% of CE values for glial cell densities across groups falls below 0.08 and that there is an outlier in the E group with a CE-value of 0.12 for the measured density. Right figure shows that 75% of CE values fall below 0.08 across groups for neuronal cell densities in layer III.

When the GCE was assessed based on the standard error of the means from the averaged case means per layer, cell-type and group, the GCE values were less than 0.10 except for the GCE of PCs in layer II of the ASD + E group, which was slightly higher than 0.10 (0.13). GCEs typically fell below 0.09 for all groups and all densities except for GCE of the ASD+E group PCD in layer II, which was 0.13. All values are reported in tables 4.15 and 4.16.

Table 4.13 Coefficients of Error in Layer II

Diagnosis	Cell Numbers				Cell Densities			
	PC (range)	NPC (range)	GC (range)	NC (range)	PC (range)	NPC (range)	GC (range)	NC (range)
TD	0.05 (0.04-0.05)	0.1 (0.09-0.12)	0.06 (0.05-0.08)	0.04 (0.04-0.05)	0.05 (0.02-0.08)	0.07 (0.05-0.10)	0.05 (0.03-0.08)	0.05 (0.01-0.08)
ASD	0.05 (0.04-0.05)	0.1 (0.08-0.12)	0.05 (0.05-0.07)	0.04 (0.04-0.05)	0.06 (0.02-0.10)	0.09 (0.08-0.15)	0.05 (0.02-0.10)	0.06 (0.03-0.09)
E	0.05 (0.04-0.07)	0.11 (0.09-0.12)	0.07 (0.05-0.08)	0.05 (0.04-0.06)	0.05 (0.03-0.06)	0.07 (0.03-0.12)	0.05 (0.02-0.10)	0.04 (0.02-0.05)
ASD + E	0.05 (0.05-0.06)	0.1 (0.09-0.11)	0.06 (0.05-0.06)	0.05 (0.04-0.05)	0.05 (0.03-0.08)	0.08 (0.06-0.09)	0.04 (0.03-0.05)	0.05 (0.02-0.06)

This table shows the mean values and ranges of the coefficients of error for both cell numbers and cell densities in layer II of the PiC per diagnostic group and per cell population. *PC*: pyramidal cells; *NPC*; non-pyramidal cells; *GC*: glial cells; *NC*: neuronal cells.

Table 4.14 Coefficients of Error in Layer III

Diagnosis	Cell Numbers				Cell Densities			
	PC (range)	NPC (range)	GC (range)	NC (range)	PC (range)	NPC (range)	GC (range)	NC (range)
TD	0.08 (0.06-0.09)	0.11 (0.09-0.12)	0.04 (0.04-0.05)	0.06 (0.05-0.07)	0.07 (0.05-0.11)	0.07 (0.02-0.14)	0.06 (0.02-0.09)	0.06 (0.03-0.09)
ASD	0.08 (0.06-0.09)	0.11 (0.10-0.12)	0.04 (0.04-0.05)	0.06 (0.05-0.07)	0.06 (0.03-0.09)	0.08 (0.05-0.10)	0.05 (0.04-0.06)	0.06 (0.05-0.09)
E	0.08 (0.07-0.10)	0.11 (0.10-0.13)	0.05 (0.04-0.05)	0.07 (0.06-0.08)	0.08 (0.04-0.11)	0.08 (0.05-0.12)	0.06 (0.03-0.12)	0.06 (0.03-0.09)
ASD + E	0.08 (0.07-0.09)	0.12 (0.10-0.14)	0.05 (0.04-0.05)	0.07 (0.06-0.08)	0.06 (0.03-0.11)	0.08 (0.02-0.13)	0.05 (0.03-0.07)	0.06 (0.02-0.09)

This table shows the mean values and ranges of the coefficients of error for both cell numbers and cell densities in layer III of the PiC per diagnostic group and per cell population. *PC*: pyramidal cells; *NPC*; non-pyramidal cells; *GC*: glial cells; *NC*: neuronal cells.

4.3.3 Effects and interactions of rmANOVA

Main effects of within-subject factors of cell-type and layer and, between-subject main effect of diagnosis and the resulting interactions between within-subject x

between-subject factors are reported for the rmANOVA. Storage time was set as a covariate.

Box's M test (M=55.63, F=0.93, df1=42, df2=2671.91, p=0.60) indicated that the observed covariance in cell densities did not differ between groups. Levene's test for equality of error variance across density measurements between groups was acceptable (all F<2, df1=3, df2=35, p>0.15). The Greenhouse-Geisser correction was used (ε<0.75) to adjust for the violation of Mauchly's tests for the assumption of sphericity for within-subject factors for layer ($\chi^2(0)$= 0.0001, p<0.0001), cell-type ($\chi^2(2)$= 8.55, p<0.05) and cell-type x layer interaction ($\chi^2(2)$=19.54, p<0.0001).

4.3.3.1 Effects of diagnosis, cell-type and cortical layer

No main effect of diagnosis on cell density was found (F=1.30, df=3, p=0.29). There was a significant main effect of layer (F=235.97, df=1, p<0.0001) and cell-type (F=424.77, df=1.64, p<0.0001). Layer-by-cell-type interaction was significant (F=320.59, df=1.39, p<0.0001) and so was the cell-type-by-diagnosis interaction (F=2.76, df=4.91, p<0.05). Layer-by-diagnosis and layer-by-cell-type-by-diagnosis interactions were not significant.

There was no main effect of storage (F(1)=0.029, p=0.866, partial η^2=0.001) and no storage-by-layer interaction (F(1)=0.285, p=0.597, partial η^2=0.008). Storage-by-cell-type interaction was significant (F(1.442)=5.068, p=0.018, partial η^2 =0.130). Similarly, storage-by-layer-by-cell-type was significant (F(1.751)=6.192, p=0.05, partial η^2 =0.154) though the partial η^2 values were low indicating that 15-20% of the variance in densities might be accounted for by a storage-by-layer-cell-type interaction. Other statistical results were not substantially affected by the inclusion of

fixation time, except that the cell-type x diagnosis effect was lost ($F>0.119$, $df>3$, $p>0.7$). The interpretation of this is considered in the discussion section.

The main effects and interactions from the rmANOVA were followed by bivariate correlational analyses using parametric Pearson's 2-tailed correlations. This was mainly to examine storage time by cell-type and layer interactions.

4.3.3.2 Storage-by-cell-type interaction

A two-tailed Pearson's bivariate correlations showed a significant positive correlation between pyramidal cell densities in layer II and storage time of tissue in formalin ($r=0.349$, $p=0.029$). A significant negative correlation between glial cell densities in layer II and storage time of tissue in formalin ($r=-0.681$, $p<0.001$) was also noted. However, when this was corrected for multiple comparisons using Bonferroni (significance level alpha (0.05) divided by the number of comparisons), the time that tissue spent in formalin had no effect on any cell-type density with all p-values greater than the corrected significance levels.

4.3.3.2 Layer-by-cell-type interaction

Two-tailed Pearson's correlation analyses showed significant correlations between cell densities within and between layers of the PiC. When adjusted for multiple comparisons, the only significant correlation that passed the Bonferroni correction was in the ASD group where PCD correlated positively with NPCD in layer III ($r=0.788$, $p=0.005$).

4.3.4 Confounding factors

Although there were no group differences for brain weight and age, separate correlational analyses were performed to examine the relationship between brain-weight and cell density as well as age and cell density overall and per diagnostic group. Based on previous studies on abnormal development of the brain in ASD and the effects of brain weight on density measurements (Courchesne 2002), it was hypothesized that brain weight might be affected by storage duration thereby affecting cell density measurements. Age also could have an effect on cell densities in the brain (Davies, Horwood et al. 1992). All analyses were subjected to appropriate Bonferroni corrections for multiple comparisons.

4.3.4.1 Bivariate correlations between age and density

There were no significant correlations between age and pyramidal, age and non-pyramidal as well as age and glial cell densities in layers II and III. This result was similar when pyramidal and non-pyramidal measurements were combined into neuronal cell densities. When examining density measurements per cell type, layer and diagnostic group and when the ASD and ASD+E mean glial cell density measurements in layer II were grouped together and correlated with age, a negative correlation was observed ($r=-0.46$, $p=0.06$) compared with an inverse trend in the TD group (figure 4.14). The difference in slopes between TD and ASD revealed a statistically significant difference in the effect of age on layer II glial cell density ($F=4.44$, $df24$, $p=0.046$). Another significant negative correlation was noted between age and pyramidal cell density in layer II only in the TD group ($r=-0.75$, $p=0.009$) whilst a negative correlation was noted between age and pyramidal cell density in

layer II in the E group (r=0.45, p=0.08). When adjusted for multiple testing using Bonferroni's, only PCD in layer II correlations with age in TD remained significant.

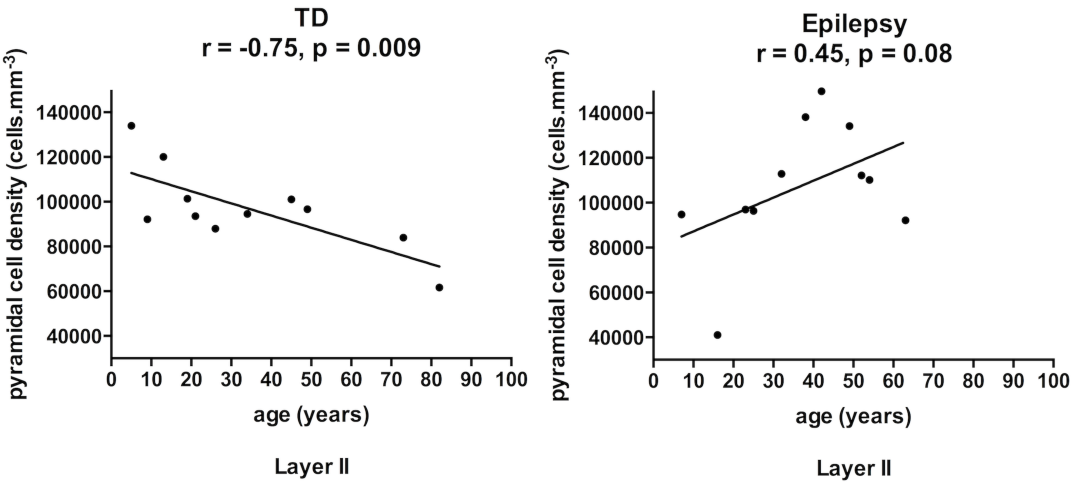


Figure 4.14 Correlations between age and pyramidal cell densities in layer II. Whilst the TD group showed a significant negative correlation, the epilepsy group showed a trend towards a positive one.

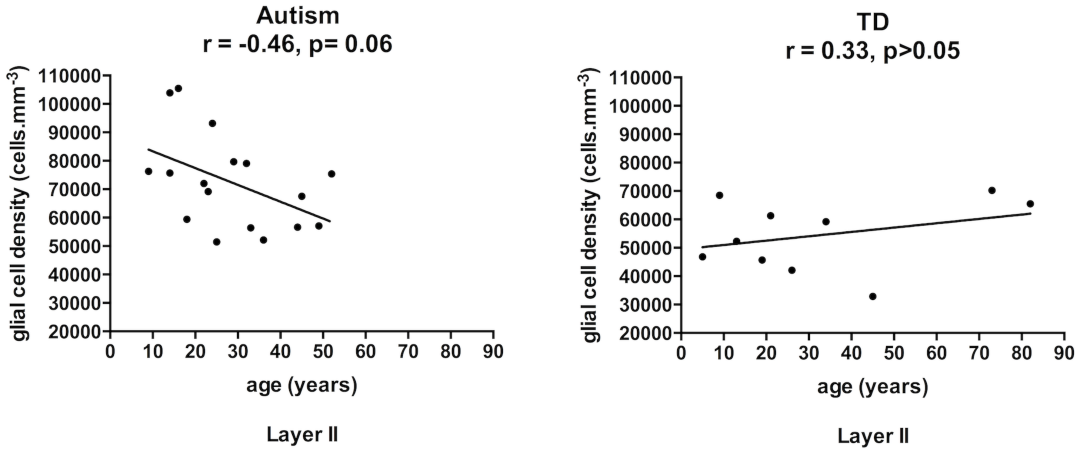


Figure 4.15 Correlations between age and glial cell densities in layer II. Glial cell densities correlated negatively with age in autism (left graph) as opposed to a trend towards a positive correlation in the TD group (right graph).

4.3.4.2 Bivariate correlations between (post-fixation) brain weight and density

There were no significant correlations between brain weight and each of PCD, NPCD and GCD. When examining these correlations by diagnostic group, layer II NPCD correlated negatively with brain weight in the TD group (r=-0.924, p=0.003), which passed the Bonferroni correction. The E group correlation tended towards an inverse one between NPCD in layer II and brain weight and scraped significance (rho=-0.589, p=0.057). These correlations were in agreement using both Pearson's and Spearman's analyses. No correlations existed between neuronal cell densities and brain weight in any diagnostic group. Brain weight did not correlate with storage duration in any group.

4.3.5 Post-hoc testing of mean cell densities between diagnostic groups

The cell-type x diagnosis interaction was followed by post hoc means testing between diagnostic groups. This showed a significant between-group difference in glial cell densities in layer II (F=4.812, df=3, p=0.007). Between-group differences were not significant for glial cell densities in layer III (F=1.126, df=3, p=0.352), pyramidal cell densities in layers II (F=0.797, df=3 p=0.504) and III (F=0.272, df=3, p=0.845); and non-pyramidal cell densities in layers II (F=1.079, df=3, p=0.371) and III (F=0.562, df=3, p=0.463).

4.3.5.1 Glial cell densities in layers II and III

In layer II, post-hoc analyses showed a significant 38.3% increase in mean glial cell densities in ASD compared with TD (p=0.014). Although mean glial cell densities increased by 34.67% in ASD+E compared with TD also in layer II, this difference

was not significant between groups (p=0.102) (see table 4.15). Both ASD+E and ASD groups had comparable means of layer II glial cell densities (3% difference).

Means in layer II were also comparable between TD and E (p>0.05). When all autism cases (ASD & ASD+E) are grouped together, mean glial densities are significantly increased in autism in comparison with both TD and E (p<0.01). There were no significant differences in mean glial cell densities in layer III across all pairwise comparisons.

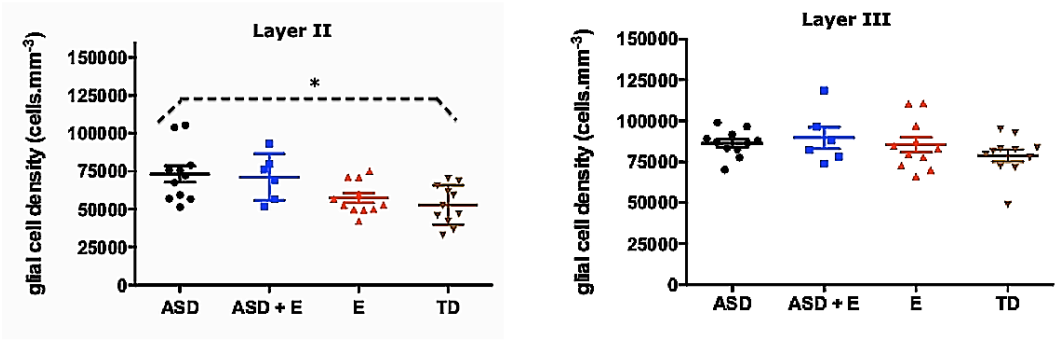


Figure 4.16 Mean glial cell densities in layers II and III. This figure shows the scatter plots of glial cell densities in all diagnostic groups in layers II and III of the PiC.

4.3.5.2 Pyramidal cell densities in layers II and III

In layer II, post-hoc analyses showed no significant differences in mean pyramidal cell densities between ASD and TD and between ASD+E and TD. When autism groups were combined and compared with TD, no differences were found. Layer II mean pyramidal cell densities were higher by 19.75% in E compared with ASD, 23.4% compared with ASD+E and 17% compared with TD though these differences were not significant (p>0.05). There were no significant differences for layer III across all pairwise comparisons.

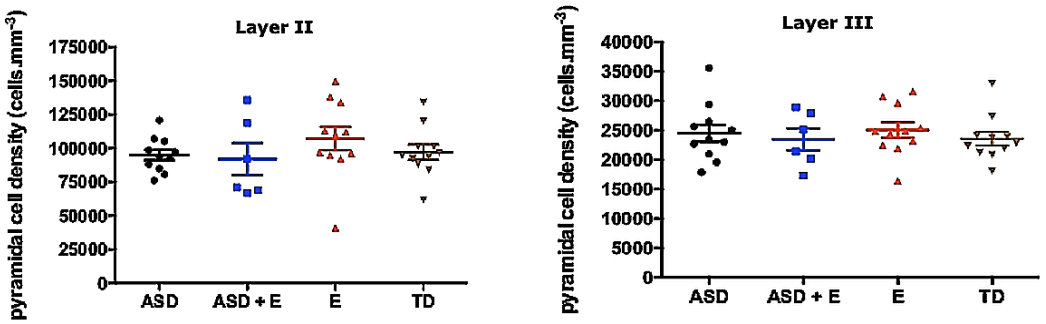


Figure 4.17 Mean pyramidal cell densities in layers II and III. This figure shows the scatter plots of pyramidal cell densities in all diagnostic groups in layers II and III of the PiC.

4.3.5.3 Non-pyramidal cell densities in layers II and III

In layers II and III, post-hoc analyses showed no significant differences in mean non-pyramidal cell densities between autism groups and TD. There was a 10% increase in layer II however in E compared with TD. No other differences were noted across groups for layer III.

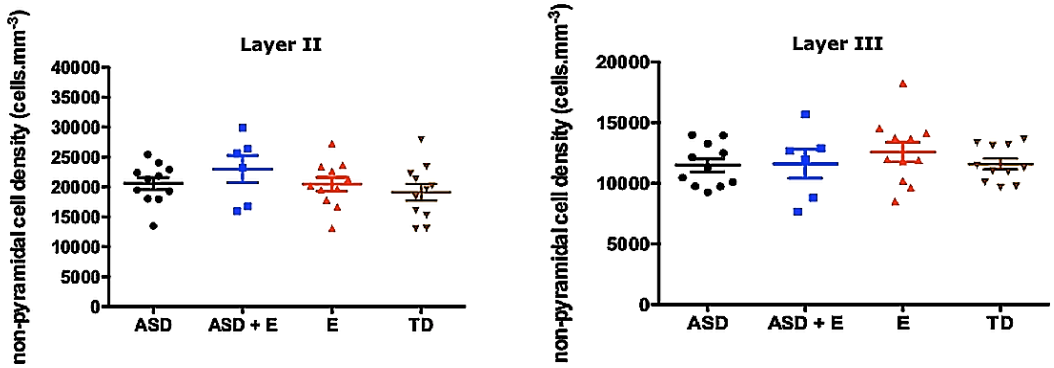


Figure 4.18 Mean non-pyramidal cell densities in layers II and III. This figure shows the scatter plots of non-pyramidal cell densities in all diagnostic groups in layers II and III of the PiC.

4.3.5.4 Neuronal cell densities in layers II and III

In layer II, post-hoc analyses showed that there were no significant differences between TD and ASD in mean neuronal cell densities. Neuronal densities were higher by 16% in the E group compared with the TD group in layer II but this difference was not significant. Mean neuronal densities were higher by 10% in the E group compared with the ASD group in layer II but that was not a significant difference either. For all remaining pairwise comparisons in layer II and layer III, no significant differences were noted in mean neuronal cell densities across groups. All means and GCEs are summarized at the end of this section.

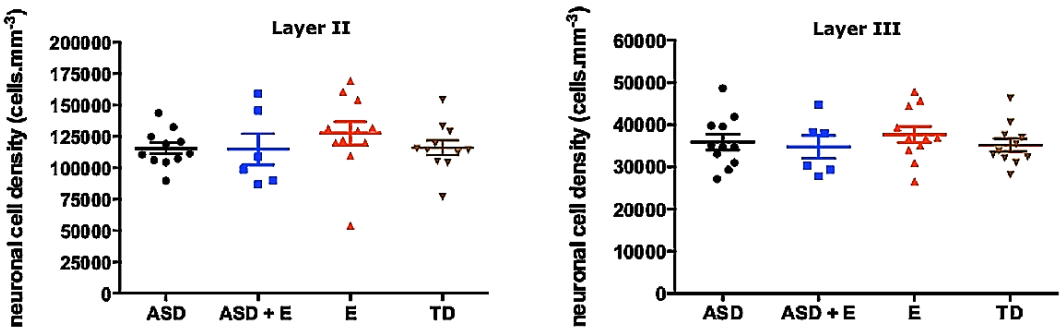


Figure 4.19 Mean neuronal cell densities in layer II and III. This figure shows the scatter plots of neuronal cell densities in all diagnostic groups in PiC layers II and III.

4.3.5.5 Summary of mean cell densities and the GCE

Below are two tables summarizing mean cell densities in layer II and III of the PiC across diagnostic groups with the GCE.

Table 4.15 Layer II cell densities and group coefficients of error

Cell type	Layer II-Cell Densities (cells/mm^3)											
	ASD (N = 11; 7M:4F)			Chronic epilepsy (N = 11; 7M:4F)			ASD + E (N=6; 5M:1F)			Comparison TD (N = 11; 5M:6F)		
	Mean (x10^3)	SD (x10^3)	GCE	Mean (x10^3)	SD (x10^3)	GCE	Mean (x10^3)	SD (x10^3)	GCE	Mean (x10^3)	SD (x10^3)	GCE
Pyramidal	94.97	12.84	0.04	113.73	20.36	0.05	92.16	29.08	0.13*	97.00	18.64	0.06
Non-Pyramidal	20.57	3.36	0.05	21.21	3.11	0.04	22.97	5.54	0.07	19.12	4.59	0.07
Glial	73.06	18.06	0.07	57.35	10.72	0.06	71.14	15.27	0.06	52.83	13.00	0.05
Neuronal	115.55	14.79	0.04	134.88	19.77	0.04	114.88	30.31	0.08	116.11	19.32	0.07

This table summarizes mean cell densities, standard deviations and group coefficients of error (GCE) in layer II across all diagnostic groups.

Table 4.16 Layer III cell densities and group coefficients of error

Cell type	Layer III-Cell Densities (cells/mm^3)											
	ASD (N = 11; 7M:4F)			Chronic epilepsy (N = 11; 7M:4F)			ASD + E (N=6; 5M:1F)			Comparison TD (N = 11; 5M:6F)		
	Mean (x10^3)	SD (x10^3)	GCE	Mean (x10^3)	SD (x10^3)	GCE	Mean (x10^3)	SD (x10^3)	GCE	Mean (x10^3)	SD (x10^3)	GCE
Pyramidal	24.52	4.90	0.06	25.05	4.38	0.05	23.49	4.58	0.08	23.60	3.87	0.05
Non-Pyramidal	11.50	1.77	0.05	12.57	2.71	0.06	11.61	2.92	0.09	11.60	1.50	0.04
Glial	86.47	8.13	0.03	85.38	15.15	0.05	89.63	16.28	0.07	78.86	12.32	0.05
Neuronal	35.93	6.18	0.05	37.70	6.38	0.05	34.73	6.62	0.08	35.19	5.02	0.04

This table summarizes mean cell densities, standard deviations and group coefficients of error (GCE) in layer III across all diagnostic groups.

4.3.6 Power of the study and sample size

The obtained results were used to calculate post-hoc power of the study at α=0.05. Effect size -f- and observed power (1-β) were calculated for each density grouped by cell-type across 4 diagnostic groups (TD, ASD, E, ASD+E). Both –f- and power were calculated based on the mean cell density per diagnostic group and the total standard deviation between the different cell density group means (N=39). For layer II, good power was demonstrated for glial cell density measurements (1-β=0.83, f=0.58). Limited power was demonstrated for pyramidal cell density (1-β=0.38, f=0.35) and

non-pyramidal cell density (1-β=0.31, f=0.31) measurements. When neurons were combined together, observed power improved to 1-β=0.53 and f=0.42. One would need to increase the number of samples to N=78 to achieve good power (superior to 0.8) at α=0.05.

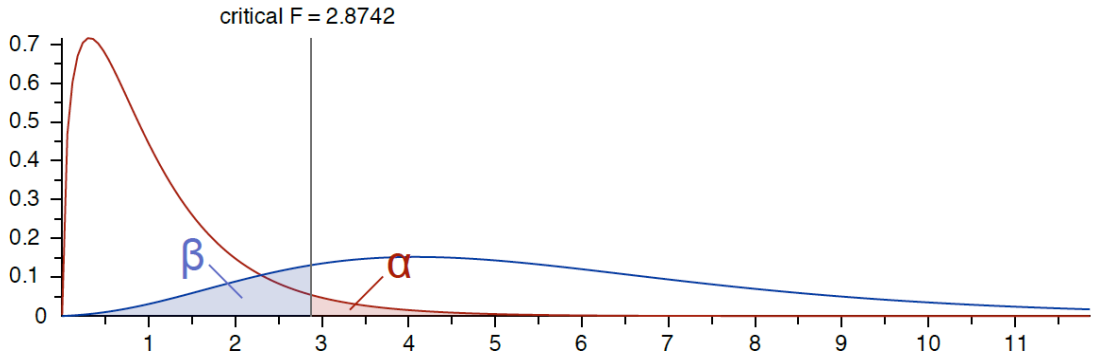


Figure 4.20 Post-hoc power of glial cell density measurements. This figure represents observed power (1-β=0.83) post-hoc of glial cell density measurements across diagnostic groups set at α=0.05. F=2.87 is the non-centrality distribution factor.

Based on means and standard deviations of cell density findings in different cortical areas reported by other researchers, a desirable sample size was estimated in designing the present study. Van Kooten et al (2008) reported neuronal density changes of 13% in layer III in the fusiform gyrus, for which a sample size of n=9 per group is estimated to provide 80% power (two-sided, target p=0.05). Larger differences have been reported for neuropil space (19%) by Casanova et al (Casanova, Buxhoeveden et al. 2002) and cell counts (64%) by Courchesne et al. (Courchesne, Mouton et al. 2011). Therefore, based on the most conservative of these findings (van Kooten et al 2008), it was estimated (power calculation based on a t-test model) that a sample size of 11 subjects per group would provide >90% power.

4.3.7 Association between cell densities and symptom severity in ASD

Glial cell densities in layers II showed a positive correlation trend in the autism group with ADI-R scores in the restricted and repetitive behaviour (RRB) domain (r=0.49, p=0.08). Layer II neuronal cell densities correlated positively with ADI-R scores in the verbal communication domain (r=0.71; p<0.05). The ADI-R questionnaire includes an item entitled 'unusual sensory interests' (item 71, code EUNSENS). The clinician rates this item according to a severity scale ranging from 0 to 2 (0=none, 1=mild, 2=severe). Correlations between item 71 scores and cell densities were not significant for any cell type.

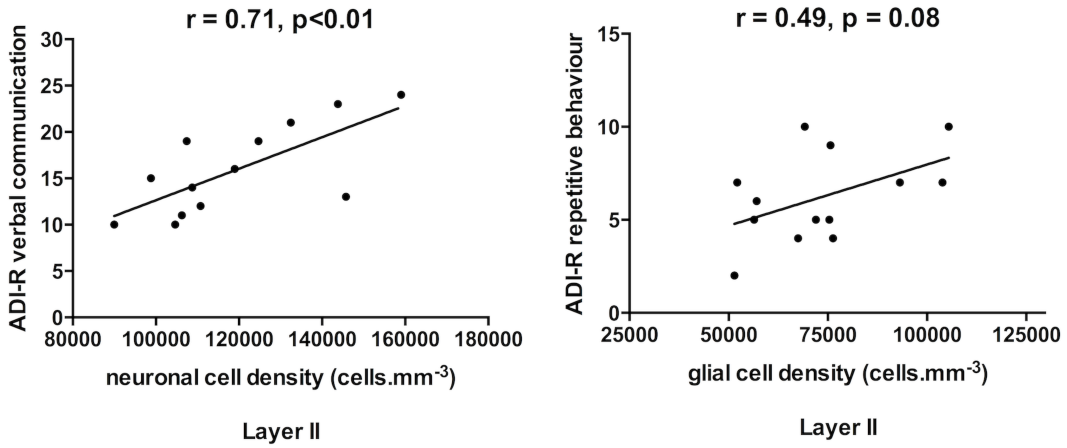


Figure 4.21 Associations between cell densities and symptom severity. Neuronal cell densities correlated positively with scores from the verbal communication domain of the ADI-R (left graph), whilst glial cell densities in layer II showed a positive trend with the ADI-R restricted and repetitive behaviour domain scores (right graph). Note that some there are missing values because it was not possible to obtain behavioural scores for all the cases.

4.4 Discussion

To the author's knowledge, this is the first study to report cell density measurements in the human piriform cortex in individuals who were diagnosed with ASD during life. Furthermore, to tease apart effects that might arise from epilepsy, ASD cases that were clinically diagnosed with epilepsy during life were separated from those who did not have epilepsy.

The main finding of this study was the significant increase in glial cell densities in layer II of the PiC in ASD compared with TD. When the combined measured mean glial cell densities in layer II from both ASD and ASD+E groups were combined into one group, a negative correlation between autism and age was observed. Pyramidal cell densities in layer correlated positively with age in the E group. When mean cell densities were correlated with severity scores in autism, significant positive correlations were observed between cell densities in layer II and domain scores of the ADI-R.

The increase in glial cell densities in layer II of the PiC is consistent with recent neuropathological studies suggesting altered glia in the cerebral cortex in ASD. Morgan et al (2010) reported increased microglial cell densities in DLPFC (Morgan, Chana et al. 2010). Vargas (2005) et al demonstrated marked astroglial activation in human ASD post-mortem tissue in the granular layer of the cerebral cortex and the cerebellum (Laurence and Fatemi 2005, Vargas, Nascimbene et al. 2005). The robustness of this result is confirmed by a high degree of inter-rater and intra-rater reliabilities, high accuracy, and good post-hoc power for glial cell density measurements in layer II for the sample size.

Increased glial cell densities in layer II of the PiC may be specific to autism. Mean glial cell densities in the ASD+E group were comparable to the ASD group increase

compared with the TD group though this was not significant. Interestingly, glial cell densities in layer II did not change in epilepsy contrary to what was predicted. Therefore, it can be suggested that the increase in glial cell densities may be independent of the epilepsy and may be characteristic of autism. This is also in line with a recent study by Courchesne et al (2010) who indeed demonstrated that the seizure component in autism did not have an effect on microglial activations in DLPFC (Morgan, Chana et al. 2010).

Neuronal densities (both pyramidal and non-pyramidal) were not significantly different between ASD and TD groups in layers II and III. With increased glial cell densities, one might expect neuronal survival to be altered thereby affecting cell densities. Post-hoc power of measured neuronal densities was limited suggesting that to detect an effect; the sample size would have needed to be doubled to achieve a power of 0.8. Some studies have indeed reported no changes in neuronal densities in ASD in fronto-temporal regions (Oblak, Rosene et al. 2011, Jacot-Descombes, Uppal et al. 2012). Therefore, preserved neuronal densities might after all reflect a true result.

No differences were observed between ASD and TD in non-pyramidal cell densities in both layers. Non-pyramidal cell densities were of interest in this study particularly in the context of the balance between excitation and inhibition. Most inhibitory GABA-ergic neurons in the PiC are non-pyramidal in shape (Suzuki and Bekkers 2007) and therefore contribute to regulating the perisomatic inhibition of pyramidal cells in layers II and III. Although differences in non-pyramidal cell densities between TD and ASD were predicted, the desired sample size to detect an effect might have needed to be very large to detect any differences in effect in this class of cells given the power analyses described previously. This would have been impossible to achieve

particularly given the time-consuming nature of manual coding. Recent studies on post-mortem human hippocampus (a neighbouring region to the PiC) in ASD have reported increases in various interneuronal densities in the cortex (Lawrence, Kemper et al. 2010). Based on cell numbers alone, this effect (if it existed in the samples) might have been masked due to several reasons: first, non-pyramidal cells (though mostly inhibitory interneurons) might have also been glutamatergic as we know that part of layer II cells are morphologically identical to non-pyramidal cells yet perform different functions. Therefore, based on their morphology alone, it could not be known which cell was excitatory and which was inhibitory. Secondly, lower counts and occurrence of non-pyramidal cells in both layers II and III compared to pyramidal and glial cells were achieved. This could account for the larger CE measurements in this class of cells where more counting boxes might have been needed to achieve a CE below 0.10. At least for layer II, it has been previously noted that GABA-ergic non-pyramidal cells were mostly concentrated near the transition area between the frontal PiC and the temporal PiC (Howard, Plailly et al. 2009). The whole PiC was sampled evenly and this study was not designed to target specific sub-regions, which might also account for the lower numbers in non-pyramidal cells. It is to be noted that if non-pyramidal and pyramidal cells are grouped together, CE measurements typically fall below 0.08.

Contrary to what was predicted, epilepsy did not affect neuronal and glial cell densities in the PiC compared with TD in the ASD+E group. The ASD+E group (like the ASD) had significantly higher glial cell densities than the E group suggesting as discussed earlier, that the epilepsy component did not affect glial cell densities in the PiC and that the result may have been due to the autism component. Studies on the pilocarpine rat model of TLE reported obliteration of parts of layer II of the PiC and

decreased neuronal cell densities (Eidt, Kendall et al. 2004). This study did not find that effect. When pyramidal cell contribution to neuronal density was assessed in the E group, there was an increase compared with the TD group in layer II but also an increase compared with the autism. A recent study found that amygdala projecting prefrontal cells supported the infralimbic and prelimbic prefrontal cortices through compensation following damage to the hippocampus (Zelikowsky, Bissiere et al. 2013). Though their findings might not affect cell density, it is interesting to consider that increased cell density in layer II may have a balancing role of the frontal microcircuitry, particularly as most of the epilepsy cases in this study showed hippocampal neuronal cell loss in the cornu ammonus 1 and 4 regions (confirmed by inspecting neuropathology reports). This result was particularly interesting especially as pyramidal cell density in layer II in the E group correlated positively with age, which was the inverse result to normal brain density changes in layer II with age (negative correlation with age in the TD group; see results section). Thus, it may be suggested that epilepsy in the PiC seemed to have no bearing except in pyramidal cell densities in layer II, which increased with age.

Although we did not have test scores of olfactory function from the autism cases during life, the positive relationship between glial cell density and the RRB domain score from the ADI-R, and the positive correlation between neuron density and the communication domain score are notable associations with symptom severity. The main function of the PiC seems to be olfactory identification but it may also act as sensory associative cortex with extracortical connections to other areas such as the prefrontal cortex and the amygdala (Johnson et al, 2000). Furthermore, these findings are broadly in support of a general increase in cell density as a feature of the cerebral cortex in autism, although modified by age. Inter-columnar spacing in ASD is

decreased (Casanova, Buxhoeveden et al. 2003) and neuronal cell densities are increased in various regions of the cortex (Lawrence, Kemper et al. 2010, Courchesne, Mouton et al. 2011). Increased cell densities in the PiC associated with more severity may be largely in support of the general increase in cell densities being a feature of the cerebral cortex in ASD.

The negative correlation between age and glial densities in autism is particularly interesting mainly because the trajectory of glial cells in the normal aging brain usually follows an inverse trend. The older we get, glial cells increase in number, neurons decrease in number, synaptic density drops and neuron-glia ratios decrease in the neocortex (Terry, DeTeresa et al. 1987). Courchesne et al suggested that autism brain size follows an abnormal early developmental trajectory that normalizes with age (Courchesne 2002). Brain size also affects cell densities. In this study, glial cell densities did not correlate with brain weight in autism and there were no correlations between age and brain-weight. Autism cases in this study were much older possibly accounting for the absence of correlations between brain size and cell densities in line with Courchesne's work. Therefore, it is interesting to consider that the negative correlation between glial cell densities and autism in layer II might be suggestive of an altered trajectory of development of glial cells in the PiC with age in autism.

Based on only cell density measurements, it is difficult to speculate on olfactory function in autism though this will be discussed further in the final chapter.

In conclusion, the role of glia in autism may be key and further experiments are required to investigate whether these increased glia are also associated with signs of pathology in the piriform cortex.

Chapter 5 Neuropathology of the piriform cortex in ASD and epilepsy

5.1 Rationale, aims and hypothesis.

In order to extend stereological investigations of the PiC, qualitative neuropathology was also performed on the previous cases. Because increased glial cell densities may suggest neuroinflammatory mechanisms in autism, the purpose here was to investigate whether signs of pathology such as hypoxia, glial fibres, early calcification and corpora amylacea may already be seen in the PiC and whether these signs were associated with the observed cytoarchitectural changes. As a brief introduction to this chapter, corpora amylacea (Ca) are briefly introduced.

Ca were first observed by Virchow (1853) in the ependyma of brain ventricles (Andree and Sedivy 2005). They are spherical basophilic aggregates formed of a mixture of short and long polysaccharides and polymerized proteins (Abel, Hebb et al. 2010). Ca have been reported in the normal aging human brain (Singhrao, Neal et al. 1993, Hoyaux, Decaestecker et al. 2000) and also in cases of hippocampal sclerosis associated with TLE (Kawamura, Morioka et al. 2002), Alzheimer's disease (Keller 2006), multiple sclerosis (Selmaj, Pawlowska et al. 2008) and myoclonic epilepsy (Sakai, Austin et al. 1968). Ca origins are thought to be mostly astrocytic (Nam, Kim et al. 2012). Ca usually accumulate in astrocytic foot-processes in the subpial, perivascular and subependymal spaces of the brain (Cavanagh 1999) and show immunoreactivity to S100 proteins, highly expressed in astrocytes and activated macrophages (Hoyaux, Decaestecker et al. 2000). There is also some evidence of the neuronal and oligodendrocytic origins of the Ca (Singhrao, Neal et al. 1994, Wilhelmus, Verhaar et al. 2011). The roles of Ca remain unclear. They were thought to be by-products of chronic hypoxia and cellular stress in human pathology

(Cavanagh 1999, Abel, Hebb et al. 2010). Biochemical analysis revealed the presence of ubiquitin, heat-shock proteins 28, 60, 70, and 72 (Martin, Mather et al. 1991, Gati and Leel-Ossy 2001), heme oxygenase-1 (Schipper, Song et al. 2009) and transglutaminase-1 (Wilhelmus, Verhaar et al. 2011) all of which are involved in the response to cellular stress. A role in neuroinflammation has also been suggested due to the presence of components of the classic and terminal complement pathways in post-mortem samples from patients who had Alzheimer's (Keller 2006) as well as their strong association with glial cells (Kawashima, Adachi et al. 1999).

In autism, only two studies have reported the presence of Ca in post-mortem tissue. Bailey et al (1998) reported in 5 autism post-mortem cases extensive Ca deposits in the cerebral cortex and the subpial space (Bailey, Luthert et al. 1998). A more recent study by Wegiel et al also reported hippocampal Ca in the granular layer in post-mortem cases of idiopathic autism (Wegiel, Schanen et al. 2012). To the author's knowledge, there are no studies on the neuropathology of the PiC in autism. Therefore, the purpose of this section was to report the broader neuropathological profile of the PiC area.

It was hypothesized that with the increased glial cell densities in the PiC, pathological Ca would be increased in autism and epilepsy.

5.2 Methods

The same post-mortem cases as in part 1 have been used here. One section of 25μm thickness stained with 0.1% cresyl-violet per case was chosen for qualitative assessments. Pathological examination of the full brain (when available) and the PiC (all cases) were examined with the assistance of Professor M. Esiri. Pathological

examination included assessing qualitatively of neuronal nuclei, size of the cell body, presence of gliosis, and Ca levels in the subpial spaces.

Qualitative pathological examination of the PiC assessed neuronal nuclei, size of the cell body, presence of gliosis, and presence of corpora amylacea (ca) in the subpial spaces. The Ca are spherical and basophilic with a relatively homogeneous dark staining. They can have various sizes and their diameter can be as high as 10 µm (Jaspar and Prick 1968). Full quantitation of Ca would require unbiased stereological sampling, which was not feasible due to time limitations. Ca density was assessed using a scoring system of 0 to 3 (0= no deposits, 1=mild, 2=moderate, 3=severe). Glial cells can have a similar size to Ca though they are easily distinguishable from the Ca because they have a thicker nuclear membrane and relatively transparent Nissl-stain of their cytoplasm. Mean levels of Ca per diagnostic group were quantified and differences assessed using a non-parametric Kruskal-Wallis one-way ANOVA. Spearman's rank-order correlations were used to correlate between measured cell densities (continuous variables) in layers II and III of the PiC and Ca levels (categorical scoring of none, mild, moderate and severe).

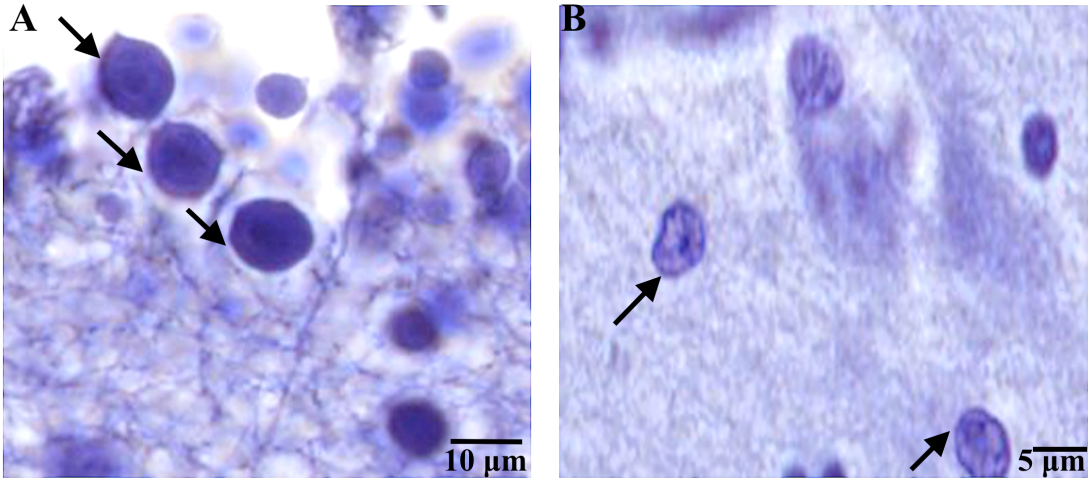


Figure 5.1 Morphology of glial cells and corpora amylacea. Left figure shows corpora amylacea and right figure glial cells.

5.3 Results

5.3.1 Pathological findings

Pathological observations showed no cortical dysgenesis (abnormal orientation of neuronal processes) generally. Trilamination was always recognizable. In some cases, the tissue was hypoxic with homogenizing changes in neurons. Numerous Ca in the perivascular, subpial, and outer layer I of the PiC were observed. Tissue gliosis was also seen in many cases. Pathological findings are summarized in table 5.1 .

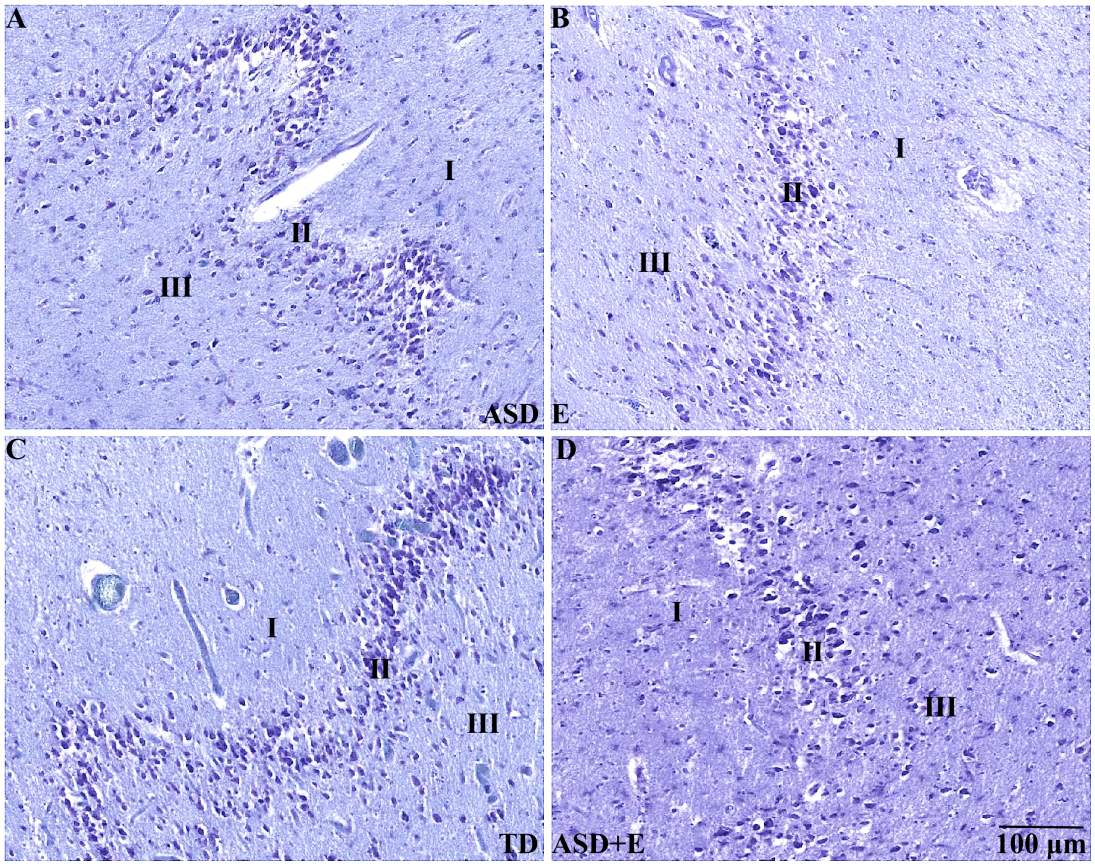


Figure 5.2 Qualitative layer II changes of the PiC in selected cases. (A) and (C) show similar laminations of the PiC and similar cell densities in layer II in ASD and TD. Though qualitatively, layer II cell densities seemed similar across all diagnostic groups, in a case of epilepsy (B) and ASD+E (D), layer II densities seemed less dense.

Table 5.1 Pathological findings of the piriform cortex. This table summarizes the pathological findings upon assessment of the piriform area in selected cases.

Diagnosis	Characteristics		
	Lamination	**Neuronal Characteristics**	**Pathological Features**
TD (n=11)	No cortical dysgenesis in TD cases. Layer II cell arrangement was non-linear in one case. PiC was a well-defined trilaminar structure with a neuron-dense layer II. Sometimes, layer II anatomical discontinuities were seen.	In two cases, homogenizing changes as a result of hypoxia were seen in neuronal populations (shrunken basophilic nucleus, eosinophilic shrunken perikaryon).	Two older cases (age>60 years old) showed numerous corpora amylacea deposits in the subpial space and around layer I of the PiC. One case showed evidence of gliosis.
ASD (n=11)	No evidence of cortical dysgenesis. In two cases, lamination sometimes appeared abnormal with signs of cell loss with more discontinuities in layer II of the trilaminar PiC.	Hypoxic changes were observed in five cases.	Nine cases showed numerous Ca deposits in the subpial space and around layer I of the PiC. Gliosis was observed in seven cases as well as presence of early calcification and glial fibers.
ASD+E (n=6)	No evidence of cortical dysgenesis. Evidence of cell loss in layer II in three cases. Unusually thick layer I in one case.	Hypoxic changes seen in one case.	All cases showed numerous Ca deposits around layer I and the subpial space. Gliosis and numerous astrocytic fibres and macrophages were also observed here in layer I.
E (n=11)	Abnormal lamination in one case.	Hypoxic changes were observed in three cases.	Three cases showed numerous Ca in the in layer I co-localising with gliosis.

5.3.2 Corpora amylacea differences between diagnostic groups

There were significant differences in Ca levels between groups (H=14.04, df=2, p=0.0009) as demonstrated by non-parametric analysis of variance to compare between means using the Kruskal-Wallis with Dunn's correction for multiple comparisons. Post-hoc testing showed that, the TD and E group did not differ in mean levels of Ca (Mean Rank Diff =-6.00, p>0.05)). The autism group had significantly higher Ca levels compared with TD (Mean Rank Diff= 15.62; p=0.0008) and tended to be higher compared with E (Mean Rank Diff = 9.62, p=0.07) (Figure 5.3). High Ca levels were also associated with higher glial cell densities in layer II (Spearman's rho=0.61, p<0.001) and a trend was observed for layer III glial densities (Spearman's rho=0.39, p=0.09). Where the Ca deposits were severe, glial fibers, macrophages and early calcification signs were also sometimes observed.

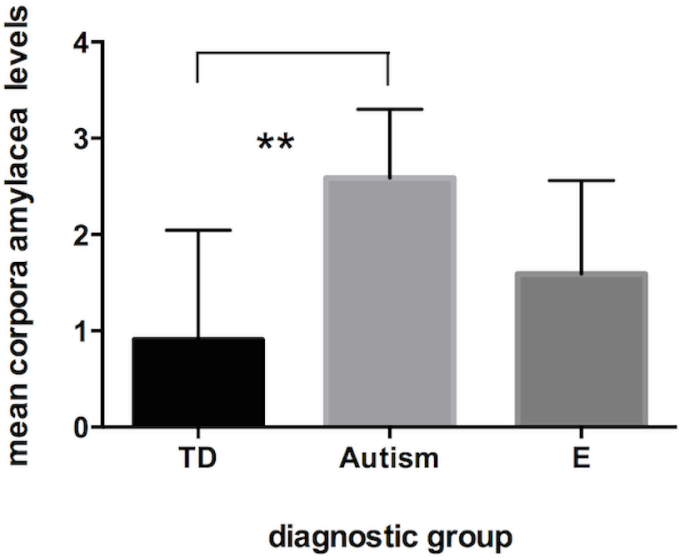


Figure 5.3 Mean corpora amylacea differences between diagnostic groups

Corpora amylacea levels were significantly increased in autism compared to both the E and TD groups. Bars represent mean levels of corpora amylacea and error bars standard deviations per diagnostic group.

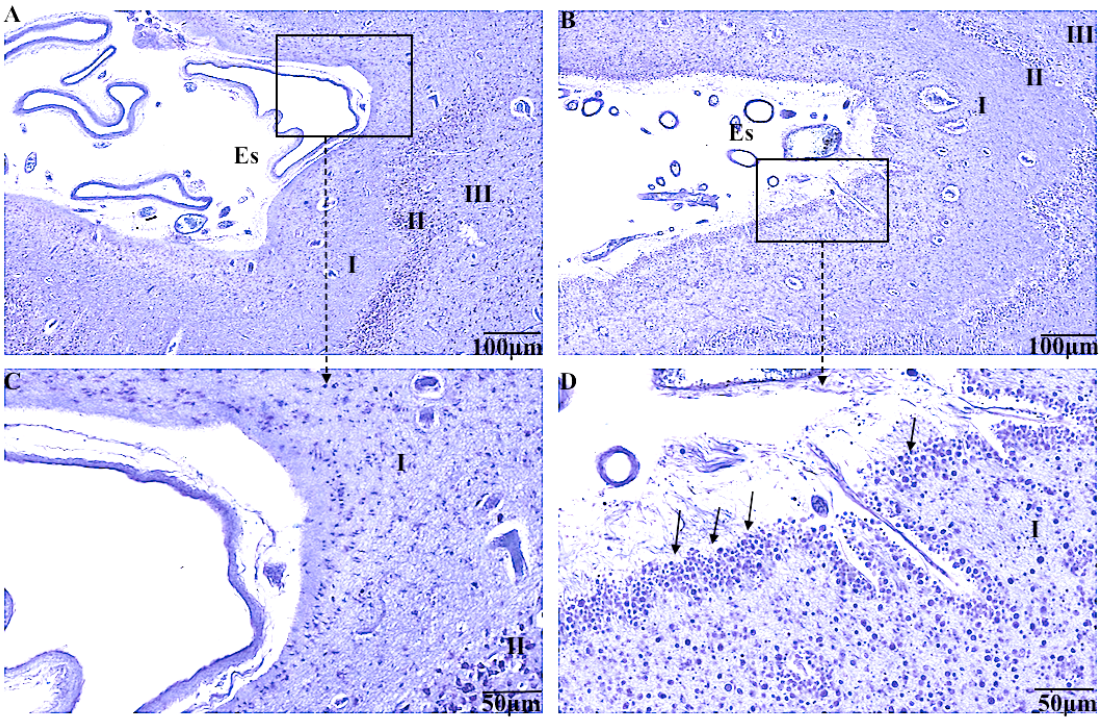


Figure 5.4 Corpora amylacea deposits in ASD compared with TD

This figure shows representative cases of ASD and TD showing in ASD high levels of corpora amylacea around layer I of the PiC at 4X (B) and 10X (D) and no corpora amylacea in TD at 4X (A) and 10X (C) magnifications in the same area. *Es*: entorhinal sulcus. Top is dorsal and left is medial.

5.3.3 Association of corpora amylacea levels with glial cell densities in ASD

High Ca levels also were also significantly associated with higher glial cell densities in layer II (Spearman's rho=0.61, $p<0.001$) and a trend was observed for layer III glial densities (Spearman's rho=0.39, $p=0.09$). Where the Ca deposits were severe, astrocytic fibers, macrophages and early calcification signs were also sometimes observed.

Table 5.2 Corpora amylacea across all diagnostic groups

	Statistic	Layer II				Layer III			
		PCD	NPCD	GCD	ND	PCD	NPCD	GCD	ND
Ca	Spearman's ρ	-.019	0.26	**0.61***	-0.15	0.02	-0.14	**0.39**	-0.08
	p-value	0.24	0.11	**0.00**	0.36	0.91	0.38	**0.09**	0.65

Spearman rho's coefficient values and p-values of correlations between cell densities in both layers across groups and Ca deposits in the outer layer of the PiC. Bold values are associations of Ca in layer I with glial densities in layers II and III of the PiC.

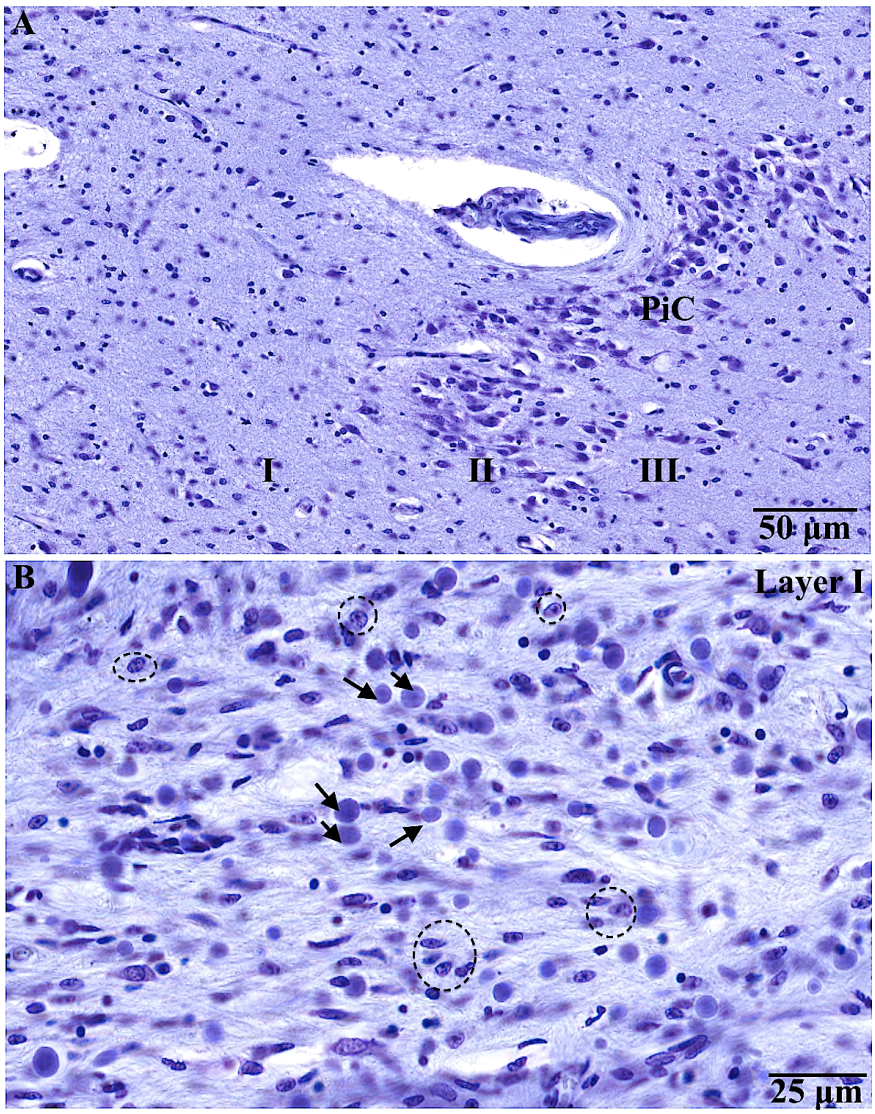


Figure 5.5 Gliosis associated with corpora amylacea levels. Top figure (A) shows gliotic tissue in an ASD+E case. At higher magnification from the same tissue,

bottom photo (B) shows cells that are consistent with the histological appearance of reactive astroglia (in dotted circles) co-localizing with many corpora amylacea (black arrows) in layer I of the PiC. Top of every figure is dorsal and left medial.

5.4 Discussion

The neuropathology of the PiC area has been under-investigated in human pathology and particularly in autism. The presence of Ca in human pathology in subpial spaces and the outer layers of the cortex is a subject of debate. Their roles remain unclear. Therefore and to extend stereological findings of increased glial cell densities in layer II of the PiC, Ca were examined in ASD, TD, ASD+E and E diagnostic groups. It was hypothesized that Ca might be increased in number in the outer layers of the PiC in ASD and E. It was also hypothesized that the amount of Ca would be associated with glial cell densities in the PiC. The main finding of this study was the 82.3% increase in Ca deposits in autism (moderate to severe) compared with TD and E groups. Glial cell densities in layer II of the PiC were positively associated with Ca deposits.

The correlation between Ca and glial cells is perhaps not surprising. It is in line with existing literature on gliosis and Ca found in the same preparations. This suggests that Ca and glial cells are related. Because Ca are thought to mostly accumulate in and originate from reactive astrocytic foot processes in response to cellular stress and neuroinflammation, this could suggest that reactive astrocytes could be contributing to this increase in glial cell densities in autism (Hoyaux, Decaestecker et al. 2000, Nam, Kim et al. 2012). In the TD group, the highest Ca accumulations were seen in the older subjects and consistently with previous reports on the increase in Ca in the cerebral cortex in aging subjects (Keller 2006).

In the chronic E group, only three cases showed high Ca accumulations contrary to what was predicted. Ca deposits are usually noted in preparations from the temporal lobe of TLE patients who had undergone surgery or from post mortem samples and are often noted to accumulate in the granular layer of the hippocampus and also the parahippocampal gyrus (Abel, Hebb et al. 2010). This has been often associated with hippocampal sclerosis. From the E case-notes and histological sections, indeed, Ca accumulations were seen in histological preparations of the hippocampus where there was severe cell loss in the CA1 region. However, no Ca accumulation was noted when there was no cell loss in the hippocampus in these cases suggesting a possible link between cell loss and Ca accumulation. Interestingly, the only case of epilepsy where a degree of cell loss was noted had more Ca in the PiC.

In conclusion, Ca deposits in outer layer I of the PiC and their association with glial cell densities in layer II and to some extent layer III suggest a characteristic changes in ASD and ASD co-morbid with epilepsy. This extends the stereological work and further suggests that glial cells may be mediating a possible neuroinflammatory response in autism early in life.

Chapter 6 Neuropathology of neighbouring regions of the PiC: the olfactory tubercle and the hippocampus in ASD and epilepsy

Neuropathological investigations were extended to include neighbouring areas of the PiC such as the olfactory tubercle (Tu) (anatomically medial to the PiC) and the hippocampus (anatomically ventral to the PiC). This was to test whether the cytoarchitecture of these areas may have been affected by pathology similarly to the PiC and whether signs of pathology such as gliosis and corpora amylacea deposition were extended to these areas. Qualitative analyses of the Tu are presented here and pilot studies on the hippocampus.

6.1 The olfactory tubercle

6.1.1 Introduction

The Tu is a trilaminar paleocortical structure known for its role in the reward system in rodents (Koob 1996, Ikemoto 2007, Lanuza, Novejarque et al. 2008). In autism, dysgenesis of the olfactory bulb and alterations to the mirror neuron system have been suggested to affect the fate of neurons migrating down to the Tu but also to functionally account for observed impairments in social behaviour (Brang and Ramachandran 2010). To the author's knowledge however, the Tu has not been previously assessed in autism in relation to olfaction.

The role of the Tu in olfactory processing is not well established although historically, this area has always been considered part of the olfactory cortex (Economo and Parker 1929, Pigache and SpringerLink (Online service) 1970, Paxinos 1990, Nieuwenhuys, Huijzen et al. 2008). Recent evidence suggests that the Tu may allow for odour discrimination as well as identification of the source of the odour as

opposed to its valence processed by the PiC (Zelano, Montag et al. 2007, Wesson and Wilson 2011). Its role in olfactory perception however remains largely unknown.

Developmentally, the Tu is formed via the convergence of cells from various developmental locations. The lamination of the Tu is achieved in parallel with that of the development of input from the olfactory bulb: this relationship between the olfactory bulb and the Tu remains central in the adult brain whereby newly born cells migrate along this axis to form interneurons in both the Tu and the PiC (Talbot, Woolf et al. 1988, Meyer, Gonzalez-Hernandez et al. 1989). With recent evidence on the neurogenic potential of the human striatum in the adult brain, the characteristics of interneurons in the Tu bordering the ventral pallidum of the striatum have yet to be elucidated (Ernst, Alkass et al. 2014, Wang, You et al. 2014).

Anatomically, in the coronal plane, the olfactory Tu in the human brain is bound laterally by the olfactory tract and the PiC, dorsally by the nucleus accumbens, the nucleus basalis of Meynert and the sub striatal terminal island, and medially by the diagonal band (Mai, Voss et al. 2008, Nieuwenhuys, Huijzen et al. 2008) (see also figure 3.1). The Tu is rich in choline and acetylcholine by virtue of receiving input from the nucleus basalis of Meynert, which supplies the entire cortical mantle (Esiri and Oppenheimer 1996). It is also rich in dopamine as it receives input from the substantia nigra. From rodent studies, the Tu receives monosynaptic olfactory input from the olfactory bulb and the PiC (Johnson, Illig et al. 2000), indirect input from the posteromedial amygdaloid nucleus (Ubeda-Banon, Novejarque et al. 2007) and also projections from the reward systems (nucleus accumbens, substantia nigra). Thus, the Tu is a multisensory area.

In humans, Price et al (1973) noted that the Tu is poorly developed and is less distinctive in primates in general than in rodents (Paxinos 1990, Nieuwenhuys,

Huijzen et al. 2008). Cytoarchitectonically, the organization of the Tu is similar to the PiC. It is hence a paleocortical structure with a superficial cell sparse plexiform layer I formed mostly of small pyramidal cells and interneurons mixed with traces of the diagonal band (Economo and Triarhou 2009). Layer II is usually very dense in formed of relatively large pyramidal neurons (Crosby and Humphrey 1941, Nieuwenhuys, Huijzen et al. 2008). Layer III is a polymorph layer formed of large multipolar neurons and also pyramidal cells and is less dense than layer II (Crosby and Humphrey 1941). Ventrally and also dorsally to layer II, the Tu is home to the characteristic granular cell clusters discovered by Julian Cajella y Sanchez in 1893 and known as the islands of Calleja. Cells in the islands of Cajella almost look like undifferentiated neurons with poorly developed dendritic trees and short unramified axons (Fallon, Riley et al. 1978, Meyer, Gonzalez-Hernandez et al. 1989). The neurons of the islands stain for acetylocholinesterase and cholineacetyltransferase due to neuropil being innervated by cholinergic inputs from the accumbens (Fallon, Riley et al. 1978). Medially to the nucleus accumbens, a large island is noted medially known as the 'masse de cellules granuliformis of Beccari' and overlaying the Tu are large multipolar neurons known as the substantia inominata of Reichert (Hsieh and Puche 2013). Interestingly, and although the Tu is much less developed in the adult human brain, granular cell clusters seem to be more developed and numerous than they are in the much more developed Tu in the rodent brain (Meyer et al, 1989). The functional implications of these developed islands in a vestigial structure are not known.

In light of the above descriptions, this part addresses first a brief anatomical description of the Tu in humans that would contribute to the paucity of anatomical studies on the area. The second part provides a descriptive and qualitative assessment

of this area to test whether gliosis, Ca deposits and any signs of inflammation extend beyond the PiC area to the Tu in autism compared with TD. It was hypothesized that Ca levels and gliosis would be increased in autism compared with TD and that a pattern of neuroinflammation similar to that observed in the PiC would be present in the Tu.

6.1.2 Methods

Qualitative analysis of the olfactory tubercle was undertaken in 28/39 post mortem cases. This was due to the fact that neurohistological sampling was initially designed for the PiC. Given that the Tu was medial to the PiC in the coronal plane, quite often the Tu was available for neuropathological examinations. Slides were scanned using the Aperio e-pathology system (Leica biosystems) and studied over a period of several weeks using image analysis software attached to the scanner (imagescope). Gliosis, satellitosis (presence of more than three oligodendrocytes as satellite cells for a neuron), lamination patterns, ectopic cell clusters, corpora amylacea deposits, granular cell clusters as well as the number of islands of Cajella and their location were investigated across the layers of the Tu. The findings are reported in the section below and are supported by high-resolution photomicrographs. Demographics of existing cases were re-assessed and tabulated (table 6.1).

Table 6.1 Demographics of tubercle cases								
Subjects	**ASD**		**Chronic E**		**ASD + E**		**Comparison TD**	
	5M:3F		5M:2F		3M:1F		4M:5F	
	Mean	**SD**	**Mean**	**SD**	**Mean**	**SD**	**Mean**	**SD**
Age at death (years)	31	14.65	42.57	15.71	30.5	5.2	34.44	27.94
Post-mortem interval (hours)	72	41.57	49.57	34.37	90	12	34.75	21.13
Storage time in formalin (years)	4.69	3.84	19	10.69	4.38	6.45	14.19	5.86
Mean fixed brain weight (grams)	1454	172.59	1471.71	147.15	1445	299.48	1493	108.6
Hemisphere	7L:1R		5L:2R		3L:1R		5L:3R:1 n/k*	
Brain bank of origin								
Harvard	0		0		0		1	
NICHD	0		0		0		1	
TWOBC	8		7		4		7	
Total Number	8		7		4		9	

Demographics of olfactory tubercle shown as means (SD) for age at death in years, the post-mortem interval in hours, storage time of tissue in formalin prior to sampling for processing in years and the fixed brain weight post-fixative in grams. A parametric one-way ANOVA (Levene's test for all independent variables respected with $p>0.05$) with post-hoc Bonferroni correction when significant differences existed shows no significant differences between groups for age ($F=0.53$, $df=3$, $p=0.668$), and brain weight ($F=0.07$, $df=3$, $p=0.98$). Storage in formalin duration was significantly different between groups ($F=4.88$, $df=3$, $p<0.01$) as well as PMI times ($F=3.72$, $df=3$, $p<0.05$). Post-hoc testing showed that the ASD+E PMI was longer than the TD group. The ASD+E and ASDE spent also significantly less time in formalin compared to the E and TD groups.

**n/k*: a paraffin-embedded control case from the institute of psychiatry (IOP) at King's College London. M: male; F: female; L: left; R: right; NICHD: Eunice **n/k*: hemisphere not known for one case. M: male; F: female; L: left; R: right; NICHD: Eunice Kennedy Shriver National Institute of Child Health and Human Development.

6.1.3 Results

Anatomical studies showed that the trilamination pattern of the Tu described in the literature is not always easily identifiable in human tissue particularly for layer II (figure 6.1). Islands of cells were not always dorsal to layer III but could also be dorsal to layer II (figure 6.1). The shapes of the cell clusters varied and so did the size and morphology of the cells within (figure 6.2). Generally, islands of cells were large and ring-like with a cell-free centre and sometimes were more diffuse and amorphous (figure 6.2). The cell size and morphology also differed with often small granular cells and sometimes larger ones intermingled with small pyramidal cells (figure 6.1).

Lamination patterns between patient groups particularly for layer II appeared to be denser in autism compared to TD and E although stereological quantification of cell density would be necessary to confirm this (figure 6.3).

Ca deposits became less dense generally in autism further medially near the plexiform layer of the Tu. This sometimes (not always) corresponded with the presence of glial fibres, contrary to predicted (figure 6.4).

More glial cells around layer I of the Tu were seen in ASD and ASD+E but not in the TD and E cases (figure 6.5). This extended to layer III. It was difficult to ascertain the type of these cells however without immunohistochemistry. Unlike the PiC, these cells had the morphology of oligodendrocytes (darkly stained nucleus) rather than astrocytes (binucleated very lightly stained cells) or microglia (rod-shaped) (figure 6.6). In some cases of autism, satellitosis was observed in layers I and III of the Tu. In one particular case of ASD+E, signs of inflammation were obvious with reactive astrocytes and microglia present in the plexiform layer and the polymorph layer of the Tu (figure 6.6). Findings are summarized in table 6.2.

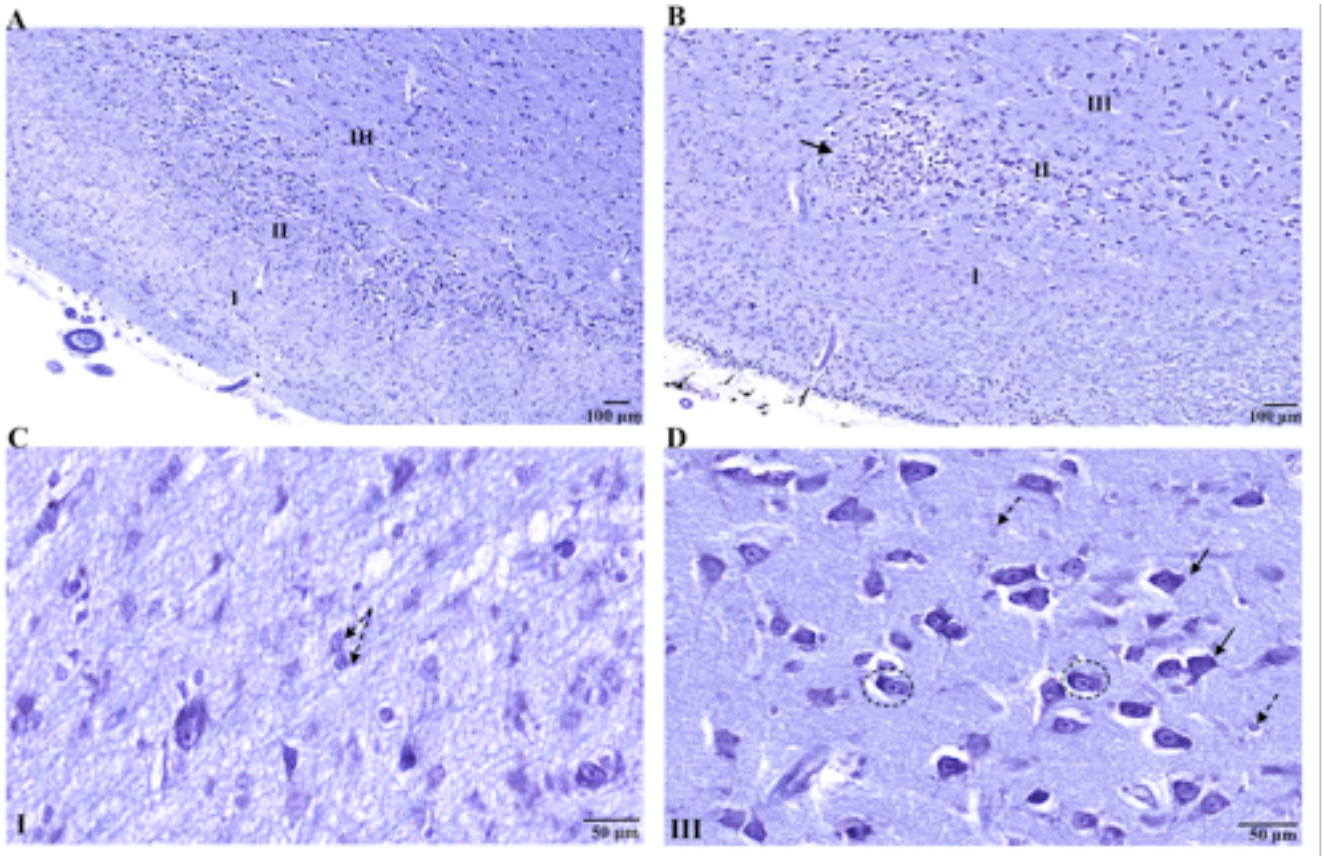


Figure 6.1 Trilamination of the tubercle. This shows in (A) the trilamination in a control case (dorsal top and left is medial). In (B), a ventral cell cluster is shown with the arrow between the pyramidal and plexiform layers. In (C) and (D), 20X magnification in the plexiform (layer I) and polymorph (layer III) layers. Dark arrows show multipolar neurons, dotted arrows show glial cells and non-pyramidal cells are represented in the dotted circles.

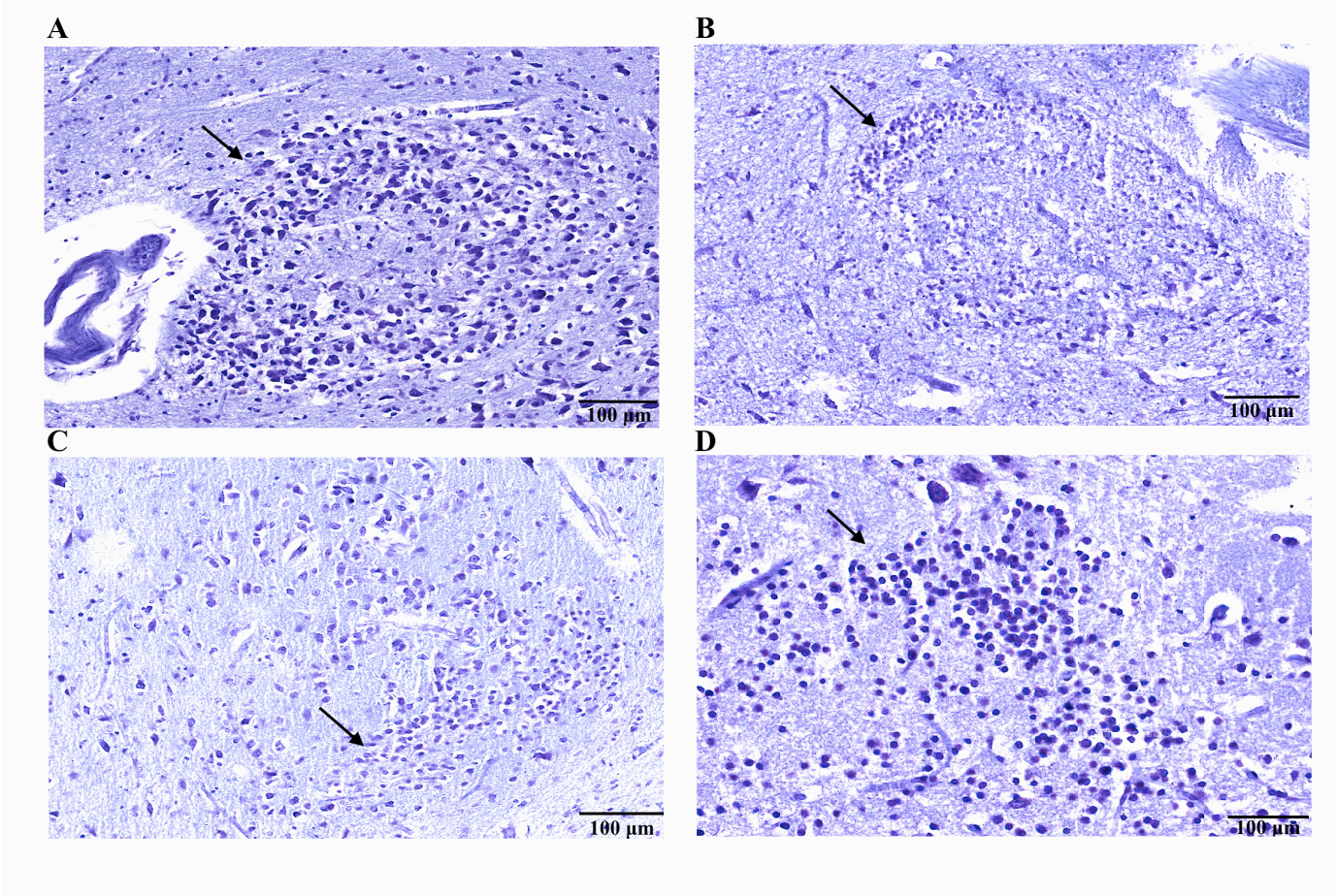


Figure 6.2 Variability in cell clusters. (A) is a case of ASD with ring like islands and (B) is a semi-arched shape in epilepsy. Bottom panel is from ASD individuals. Cell size and cell morphology are variable.10X with left of the figures medial and top is dorsal.

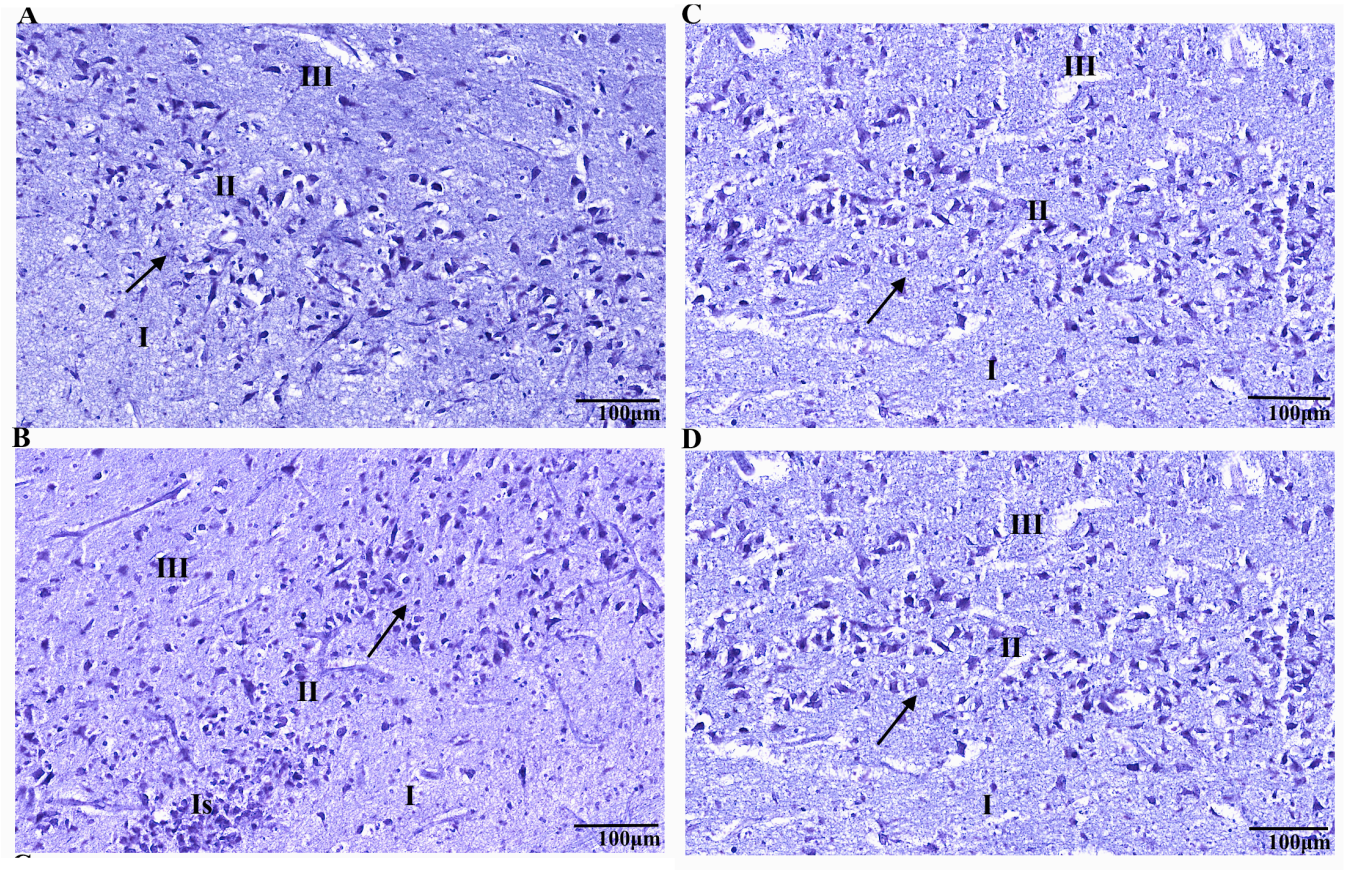


Figure 6.3 Cell densities in layer II of the tubercle. This shows density of cells in layer II in TD (A), ASD (B), E (C, D). Cells seem smaller in ASD and denser than in TD. The black arrow indicates layer II. *Is*: ventral island, representing clusters of cells in (B). Photos were taken at 10X.

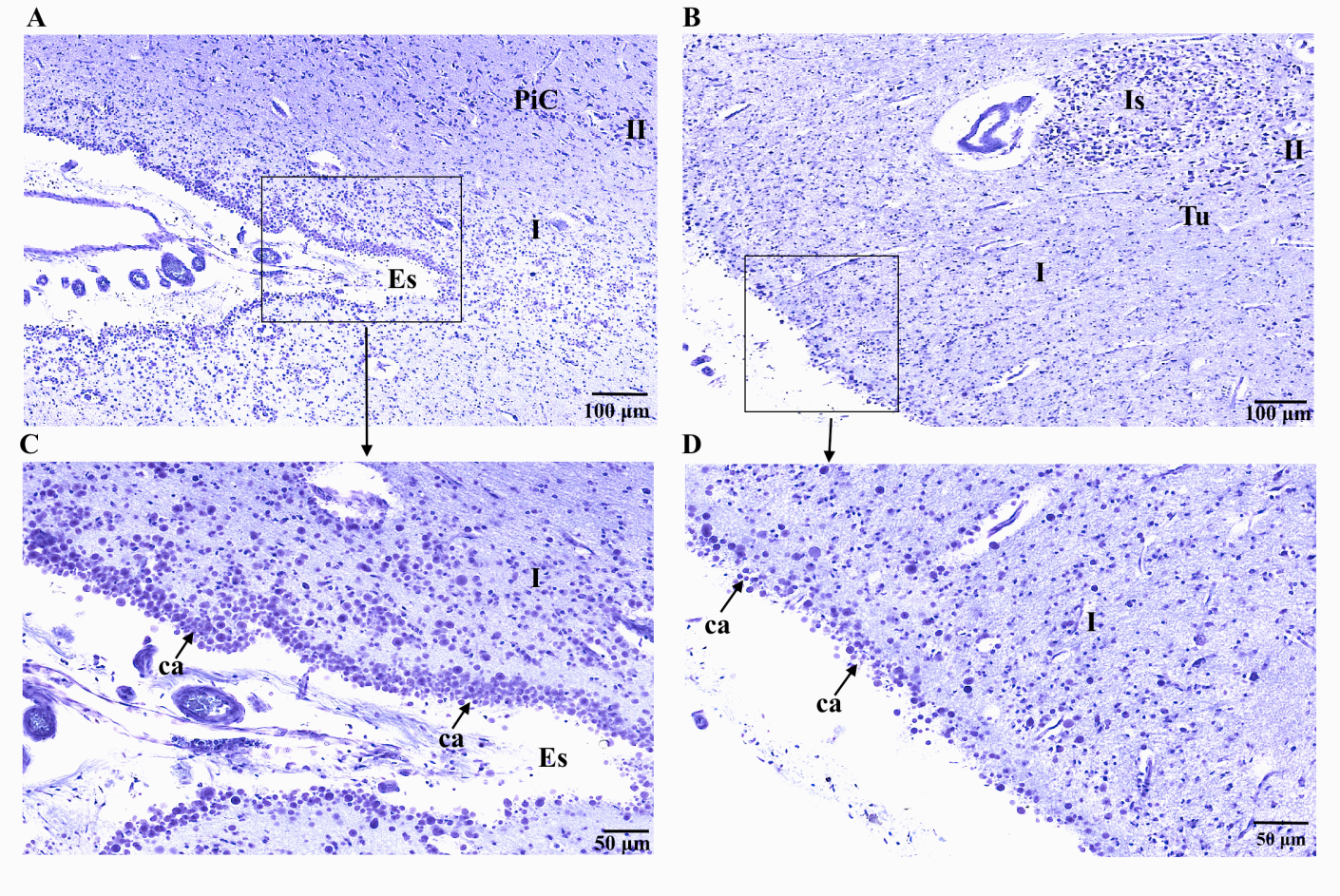


Figure 6.4 Ca deposits in the Tu in autism. (A), (B), (C) and (D) show the plexiform layer I covered with Ca in the PiC (A) & (C) and the Tu (B, D). (A) & (B) are taken at 4X, (C) & (D) are taken at 10X. The arrows point out to a magnified view of the selected area. Top of each figure is dorsal and left is medial. (B), (D) are medial to the PiC. *ca:* corpora amylacea*, Es*: entorhinal sulcus, *Is*: island of cells, *PiC*: piriform cortex; *I, II, III*; layers I, II and III.

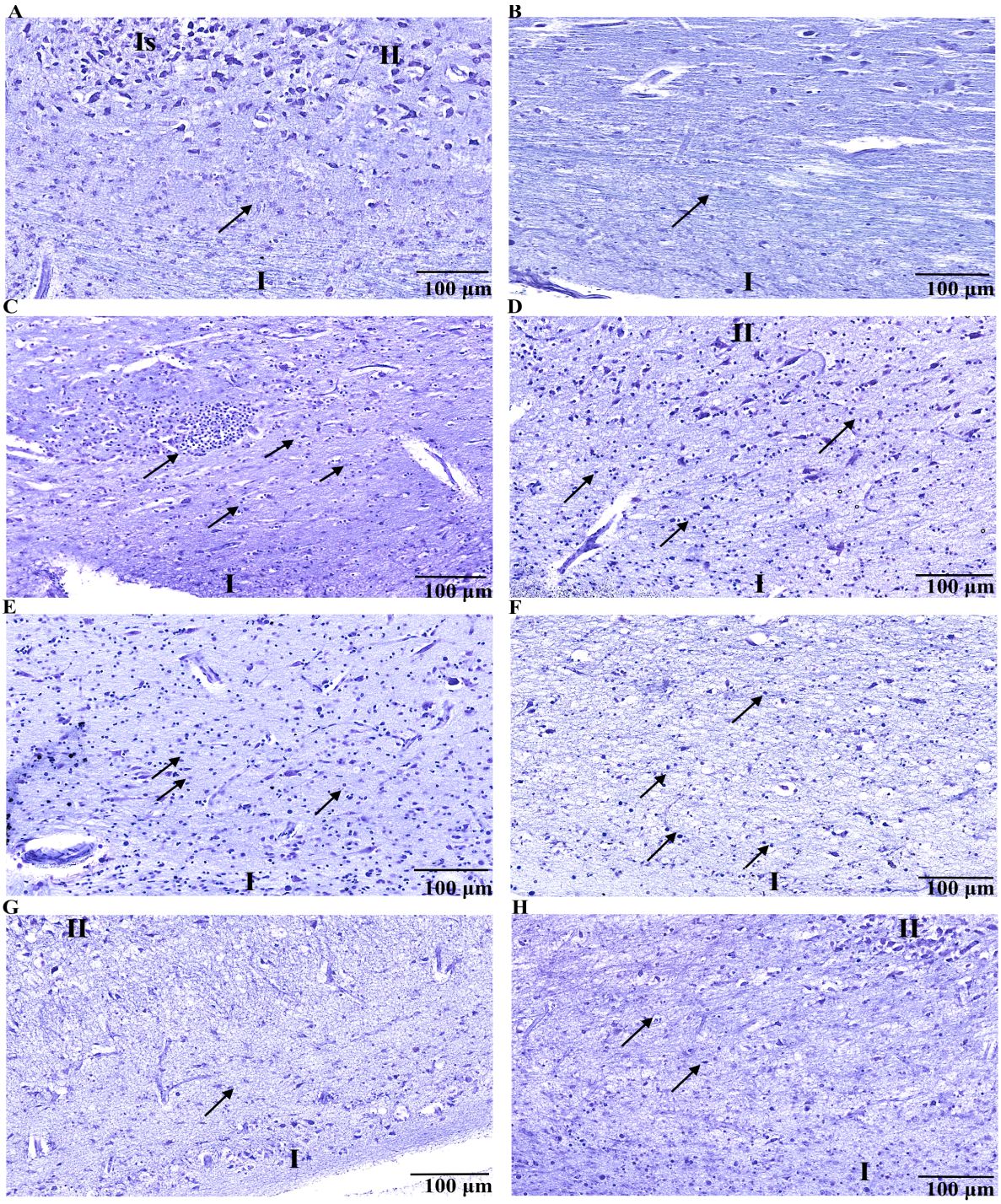


Figure 6.5 Glial cells in the tubercle. The figure above shows increased presence of glial cells in 4 cases of ASD (C, D) and ASD+E (E, F) compared to TD (A, B) and E (G, H) in the plexiform layer of the Tu (layer I). In (C), a glial nodule can be seen. Black arrows indicate the presence of darkly stained glial cells. Top of each figure is dorsal and left is medial. *I* represents layer I and when visible, layer II is indicated. *Is*: island of clusters of cells ventral to layer II.

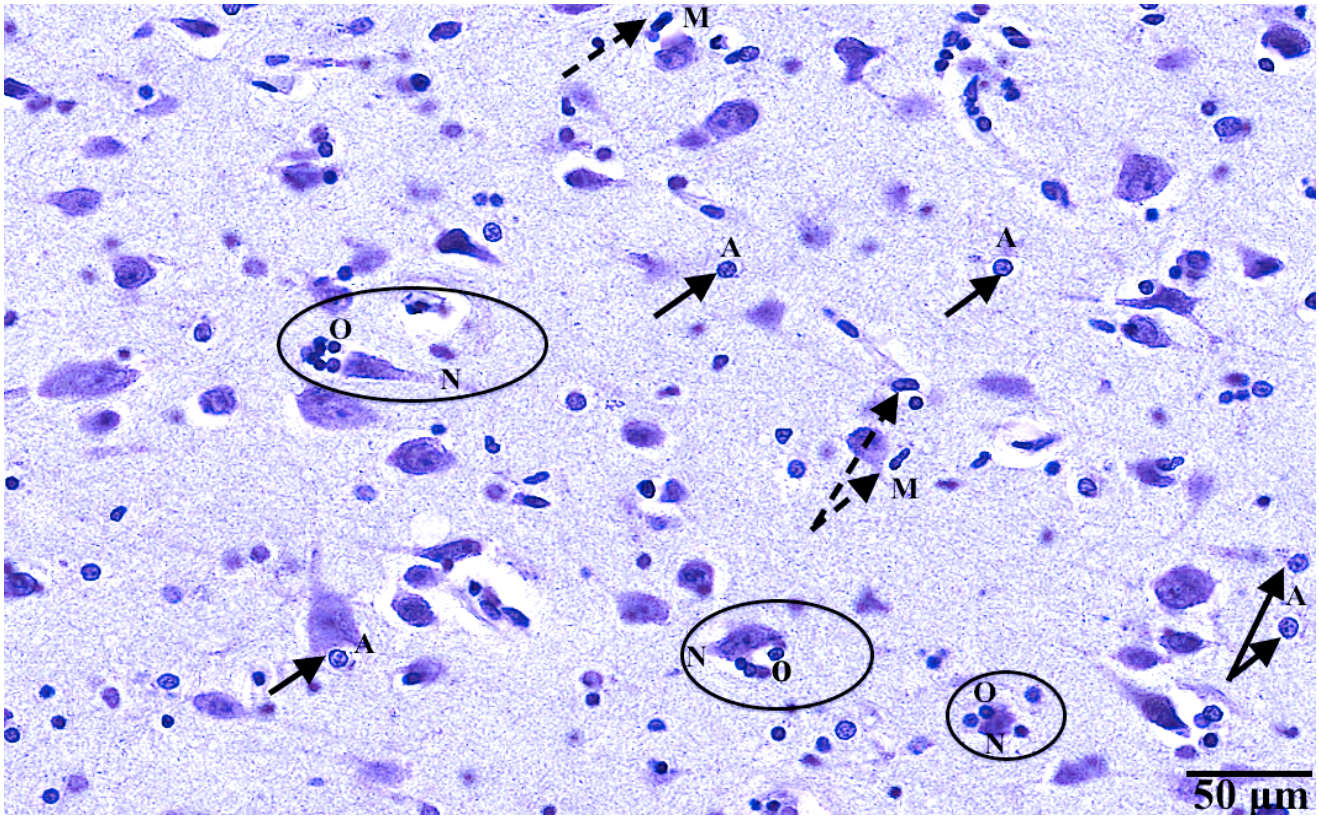


Figure 6.6 Satellitosis in an autism and epilepsy case. Case of ASD+E showing satellitosis of a neuron by oligodendrocytes in the polymorph layer (layer III) of the Tu adjacent to layer III of the PiC. Satellitosis is shown by the black circles around one neuron (N) and oligodendrocytes (O). Astrocytes can also be seen (A) and microglia (M). Photo was taken at 20X magnification. Top is dorsal and left is medial.

Table 6.2 Pathological findings from qualitative analysis of the olfactory tubercle in ASD, ASD+E, TD and E.

Diagnosis	Pathology				
	Lamination	**Gliosis**	**Corpora amylacea**	**Granular cell clusters**	**Other features**
TD (n=9)	Layer I: plexiform, Layer II: sometimes a dense layer though short, sometimes long and diffuse and less dense. Layer III: polymorph and has multipolar cells	Observed in only one case	Mild - moderate deposits observed in two cases. In these cases, deposits were more severe closer to the PiC. They disperse further medially in the frontal area	Cell clusters/islands in all cases around layer III. Three to five islands can be seen. Dorsal islands have a halo and fusiform neurons entering the islands.	NB of Meynert is visible dorsally and medially. The substantia perforata anterior is also visible in seven cases.
ASD (n=8)	Trilamination is obvious in three cases and less clear in others A single case has a layer II that undulates dorsomedially and is patchy and discontinuous.	Tu is generally gliotic in seven cases with five cases being severe. Gliosis becomes prominent more dorsally.	Much lower Ca deposits compared to PiC area. Ca levels dropped in all cases frontomedially .	Islands and granular cell clusters are more diffuse with smaller cells and they numerous (5-7) compared to TD.	Satellitosis in three cases. Ring-like islands of cells in one case.
ASD+E (n=4)	Trilamination particularly between layers II and III is sometimes lost	Very gliotic in except one case, which showed moderate gliosis.	Ca deposits are less severe than in the PiC/entorhinal area and go as deep as layer II in one case.	Islands are lower in number and granular cells are small in size. (3-4)	In one case, microgliosis and gliosis in layer I of the tubercle and one case has satellitosis with large neurons.
E (n=7)	Trilamination is visible sometimes	Two of the cases have mild gliosis in layer I and II of the tubercle	One case has very dense Ca in layer I	3-4 islands and one case has no islands/remnants of islands.	Semi-arched islands in one case

6.1.4 Discussion

The studies above demonstrated first that the anatomy of the olfactory tubercle is much more challenging to delineate in human tissue without a full 3D-reconstruction of the structure done through antero-posterior mapping of the Tu in a few TD cases of various age ranges. Furthermore, luxol fast blue counterstained with Nissl would be necessary to determine the dimensions of the Tu, its anatomical boundaries and to address inter-individual variability in the anatomy. A stereological study would be appropriate to measure cell densities in the Tu and to investigate the type of molecular marker that neurons and glial cells in particular express. This was however beyond the scope of this thesis.

Pathological examination of the Tu showed that, in autism, Ca deposits decreased medially to the PiC area near the plexiform layer of the olfactory Tu. This was not predicted. Though Ca deposits in the PiC were associated with the presence of pathological glial fibers from astrocytes in layer I, this was not always the case in the Tu. It was recently shown that the striatum is an area of adult neurogenesis (Ernst, Alkass et al. 2014). Therefore, it may be suggested that possibly the turnover of cells in this area may account for the lesser densities of the Ca, which are deposits associated with locally chronic inflammatory processes (Nam, Kim et al. 2012). Immunohistochemical staining of astrocyte, oligodendrocyte, microglial and neuronal-specific proteins in the Ca deposits around the Tu area would be necessary to assess the origins of these Ca. Interestingly, more oligodendrocyte-resembling cells in the Tu were observed in autism cases also around layer I. Immunohistochemical staining of these cells would be also necessary to ascertain whether they are glial or neuronal in origin. Though cell densities appeared to be denser in layer II in some cases of autism, it would be appropriate to also quantify these stereologically to get an

accurate estimate of the density in this novel area. Increased neuronal cell densities are indeed consistent with findings on increased cell packing densities in the cortex of autism cases (Courchesne, Mouton et al. 2011)

Based on these preliminary findings, pathological inflammation encountered in the PiC area does not seem to extend to the same degree to the Tu. This may be because the Tu is involved primarily in the reward system whereas the PiC is primarily an olfactory area. This may further support the investigation of olfactory dysfunction in autism, where pathological changes may be more specific to the PiC area. However, stereological quantification methods are necessary to investigate layer-specific densities as qualitative analyses alone are not sufficient to determine whether cell densities have changed in the Tu compared with the PiC in autism. Finally, measuring cell size in layers of the PiC, cortical thickness and layer depth measurements as well as characterization of pathology using immunohistochemistry are required to investigate further the neuroanatomy and neuropathology of this area of the brain in autism and the implications of cytoarchitectural changes on function.

6.2 The hippocampus pilot studies in ASD

6.2.1 Introduction

Some memory functions in autism such as temporal order memory, source memory and working memory are impaired in adolescents and children with autism whilst short and long-term recognition are sometimes spared (Bennetto, Pennington et al. 1996, Taylor, Donner et al. 2012). Reduced right hippocampal activation using fMRI was demonstrated in young children with ASD in working memory tasks (Taylor, Donner et al. 2012). Interestingly, the autism valproate model shows enhanced spatial memory correlating positively with neuronal cell densities in all hippocampal subfields (Edalatmanesh, Nikfarjam et al. 2013). The hippocampus is where working memories are transferred into long-term storage engrams (Duvernoy, Cattin et al. 2013). Given its fundamental role in memory formation alongside the frontal cortex, the hippocampus has attracted a considerable number of neuropathological studies to investigate cytoarchitectonic changes that might be associated with differences in memory performance in autism compared with the typically developing population. Increased cell-packing neuronal density in all CA subfields and the subiculum as well as reduced pyramidal cell size in post-mortem cases of infantile autism has been previously reported (Kemper and Bauman 1993, Kemper and Bauman 1998). A study by Bailey et al (1998) however showed in 5 post-mortem cases of ASD that there were no signs of increased neuronal densities in the various CA regions contradicting the Kemper study (Bailey, Luthert et al. 1998). A Golgi-staining study of the CA1 and CA4 neurons showed decreased dendritic arbours in autism (Raymond, Bauman et al. 1996). Thus, it is unclear whether cell density changes in the hippocampus are increased or decreased.

Similarly to the PiC, the hippocampus is also an epileptogenic structure in humans and rodents and it has attracted a lot of research into autism mainly because of the co-morbidity of autism cases with epilepsy. Interestingly, the different CA regions of the hippocampus have different resistances to seizures: whilst the CA3 neurons are highly resistant, the CA1 and CA4 neurons tend to be less resistant and more vulnerable and cell loss is often characteristic of these areas in epilepsy (Thom 2014). A recent study by Papadakis et al (2013) demonstrated that neurons that survived hypoxic insults showed increased levels of the hamartin protein in the CA3 region, thereby suggesting one molecular mechanism by which neurons may resist seizures (Papadakis, Hadley et al. 2013). Lawrence et al. (2010) showed that GABA-ergic CB interneuronal densities in autism were reduced in the dentate gyrus and the CA4 whilst CR interneuronal densities in the CA1 and PV interneuronal densities in the CA1 and CA3 were increased in autism compared with controls (Lawrence, Kemper et al. 2010). Overall, the consensus on the cytoarchitectonics of the hippocampal formation is far from established. Two subfields, the CA1 and CA3 areas were chosen here for analyses given the difference in their vulnerability to seizures. Pyramidal, non-pyramidal and glial cell densities were quantified. It was hypothesized that in the CA1 and CA3 areas, pyramidal, non-pyramidal and glial cell densities would be increased in autism compared with the TD population. It was also hypothesized that in E, increased glial cell densities would be observed in the CA1 and CA3 and decreased neuronal cell densities in the CA1 area compared to the CA3 area. For reasons of time limitations, only the pilot studies and the stereological sampling strategy were undertaken and are presented here.

6.2.2 Methods

6.2.2.1 Neurohistological sampling and hippocampal anatomy

Post-mortem cases were selected as previously specified (same as the PiC). Consent to use tissue in medical research was granted in conformity with existing hospital and coroner's procedures. The temporal lobes were cut into 5-mm-thick coronal slices and the full hippocampus was available for histological analyses. Each block was embedded in paraffin wax, and 2 x 25-µm-thick sections were cut from the anterior face, mounted onto coated slides, stained with Nissl-stain and coverslipped for the pilot studies.

The anatomical boundaries of the hippocampal formation in humans are very well established. The hippocampus is located in the medial part of the temporal lobe and it forms the medial wall of the lateral ventricle in this area. The hippocampal regions are the dentate gyrus and the CAs divided into four regions designated by CA1 to CA4. The CA1 region fuses with the subiculum, which is connected to the entorhinal cortex onto the parahippocampal gyrus of the temporal lobe (Duvernoy, Cattin et al. 2013)

Hippocampal afferents are mainly from the septum and hypothalamus via the fornix and from the adjacent entorhinal cortex. Outputs from the hippocampus pass primarily through the fornix and a large number of projections feed back to the entorhinal cortex (Duvernoy, Cattin et al. 2013). The structure of the hippocampus and its components are illustrated in figure 6.7.

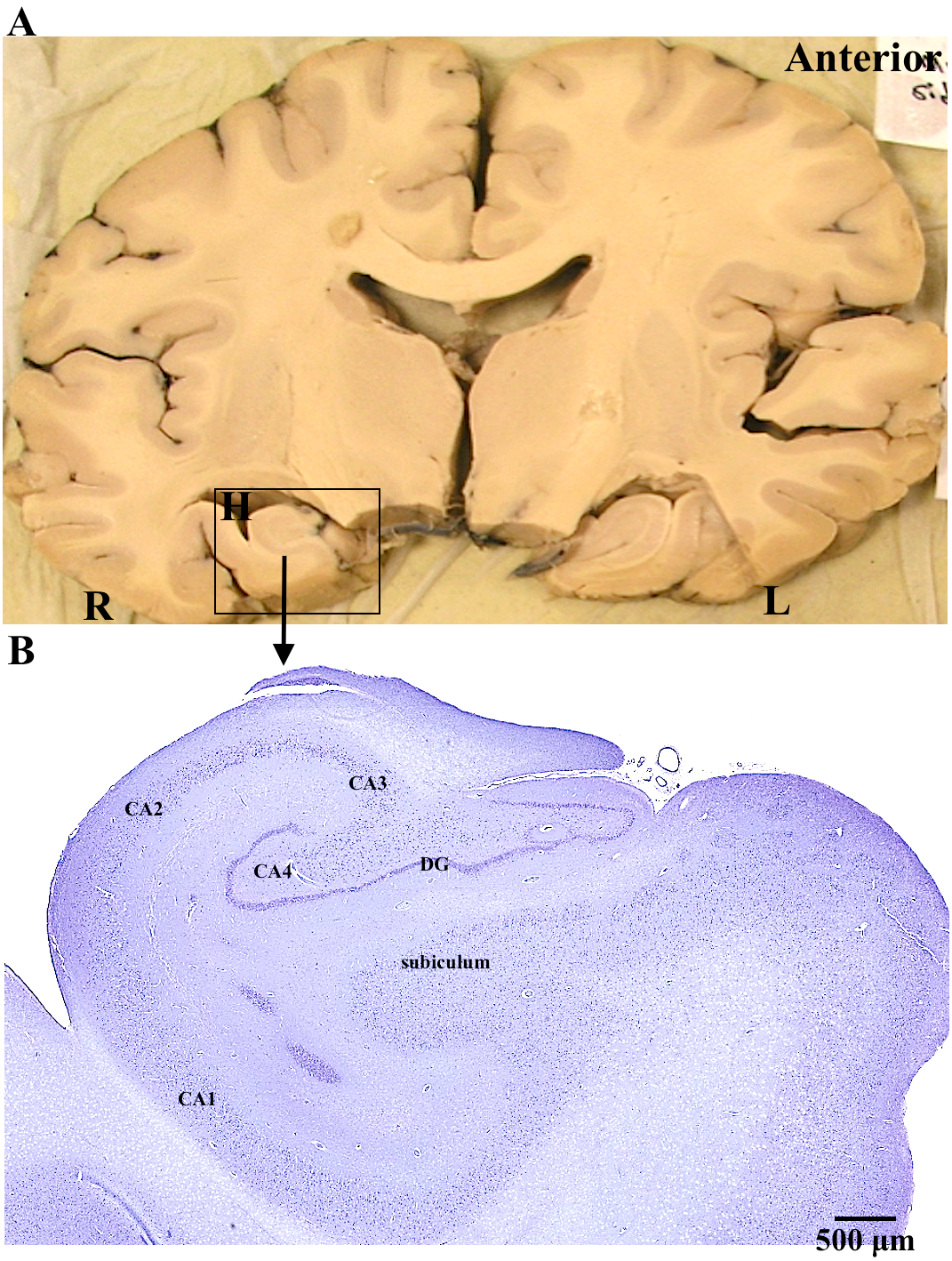


Figure 6.7 Sampling of the hippocampus. Neurohistological sampling of the hippocampus from the right hemisphere in a coronal slice showing in (A), the right hippocampus on the anterior side of the slice. (B) shows cresyl violet staining and photo at 0.5X of the right hippocampus with the 4 cornu ammoni (CA1, CA2, CA3 and CA4) and the dentate gyrus (DG). Top of the photo is dorsal and left is lateral.

6.2.2.2 Pilot stereological studies

For neuronal densities, it was established that the counting grid should be calibrated at 90 μm x 90 μm to count on average 1 to 3 cells per counting box in the CA1 and CA3 subfields of the hippocampus. For glial densities in the hippocampus, the counting grid dimensions were established to be 50 μm x 50 μm across all the subfields. The counts were done on a microscope with a high-numerical aperture (NA = 1.4) and with oil-immersion.

General counting rules involved counting cells at a 60X magnification. To view all the cells in a counting box, the focus was changed at least three times to make sure all the cells come into view and are counted per counting box.

Definition of counting cells in the hippocampus

A neuron is defined as a large pyramidal cell in the CA1 to the CA3 regions. The neuron is more triangular-shaped in the CA4-region with Nissl-substance in the cytoplasm and a vesicular nucleus containing a prominent nucleolus. A granular cell is a small round neuronal cell in the dentate gyrus. A glial cell is defined as a cell with a nucleus that is globular (astrocyte) and has a pale staining or ellipsoid/rodlike (microglia) across all the subfields (see figure 6.8 below).

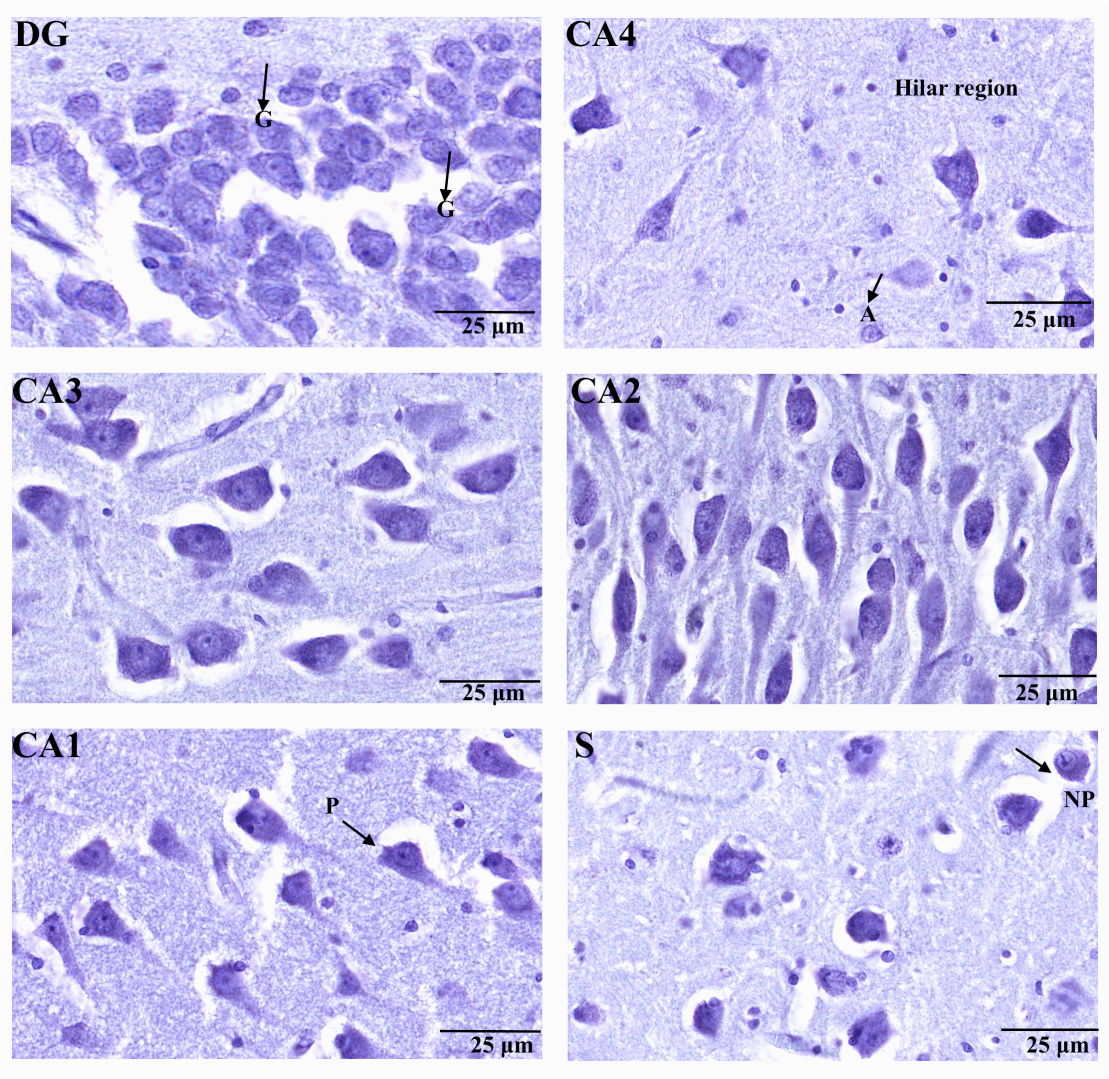


Figure 6.8 Cell morphologies in hippocampal subfields. Different neuronal morphologies can be seen in the hippocampal subfields and the dentate gyrus. *A*: astrocyte, *G:* granular cell; *NP*: non-pyramidal cell; *P*: pyramidal cell. Photos taken at 40X.

Definition of neuron-containing layers of the hippocampus

For the definition of the neuron counting layers of the hippocampus, Duvernoy's (1988) descriptions are used. Neuronal and glial cell densities were determined for the neuronal cell layer of CA1, CA2, CA3, CA4 and the granular layer of the dentate gyrus. The pyramidal cell layer of the CA1 is situated between the subiculum and the

CA2 medial to the temporal horn of the lateral ventricle. In control hippocampus, CA pyramidal cells are triangular, smaller and less densely packed than those of CA2. The transition zone between subiculum and CA1, and CA1 and CA2 was marked by a change in the width of the pyramidal cell layer which was relatively easy to identify between CA1 and CA2 but more difficult and arbitrary for the transition with between CA1 and the subiculum. The pyramidal cell layer is densely packed and neurons are large in CA2. However, the neuronal layer in CA2 is characteristically narrow. The transition between CA2 and CA3 is not clear from the control slides and therefore, the delineation was arbitrary. CA4 is formed of nerve cells that are rather large, ovoid and more loosely arranged than the neurons in CA1, CA2 and CA3. As part of the CA3 enters the hilar region (CA4) and also, the proximity between the CA4 neurons and the granular layer of the dentate gyrus, at least one counting box distance of 90 μm was set to avoid counting neurons from the CA3 or the dentate gyrus as part of the CA4 neuronal counts. The granular cell layer was easy to identify as densely packed round nerve cells around the hilus.

Number of counting boxes to determine cell densities in the hippocampus

As a pilot study, it was important to establish the number of counting boxes required to determine the cell densities in the different hippocampal sub-regions. For this purpose, three control hippocampal sections were chosen to carry out the study. The CA1 region was chosen to calculate the neuronal densities using 10, 25, 50, 100 and 200 counting boxes. A 90 μm x 90 μm acetate grid was superimposed on the screen for the neuronal counts and a 50 μm x 50 μm acetate grid was superimposed on the screen for the glial cell counts. The Axiovision stereology software moves the counting boxes systematically according to defined distances between probes (150 μm

x 150 μm) and a z-depth of 20 μm. Counting was done at 60X magnification and the counting box was moved systematically along CA1 by switching to lower magnification (10X) then going back to 60X to do the cell counts in the new area.

Neuronal and glial cell densities were calculated in cells per square millimeter and then converted to cubic millimeter (see below). The number of counting boxes to determine the cell density in the hippocampus subfields was 50. Cell densities were quantified as specified previously.

Table 6.3 – CA1 Neuronal Cell Density

Counting boxes	**Neuronal Density/unit area**		**Neuronal density/unit volume**	
(n = 3)	**Mean (mm^{-2})**	**SD**	**Mean (mm^{-3})**	**SD**
200	468	63	18717	2532
100	455	46	18206	1838
50	391	44	15655	1761
25	527	71	21080	2854
10	475	74	19019	2962

This shows the mean neuronal density in CA1. The mean is calculated by adding the densities obtained in three sections for the same number of counting boxes and then dividing by the total number of sections (n =3). ND1 is neuronal density per unit area and ND2 is neuronal density per unit volume. SD1 is the standard deviation from the mean ND1 and SD2 is the standard deviation from the mean ND2.

Table 6.4 – CA1 Glial Cell Density

Counting boxes (n = 3)	Glial Density/unit area		Glial Density/unit volume	
	Mean (mm^{-2})	SD1	Mean (mm^{-3})	SD2
200	608	59	24307	2352
100	618	75	24733	3003
50	588	41	23507	1641
25	576	102	23027	4077
10	571	29	22853	1171

This shows the mean glial density in CA1. The mean is calculated by adding the densities obtained in three sections for the same number of counting boxes and then dividing by the total number of sections (n =3). GD1 is glial density per unit area and GD2 is neuronal density per unit volume. SD1 is the standard deviation from the mean GD1 and SD2 is the standard deviation from the mean GD2.

6.2.3 Conclusion of the pilot study

Finally, this pilot study determined how many counting boxes were required to obtain a representative density in the CA1 region. This would be applicable also to the CA3 region given the proximity in cell densities in TDs in both regions. The next stage would be would be to quantify cell densities in all cases using the above design.

In conclusion, the above studies set the stage for further investigations of the neuropathology of both the tubercle and the hippocampus in ASDs in order to determine whether cytoarchitectonic changes might correspond to symptomatology.

Chapter 7 Magnetoencephalography studies of autism spectrum disorders

Thus far, the neuropathology and detailed neuroanatomy of the piriform cortex were investigated in autism and epilepsy. Post-mortem studies of this primary sensory area involved in olfactory processing showed changes in glial cell densities in autism. The neuropathology also showed associations between pathological deposits in the PiC area and glial cell densities. The neuropathology of the olfactory tubercle was also assessed and interestingly, the local changes seen in the PiC did not seem to translate to the tubercle although this needs further investigation. Pilot work was also presented on both hippocampal cell cultures and post-mortem human hippocampal tissue. Post-mortem and *in vitro* investigations are invaluable for assessing the cellular constitution of areas of the cerebral cortex. However, they do not allow us to investigate function in living cells. A substantial level of complexity is added when many cell populations of the cerebral cortex are activated simultaneously to ensure that a sensory function is carried out properly. In response to a visual stimulus for example, neurons of the primary sensory visual areas located in the occipital pole synchronize their firing to an oscillatory mode in the gamma band above 30 Hz hence supporting object recognition (Tallon-Baudry and Bertrand 1999, Singer 2001). In this part of this thesis, the neural correlates underlying superior processing in the visual sensory domain in ASD are investigated in MEG recordings. First, an overview of the relevant technology is presented followed by a discussion of the putative roles of gamma oscillations in health and disease.

7.1 Magnetoencephalography: An overview

Magnetoencephalography (MEG) is a non-invasive technique that enables us to record brain activity with a high temporal resolution of less than a millisecond and with relatively good spatial resolution of a few millimetres. Magnetic fields are generated by post-synaptic currents flowing in neurons firing in response to a stimulus (Braeutigam 2013). Field changes are detected and amplified by superconducting quantum interference devices (SQUID) that respond to changes in magnetic flux captured by the pick-up coils (Vrba and Robinson 2001).

MEG is preferentially sensitive to tangential currents in the sulci that generate magnetic fields that reach the surface of the head unlike radial currents in the gyri seen in EEG recordings for example and that do not reach the surface (Ahlfors, Han et al. 2010). Magnetic fields generated by single nerve cells are too weak to be measured outside the head. Typically, detectable field changes require thousands of neighbouring neurons to carry aligned currents of suitable strengths and duration to allow for spatial and temporal summations (Plonsey 1982). The main sources of magnetic fields are from postsynaptic currents flowing through the apical dendrites of cortical pyramidal cells rather than currents associated with action potentials or other electro-chemical processes (Plonsey 1982).

Pick-up coil configuration determines what the detector is measuring with a simple planar coil measuring magnetic field changes perpendicular to the plane of the coil, and a figure-of-eight-shaped coil measuring changes in the spatial field gradient (Schwartz, Edgar et al. 2010). The SQUID transforms the magnetic fields into electrical voltages. The Oxford Human Brain activity centre MEG scanner used in this study is in a magnetically shielded room (see figure 7.1). Magnetic fields are recorded with a helmet-shaped array of 102 SQUID devices with each 3 pick-up coils

hence forming 306 channels around the head. Two first-order planar gradiometers are mostly sensitive to tangential neuronal currents flowing in the region below the device and henceforth allow the measurement of two orthogonal spatial gradients of the magnetic field in the longitudinal and latitudinal directions. The magnetometer coil is more sensitive to the deeper sources and the distance between cortex and detector is about 4-5 cm (Braeutigam 2013).

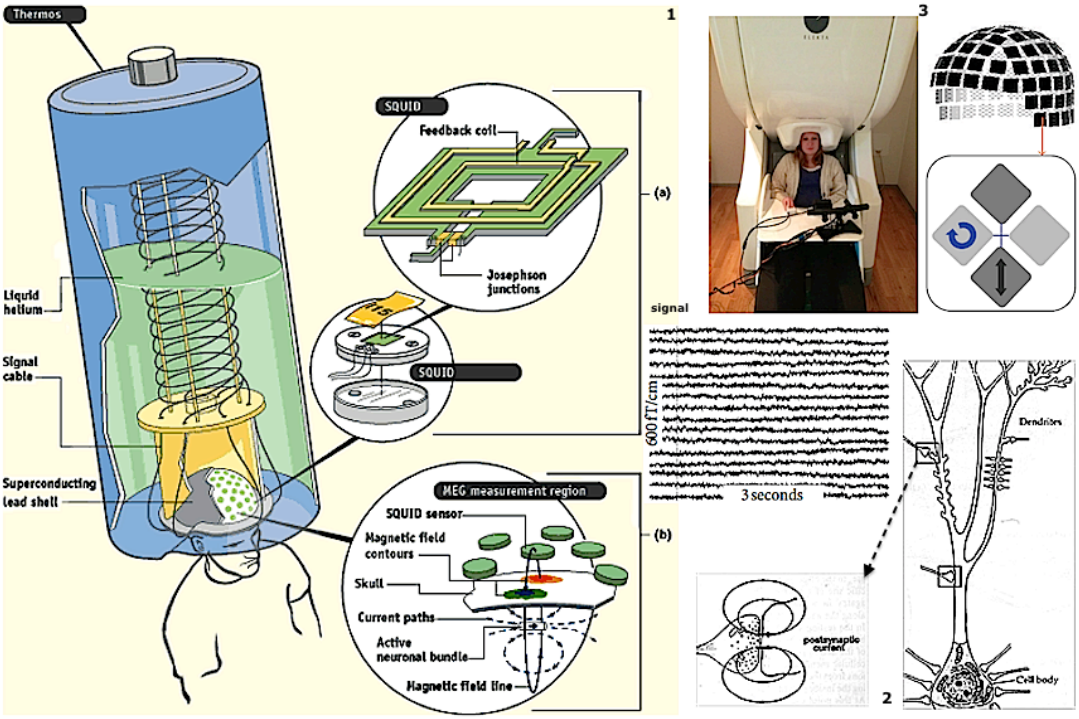


Figure 7.1 MEG measurements. This figure has been modified from Braeutigam (2013) (Braeutigam 2013) and (LLC 2008). (1) This shows a schematic representation of the MEG helmet array of SQUID sensors operating at the temperature of liquid Helium (-269°C). The coil contained within each SQUID sensor receives brain fields and is coupled magnetically to the SQUID, which produces a voltage proportional to the magnetic field received by the coil. Part a) in (1) shows the SQUID superconducting region in green and two Josephson junctions with electrical resistance allowing the measurement of voltage proportional to the magnetic flux of the SQUID square hole. The feedback coil shown couples magnetically the SQUID to

the pick-up coil in the SQUID sensor. (b) This shows the magnetic field produced by neuronal brain currents with the red region showing the strongest field in the direction that is out of the skull and the blue region showing the strongest field in the direction that is towards the skull. (2) This shows that postsynaptic currents are carried along the apical dendrites of cortical pyramidal cells. (3) This shows the OHBA MEG scanner used in this study with the 102 detector helmet-shaped array with two-first order gradiometers (diamonds) measuring magnetic field gradients along perpendicular directions and one magnetometer (grey coil) measuring the magnetic field. Signals obtained from MEG recordings show the magnetic field or gradient as a function of time for 16 channels (Elekta Neuromag, OY, Helsinki).

7.1.1 Artefact correction

Once MEG data are collected, one proceeds to correcting signals from physiological artefacts such as heartbeats and eye-blinks. Head movement is also accounted for and artefacts due to head position are removed from the traces (Braeutigam 2013). Finally, implanted materials also interfere with MEG tracings by generating non-physiological magnetic fields in situ that affect the signal. There are no universal methods to correct for these artefacts. However, reliable MEG-data might still be obtained with in-house methods of correction (Carrette, De Tiege et al. 2011).

7.1.2 Source localization

This section is only included here for thoroughness of MEG methods. All source estimation methods are based on the theory of electromagnetism governed by Maxwell's equations that relate the spatial and temporal derivatives of the electric and magnetic fields to the charges and currents identified within a specific volume that

has its own geometry, magnetic permeability and electric permittivity (Braeutigam 2013). However, major challenges arise when attempting to localize the neural generators of the signal recorded by the detectors. The first challenge is known as the 'forward problem', which relates to the calculation of the magnetic field numerically or analytically by knowing the properties of the milieu as well as the traversing currents (Jackson 1963, Wendel, Vaisanen et al. 2009). This precedes any source localization analyses. The second challenge is known as the 'inverse problem' and mainly regards the estimation of intra-cranial current sources from extra-cranial MEG recordings (Garnero, Baillet et al. 1999). The root of the inverse problem stems from the fact that silent yet neurophysiologically relevant currents may not be recorded by the detectors even if we increased the number of channels or improved the quality of the data. Typically, the inverse problem is addressed through a simplification of the description of the sources and by posing physiologically relevant assumptions (Braeutigam 2013). Imaging techniques, equivalent current dipole methods and beamforming can be used to address the inverse problem but are beyond the scope of this thesis and therefore will not be discussed (Hansen, Kringelbach et al. 2010).

7.1.3 Analytical tools

MEG recordings provide readings of the variation in time of magnetic fields generated by brain electrical activity detected over the head. Event-related fields and time-frequency analyses of oscillatory activities are two analytical approaches that are discussed below and that are relevant in the context of this thesis.

Event-Related Fields (ERF)

ERFs in MEG (or ERPs in EEG recordings) represent electrophysiological measurements of brain responses following stereotyped visual, auditory or other stimuli. The stimulus-specific neural response is obtained by averaging the data from the retrieved signal hence yielding a mean waveform per subject (the evoked response). ERFs are useful in: 1) providing a continuous measure of visual processing for example (or any perceptual process) between the stimulus and the response; 2) providing output from a large number of individual cognitive processes; and 3) providing an online measure of the processing of sensory stimuli in the absence of a behavioural response. One of the main disadvantages of ERFs is that the interpretation of their functional significance is less clear than that of behavioural responses (Hansen, Kringelbach et al. 2010).

Time-Frequency analysis

The frequency content of MEG recordings and their variation with time are obtained by applying specific algorithms to the data. Oscillatory brain activity is considered in the context of well-defined stimuli (Braeutigam 2013, Wacker and Witte 2013). Two responses can be noted: evoked oscillatory responses which appear at the same latency and phase in each trial and induced oscillatory responses which appear with jitter in phase from one trial to another and are not detected by averaging (see also next section) (Tallon-Baudry and Bertrand 1999). Many brain rhythms are assumed to modulate attentional and perceptual processes and extracting them allows us to map by the millisecond changes in neuronal synchrony in response to sensory stimuli.

7.1.4 Clinical applications in ASD

MEG-technology is being used extensively in epilepsy surgery. The fact that MEG is non-invasive and has a relatively friendly set-up have made it an appealing technology that has been used in the investigation of the neural correlates underlying behaviour in ASD. In particular, MEG has been used to investigate sensory processes in autism as well as epileptiform activity. MEG studies in autism, however, remain relatively rare.

7.2 Roles of gamma oscillations

Brain rhythms at frequencies of 30 Hz and above are known as gamma oscillations and have been associated with cognitively active states and implicated in a variety of functions including visual perception (Tallon-Baudry 2009), audition (Canolty, Edwards et al. 2006), memory (Chaumon, Drouet et al. 2008) and olfaction (Jung, Hudry et al. 2006). These oscillations have been described in several brain areas including the visual cortex (Muthukumaraswamy, Singh et al.), the hippocampus (Bartos, Vida et al. 2007) and the olfactory bulb (Jung, Hudry et al. 2006). Evidence for the roles of gamma oscillations comes from *in vitro* studies on brain slices, and *in vivo* studies on animals and human subjects. In brief, *in vitro* studies corroborated by *in vivo* studies suggest a close association between gamma oscillations and the firing of inhibitory cells thereby suggesting their implication in the balance between excitation and inhibition. *In vivo* studies utilizing visual stimuli to induce/evoke gamma oscillations in animal and human subjects suggest a role in visual processes and perception. In this section, the main *in vitro* and *in vivo* experiments that have led to the elucidation of the roles of gamma oscillations are reviewed. The distinction between evoked and induced gamma responses is discussed first.

7.2.1 Evoked and induced gamma-band responses

Evoked and induced bursts in gamma activity typically follow transient neural responses (ERFs) in MEG, which are broadband signals time and phase-locked to stimulus onset and can be traced by averaging trials. Evoked gamma responses are narrow-band signals that are time and phase-locked to the stimulus and require time-frequency transformation prior to their extraction with averaging. Induced gamma responses, however, are time-locked to stimulus onset (Tallon-Baudry and Bertrand 1999). Time-frequency transformation and power measurements are performed prior to their extraction with averaging.

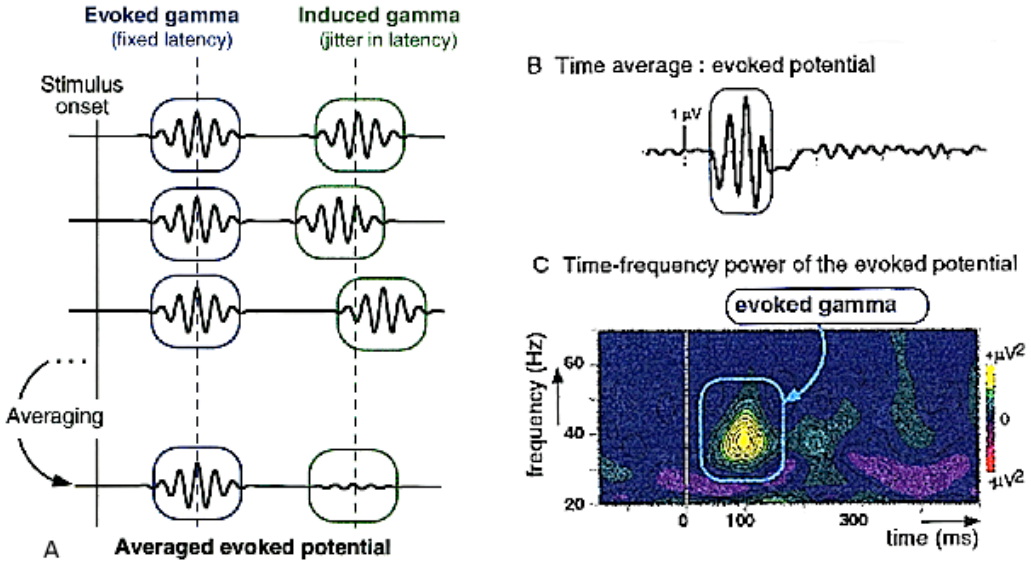


Figure 7.2 Evoked and induced gamma. This figure has been modified from (Tallon-Baudry and Bertrand 1999). (A) shows the two types of gamma-band MEG recordings with evoked gamma (blue) in single trials that is time and phase-locked to stimulus onset and therefore is visible with averaging as opposed to induced gamma that is marked by a jitter in latency and therefore is not visible by averaging from single trials. (B) shows an averaged evoked potential that following convolvement of the signal by a Morelet wavelet (see methods section) allows the visualisation in time

and frequency in (C) of the evoked gamma-band response (30-50 hz) between 80 and 130 ms. The induced response is not shown here.

7.2 2 Roles of gamma in visual processing

In 1989, Gray et al showed that in response to moving bars, populations of cortical neurons from an anaesthetized cat exhibited changes in their firing rates co-occurring with the generation of locally synchronized gamma oscillations (Gray, Konig et al. 1989). These evoked oscillations were phase-locked where the firing spikes of individual units oscillated at the same frequency as the recorded visually evoked field. This experiment is one of many that have had a tremendous impact on systems neuroscience suggesting a link between cellular electrophysiology and visual function (Traub and Whittington 2010). Tallon-Baudry distinguishes between local and long-range oscillatory synchrony in the gamma range: the former is defined by a power increase in a given frequency at the MEG sensor and reflects within-area neural interactions and the latter is defined by phase synchronization at a given frequency which reflects between-area neural interactions (Tallon-Baudry 2009). For example, small moving bars induce gamma locally and long moving bars reveal gamma band synchronization between two separate cortical sites as the ends of the moving bar represent separate visual fields but similar orientations (Traub and Whittington 2010).

The scientific literature is full of visual paradigms that have been used to elicit gamma oscillations. Using illusory Kanizsa triangles, locally-induced gamma activity through a 30-80 Hz burst between 200 and 300 ms after onset is demonstrated in the visual areas (Tallon-Baudry, Bertrand et al. 1997) and a strong negative correlation is demonstrated between the latency of this gamma burst and object recognition delays (Tallon-Baudry, Bertrand et al. 1997). Arguably, the very first electrophysiology

paper to report findings on long-range oscillatory synchrony in the gamma-range was an EEG study by Rodriguez et al (1999) in healthy controls (Rodriguez, George et al. 1999). Individuals had to assess whether they perceived a face or not. The group found increased evoked gamma phase-locking in response to the perception condition between the occipito-temporal and parietal regions and concluded that gamma oscillation mechanisms were not restricted to local visual feature-binding but also seemed to facilitate long-range cognitive integration. Thus, local and long-range gamma oscillations are implicated in visual processing.

Initially, gamma oscillations were suggested to be an epiphenomenon in visual processes. However, Vidal et al (2006) showed that oscillatory synchrony in this range can be highly specialized and dependent on the grouping properties of the stimulus (coherent versus incoherent) whereby coherent percepts elicited a central-occipital high-gamma response (70-120 Hz) as opposed to a more parietal low gamma response (44-66 Hz) with attention-related stimuli (Vidal, Chaumon et al. 2006). Therefore, oscillatory synchrony in the gamma range is commonly assumed to play an important role in cognitive visual processes of object representation as well as attention and can be specific.

There are few studies that have demonstrated how gamma oscillation synchrony might relate to perception. Roelfsma et al (1994) showed that when visual images were presented to both eyes in surgically-induced strabismic amblyopia in cats, synchronized activity of pairs of neurons in the gamma range was only observable in the healthy eye (Roelfsema, Konig et al. 1994). Fries et al (1997) showed that neurons from the healthy eye increased their oscillatory synchrony in the gamma range when awake strabismic cats 'perceived' the visual stimulus as opposed to the reverse scenario when they did not (Fries, Roelfsema et al. 1997). Tallon-Baudry et al (2005)

proposed a relationship between perception and enhanced oscillatory synchrony in the gamma range modulated by attentional processes through synchrony in the beta range in the fusiform gyrus and the lateral occipital cortex (Tallon-Baudry, Bertrand et al. 2005). Thus, gamma oscillatory synchrony appears to play a role in visual perception.

7.2.3 Cellular mechanisms of gamma and the E/I balance

There were many *in vivo* attempts to investigate the type of interaction between synapses and gamma oscillations. An experiment by Jagadeesh et al (1992) found that induced gamma oscillations in cat visual cortex were associated with gamma frequency changes in synaptic potentials suggesting that these synaptic interactions might be generating the rhythm (Jagadeesh, Gray et al. 1992). Fast rhythmic bursting cells (cortical cells that generate fast oscillations upon current injection) have been also suggested to be involved in driving induced gamma in cat visual cortex (Cardin, Palmer et al. 2005).

Evoked visual gamma *in vivo* synaptic mechanisms are not known. Most of our understanding of the cellular mechanisms underlying evoked gamma oscillations is based on electrophysiological data from hippocampal slices *in vitro* (Traub and Whittington 2010, Buzsaki and Wang 2012). Tetanic gamma recordings (in the absence of sensory input) seem to be associated with slow intracellular depolarizations in pyramidal cells and interneurons with similar latencies to *in vivo* recordings suggesting a coordinated interaction between excitation and inhibition to generate gamma (Whittington, Doheny et al. 2001). The synchrony and period of these oscillations seem to be determined by $GABA_A$ receptor-mediated perisomatic inhibition postsynaptic potentials and both the CA1 and CA2 sites of the hippocampus synchronized tightly in this experiment (Whittington, Doheny et al.

2001). Phasic excitation of perisomatic-inhibition through parvalbumin-positive interneurons seems also critical for persistent gamma oscillation generation at least in the CA3 area of the hippocampus and Buhl (1998) suggested that rhythm generation on this range depended upon optimal preservation of the inhibitory circuitry (Buhl, Tamas et al. 1998). A recent paper by Sohal et al (2009) demonstrated through opto-genetic techniques that inhibiting parvalbumin interneurons in mouse prefrontal cortex suppressed phase-locked evoked gamma activity. Furthermore, when fast-spiking PV interneurons were injected with trains of simulated excitatory post-synaptic currents and driven by flashes of light to emulate feedback inhibition, gamma-band power was markedly enhanced (Sohal, Zhang et al. 2009). To the author's knowledge, this is the first paper to suggest a direct association *in vivo* between evoked gamma oscillations and the E/I balance in neocortex.

Further possible associations between visual gamma and the E/I balance can be extrapolated from systems neuroscience papers in humans. Muthukumaraswamy et al (2009) demonstrated that *in vivo* levels of GABA neurotransmitter correlated with the peak frequency of sustained induced gamma oscillations in response to high-contast gratings in human medial visual cortex further supporting a role of gamma oscillations in the balance between excitation and inhibition (Muthukumaraswamy, Edden et al. 2009). The same group also showed that elevating endogenous GABA levels modulated evoked gamma-band frequency through GAT-1 blockade hence suggesting a more direct link with inhibitory synaptic density and gamma rhythm generation (Muthukumaraswamy, Myers et al. 2013). It should be noted however that the validity of these observations has been recently challenged by a large-scale study (Cousijn, Haegens et al. 2014). Finally, and on a structural level, the integrity of GABAergic interneuronal connections within cortical minicolumns seems to be

crucial for the generation of gamma oscillations: it is suggested that the quality of MEG recordings depends on the coherent activity of dendritic bundles across many minicolumns (Buzsaki and Wang 2012).

Hence, oscillatory synchrony in the gamma range appears to be associated with the balance between excitation and inhibition in human visual cortex *in vivo* and the hippocampus *in vitro.*

7.2.4 Summary

Gamma oscillations are assumed to play a role in visual processing and perception. Phasic excitation of inhibitory circuits seems to be critical for the generation of gamma oscillations. *In vitro* and *in vivo* studies show a correlation between inhibitory neurotransmitters and evoked gamma in the visual cortex. Gamma oscillations have been examined in the context of neurodevelopmental disorders such as ASD. In the following chapter, gamma oscillation findings in ASD are reviewed.

7.3 Gamma oscillations in ASD: a review of the MEG and EEG literature

Anomalies in gamma oscillations have been reported in ASD. Studies have covered local and long-range oscillatory synchrony measurements in the gamma range in response to auditory, visual and language stimuli and also in resting-state paradigms. Gamma-band power changes in ASD are often reported and this has been criticized on the grounds that local gamma power might be reflecting saccadic activity in the temporal lobe rather than cognitive processes (Carl, Acik et al. 2012). Much fewer studies have examined long-range gamma phase-synchrony in ASD. Uhlhaas suggested that high inter-hemispheric gamma phase-synchrony in primary visual cortex might be mediated by axonal tracts spanning both hemispheres (Uhlhaas and

Singer 2007, Uhlhaas, Pipa et al. 2009, Uhlhaas, Roux et al. 2009). Furthermore, severing inter-hemispheric tracts creates phase lag thereby abolishing synchrony. A MEG study by Braeutigam et al showed that γ-oscillations were modulated by the type of the task in healthy controls in response to congruous and incongruous word stimuli at distinct long latencies (300-600 ms) and suggested that measuring coherent phase-locked γ-band oscillations could provide independent information on brain dynamics when local power measurements provided little information about synchronized activity (Braeutigam, Bailey et al. 2001). Therefore, measuring oscillatory phase-synchrony in the gamma range in ASD might provide valuable information on synchronized brain activity in cognitive tasks. A review of the EEG/MEG studies that have reported changes in gamma power and gamma phase locking in ASD is presented here.

7.3.1 Evidence of gamma anomalies in resting-state paradigms

EEG and MEG resting-state studies reveal gamma abnormalities in ASD although it is unclear whether gamma-band power increases or decreases in resting-state recordings. Some groups have demonstrated right laterality of reduced gamma power in ASD in resting-state eyes-open paradigms using EEG recordings (Sheikhani, Behnam et al. 2012, Maxwell, Villalobos et al. 2013). MEG studies by Cornew et al (2012) and EEG studies by Orekhova et al (2007) and Lushchekina et al (2010) however, found a rather different effect with eyes-closed resting-state paradigms and increased gamma-band power in posterior regions (no hemispheric asymmetry) in autistic adults and children (Orekhova, Stroganova et al. 2007, Lushchekina, Podreznaia et al. 2010, Cornew, Roberts et al. 2012). Furthermore, where correlations with behavioural scores were attempted, increased temporal and parietal alpha but not gamma power was associated with greater symptom severity. In general, the increase

in resting-state gamma power in ASD has been attributed to a possible imbalance between excitation and inhibition being at the core of ASD pathophysiology.

7.3.2 Evidence of gamma anomalies in response to visual stimuli

Atypical visual processing in ASD has been associated with anomalies in gamma oscillations. Some groups report induced responses, others report evoked responses and rarely, groups report findings on both. Generally, gamma anomalies reported in response to visual stimuli involve paradigms relating to face processing, visual grouping (e.g. Kanisza figures), and visual orientation (Gabor patches).

Face processing

Phase-locked γ-range responses have been investigated in one MEG study. Sun et al (2012) demonstrated lower detection rates of upright Mooney faces in ASD. This was followed by a reduction in evoked γ-band power and phase locking in fronto-parietal regions in the ASD group compared to neurotypical subjects. Interestingly, visual activation in response to Mooney faces was stronger in the ASD group, suggesting atypical modulation of high-frequency power in fronto-parietal regions in ASD (Sun, Grutzner et al. 2012). Using MEG, Wright et al (2012) showed that children with ASD had an absent induced gamma response over right lateral occipital areas in response to faces though the evoked response remained relatively intact when subjects viewed emotions on faces (MEG study), suggesting impaired perceptual binding in ASD (Wright, Alderson-Day et al. 2012). A very recent MEG study by Khan et al investigated phase-amplitude coupling (PAC: phase at low frequency modulates high-frequency amplitude) between alpha-band phase and gamma-amplitude in the fusiform area of ASD individuals in response to faces and showed an overall

reduction in PAC in the absence of gamma or alpha power reductions suggesting that the timing of gamma and not the amount of gamma is atypical in ASD. Overall, the group also reported decreases in long-range and local connectivity in ASD (Khan, Gramfort et al. 2013). A MEG study by Richard et al (2013) found reduced prefrontal induced gamma activity in young adults in response to eye-gaze processing in ASD, suggesting that impaired generation of neural synchrony in the gamma range in the PFC might account for deficits in socio-cognitive functions in ASD (Richard, Lajiness-O'Neill et al. 2013). Finally, an EEG study by Grice et al (2001) found that children with ASD showed a decrease in induced gamma activation in frontal regions in response to upright faces compared with the neurotypicals, further suggesting alterations in perceptual binding and configural processing in ASD (Grice, Spratling et al. 2001). In summary, in face-processing tasks, induced and evoked gamma activities are reduced in ASD compared with TDs.

Lower order visual processing paradigms (Gabor patches)

A MEG study by Snijders et al (2013) found that in response to visual Gabor patches with changing orientations of stimulus elements, ASD adults showed a weaker gamma steady-state 60 Hz response that was not sensitive to contextual modulation unlike the TD group who showed a stronger signal (Snijders, Milivojevic et al. 2013). An EEG study by Milne et al (2009) showed that induced gamma-band power was decreased in the striate and extrastriate cortices in ASD in response to Gabor patches of varying spatial frequency (Milne, Scope et al. 2009). These studies suggest that alterations in gamma power might underlie atypical visual processing in ASD.

Kanizsa stimuli

Phase-locked gamma activity was only reported by one EEG study in response to Kanizsa stimuli in ASD. Stroganova et al (2012) observed reduced phase-locked evoked gamma activity in response to Kanisza stimuli in a group of children with ASD located to the parieto-occipital cortices at latencies between 40-270 ms. Since the early response to Kanisza stimuli was located in the visual cortex in both TD and ASD with similar activations (40-120 ms), the group concluded that ASD children relied heavily on lower-order processing in the visual areas as the 40-270 ms response was more specialized and therefore is part of higher-order processing (Stroganova, Orekhova et al. 2012). Interestingly, an earlier EEG study on children with autism conducted by Brown et al (2005) reported increased induced parietal gamma activity in response to Kanizsa stimuli, suggesting decreased inhibitory processing in ASD (Brown, Gruber et al. 2005). Overall, these findings suggest atypical visual perception in ASD though it is unclear whether gamma activity increases or decreases in response to illusory contour stimuli.

Video stimuli

In ASD, changes in gamma-band activity in response to videos have been reported. In one MEG study, the task was passive and individuals only watched colourful animated images that had an auditory component. Kikuchi et al (2011, 2013) showed that evoked gamma-band phase-locked activity was increased in 3-4 year old children with ASD with a right-lateralization but no lateralization in the older group (7-8 years old) for the same stimuli (Kikuchi, Shitamichi et al. 2013). These findings were not in agreement with an EEG study by Machado et al (2013) who showed that ASD individuals had lower gamma-band coherence values than controls in the occipital

regions when they passively watched cartoons with and without auditory tones although right lateralization of responses was also achieved here (Machado, Estevez et al. 2013). Thus, in response to video stimuli, gamma-band anomalies are also reported in ASD.

7.3.3 Gamma anomalies in response to auditory & language stimuli

Briefly, studies on auditory gamma responses have more consistently reported reductions in evoked activity and phase locking across trials in ASD individuals. Only the MEG-studies in the area are reviewed below. Rojas and colleagues focused on gamma abnormalities in first-degree relatives of children with ASD. In response to a word recognition task, parents of children with ASD (pASD) had increased total gamma-band power compared with the TD group over occipital cortices. However, evoked gamma and beta activities were increased in the pASD group with no difference in the inter-trial phase-locking factor (PLF) between groups (McFadden, Hepburn et al. 2012). The group also measured induced and evoked gamma-band transient and steady state auditory responses (40Hz) and showed a consistent reduction in evoked steady-state power and total power across all three auditory conditions at 32, 40 and 48 Hz. The PLF was overall reduced significantly in the pASD group (Rojas, Teale et al. 2011). Findings of this study were consistent with an earlier study in children and adolescents with ASD studied by the same group, where they showed left hemisphere reduced steady-state gamma power in response to auditory clicks in the ASD group (Wilson, Rojas et al. 2007). The group measured transient auditory responses in ASD at 40Hz and showed that induced gamma-band power increased in ASD whilst evoked gamma-band power and phase-locking decreased in ASD (Rojas, Maharajh et al. 2008). pASD studies suggest that gamma-

band phase consistency and changes in evoked and induced power in response to the considered paradigms could constitute possible endophenotypes for ASD.

In terms of language processing, only one MEG study examined evoked gamma phase locking in ASD. Braeutigam et al (2008) measured phase-locked evoked γ-band oscillations in ASD in a contextual integration task. The group found that incongruous words elicited weaker evoked gamma responses in the ASD group over left temporal cortices whilst congruous words elicited stronger and more prolonged oscillations in the central and prefrontal areas in ASD. The group concluded that γ-band responses supported sustained cortical synchronization across segregated areas in ASD (Braeutigam, Swithenby et al. 2008).

7.3.4 Evidence on gamma oscillation anomalies in relation to the E/I balance

It has been speculated that atypical visual perception in ASD might stem from an imbalance between excitation and inhibition. A common finding in ASD is reduced spacing between minicolumns in the neocortex (Casanova, Buxhoeveden et al. 2003) and gamma oscillations have been suggested to depend on the integrity of dendritic bundles and controlled perisomatic GABA-ergic inhibition through parvalbumin interneurons (Buzsaki and Wang 2012). There is also a wealth of evidence in the animal literature of parvalbumin interneuron dysfunction in autism suggesting that gamma oscillatory synchrony might be implicated in the balance between excitation and inhibition in autism (Gogolla, Leblanc et al. 2009, Marin 2012). Furthermore, changes in the parvalbumin system have been shown to directly relate to ASD symptomatology (Saunders, Tatard-Leitman et al. 2013). Interestingly, repetitive transcranial magnetic stimulation (rTMS) in ASD increased the discrimination of gamma-band power differences between target and non-target visual stimuli to

baseline and caused significant improvement in responses on behavioural questionnaires of irritability and repetitive behaviour (Baruth, Casanova et al. 2010). This was more direct evidence on how modulating gamma and thereby the balance between excitation and inhibition can directly affect symptom severity.

In summary, autism individuals seem to have characteristic gamma responses to visual, auditory and language stimuli in comparison with the typically developing population. Interestingly, these differences do not always appear to be a disadvantage particularly when it comes to task performance, where individuals with autism seem to do better when the task requires heightened perceptual and sensory abilities. It is unclear whether these performance superiorities are characterized by the underlying gamma-band activity differences suggesting that the 'anomaly' in the gamma response may not necessarily mean 'impairment' but on the contrary, a possible advantage in ASD.

Chapter 8 Gamma oscillations in perceptual simultaneity in ASD: time-frequency analyses of magnetoencephalographic recordings

8.1 Rationale and hypothesis

Reduced evoked gamma responses in response to visual stimuli such as faces, illusory figures and Gabor patches in ASD are relatively consistent findings in the literature. Oscillatory synchrony in the gamma range reflects enhanced cortical processing *in vivo* and gamma power is increased through feedback inhibition of cortical pyramidal cells by parvalbumin interneurons in the neocortex and is therefore implicated in the balance between excitation and inhibition in cortical networks. Not much is known about the phase synchrony of gamma oscillations in visual processing in ASD. Evoked gamma responses have usually a very early onset in response to visual stimuli (50-150 ms) and their role in feature binding remains unclear, unlike the better-established role of induced gamma oscillations.

Not much is known either about the role of gamma in the perception of simultaneity. Individuals with ASD exhibit lower visual simultaneity thresholds in tasks relating to the temporal coding of event structure, defined as the processing of the temporal relationships between events such as the relative simultaneity or asynchrony of events. Falter *et al*. showed that ASD individuals have increased parsing of temporal event structure and a decreased capacity for integration over time (Falter, Elliott et al. 2012). They also showed that ASD subjects have an enhanced temporal resolution in a perception simultaneity task and superior access to early visual processing stages in the task that are associated with superior task performance compared with the TD group. In this paper, individuals had to assess between real (simultaneous) and apparent (asynchronous) visual simultaneity in three conditions: SIM (two bars appear simultaneously on a screen), SHORT (second bar appears with a 17 ms delay

from the first bar) and LONG (second bar appears with a 117 ms delay from the first bar) conditions. Behaviourally, the ASD group gave significantly fewer 'simultaneous' responses in the SHORT condition compared with the TD group. Event-related field analyses showed that the strongest evoked potentials were at 130 ms at occipital cortices in both groups (see figure 8.1 below). Event-related power differences were significantly higher between the simultaneous and the asynchronous SHORT condition in ASD suggesting an increase in neural processes, which could support perceptual differentiation between conditions in that group even if the behavioural outcome was simultaneous (Falter, Braeutigam et al. 2013).

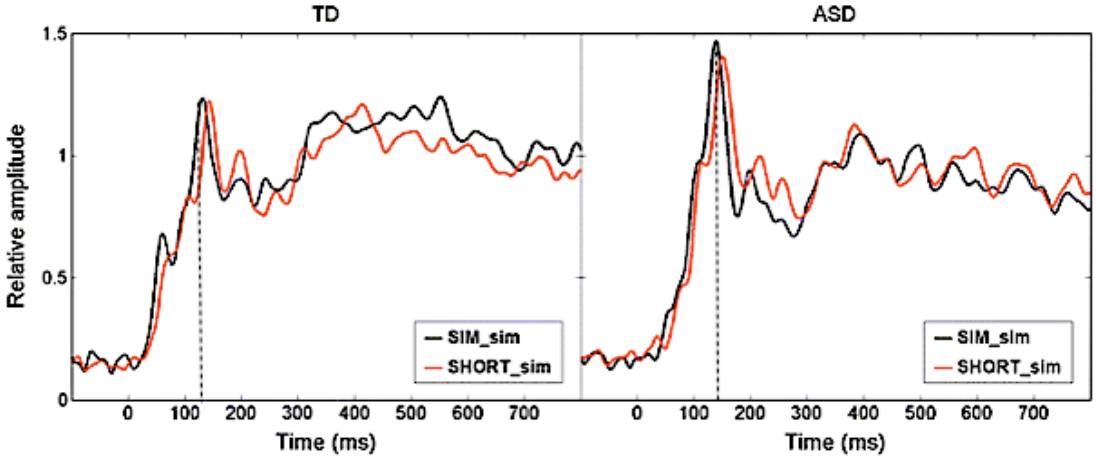


Figure 8.1 Event related fields in perceptual simultaneity. This figure was modified from Falter et al (2013) and shows the grand root-mean-square (rms) signals in the SIM_sim (SIM condition, 'simultaneous' response) and SHORT_sim (SHORT condition, 'simultaneous' response) conditions in TD and ASD. The dotted line represents the strongest peak observed at a latency of 130 ms in occipital cortices. The global rms-curves were obtained through summation over all channels and all participants within a participant group and stimulus onset was at 0 ms.

When latency differences (LATDIFF) were correlated with performance differences (PERFDIFF) at 130 ms in the ASD group, a significant negative correlation was reported suggesting that early brain response latency predicted performance in the ASD group only (see figure 8.2 below).

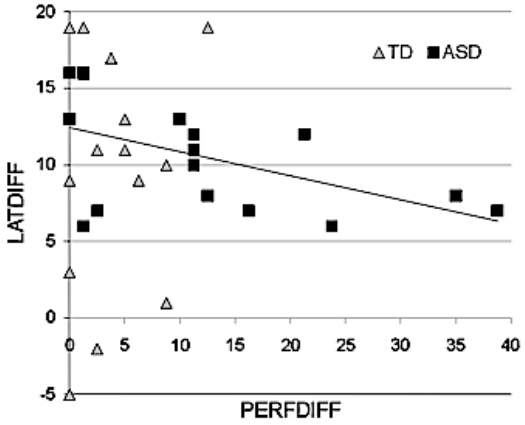


Figure 8.2 Correlation between performance difference and latency difference. This figure was used with permission from Falter et al (2013) and shows a significant negative correlation of the performance difference (PERFDIFF) with the latency difference (LATDIFF) between the SIM_sim and SHORT_sim conditions in the ASD group. There was no correlation in the TD group.

The neural correlates underlying superior visual processing in perceptual simultaneity and enhanced temporal resolution have yet to be addressed. Gamma oscillatory synchrony may underlie visual atypicalities in ASD and decreased gamma synchrony has been associated with diminished task performance (McFadden, Hepburn et al. 2012, Sedley and Cunningham 2013). However, the roles of gamma synchrony in predicting performance under certain conditions of perceptual simultaneity are unknown. With permission from Falter et al (2013), previously collected MEG-recordings were used to extract using time-frequency analyses evoked gamma

oscillations. Trial-by-trial phase consistency of the γ-band evoked response in 17 individuals with ASD and 17 TD in the task.

Hypothesis

It was hypothesized that increased oscillatory activity in the gamma-band would predict enhanced feature binding in the visual time perception task and result in worse task performance under certain conditions.

8.2 Methodology[5]

8.2.1 Participants

Participant data were obtained with permission from Falter et al (2013) (Falter, Braeutigam et al. 2013). Full recruitment details have been specified elsewhere. In brief, 17 individuals with a clinical diagnosis of ASD (16-38 years) were recruited through advertising and their diagnosis confirmed using the ADI-R and the ADOS-G diagnostic assessments. Verbal, performance, and full-scale IQ scores were assessed using the Wechsler Abbreviated Scale of Intelligence, WASI (Wechsler 1999). Participants with a diagnosis of a co-morbid psychiatric disorder, current medication, and a full-scale IQ < 85 were excluded from the study. Out of the 17 participants, 14 had a diagnosis of Asperger syndrome (n = 14) and 2 were diagnosed as high-functioning autism (n = 3) according to DSM-IV-TR. (see Table 8.1). 17 TD participants (15–38 years) were recruited and exclusion criteria for the TD group were any psychiatric diagnoses, any medication, and a full scale IQ < 85 (see Table 24). The ASD and TD groups were matched for chronological age, verbal IQ, and performance IQ (largest $t(30) = 1.08$, $p = .29$). All participants had normal or corrected-to-normal vision. Written informed consent was obtained from all participants prior to any testing. The National Research Ethics Service UK granted ethical approval for the study (see Appendix K for ADOS-G definition).

[5] Participant details, behavioural data and MEG-recordings were obtained with permission from C.M. Falter and S. Braeutigam. In this section, we summarize the methodology for thoroughness. My work involved extracting brain rhythms from MEG-recordings using time-frequency analyses.

Table 8.1 Demographics and Diagnostic Scores of ASD and TD Subjects

Participant Demographics and Scores	Diagnosis		*t* Statistic
	ASD (n=17) Mean (SD), range	TD (n=17) Mean (SD), range	*t*(30), *p* value*
Age (years)	24.3 (7.2), 16.8-38.3	26.1 (6.7), 15.8-38.5	0.73, 0.41 (ns)
Gender	16M:1F	13M:4F	--
ADOS-G (communication domain)**	3 (2), 1-7	--	--
ADOS-G (reciprocal social interaction domain)	6 (3), 1-11	--	--
ADOS-G (stereotypical behaviour and restricted interests domain)	1 (1), 0-4	--	--
ADI-R *(social interaction domain)**	17 (5), 10-25	--	--
ADI-R (communications domain)	15 (4), 9-21	--	--
ADI-R (restricted interests domain)	5 (3), 2-10	--	--
Verbal IQ****	114 (9), 99-127	114 (12), 99-139	0.10, 0.92 (ns)
Performance IQ	112 (15), 75-136	117 (9), 104-136	1.08, 0.29 (ns)
Full-Scale IQ	115 (11), 88-131	117 (10), 101-141	0.59, 0.56 (ns)

Demographics of ASD and TD subjects showing age of participants and their clinical scores. Data are shown as mean (standard deviation), range. **p* value obtained from comparing means using a parametric unpaired t-test that assumes equal variances (verified using Hartley's *F*-test)) **Scores calculated by using the Autism Diagnostic Observation Schedule- Generic in three domains (Lord, Risi et al. 2000) ***Scores calculated by using the Autism Diagnostic Interview-Revised in three domains (Lord, Rutter et al. 1994). ****Intellectual Quotient (verbal, performance, full-scale) calculated using the Wechsler Abbreviated Scale of Intelligence (Wechsler 1999).

8.2.2 Experimental paradigm and design

In the current study, a modified version of the perceptual simultaneity task designed by Elliott et al (2007) (Elliott, Shi et al. 2007) was used in order to facilitate between-condition comparisons using MEG. The experiment was conducted in a dimly lit scanning room (mean screen surround luminance 0.1 cd/m^2) to reduce the impact of onscreen persistence, with stimulus luminance maintained at 0.4 cd/m^2 upon a background field of 0.075 cd/m^2. Stimuli were generated and presented using Inquisit 3 (Software 2003) and back-projected onto a translucent screen. Participants viewed two white bar stimuli (subtending 4.6° of visual angle vertically and 0.5° horizontally) which were positioned to the left and right of the centre of the screen (randomized side of first stimulus) with a distance of 7.2° visual angle between them. In contrast to a previous version of this task where stimuli faded over as luminance increased (Falter, Elliott et al. 2012), the current experiment used simple onset stimuli in order to simplify the MEG analysis.

Three conditions were presented in pseudo-randomized order: a) two vertical bars appeared simultaneously on the screen (SIM condition); b) asynchronously with a 17 ms delay (SHORT condition); c) asynchronously but with a much longer delay of 117 ms (LONG condition). The main reason for including the LONG condition was to maintain attention throughout the task by presenting perceptually different trials. Each trial started with a blank 500 ms ISI followed by stimulus presentation with simultaneous or asynchronous onset and a simultaneous offset of 17 ms after second stimulus onset. A response cue was presented 1500 ms after stimulus offset. Participants were asked to respond if the two bars were simultaneous or asynchronous by pressing one of two buttons. Participants were instructed to avoid eye movements during stimulus presentations and to restrict eye blinks and button presses to when the

response cue appeared. The response cue remained on the screen until a response was provided. There was no feedback on performance. Participants completed a practice block of 10 trials followed by four experimental blocks consisting of 60 trials each. Each stimulus was presented 80 times for a total of 240 trials.

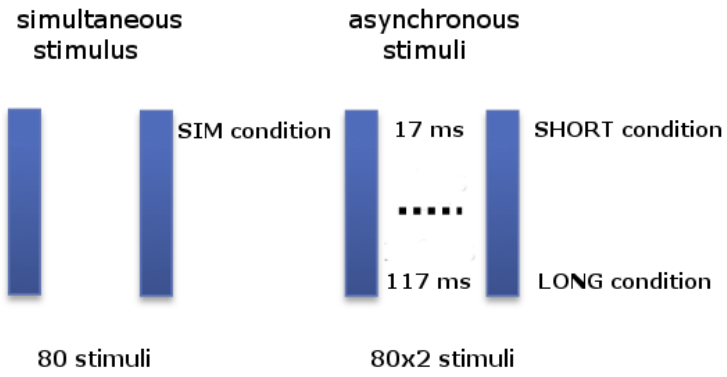


Figure 8.3 Visual paradigm of perceptual simultaneity. This figure shows the stimuli that participants had to assess. The bars appear simultaneously (SIM condition) or asynchronously with either a delay of 17 ms (SHORT condition) or 117 ms (LONG condition). Stimuli appear in a pseudo-random order for a total of 240 trials, 80 of each stimulus. The response cue duration is 1500 ms.

8.2.3 Data Acquisition

Measurements were performed using a Neuromag-306 VectorView™ system, the characteristics of which have been specified in the MEG-technology chapter of this thesis (see chapter 7). The data were sampled at 1,000 Hz (0.03–330 Hz anti-alias filter; artefact correction using Maxfilter™; 40 Hz low-pass filter before subsequent analysis) and corrected for variation in individual head position before analysis using MaxMove™ (part of the scanner software package). Physiological artefacts were identified from the recorded electrooculograms and electrocardiograms. MEG traces with coinciding eye-blinks were corrected using a PCA-based approach (in-house

software; algorithm based on spatial confound and sensor data correction routines provided by SPM8; see also (Berg and Scherg 1994). A small number of epochs (<5 %) had to be excluded from the analysis due to other artefacts. Dr. Sven Braeutigam, Dr. Sarah Carrington, Dr. Christine Falter and Professor Anthony Bailey were responsible for the acquisition of MEG data.

8.2.4 Event-related fields

Evoked responses were useful in the principal component analyses as indicated in the subsequent section. Evoked responses were averaged separately for each participant and for each of the three conditions. A baseline was established by averaging signal strength over 100 ms preceding the onset of the first stimulus. A latency range of 0 to 1000 ms after stimulus onset was chosen for analyses. The remainder of this sub-section is included for reasons of thoroughness as the method was used in the Falter paper.

Statistical differences in ERFs between the conditions of interest across participants were analyzed employing a time-dependent measure P(t) (Braeutigam, Rose et al. 2004).

$$P(t) = prob(\chi^2) := prob((-2\sum_{i=1}^{N} \ln f_i(t)) \tag{10}$$

N denotes the number of channels (see equation (10)). For each channel, f(t) denotes a non-parametric statistical test applied to evoked fields of interest. For each significant interval [P(t) < 0.01], the spatial distribution of the significant difference was given by f_i. Correspondence between the spatial distribution of the significant difference and the spatial distribution of ERFs (using grand-average power maps = root-mean-square

of the two gradiometers in a pair) was explored. Two different non-parametric tests (f) were used in the formula above dependent on the nature of the comparison. Wilcoxon and Mann–Whitney u tests were used for within and between group analyses, respectively. ERF data were used to help with PCA analyses the identification of latencies of interest for subsequent t/f analyses (Falter, Braeutigam et al. 2013).

8.2.5 Principal variance components of evoked responses

PCA analyses of evoked responses (broadband, all frequencies) were used to identify maximal signal variance in time to subsequently pursue time-frequency analyses. The first components of principal variance for evoked responses across all frequencies in the SIM and SHORT conditions ('simultaneous' response) in TD and ASD were plotted against time. This revealed that all major peaks were observed before 250 ms.

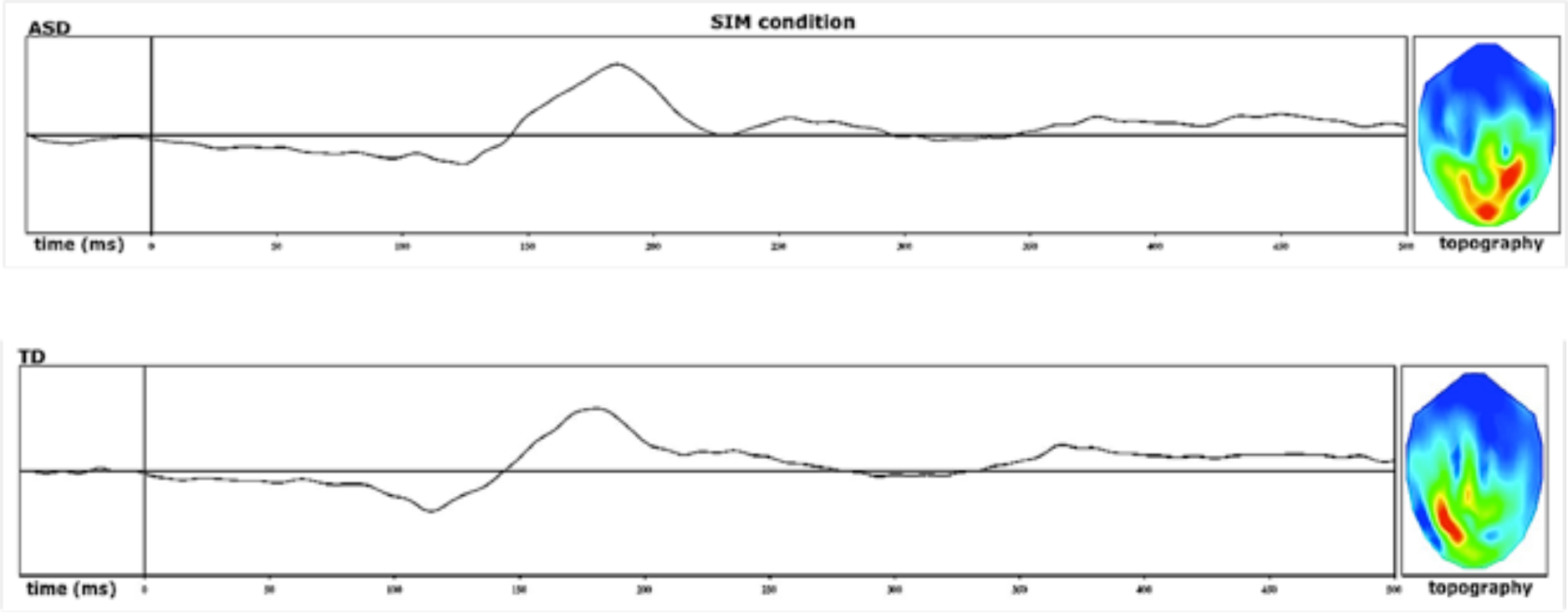


Figure 8.4 Signal variance between TD and ASD in the simultaneous conditions. This figure shows maximal signal variance across SIM condition in ASD and TD against time with an occipital localisation as shown by the topographical maps on the right.

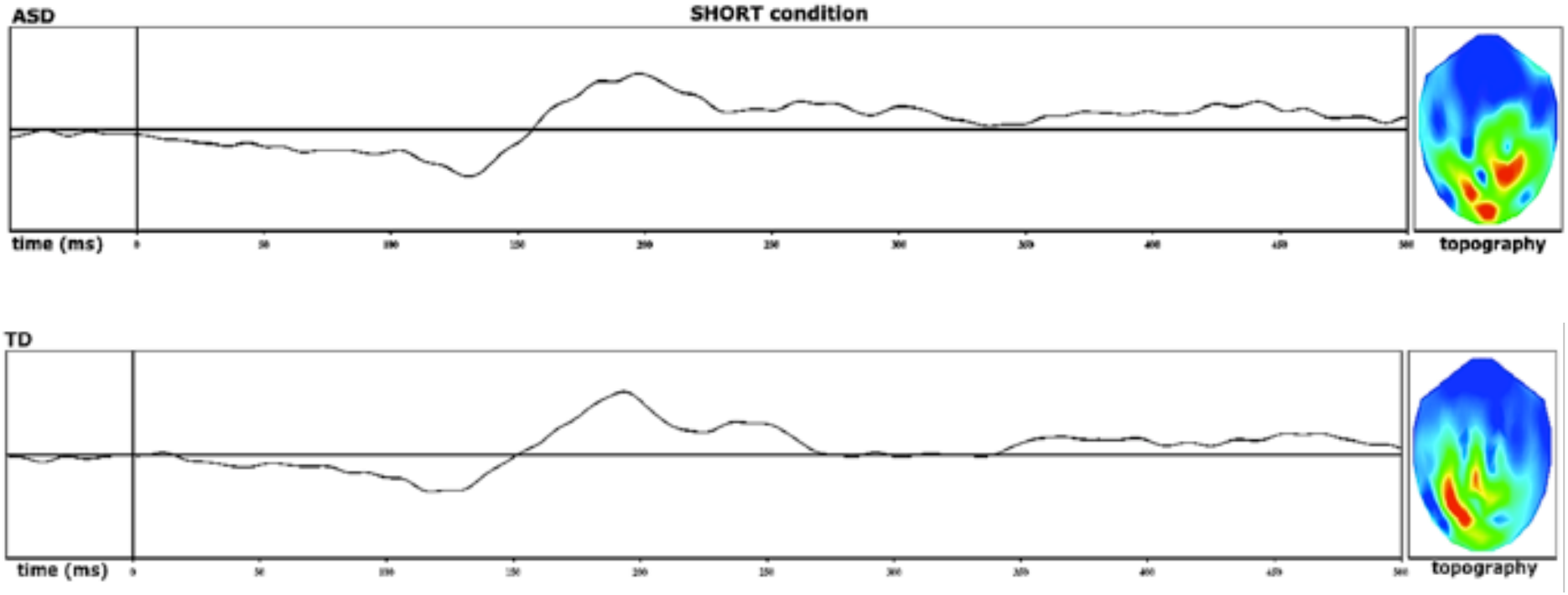


Figure 8.5 Signal variance between TD and ASD in SHORT condition. This figure shows maximal signal variance across SHORT condition in ASD and TD against time with an occipital localisation as shown by the topographical maps on the right.

8.2.6 Time-frequency analyses

In order to assess changes in oscillatory activity in the gamma range, one resorts to signal decomposition by using wavelets that allow the extraction of both signal power and phase centred at time and frequency. Tallon-Baudry described a method to convolve the signal with a Morlet wavelet $w(t,f_0)$ to perform (t,f) analyses in the gamma range. They proposed that a much better compromise would be achieved between temporal and frequency resolutions (Tallon-Baudry and Bertrand 1999). Phase locking of gamma-waves to stimuli has been proposed as a specific feature in many cognitive processes (Braeutigam, Bailey et al. 2001, Singer 2001, Uhlhaas and Singer 2007). In this study, gamma-band responses were analysed using a robust measure of phase-locking γ_D (gamma density) described previously by Braeutigam et al (2001) (Braeutigam, Bailey et al. 2001, Braeutigam, Rose et al. 2004). The method involves a Gabor wavelet transformation, a bootstrap evaluation and a rejection procedure in order to identify points (t,f) in time and frequency of high phase-locking that is independent of *γ-power*. As a consequence of the wavelet transformation, the gamma density carries with it uncertainties in time and frequency (see table 8.2). γ_D is defined for each subject, channel and condition (see also figure 8.6).

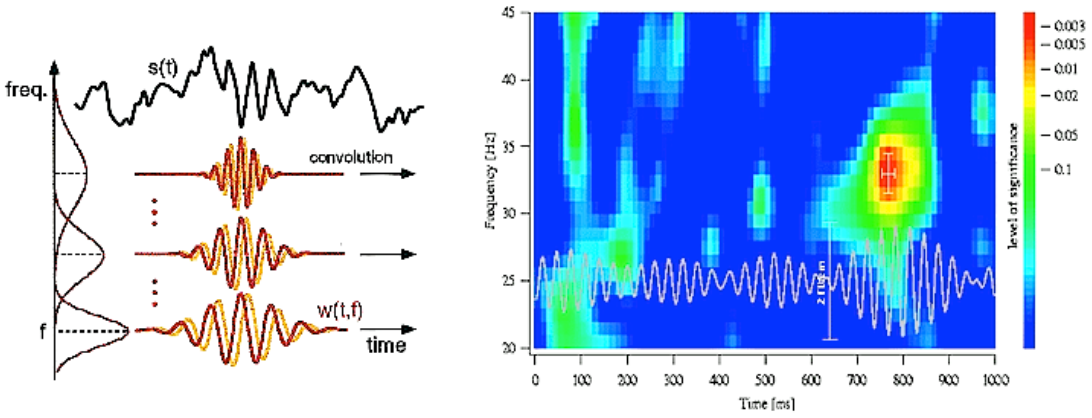


Figure 8.6 Gabor wavelet convolution of the signal. This figure represents the convolution of the signal to be analyzed by a Gabor wavelet (left, (Tallon-Baudry

2009)) and the resulting time-frequency plane with a superimposed wavelet on the frame (right, (Braeutigam, Bailey et al. 2001)). Briefly, signal s(t) is convoluted by a complex Gabor wavelet with w(t,f) as characteristics and having a Gaussian shape both in time (SD, σ_t) and in frequency domains ($\sigma_f=1/(2\pi\sigma_t)$ (Tallon-Baudry 2009).

Statistically significant differences between phase-locked γ-responses to the simultaneous and asynchronous stimuli are identified for as follows. For each channel, a local measure τ_i (applied to γ_D) of the significance of difference between phase-locking densities across subjects is obtained. Subsequently, a global measure of significance across all channels is obtained:

$$P\gamma_D(t,f) := prob(\chi^2_{\gamma_D}) = prob(-2\sum_{i=1}^{N}\ln\tau_i(t,f)) \quad (11)$$

where N denotes the number of channels.

Finally, non-parametric statistical tests incorporated in equation (11) were:

1) One two-level (2 for group, 2 for condition) non-parametric ANOVA test ((TD, ASD) x (SIM, SHORT)) to examine main effects of group, condition and group x condition interaction in γ phase locking. It is important to note that throughout the entire t/f analyses presented in the results, all the interactions and main effects from one and only one ANOVA are presented in t/f planes and global root mean square signal maps.
2) Post-hoc statistical tests included a Wilcoxon-rank test to examine within group differences in phase locking and a Mann-Whitney u test to examine between group differences in phase locking.

Table 8.2 Frequency and time uncertainties

Frequency (*f*) (Hz)	**Frequency Uncertainty** $\sigma_f = \frac{f}{K}$	**Time Uncertainty** $\sigma_t = \frac{1}{2\pi\sigma_f}$
30	3.75	42.46
32	4.00	39.81
34	4.25	37.47
36	4.50	35.39
38	4.75	33.52
40	5.00	31.85
42	5.25	30.33
44	5.50	28.95
46	5.75	27.69
48	6.00	26.54
50	6.25	25.48
52	6.50	24.50
54	6.75	23.59
56	7.00	22.75
58	7.25	21.96
60	7.50	21.23
62	7.75	20.55
64	8.00	19.90
66	8.25	19.30
68	8.50	18.73
70	8.75	18.20
72	9.00	17.69
74	9.25	17.21
76	9.50	16.76
78	9.75	16.33
80	10.00	15.92

This shows uncertainties in time and frequency of γ-modes associated with the Gabor transformation. (σ_f=uncertainty in frequency, σ_t = uncertainty in time, K=8).

8.2.7 Choice of gamma frequency range (30-80 Hz)

Phase jitters are present because of experimental constraints and neurophysiological variability. At the lower 30 Hz limit of the gamma range, signal phase-aligment is maximal (A=0.9). Phase jitters become more important at higher frequencies, thereby, reducing maximal phase-alignment. This is due to equipment constraints. The 80 Hz frequency has been chosen as a cut-off off point because of simulations showing low phase-alignment and more jittering beyond this point (A=0.3). Therefore, the 30-80 Hz gamma range was used in all subsequent analyses.

8.2.8 Strengths and weaknesses of MEG analyses

The above method of analysis though different to standard methods achieves similar results. It has been reviewed and accepted by many reviewers over time and published in many scientific articles (Braeutigam, Bailey et al. 2001, Braeutigam, Rose et al. 2004, Bailey, Braeutigam et al. 2005, Braeutigam, Swithenby et al. 2008, Braeutigam 2013) as well as independently validated by researchers using independently developed software (OSL) based on the well-known package SPM8 (Dr. Elizabeth Tunbridge). The approach used here is similar to that adopted in open source software packages for electrophysiological analyses such as fieldtrip (Oostenveld, Fries et al. 2011). The main advantages of the method is that it does not require a pre-selected region of interest, utilizes all the available data and provides a global time-dependent statistic based on general assumptions to allow both parametric and non-parametric designs. However, the main drawbacks are that it can be over-conservative and is mostly applicable in signal space and not source space. Finally, the intepretation of the results may be rendered difficult with strong volume conduction effects, which is also a possible drawback for most signal-space approaches.

8.2.9 Summary of the analyses

The analyses are summarized in the diagram below.

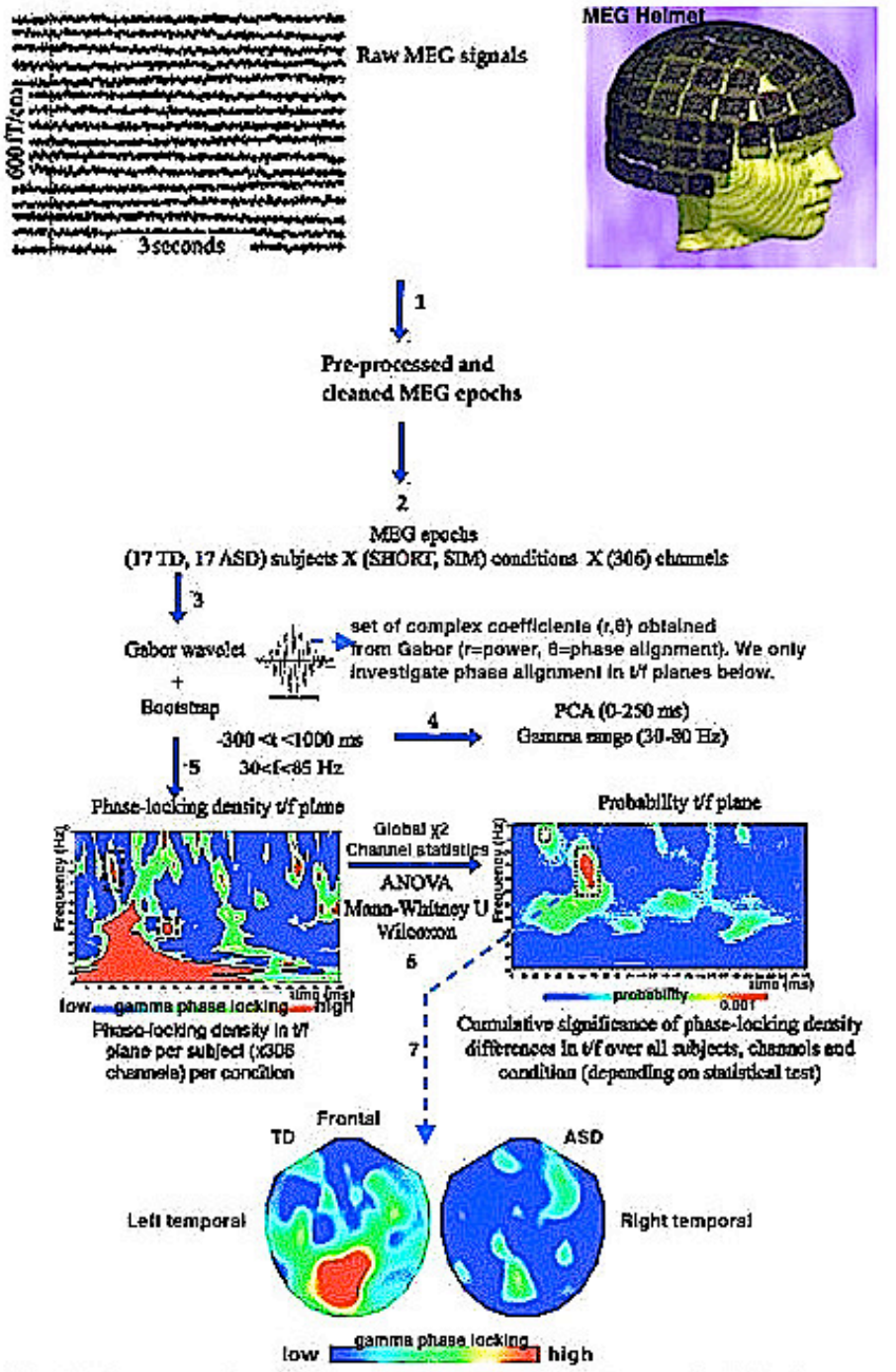


Figure 8.7 Summary of analysis. This figure indicates a brief summary of the steps of the analyses. (1) Raw MEG recordings are extracted, pre-processed and cleaned

from artefacts then grouped per subject, condition and channel. (2) From the MEG epochs, the signal (for each subject, condition and channel) is convolved with a Gabor wavelet transform to extract frequency content of the signals against time. (3) This is followed by a bootstrap assessment to give an estimate of phase-locking density per subject, channel and condition (5). Data are analyzed between -300-1000 ms and 5-85 Hz. (4) Using a PCA-based approach, maximal signal variation in time is observed before 250 ms. The gamma range chosen for analyses is 30-80 Hz (see 8.2.7). In (6), non-parametric statistical tests are applied to the data to obtain a cumulative significance of phase-locking density differences in t/f over all subjects, channels and condition. This depends on the nature of the comparison. Finally, grms values are extracted and mapped onto 2D planes to show strength of gamma phase locking over various cortical locations and integrated over the t/f interval of the significant difference between groups (7).

8.3 Results

8.3.1 Behavioural results

Mean percentages of 'simultaneous' responses and standard deviations for both groups were calculated. A D'Agostino Pearson and Omnibus normality test showed that data were normally distributed ($p>0.05$). Maulchy's test for sphericity was applied to evaluate the assumption of equality of variance and compound symmetry across conditions and was significant ($p<0.05$) suggesting inequality of variance. A Hyhn-Feldt correction of sphericity was applied as a result ($\varepsilon>0.75$). A split-plot ANOVA with one between-subject factor of group (ASD, TD) and one within-within subject factor of condition (SIM, SHORT, LONG) was performed. The results shown here are for the simultaneous response outcome. There was a significant main effect of condition ($F(2,62) = 950.43$, $p < .001$, partial $\eta^2 = .97$, Huynh–Feldt corrected) and a main effect for group ($F(1,31) = 6.96$, $p = .013$, partial $\eta^2 = .183$) suggesting that both groups differed significantly across the three conditions for the simultaneous outcome. The interaction between group and condition was significant ($F(2,62) = 17.39$, $p = .001$, partial $\eta^2 = .36$). A Bonferroni correction was chosen as a post-hoc test as it has more control over type-I error rates. Post hoc testing revealed that the ASD group gave significantly fewer 'simultaneous' responses in the SHORT condition ($p = .01$); ASD = 74.34 ± 20.36, TD = 92.21 ± 6.56; more 'simultaneous' responses in the LONG condition ($p = .016$; ASD = 8.38 ± 8.31, TD = 2.29 ± 0.55) compared to the TD group. Mean responses between groups were not significantly different from each other in the SIM condition.

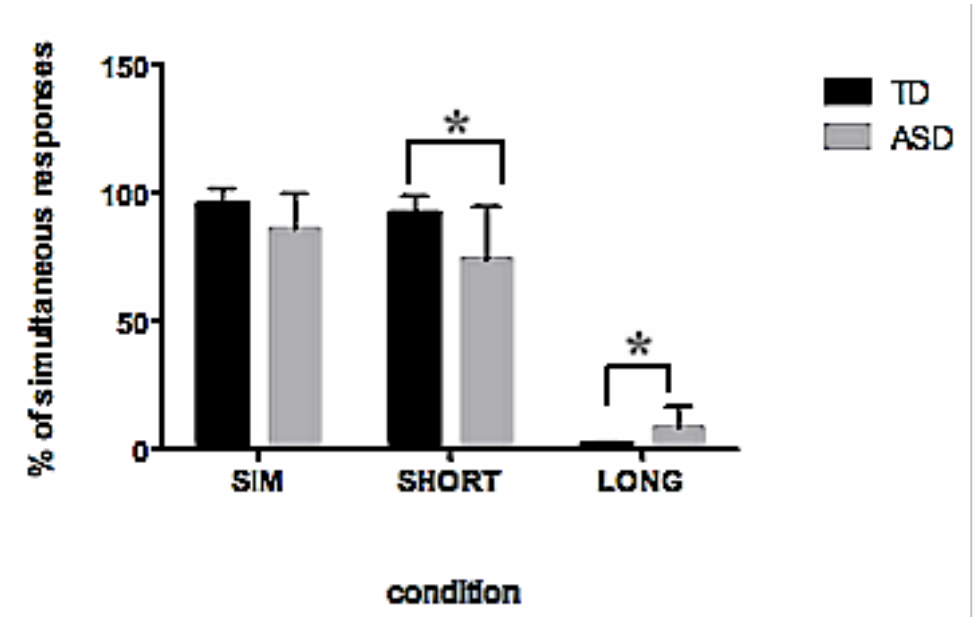


Figure 8.8 Mean percentage of simultaneous responses. The figure shows the mean percentage responses and SEM of the responses (simultaneous) to the SIM, SHORT and LONG stimuli for 17 TD and 17 ASD subjects.

Table 8.3 Percentage of simultaneous responses with standard deviations.

Condition	Diagnosis	
	TD	**ASD**
SIM	95.96 (5.82)	86.03 (13.84)
SHORT	92.21 (6.56)	74.34 (20.36)
LONG	2.29(0.55)	8.38 (8.31)

Mean percentages of simultaneous responses between ASD and TD in the SIM, SHORT and LONG conditions. Representation is as mean (SD).

8.3.2 Time-Frequency planes and analyses

Time-frequency analyses of MEG-recordings in the gamma range (30-80 Hz) and in a temporal window (0 to 250 ms) based on PCA analyses are presented here. Differences in lower frequency ranges as well as those beyond 250 ms are presented at the end of the results section. All analyses are correlated with the same behavioural

outcome and that is when subjects say ‘simultaneous’ in both the SHORT and SIM conditions.

Non-parametric analysis of variance examined the significance of the interaction between group (TD, ASD) and condition (SIM, SHORT) in time and frequency. ‘Simultaneous’ response epochs (both SHORT and SIM conditions) were subsequently divided within the TD group and the ANOVA-rank analyses were repeated to examine interactions within this group. The purpose of these tests was to determine the main effects of condition, group and interactions between group and condition for TD and ASD and also within TD to determine evoked phase-locked gamma latencies and frequencies of interest for post-hoc analyses. The following sections all derive from one ANOVA.

8.3.2.1 ANOVA interaction between group and condition

A significant ($p<0.001$) interaction between group and condition was noted in evoked gamma phase-locking in the 73-80 Hz frequency range at very early latencies between 20 and 40 ms (see below) after stimulus onset at t=0 ms. Another significant ($p<0.001$) interaction was noted between 45-80 Hz at early latency ranges (10-90 ms). Other significant interactions were also noted between 95 and 110 ms for 45-50 Hz frequencies; 125-155 ms for 50-60 Hz frequencies and 180-220 ms for frequencies between 40-50 Hz.

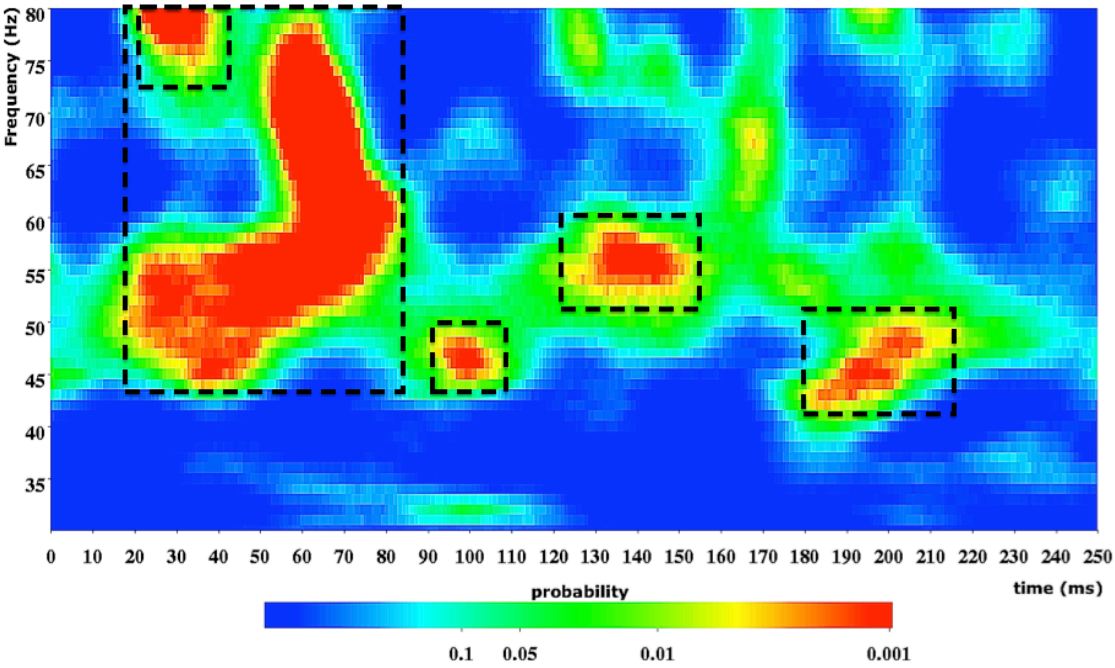


Figure 8.9 Interaction between group and condition. This examines the interaction between group (TD, ASD) and condition (SIM, SHORT) as a function of time and frequency. The significance of phase-locking interactions over all channels for all subjects between 0-250 ms and 30-80 Hz frequencies is shown in the red clusters. Rectangles denote areas of significance.

8.3.2.2 ANOVA main effect of group

There was a significant main effect of group ($p<0.01$) in evoked gamma phase locking (54-70 Hz) between 70 and 120 ms from stimulus onset (t=0 ms). Grand average calculation of evoked gamma phase-locking integrated over time and frequency of the main effect for group showed that phase-locking was higher in the TD group and was located to the occipital pole (see figure 8.10, see also appendix J).

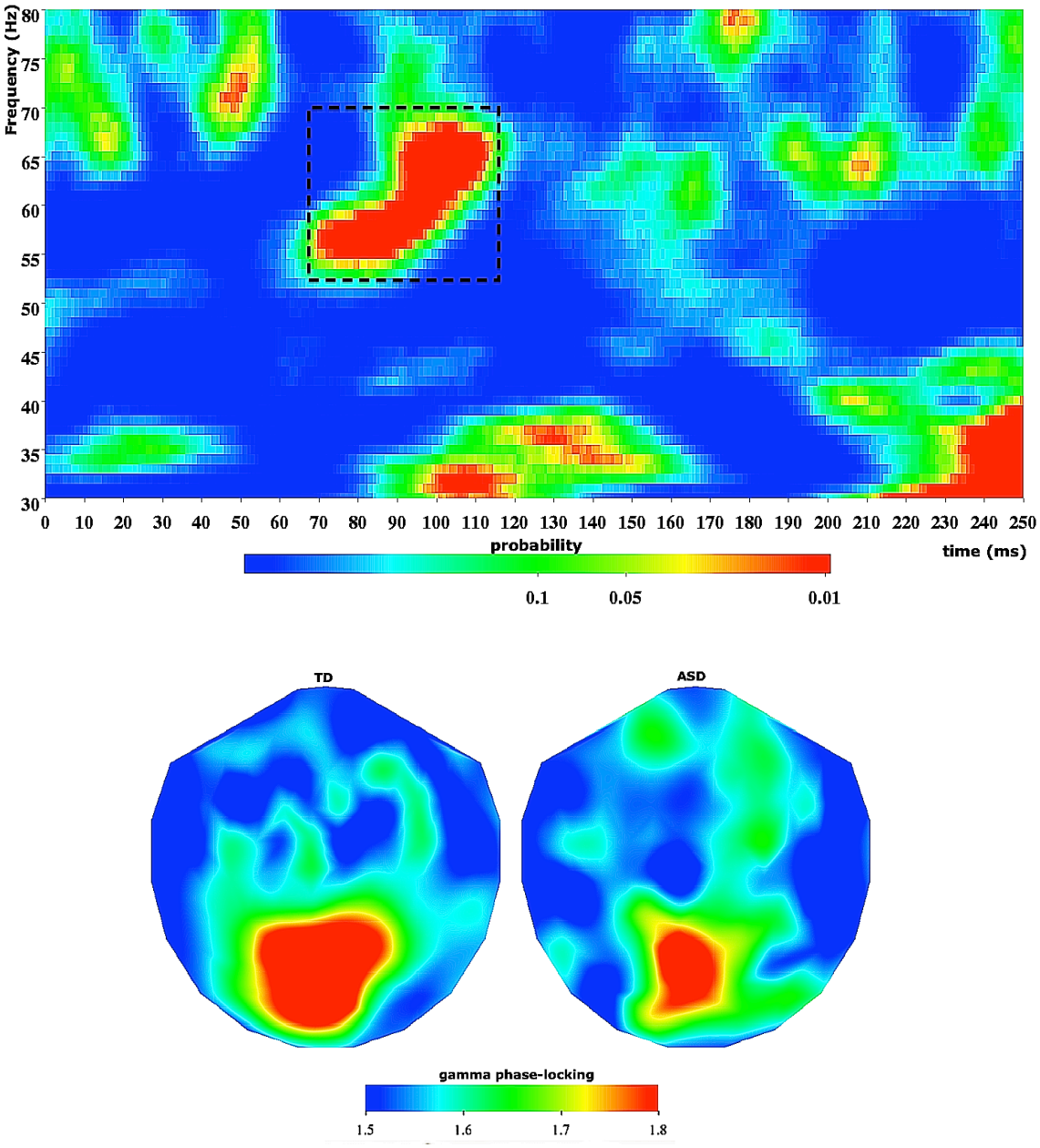


Figure 8.10 Main effect of group. This shows the main effect of group as a function of time and frequency (top) and averaged occipital evoked gamma phase-locking for the main effect of group between 54-70 Hz and 70-120 ms in TD and ASD (bottom).

8.3.2.3 ANOVA main effect of condition

The time-frequency plane shows a significant main effect of condition ($p < 0.001$) in evoked gamma phase locking between 30-45 Hz at early latencies (90-160 ms). Calculation of the grand average of evoked gamma phase-locking integrated over

time and frequency of the main effect for condition showed that phase-locking was higher in the SIM condition than the SHORT condition and was located to the occipital pole.

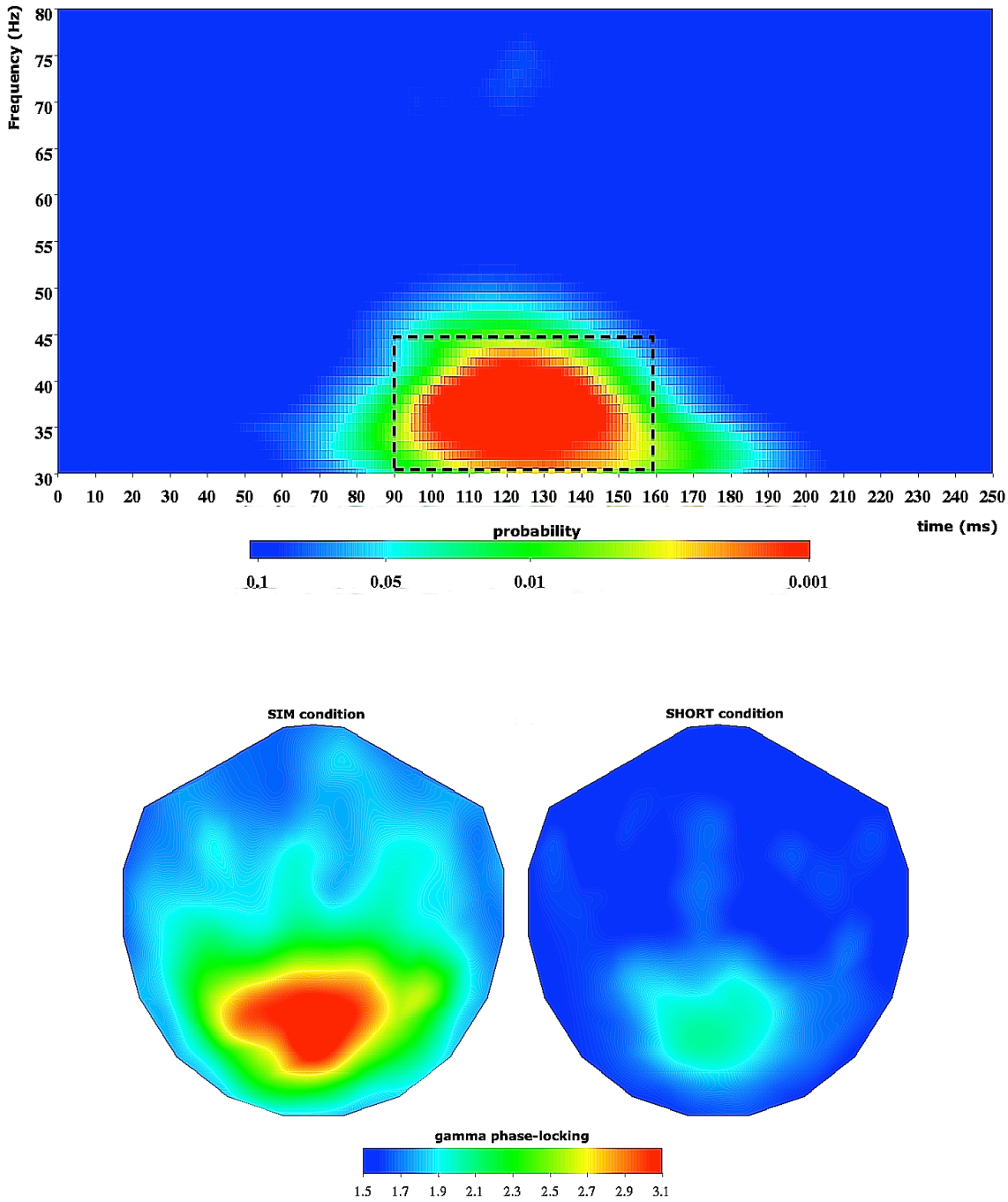


Figure 8.11 Main effect of condition. This figure represents the main effect of condition as a function of time and frequency (top) and occipital evoked gamma

phase-locking in the SIM and SHORT conditions between 30-45 Hz and 90-160 ms (bottom).

8.3.2.4 Post-hoc analyses of main ANOVA interaction: Mann-Whitney U for between-group differences

Post-hoc testing using the Mann-Whitney U was applied to examine inter-group mean evoked gamma phase-locking differences in time and frequency for each condition separately.

The SIM condition

Time-frequency representation of the significant differences between TD and ASD in evoked gamma phase-locking shows no significant ($p>0.01$) differences between 35-80 Hz for latencies between 0 and 180 ms. There was a significant difference ($p<0.01$) in evoked gamma phase-locking between 90-120 ms for 30-35 Hz frequency ranges and also another difference between 180-200 ms for 45-50 Hz frequency ranges.

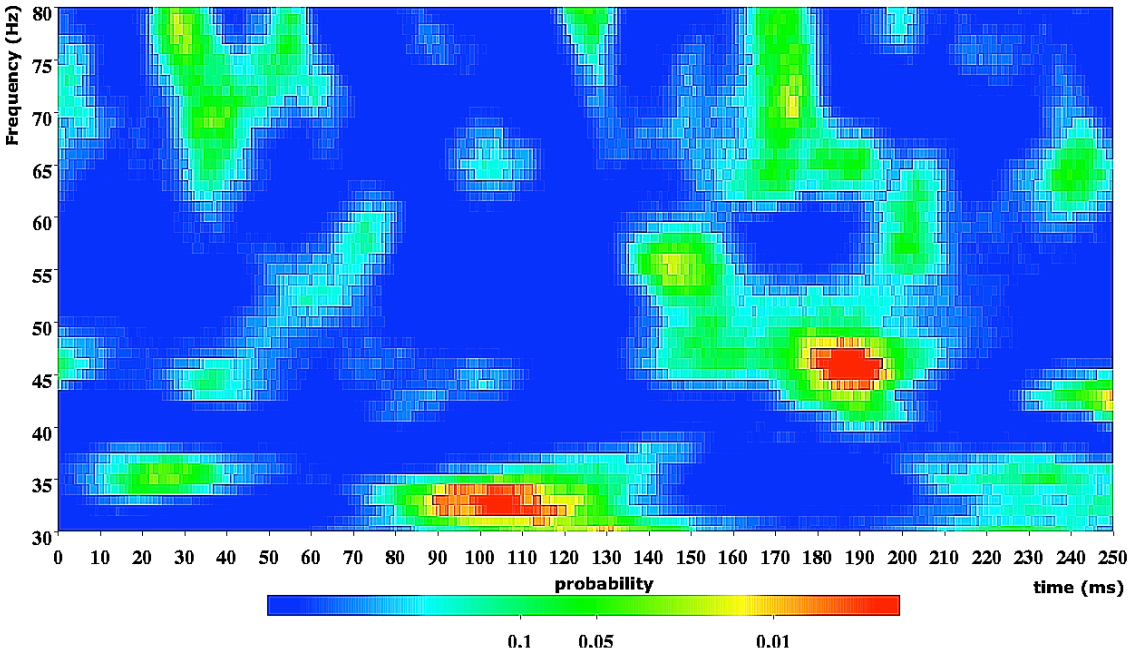


Figure 8.12 Between-group differences in the simultaneous condition. This figure represents the probability in time and frequency of significant differences in evoked gamma phase locked responses following the SIM condition between 0-250 ms and 30-80 Hz between TD and ASD.

The SHORT condition

Time-frequency representation of the significant differences between TD and ASD in evoked gamma phase-locking shows significant ($p<0.01$) differences between 48-70 Hz for latencies between 10 and 140 ms. There were also significant differences ($p<0.01$) in evoked gamma phase-locking between 20-40 ms for 75-80 Hz frequency ranges and also another difference between 160-180 ms for 55-65 Hz frequency ranges.

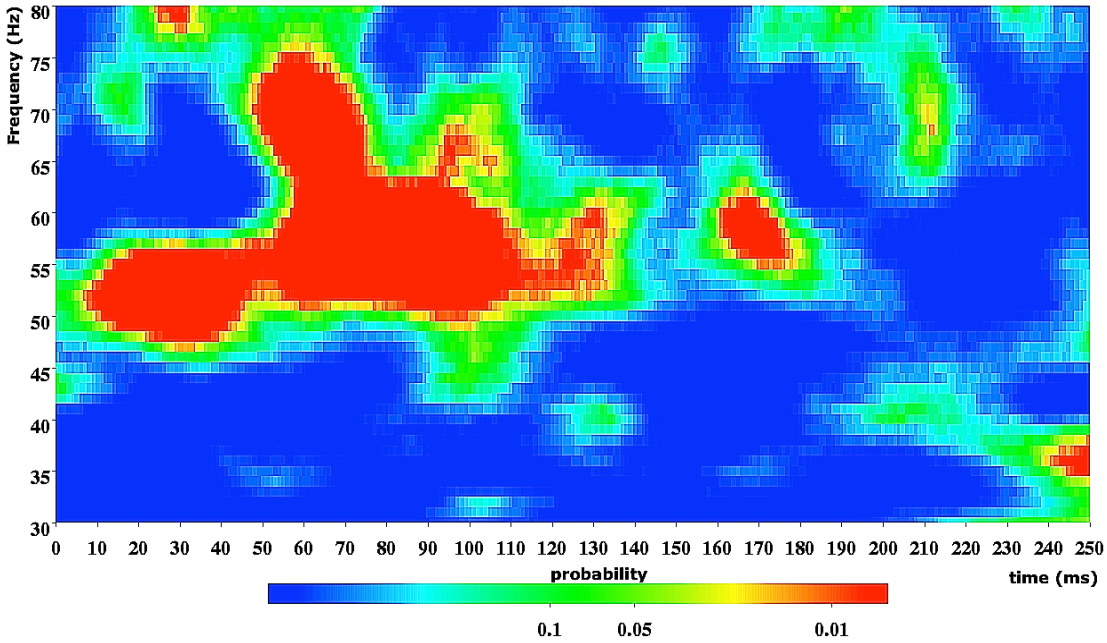


Figure 8.13 Between-group differences in the short condition. This figure represents the probability in time and frequency of significant differences in evoked gamma phase locked responses following the SHORT condition between 0-250 ms and 30-80 Hz between TD and ASD.

8.3.2.5 Mann-Whitney U for between-group differences for different conditions

Between-group differences using Mann-Whitney U for different conditions are shown below.

TD in SHORT versus ASD in SIM

Time-frequency representation of the significant differences between TD in SHORT condition and ASD in SIM condition in evoked gamma phase-locking shows significant ($p<0.01$) differences between 30-45 Hz for latencies between 100 and 160 ms.

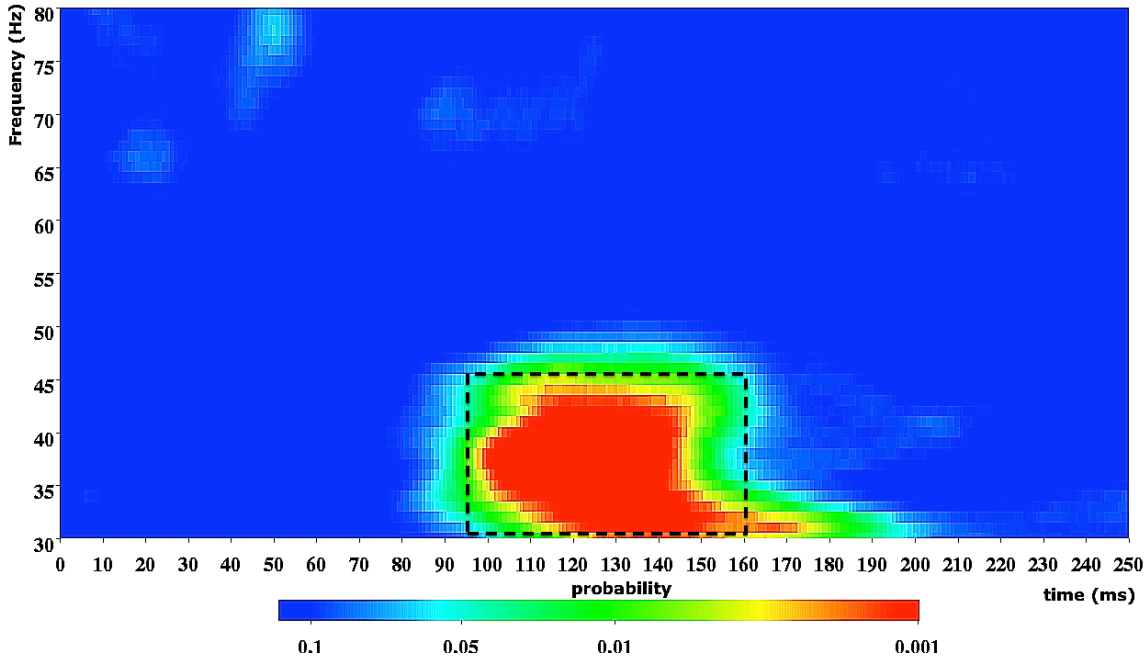


Figure 8.14 Between-group differences in different conditions (1). This figure represents the probability in time and frequency of significant differences in evoked gamma phase locked responses following the SHORT condition in TD and SIM condition in ASD between 0-250 ms and 30-80 Hz. Rectangle denotes the significant difference.

TD in SIM versus ASD in SHORT

Time-frequency representation of the significant differences between TD in SHORT condition and ASD in SIM condition in evoked gamma phase-locking shows significant ($p<0.01$) differences between 30-45 Hz for latencies between 80 and 170 ms.

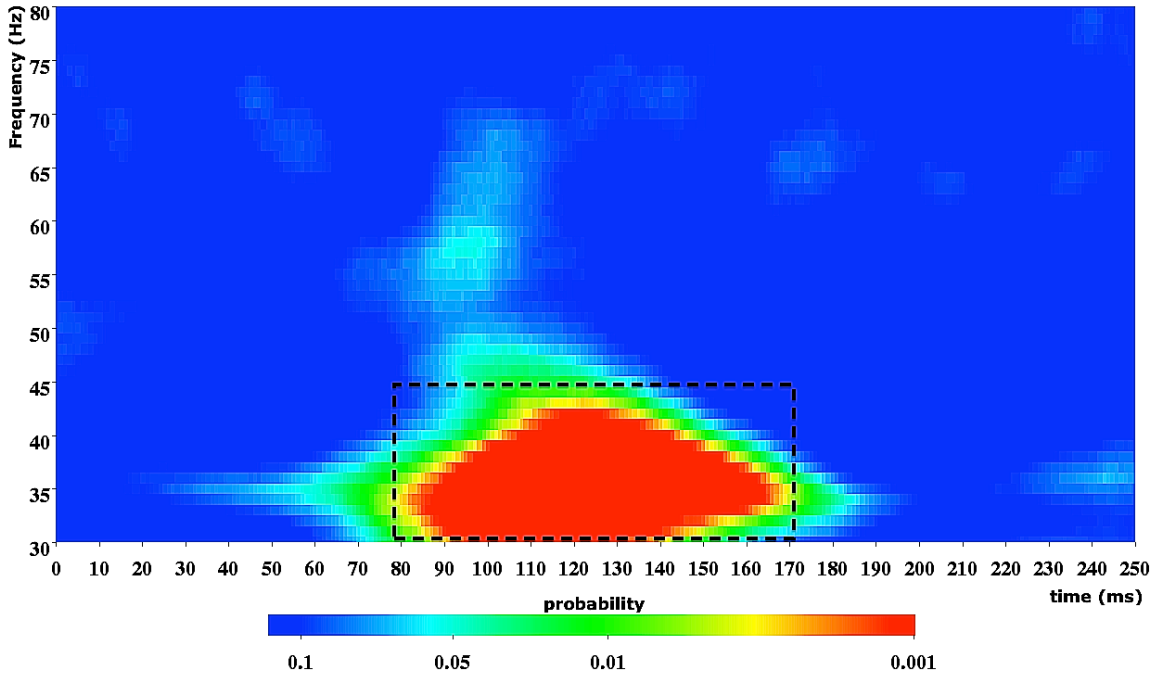


Figure 8.15 Between-group differences in different conditions (2). This figure represents the probability in time and frequency of significant differences in evoked gamma phase locked responses following the SHORT condition in ASD and SIM condition in TD between 0-250 ms and 30-80 Hz. Rectangle denotes the significant difference.

8.3.2.6 Within-group comparisons between conditions

Within group comparisons are presented below.

TD group

Time-frequency representation of the significant differences within the TD group between the SHORT and SIM conditions in evoked gamma phase-locking shows significant ($p<0.01$) differences between 30-45 Hz for latencies between 100 and 155 ms.

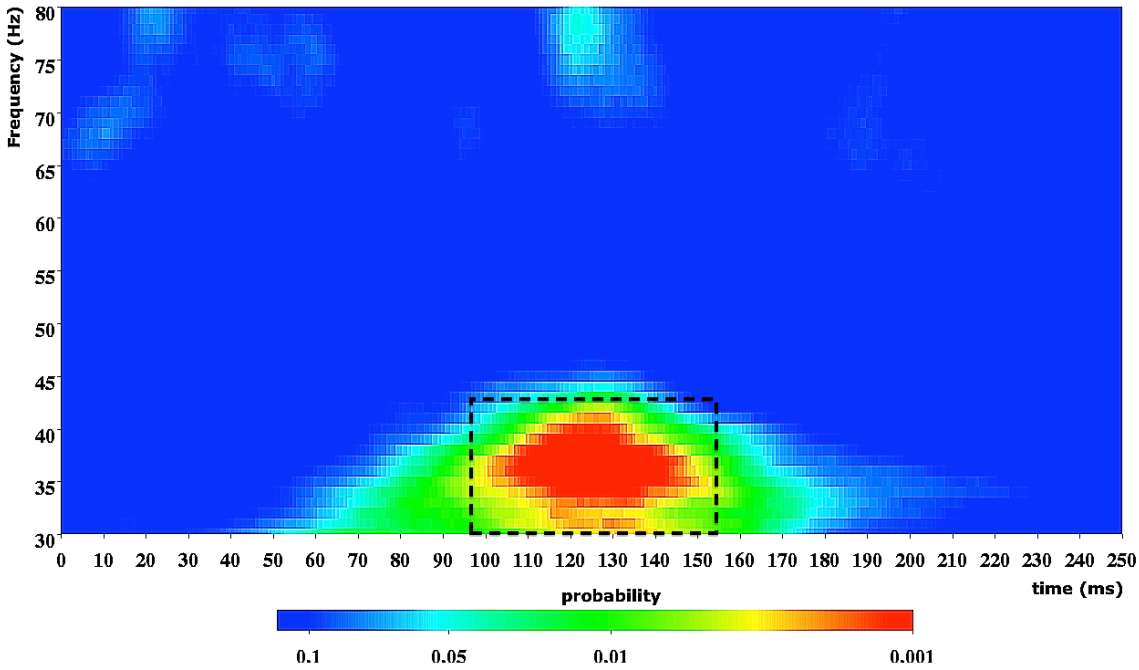


Figure 8.16 Within-TD differences between SHORT and SIM conditions. This figure shows a significant evoked gamma phase-locking between the SHORT and SIM conditions in the TD group at 30-45 Hz frequencies between 100-155 ms. Rectangle denotes the significant difference.

ASD group

Time-frequency representation of the significant differences within the ASD group between the SHORT and SIM conditions in evoked gamma phase-locking shows significant ($p<0.01$) differences between 30-50 Hz for latencies between 90 and 160 ms.

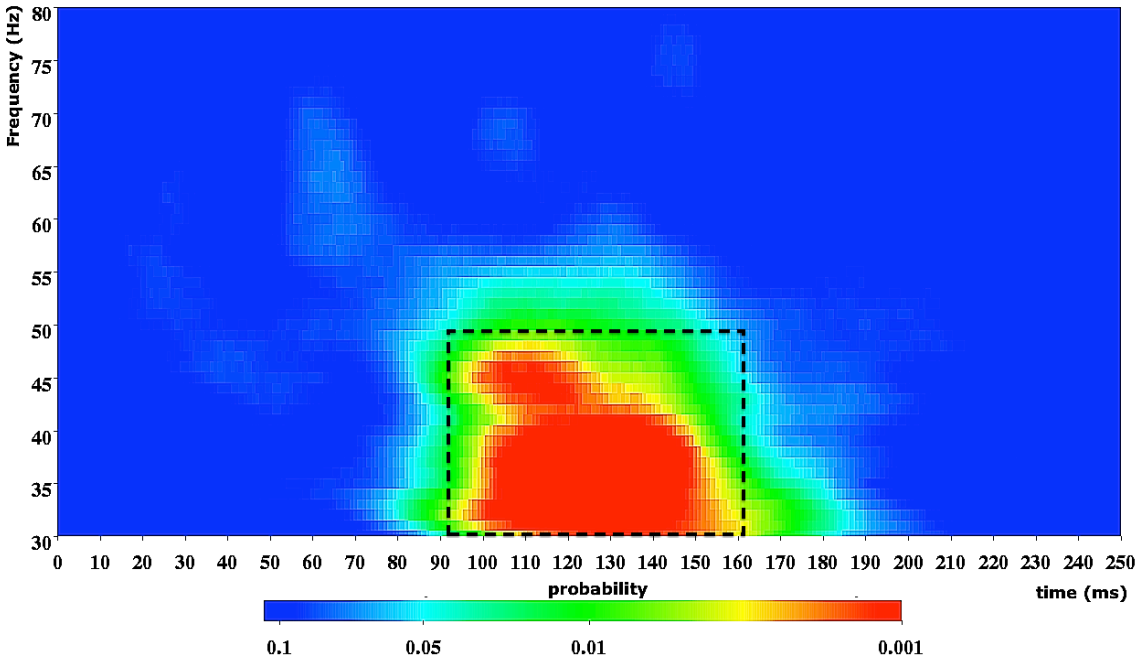


Figure 8.17 Within-ASD differences between SHORT and SIM conditions. This figure shows a significant evoked gamma phase-locking between the SHORT and SIM conditions in the ASD group at 30-50 Hz frequencies between 90-160 ms. Rectangle denotes the significant difference.

8.3.2.7 ANOVA interaction within the TD group

The time-frequency plane shows that within the TD group x condition interaction is significant ($p<0.01$) between 45-65 Hz for latencies between 40-120 ms, 45-70 Hz for latencies between 120-170 ms and 70-80 Hz between 60 and 90 ms. From the main ANOVA-rank interaction plane for group x condition for ASD and TD and the within-TD interaction plane, two evoked phase locked gamma ranges of interest were determined in order to pursue in post-hoc analyses for differences between TD and ASD and to perform phase-locking correlations with severity scores of the ADI-R and ADOS-G scores in the ASD group.

The first interval is the 50-80 Hz gamma range for latencies between 50-80 ms. The second interval is the earlier higher gamma range at 70-80 Hz between 20-40 ms.

When the main group and condition effects were plotted in time and frequency, no main effects were seen between 50-80 Hz for latencies between 20-150 ms.

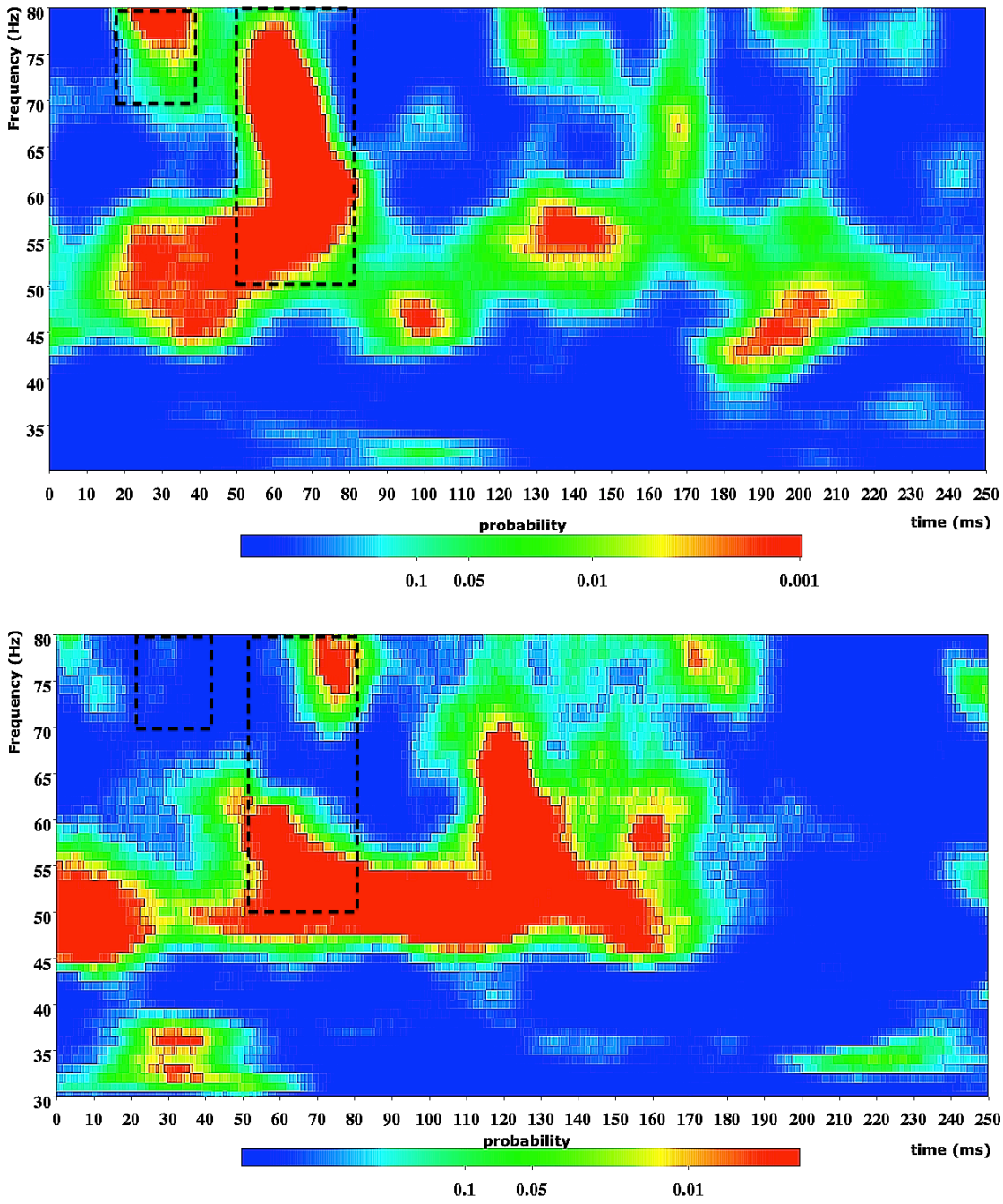


Figure 8.18 Identification of time and frequency intervals of interest. Top figure shows group x condition interaction from our main ANOVA-rank for both TD and ASD with the two t/f interval of interest: 1st interval is 70-80 Hz gamma range between 20-40 ms latencies (left rectangle) and 2nd interval is 50-80 Hz gamma range

between 50-80 ms latencies (right rectangle). Bottom figure shows the within TD group x condition interaction in evoked phase-locked gamma range. The left and right rectangles in this figure highlight the gamma intervals that are not present within the TD group when we perform the ANOVA-rank analyses.

Plotting within TD group main effects shows no main condition and group effects within the latencies and gamma ranges of interest.

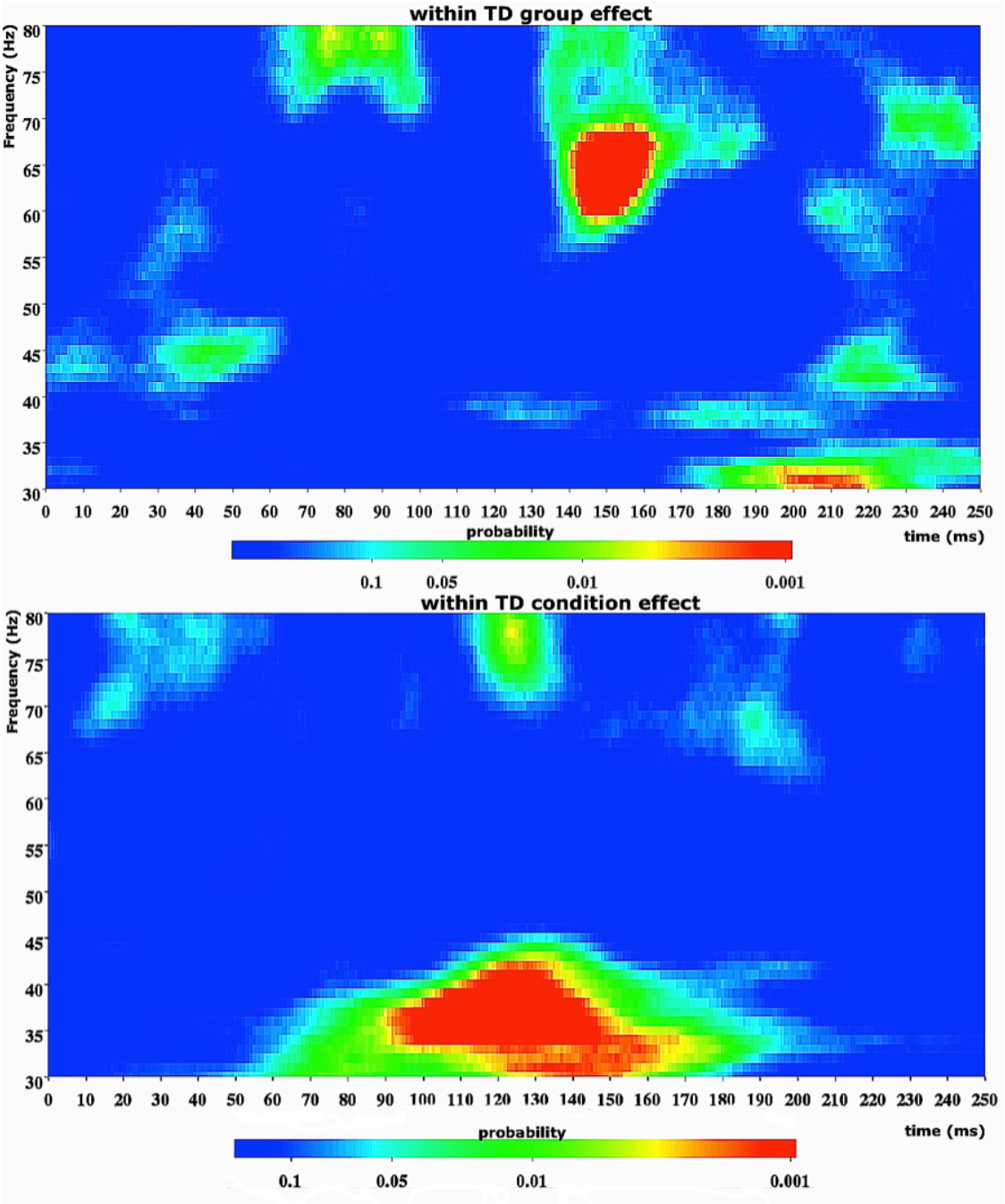


Figure 8.19 Within-TD group and condition effects. Top plot shows no main effect of group with the gamma ranges of interest (top plot). Bottom plot shows a main effect of condition.

8.3.2.8 Evoked gamma phase-locking at 50-80 Hz/ 50-80 ms

The first gamma interval of interest was 50-80 Hz/50-80 ms where differences between ASD and TD were identified in both conditions.

SIM condition between ASD and TD

The time-frequency plane after the Mann Whitney U statistic is shown below to determine significant differences in evoked gamma phase locking between TD and ASD. Between 50-80 Hz at 50-80 ms, there are no significant differences between TD and ASD. Evoked gamma phase-locking in TD and ASD was occipital.

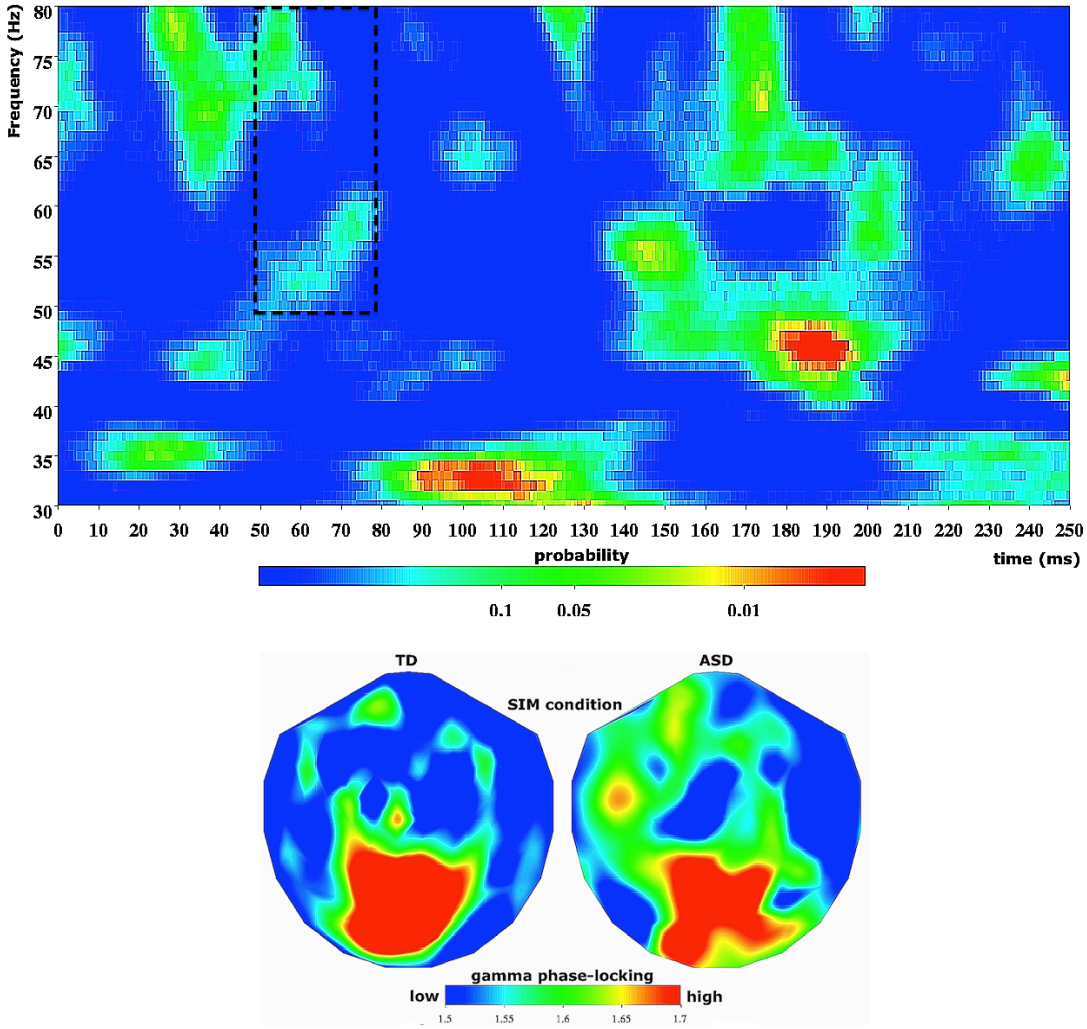


Figure 8.20 Between-group differences in the SIM condition in t/f interval of interest. The t/f plane showing differences in evoked gamma phase locking in the SIM condition between ASD and TD is represented in the top figure. Rectangle denotes no significant differences between 50-80 ms latencies and 50-80 Hz between

groups. Bottom figure shows that evoked gamma phase-locking pattern is occipital and similar between TD and ASD in the SIM condition.

SHORT condition between TD and ASD

Time-frequency plane after applying the Mann Whitney U statistic to determine significant differences in evoked gamma phase locking between TD and ASD is shown below. Between 50-80 Hz at 50-80 ms, there is a significant difference between TD and ASD in that range. The directionality of that difference shows a significantly reduced occipital evoked phase-locked gamma response in the ASD group compared with the TD group.

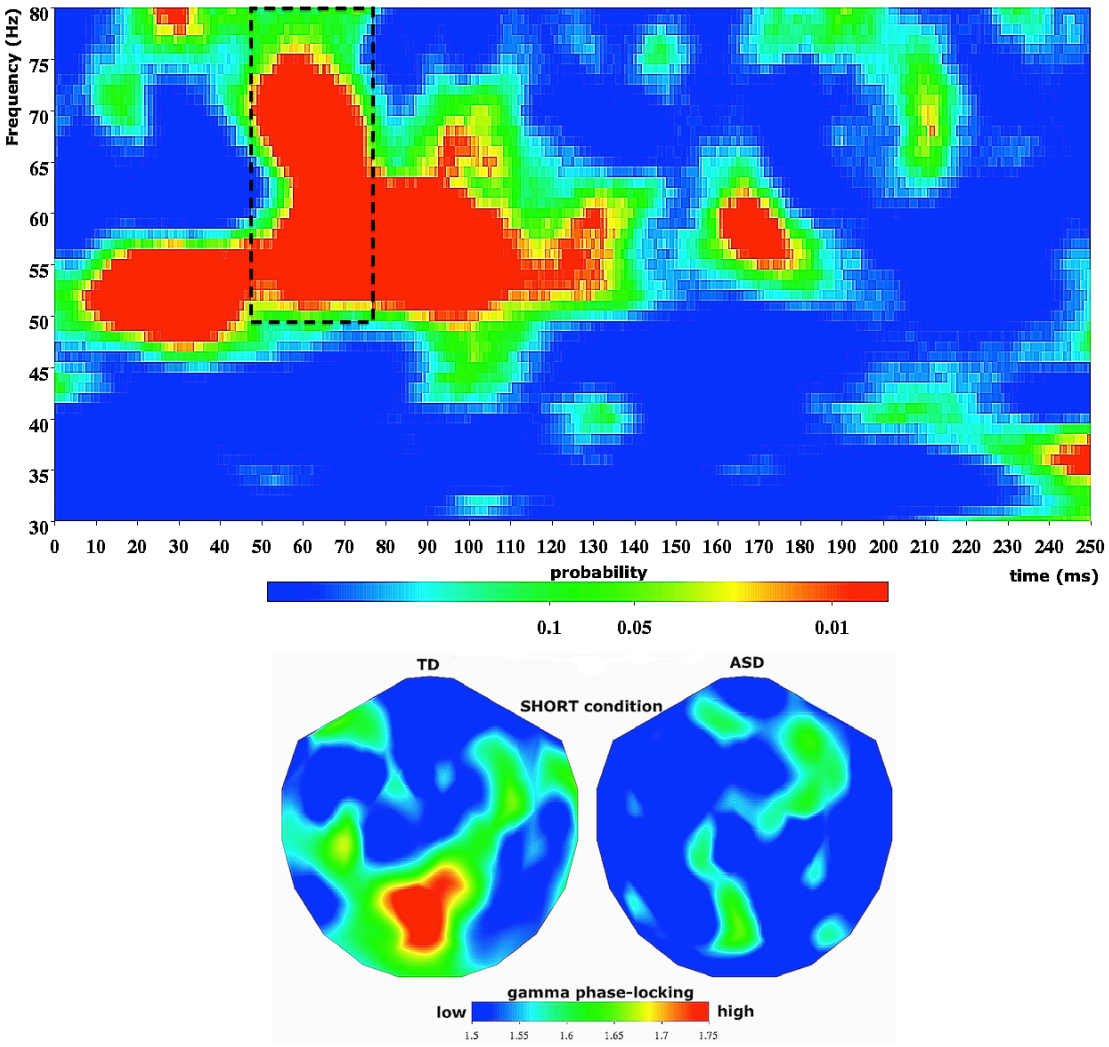


Figure 8.21 Between-group differences in the SHORT condition in t/f interval of interest. The t/f plane showing differences in evoked gamma phase locking in the SHORT condition between ASD and TD is represented in the top figure. Rectangle denotes significant differences between 50-80 ms latencies and 50-80 Hz between groups. Bottom figure shows that evoked gamma phase locking pattern is occipital and is markedly reduced in the ASD group the SHORT condition.

After mapping evoked gamma phase locking between groups, a numerical value was extracted in the SHORT condition corresponding to gamma phase locking. This was done by extracting the maximal channel value from the phase-locking map of each

individual in both groups. These values were subsequently averaged per group and condition and compared using a Mann-Whitney u non-parametric test between and within groups. In the SIM condition, mean phase locking is not significantly different between groups. However, it is significantly reduced in the ASD group in the SHORT condition (p=0.0007).

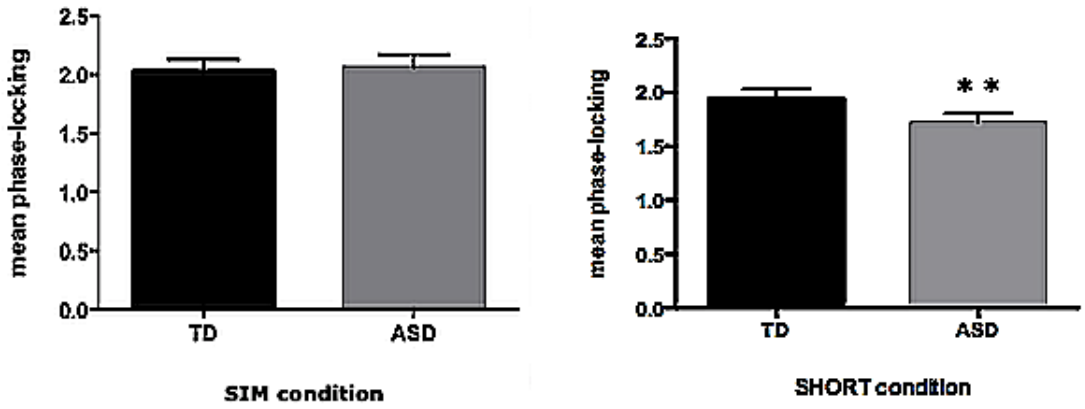


Figure 8.22 Mean phase locking between TD and ASD in SIM and SHORT conditions. This figure shows Mann-Whitney u testing of mean phase locking differences between TD and ASD in the SHORT and SIM conditions.

Wilcoxon testing for within-group differences between conditions was applied: the TD group showed no differences in mean phase-locking between conditions, whilst the ASD group showed a significant reduction in mean phase-locking (p=0.004) in the SHORT condition compared to the SIM condition.

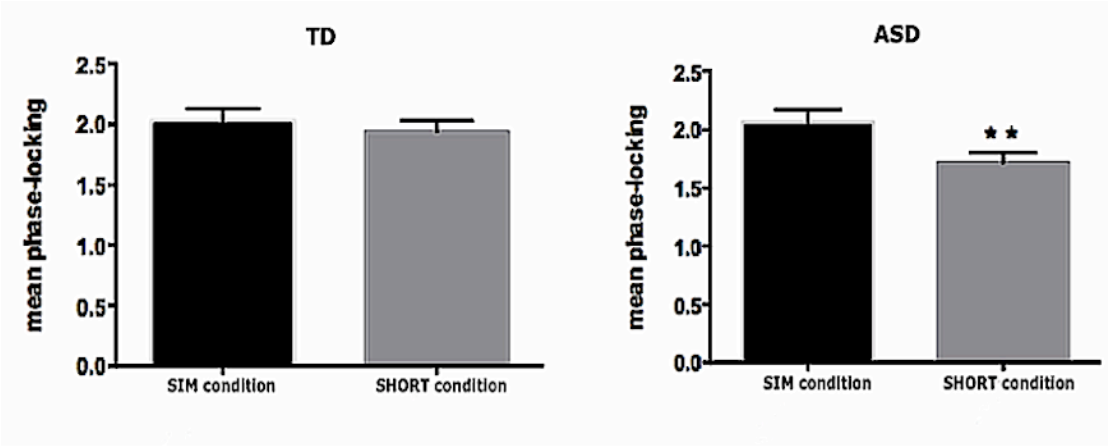


Figure 8.23 Mean phase locking between conditions in TD and ASD. This figure shows Wilcoxon-testing of mean phase locking differences within the TD and ASD groups between SHORT and SIM conditions.

8.3.2.9 Evoked gamma phase-locking between 70-80 Hz at 20-40 ms

The second gamma interval of interest was 70-80 Hz/20-40 ms where differences between ASD and TD were identified in both conditions.

SIM condition between TD and ASD

Time-frequency plane after applying the Mann-Whitney U statistic to determine significant differences in evoked gamma phase locking between TD and ASD is shown below. Between 70-80 Hz at 20-40 ms, there are no significant differences between TD and ASD ($p>0.01$). Evoked gamma phase locking in TD was central with right laterality and more centro-temporal with left laterality in the ASD group.

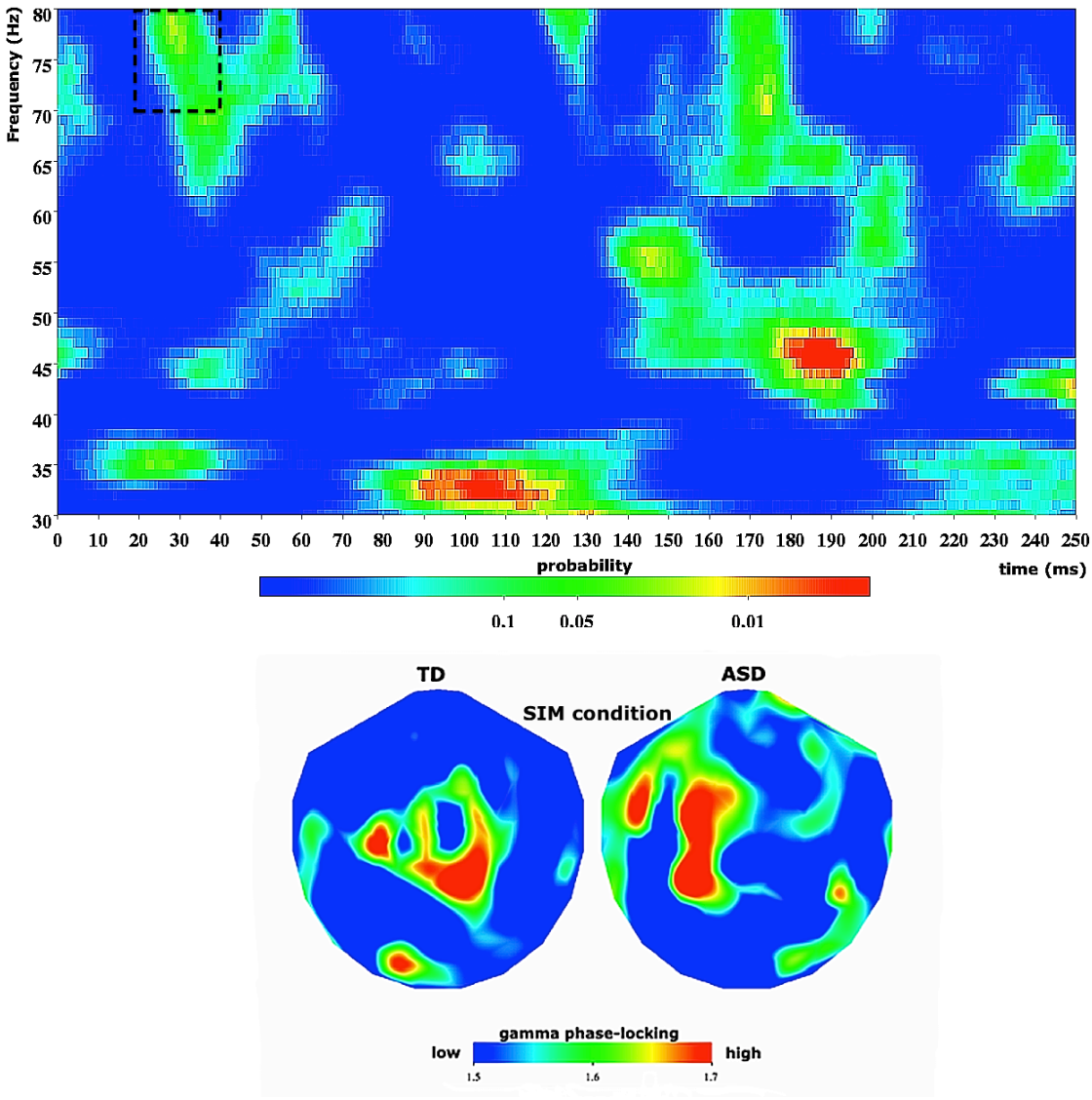


Figure 8.24 Between-group differences in higher gamma range in the SIM condition. The t/f plane showing differences in evoked gamma phase locking in the SIM condition between ASD and TD is represented in the top figure. Rectangle denotes no significant differences between 20-40 ms latencies and 70-80 Hz between groups. Bottom figure shows that evoked gamma phase-locking pattern is left centro-temporal in ASD and right central in the TD group.

SHORT condition between TD and ASD

Time-frequency plane after applying the Mann-Whitney U statistic to determine significant differences in evoked gamma phase locking between TD and ASD is shown below. Between 70-80 Hz at 20-40 ms, there is a significant difference between TD and ASD ($p<0.01$). Right frontal evoked gamma phase-locking in ASD is increased compared with the TD group.

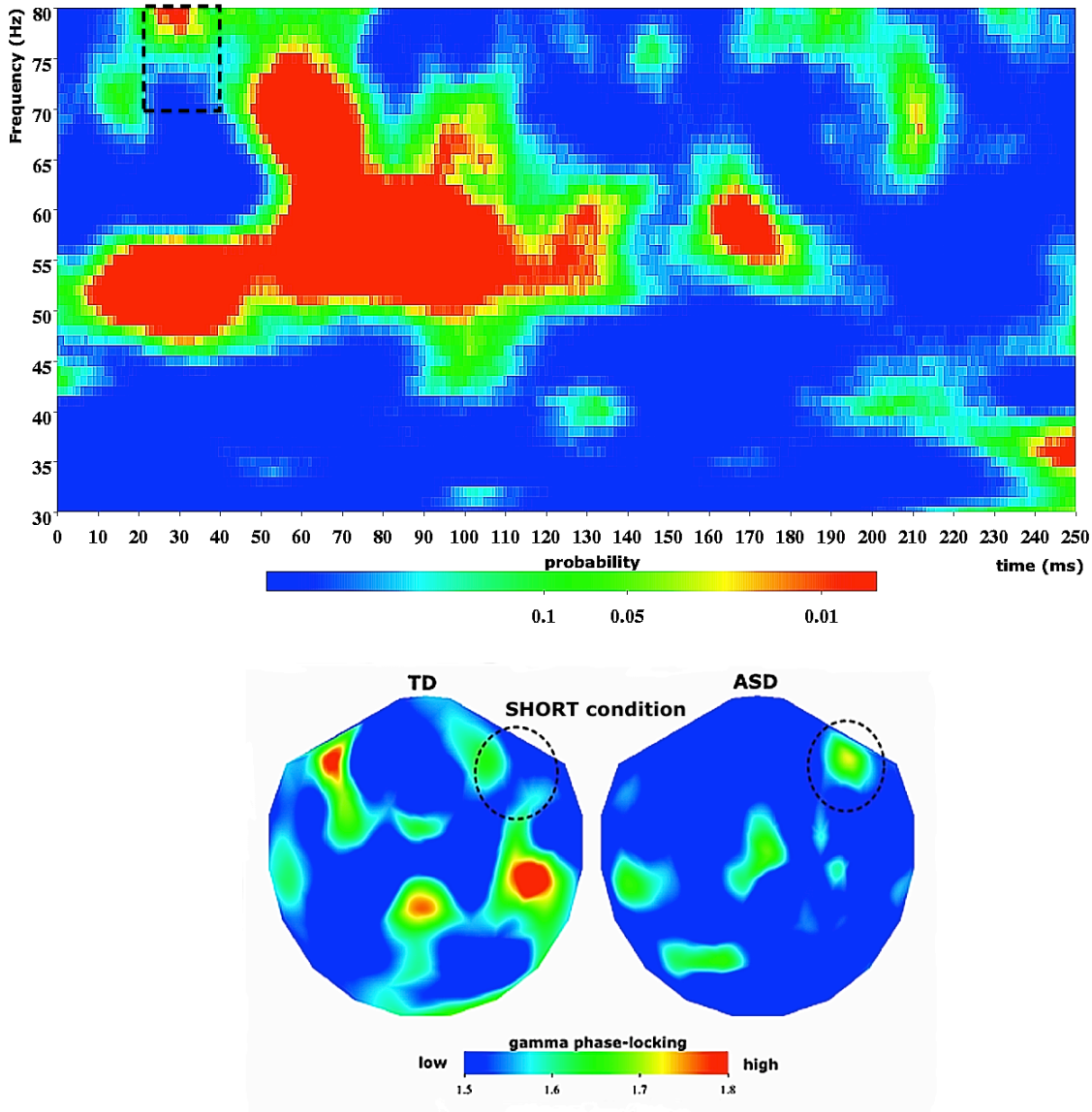


Figure 8.25 Between-group differences in higher gamma range in the SHORT condition. The t/f plane showing differences in evoked gamma phase locking in the SHORT condition between ASD and TD is represented in the top figure. Rectangle

denotes significant differences between 20-40 ms latencies and 70-80 Hz between groups. Bottom figure shows that right frontal evoked gamma phase-locking pattern is increased in the ASD group compared with the TD group in the SHORT condition.

Extraction of evoked gamma-phase locking maximal channel value as previously and performing between group Mann-Whitney U analyses shows an increase in ASD compared with TD in right frontal evoked gamma phase locking.

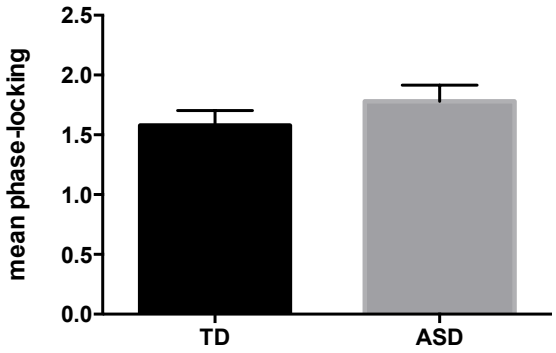


Figure 8.26 Mean phase locking differences in higher gamma in the SHORT condition between TD and ASD. The figure shows the increase in ASD compared with TD of right frontal evoked gamma phase locking between 70-80 Hz at 20-40 ms latencies.

8.3.3 Phase locking correlations with symptom severity

ADOS-G and ADI-R domain scores were correlated with occipital and right frontal gamma phase locking to show associations between ASD severity and the gamma response in the SHORT condition.

8.3.3.1 (50-80 ms/50-80 Hz) t/f range

Evoked gamma phase-locking measures at the occipital pole in the 50-80 Hz and at 50-80 ms latency in the SHORT-condition (‘simultaneous’ response) were correlated

using Spearman with ADI-R and ADOS-G scores from the subjects. Two values were excluded from the analysis: we did not have ADOS-G and ADI-R scores for one subject and one phase-locking value was detected as an outlier using R software. Therefore, 15 ASD individuals were retained for correlation analyses.

There was a significant inverse correlation between ADOS-G scores in the reciprocal social interaction domain (RSI) ($r=-0.54$; $p<0.05$) and evoked 50-80 Hz gamma phase locking in the 50-80 ms latency range. There were no significant correlations between evoked gamma phase locking in the 50-80 Hz range and 50-80 ms latency and ADI-R scores in the different domains in the SHORT condition.

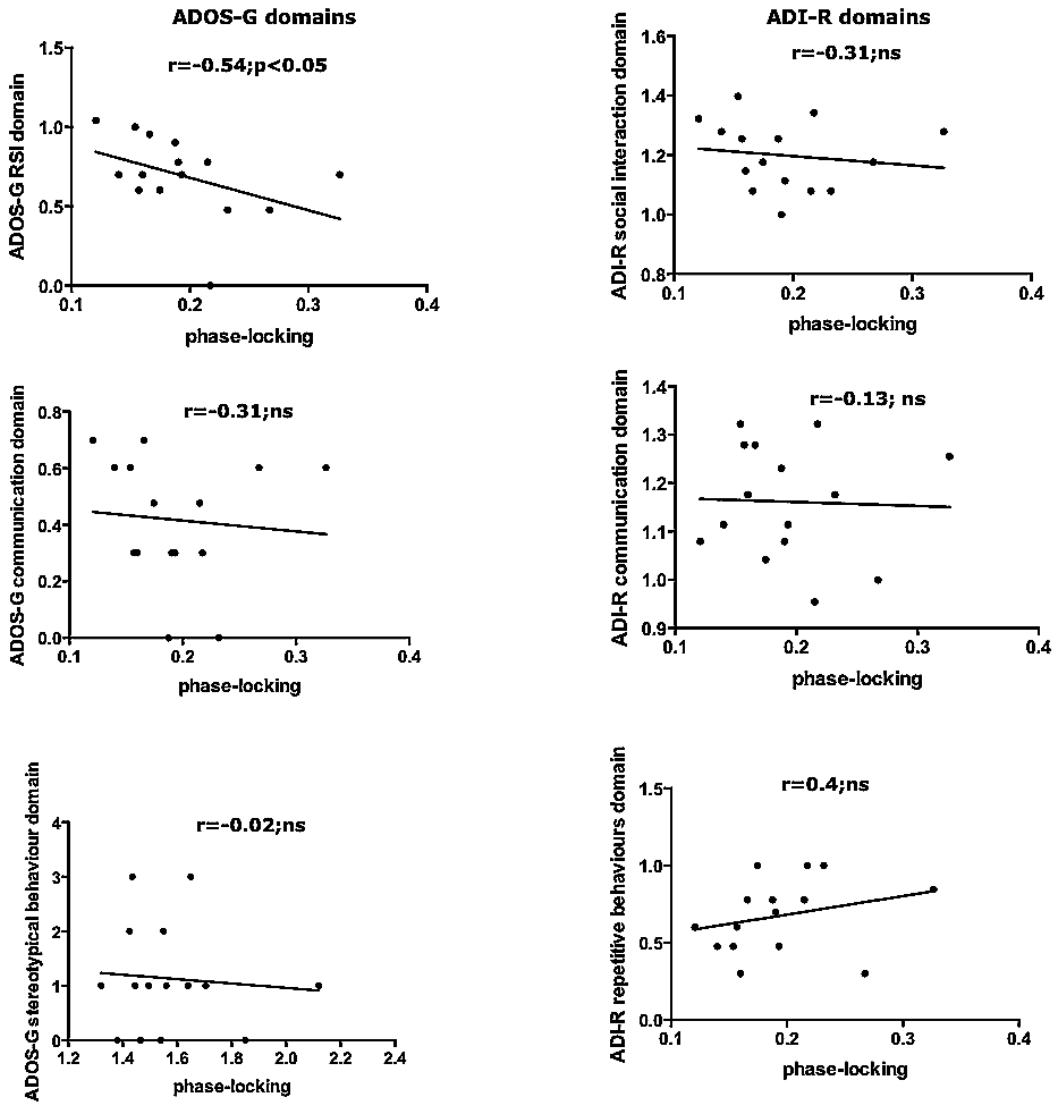


Figure 8.27 Correlations between gamma phase locking and severity scores in the first t/f interval. Figure above shows correlations of ADOS-G and ADI-R domain scores in the SHORT condition with phase-locking values in the 50-80 Hz and 50-80 ms ranges. Data have been log-transformed except for ADOS-G stereotypical behaviour domain, where scores were sometimes equal to 0.

An analysis of the variance of ADOS-G scores shows maximum variance in ADOS-G scores in the RSI domain as opposed to lower variance in ADOS-G communication and stereotypical behaviour domains

Table 8.4 Dispersion of ADOS-G domain scores

	ADOS-G Domain Scores		
	Communication	**RSI**	**Stereotypical behaviour**
Variance	1.78	7.67	0.98
Minimum	1	1	0
Maximum	5	11	3
Range	4	10	3

An analysis of the variance of ADOS-G scores shows maximum variance in ADOS-G scores in the RSI domain as opposed to lower variance in ADOS-G communication and stereotypical behaviour domains

8.3.3.2 (20-40 ms/70-80 Hz) t/f range

There was a significant positive correlation between ADOS-G scores in the reciprocal social interaction domain (RSI) ($r=0.54$; $p<0.05$) and evoked 70-80 Hz gamma phase locking in the 20-40 ms latency range. There were no other significant correlations between evoked gamma phase locking in this range and ADI-R scores in the different domains in the SHORT condition.

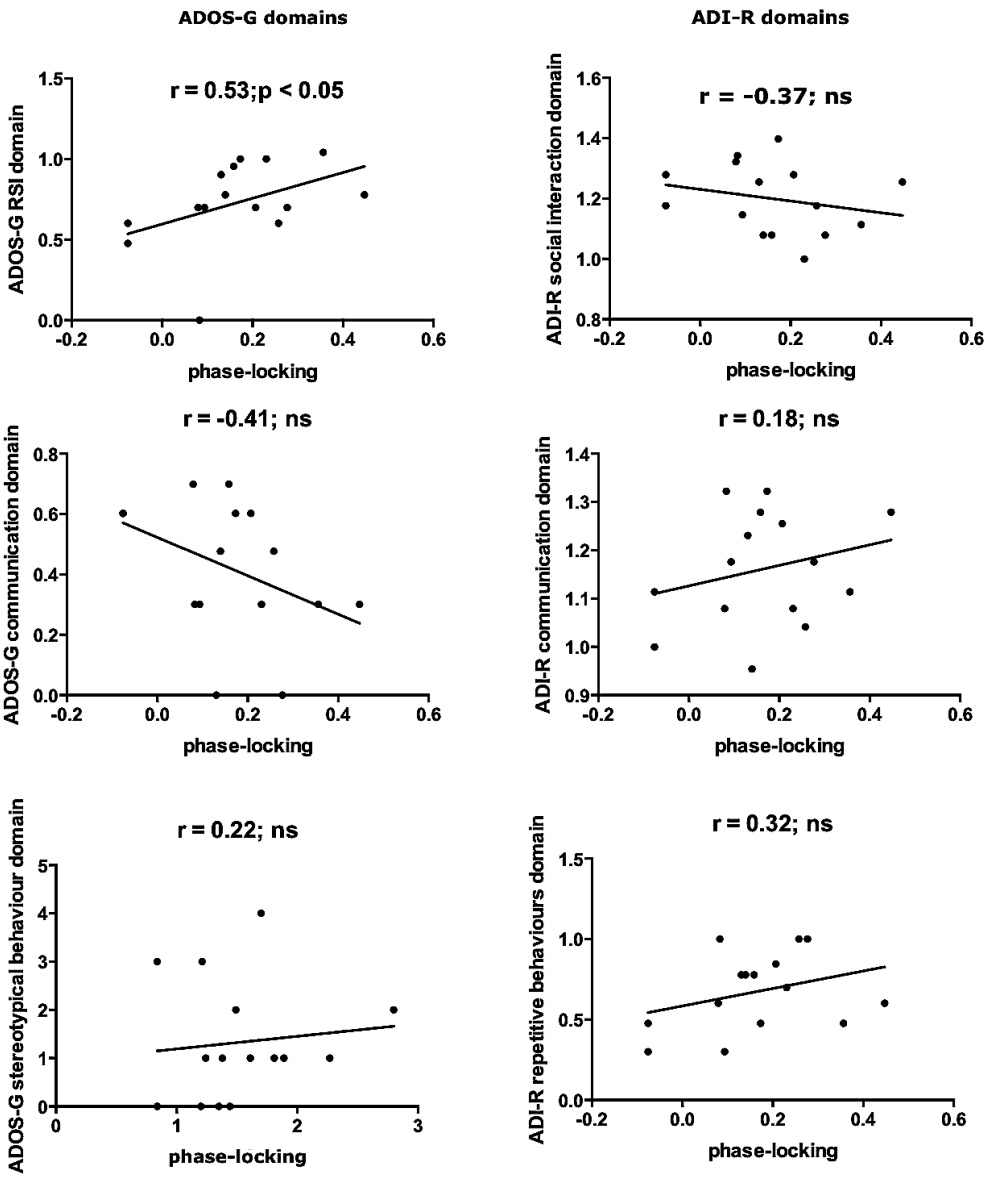


Figure 8.28 Correlations between gamma phase locking and severity scores in the second t/f interval. Figure above shows correlations of ADOS-G and ADI-R domain scores in the SHORT condition with phase-locking values in the 70-80 Hz and 20-40 ms ranges. Data have been log-transformed except for ADOS-G stereotypical behaviour domain, where scores were sometimes equal to 0.

8.3.4 Validity and robustness of findings

To assess the robustness of the above results, several verifications were undertaken. These are outlined below.

8.3.4.1 Increasing the scale of main ANOVA interaction

Increasing the scaling of the time-frequency plane of the group x condition interaction plane illustrates that the 50-80 Hz at 50-80 ms gamma range as well as the 70-80 Hz at 20-40 ms are the intervals where the effects are strongest.

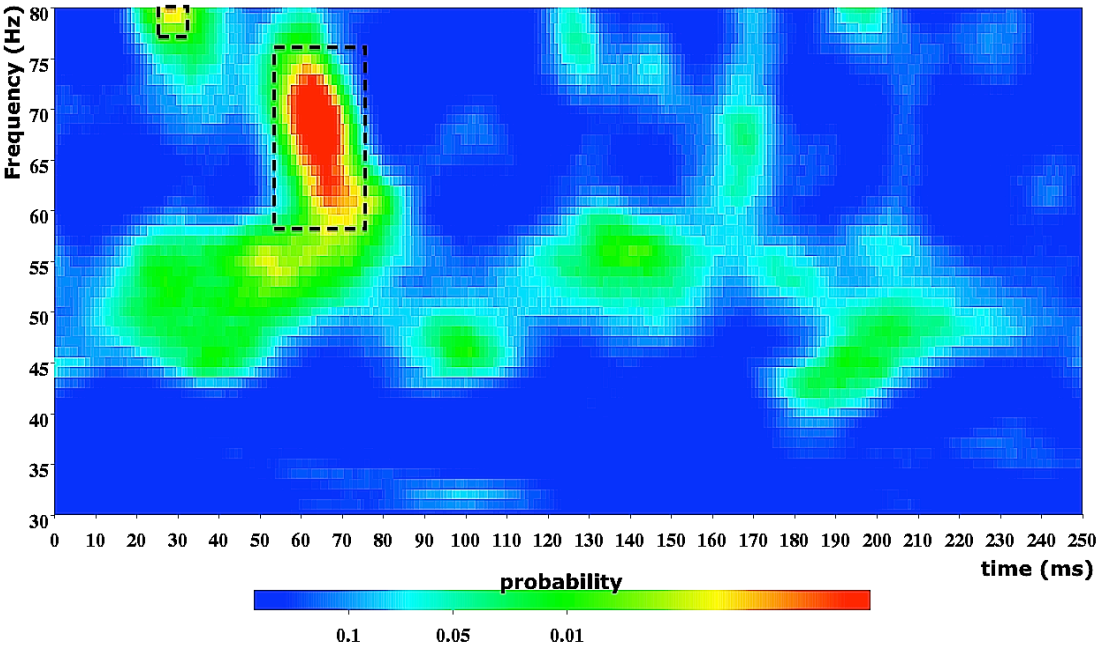


Figure 8.29 Increased scale of ANOVA interaction. This figure shows the strongest gamma ranges remaining after increasing the scaling in the t/f plane of the group x condition interaction in the ANOVA-rank. The highest frequency is indeed captured in the early cluster (20-40 ms/70-80 Hz) even if plotting in the y-axis is increased to 85 Hz to capture the full interaction (entire red area) in this early cluster.

8.3.4.2 Taking a larger evoked gamma time interval

Even if the time interval is increased (40-120 ms) to include earlier and later latencies on the 50-80 ms/50-80 Hz gamma range, occipital phase-locking is reduced and more importantly, the negative correlation between ADOS-G (RSI) and evoked gamma phase-locking in this range still holds with $p<0.05$.

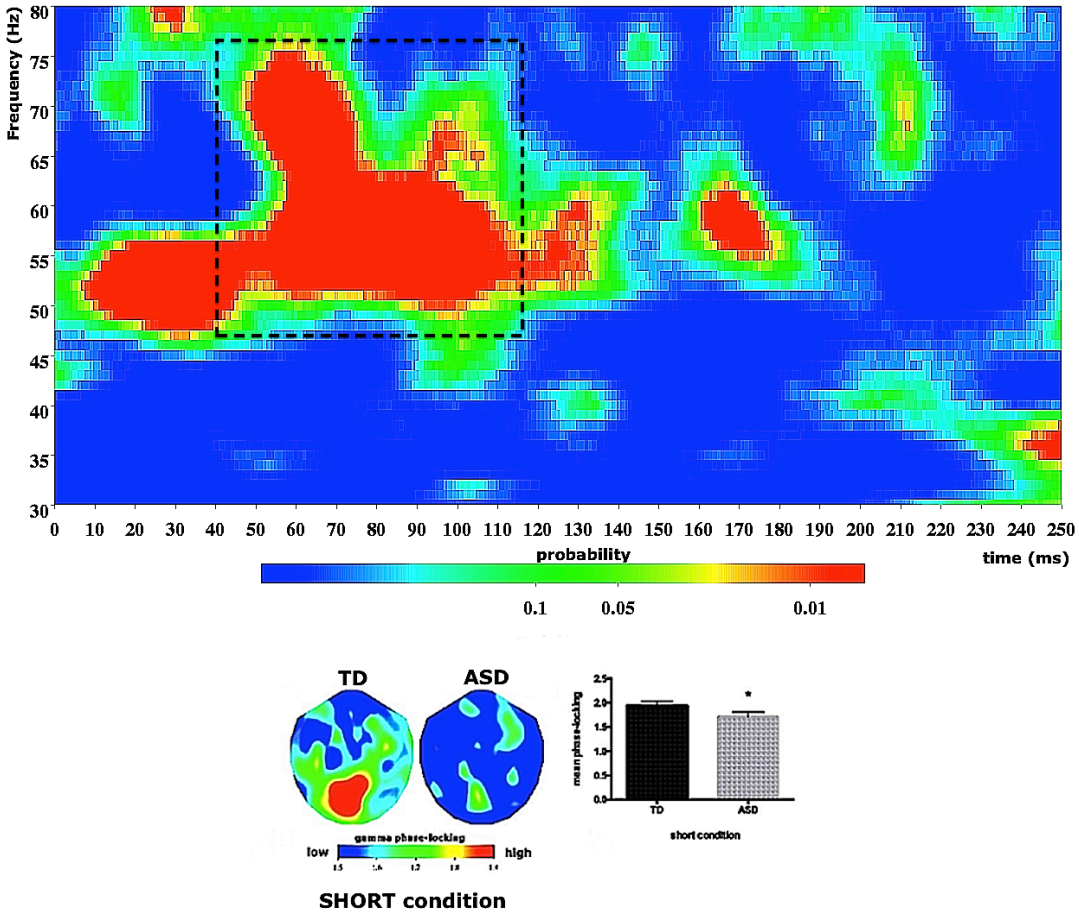


Figure 8.30 Inclusion of a larger t/f interval of significance. This figure above shows the integration over time to include earlier and later latencies of evoked gamma phase locking between 50-80 Hz at a latency range between 40-120 ms. Top figure shows the Mann-Whitney U plane with the rectangle denoting a significant difference in evoked gamma phase locking between TD and ASD. Bottom left figure shows that occipital phase locking is reduced in the ASD group in this integration and bottom

right figure shows that the difference in the maximal channel value is decreased in the ASD group compared with the TD group and is still significant (p=0.03).

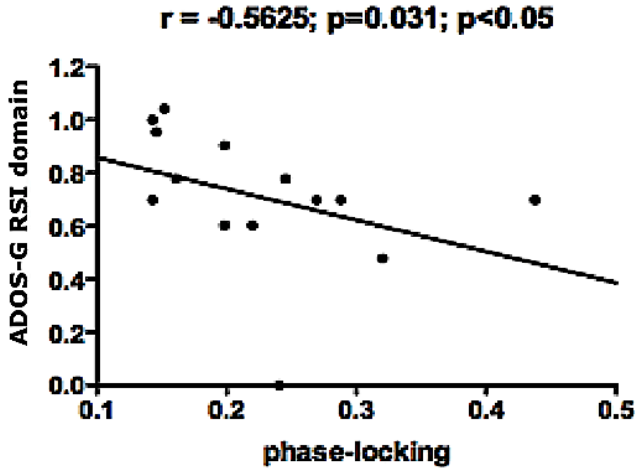


Figure 8.31 Strength of the association between symptom severity and gamma phase locking. This figure shows that the inverse correlation still holds between the ADOS-G RSI domain and mean gamma phase-locking in the ASD group even if we consider a larger temporal integration.

8.3.4.3 Mapping evoked gamma in TD & ASD in both conditions

To verify that there was no averaging artefact and to confirm that the reduction in occipital phase-locking (50-80 Hz) at early latencies (50-80 ms) is consistent across all individuals in ASD, individual phase-locking averages were plotted in all 34 individuals by choosing a slightly larger latency interval that includes our interval of choice. In 15/17 individuals with ASD, reduced evoked gamma phase-locking in the SHORT condition compared to the SIM condition can be seen at the occipital pole. In the TD group, 14/17 individuals show that gamma phase locking (50-80 Hz) is similar between SHORT and SIM at the occipital pole at early latencies (50-80 ms).

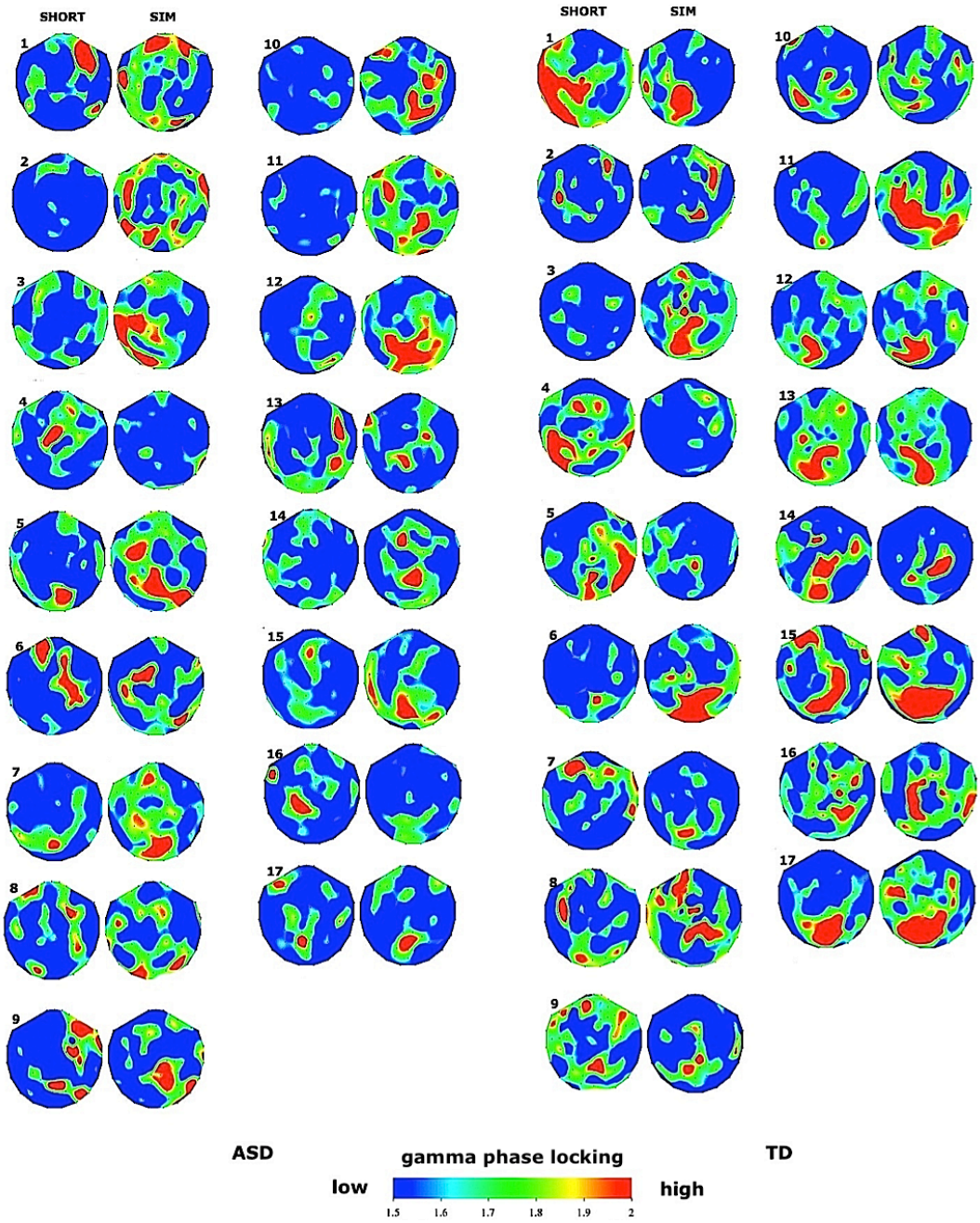


Figure 8.32 Individual phase locking averages in the gamma range (50-80 Hz) at latencies between 50 and 110 ms. Generally, ASD individuals show reduced gamma phase locking in the SHORT condition compared to the SIM condition at the occipital pole as opposed to the TD group, where generally, gamma phase locking is unaltered between SHORT and SIM conditions.

8.3.4.4 Excluding the TDs who performed well on the task

5 TD individuals who performed well in the SHORT condition were removed from the analyses and the Mann-Whitney U time-frequency plane was plotted to detect differences in evoked gamma phase locking between the remaining TDs (non-ASD-like) and the ASD group. Despite the removal of data from these 5 individuals, the result persists and is robust and the 50-80 Hz/50-80 ms gamma range is still visible in the t/f plane. Occipital phase locking is also markedly reduced in the ASD group compared with the non-ASD-like group.

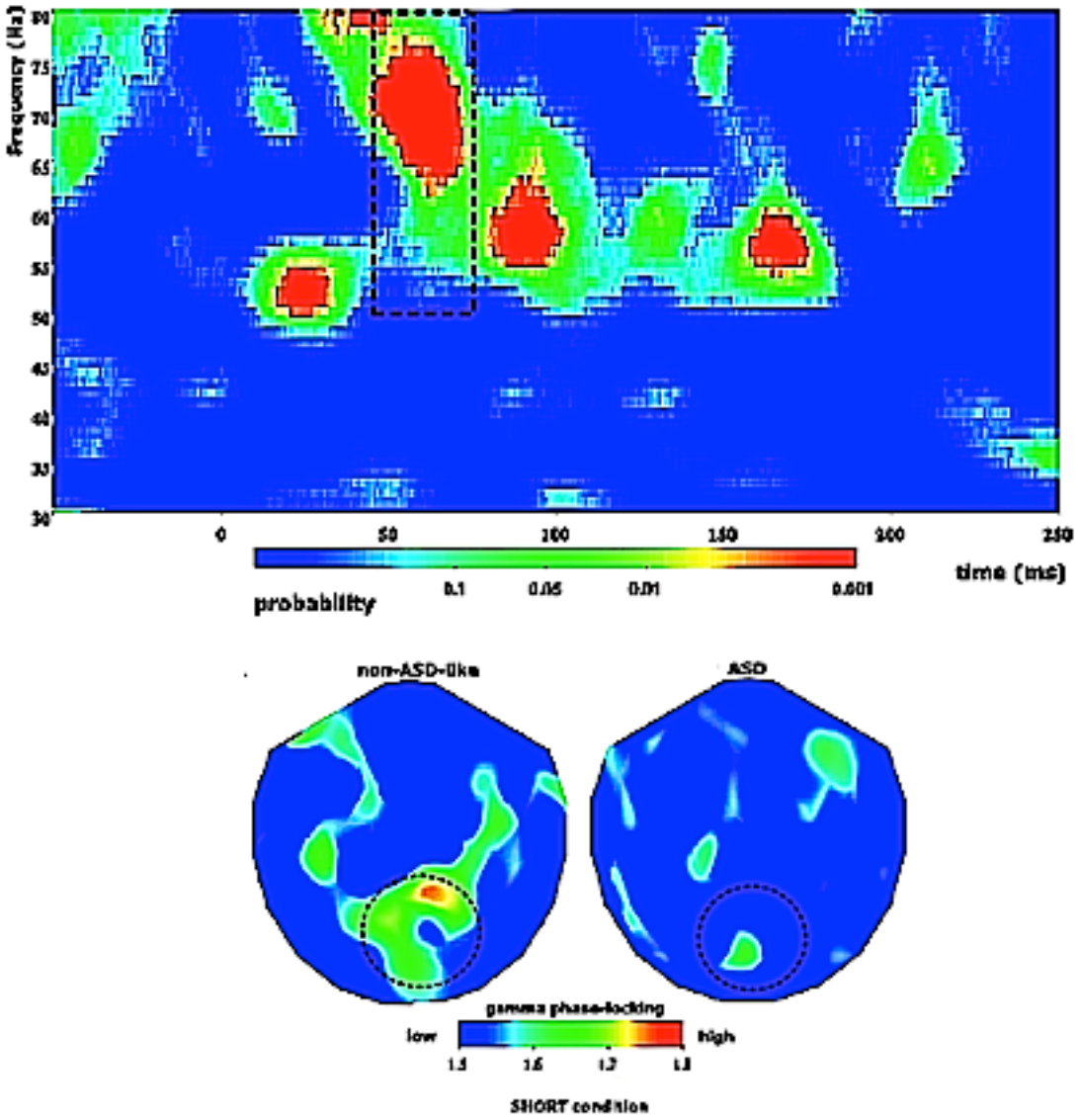


Figure 8.33 Exclusion of top TD performers on the SHORT condition. Top figure

illustrates the t/f plane showing a significant evoked gamma phase locking difference between non-ASD-like and ASD after removing the 5 high-performing TDs in the SHORT condition. Bottom figure shows a reduction in occipital phase locking in the TD group.

8.3.5 The LONG Condition

Time-frequency analysis of evoked phase locked gamma activity in the LONG condition between TD and ASD showed no difference between groups (dotted circle in figure 8.34) at latencies less than 120 ms from the presentation of the first stimulus. This is demonstrating that task performance alone did not give a gamma effect. Significant differences were noted after 120 ms in the lower gamma range of 30-38 Hz between 130-180 ms, which was predominantly occipital and with higher phase locking in ASD compared with TD. The significant difference in the higher gamma range of 70-80 Hz between 130-150 ms was stronger right frontally in TD compared with ASD. The 40-65 Hz between 120-160 ms significant difference between groups was shown to be stronger in the centro-parietal and right occipital areas in ASD compared with TD. Finally, there was also a significant difference between groups between 190-240 ms and at a gamma range of 55-80 Hz. The TD group in this interval showed a more occipital response as opposed to a more centro-parietal response in the ASD group.

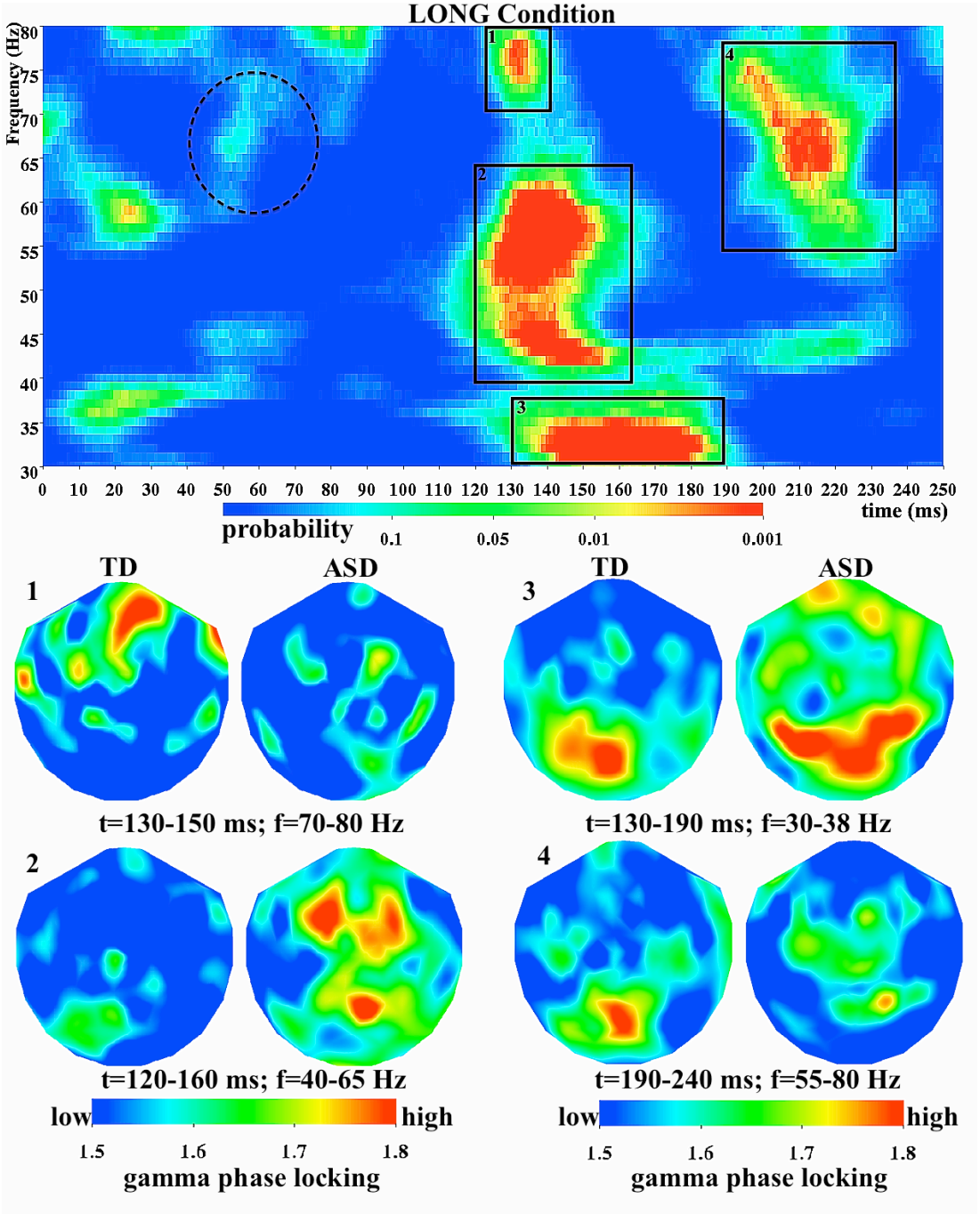


Figure 8.34 LONG condition between TD and ASD. Top figure illustrates the t/f plane in the LONG condition correlated with the non-simultaneous behavioural outcome. The significant evoked gamma phase locking differences between ASD and TD are shown by the squares (1, 2, 3 and 4) and the dotted circle represents the previously investigated intervals with no difference between groups in this gamma

range. Below the t/f planes, phase locking (grms values) per group are shown with the numbers (1, 2, 3 and 4) associated with the squares in the t/f plane.

8.3.6 Other evoked phase locking differences in the SHORT condition

Phase-locking differences in t/f between TD and ASD existed in the gamma range after 250 ms and also in the lower frequency ranges (<25 Hz) in this condition. These are shown below.

8.3.6.1 Gamma differences in the SHORT condition after 250 ms

There were further evoked gamma differences between 30-80 Hz and between 250-1000 ms in the SHORT condition. These are illustrated in the following page.

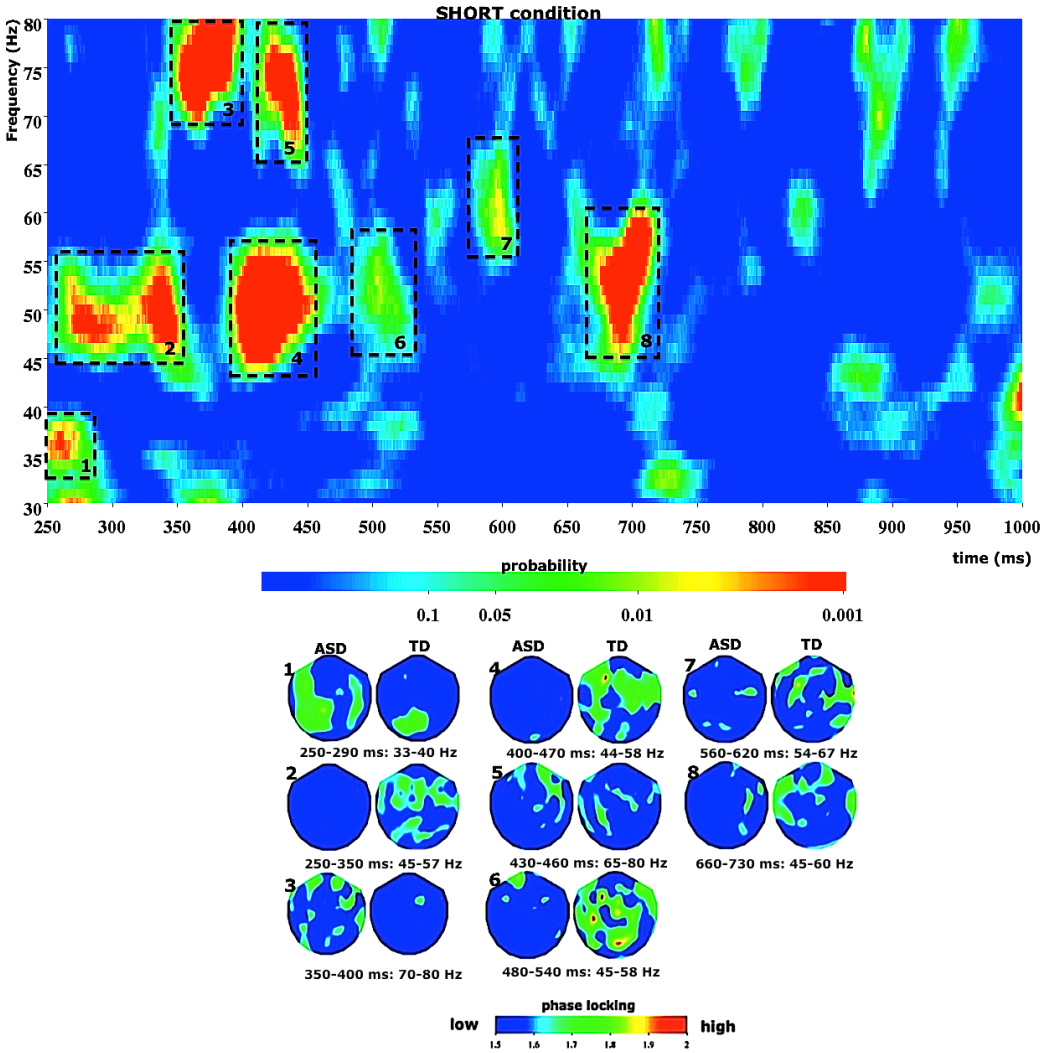


Figure 8.35 Gamma differences in the SHORT condition at later latencies. This shows mapping of phase-locking differences across the time-frequency plane between TD and ASD over latencies > 250 ms and gamma frequency ranges (30-80 Hz) in the SHORT condition. Plots 1 and 3 in the bottom figure show an increase in gamma phase locking in ASD compared with TD whilst the remaining plots show generally reduced gamma phase-locking in ASD compared with TD.

8.3.6.2 Lower frequencies in the SHORT condition

The Mann-Whitney U time-frequency plane also shows a significant difference in evoked beta phase-locking between ASD and TD at latencies between 50-400 ms and

a frequency range between 15-24 Hz. Beta phase-locking is occipital and also reduced in ASD.

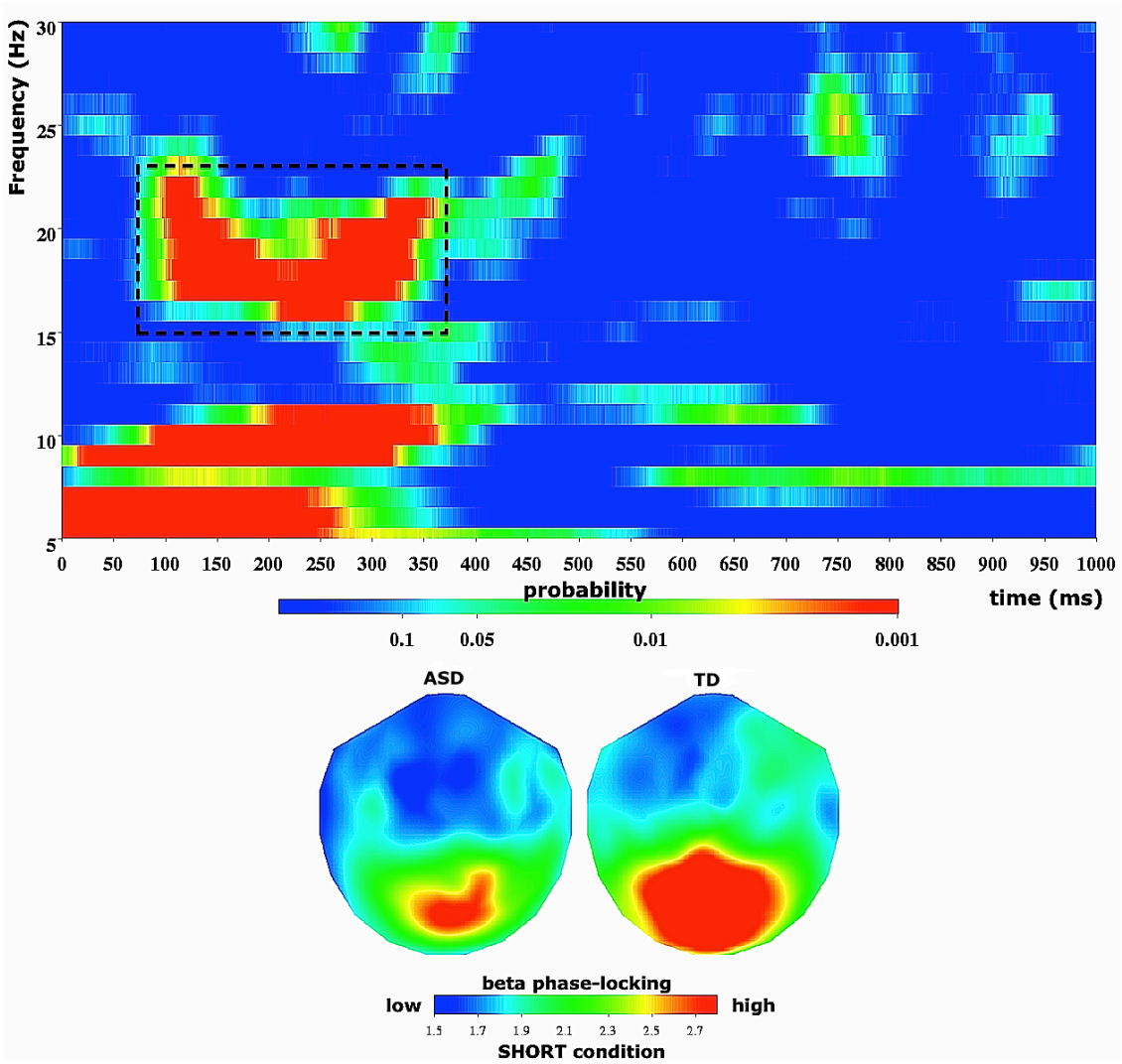


Figure 8.36 Beta differences in the SHORT condition. The top figure shows the t/f plane after applying the Mann-Whitney u in the SHORT-condition to detect significant differences between TD and ASD at lower frequencies (<30 Hz) and from 0-1000 ms latencies. Rectangle denotes a significant difference in evoked beta phase locking. Bottom figure shows occipital reduction in beta phase locking in the ASD group compared with the TD group.

8.4 Discussion

This study examined the neural correlates underlying enhanced temporal resolution and superior performance of ASD individuals in a perceptual simultaneity task. 34 individuals (17 ASD, 17 TD) judged between real and apparent simultaneity in three conditions (SHORT, LONG, SIM) (Falter, Braeutigam et al. 2013). Using time-frequency analyses, trial-by-trial phase consistency of oscillatory synchrony in the gamma range (30-80 Hz) was investigated in the SHORT, SIM and LONG conditions in ASD and TD. Gamma oscillatory synchrony is thought to underlie visual processing events and has roles in visual grouping and perceptual binding (Tallon-Baudry 2009). Given that gamma oscillations in response to various visual stimuli (face-processing stimuli (Wright, Alderson-Day et al. 2012), illusory contours (Stroganova, Orekhova et al. 2012), video stimuli (Kikuchi, Shitamichi et al. 2013), Gabor patches (Milne, Scope et al. 2009)) and in resting-state paradigms (Cornew, Roberts et al. 2012)) are altered in ASD, it was hypothesized that a reduction in gamma-band synchrony may underlie the enhanced temporal resolution in perceptual simultaneity in ASD. MEG studies on evoked gamma responses in visual processing are very rare and this is the first study to investigate evoked gamma responses in perceptual simultaneity in ASD.

Summary of findings

At the behavioural level and consistent with the study by Falter (2013), individuals with ASD were 4 times more likely to distinguish apparent simultaneity in the SHORT condition compared with the TD group. In the LONG condition however, ASD individuals were less likely to give the correct behavioural outcome compared with the TD group.

At the level of the neurophysiological response, a highly complex interaction between subject group and experimental condition was observed in the t/f planes, where this interaction was partly overlapping with a group effect suggesting higher gamma over occipital cortices in TDs at latencies typically associated with the primary visual response at around 100 ms.

In contrast, the pattern of significance was clearly (in terms of the available resolution of the t/f planes), distinct from a condition effect suggesting higher occipital low-gamma following SIM compared to SHORT stimuli at about 130 ms. Importantly, an intra-TD analyses allowed to reduce the complexity of the interaction to two t/f regions robustly sensitive to ASD over and above differences in performance. In particular, an early visual (50-80 Hz/50-80 ms) effect suggested an ASD-specific reduction of high gamma over occipital cortices in the SHORT condition. Critically, this gamma activity was significantly and negatively associated with symptom severity in patients. An even earlier effect at earlier latencies (20-40 ms) and at higher gamma frequencies (70-80 Hz) showed a right frontal increase in phase locked gamma where the gamma activity was significantly and positively correlated with symptom severity in the ASD group. Additionally, outside the main t/f region of interest, increased gamma in ASD compared with TD was observed at longer latencies but at similar frequencies. In the LONG condition, gamma responses could be dissociated into three frequency ranges: occipital lower gamma (30-40 Hz) stronger in ASD, a right frontal higher gamma (70-80 Hz) stronger in TD and within the t/f interval of interest (50-80 Hz), a more diffuse and spread out parietal, central and occipital gamma stronger in ASD immediately following the appearance of the second bar. Finally, also within (50-80 Hz), occipital gamma became weaker in ASD at later latencies (190-240 ms).

Superior performance of ASD in perceptual simultaneity

Superior performance in the SHORT condition in ASD might be conceptually consistent with superior visuo-perceptual processing being associated with WCC theory (Shah and Frith 1983), suggesting higher local processing abilities and attention to fine task details in comparison with TDs. Interestingly, individuals with ASD did not perform as well in the LONG task. It can be speculated that as they anticipated the appearance of the second bar, individuals with ASD may have become more distracted resulting in an erroneous behavioural outcome on some occasions. It is to be noted however that they still performed relatively well in this condition though they seemed to be more prone to errors. Therefore, perhaps with extremely high temporal resolutions such as those encountered in the SHORT condition, the ASD brain being more task-focused and less distracted may result in better task performance.

Oscillatory synchrony in the gamma range in the SHORT and SIM conditions in the 50-80 ms/50-80 Hz interval

In the SIM condition, evoked phase-locked gamma activity was located to the occipital visual areas in both TD and ASD. Behaviourally, both groups perceived the stimulus as simultaneous and phase locking was similar between groups thereby explaining why the Mann-Whitney U t/f plane showed no difference in the interval of interest. Evoked phase-locked gamma activity in response to real simultaneity might play a role in binding both vertical bars into the same visually coherent event within the same time window in line with the binding-by-synchrony hypothesis (Tallon-Baudry 2003). In the SHORT condition, occipital evoked phase-locked gamma activity was significantly reduced in the ASD group compared with the TD group in response to apparent simultaneity. This reduction was consistent across 15/17 ASD

individuals. Reduction in evoked phase-locked gamma is consistent with a study by Stroganova et al (2012) who observed reduced evoked phase-locked gamma activity in response to Kanisza stimuli in a group of children with ASD. This located to the parieto-occipital cortices at latencies between 40-120 ms (Stroganova, Orekhova et al. 2012). The Mann-Whitney U t/f plane in this condition showed a much larger difference in evoked activity between ASD and TD between 10-90 ms and 45-80 Hz. However, plotting the group x condition interaction within the TD group demonstrated that the 50-80 Hz/50-80 ms interval was more specific to ASD whilst the remaining differences related to task performance in both groups.

Behaviourally, the ASD group was better at recognizing apparent simultaneity than the TD group. Though reduced evoked gamma phase locking has been associated with impaired visual processing, it seems to be advantageous to task performance in ASD. Although the false behavioural outcome has been communicated, ASD subjects may have recognized at the neural level apparent simultaneity demonstrated by the reduction in evoked gamma phase locking. Gamma activity burst is usually observed when objects are perceived as part of the same percept. It is interesting to consider that in the SHORT condition, the visual scene might have been perceived as two distinct stimuli in ASD, thereby reflecting the true response. In contrast to the ASD group, phase-locked gamma activity was similar to the SIM condition in the TD group possibly indicating that the visual scene was bound into one percept therefore masking apparent simultaneity at the neural level. Thus, reduced gamma oscillatory synchrony in apparent simultaneity in ASD might be supportive of superior task performance through reduced binding.

Reductions in occipital evoked gamma phase locking were associated with stronger ASD severity in the RSI domain. This was demonstrated by a strong negative

correlation between phase locking and ADOS-G scores in the RSI domain. This is in line findings from other groups who have also identified correlations between the ADOS-G scores and gamma responses motivating further research into gamma as a biomarker for ASD (Uhlhaas and Singer 2007, Khan, Gramfort et al. 2013).

Oscillatory synchrony in the gamma range in the SHORT and SIM conditions in the 20-40 ms/70-80 Hz interval

In addition to occipital gamma, gamma phase locking over frontal areas was increased in the ASD group in the SHORT condition. This was associated with stronger symptom severity in the ADOS-G RSI domain thereby demonstrating a response specific to ASD. Frontal activation in ASD in response to visual stimuli has been noted in many studies (Spencer, Holt et al. 2012). The very early latency of this higher gamma response is interesting and involves areas of the brain implicated in executive control. Due to the highly repetitive nature of the task and the practice block prior to the actual task, individuals with ASD might be expecting the stimulus thereby implicating executive areas prior to stimulus recognition at the neural level at later latencies in the visual areas.

Oscillatory synchrony in the LONG condition

In this condition, gamma responses at the presentation of the second bar could be dissociated into a high gamma right frontal anticipatory response in the TD group coupled with visual binding mechanisms within 50-80 Hz gamma frequencies and also the lower gamma frequencies 30-40 Hz. However, the anticipatory neurophysiological response in ASD seemed confined to the 50-80 Hz range and not the higher gamma range, unlike the TDs. Perceptual binding occurred in ASD at lower gamma frequencies similarly to the TDs (30-40 Hz). Interestingly, within the 50-80 Hz range, the ASD response was quite spread out over many brain areas

including the occipital cortex, parietal, central and temporal areas suggesting a possibly more 'noisy' brain. With the attenuation of the extremely high temporal resolution of the task in the SHORT condition, the ASD brain may be relegating visual binding processes to the lower gamma range in the LONG condition only. Speculatively, the inability to visually bind stimuli in the LONG condition in the 50-80 Hz frequency range may somehow predict the behavioural response and predispose the ASD group to more errors. At later latencies (190-240 ms), both the ASD group showed stronger occipital gamma response, which might suggest eventual perceptual binding (Grutzner, Uhlhaas et al. 2010).

Oscillatory synchrony at later latencies and other frequencies

Evoked gamma differences between TD and ASD in the SHORT condition were also observed beyond 250 ms. Interestingly, two narrow t/f intervals at lower (33-40Hz: 250-290ms) and higher gamma (70-80Hz: 350-400ms) frequencies between 250-400 ms showed increases in evoked gamma phase locking in ASD compared with TD. At lower frequencies (<30 Hz), evoked occipital evoked beta phase-locked activity decreased in the ASD group compared with the TD group in the SHORT condition. It is beyond the scope of this chapter to discuss all these differences. However, a number of studies have proposed that lower frequency gamma phase-locking might be associated with enhanced visual-processing (Salari, Buchel et al. 2012) and unconscious learning (Chaumon, Drouet et al. 2008, Chaumon, Schwartz et al. 2009) thereby facilitating higher order perceptual grouping in the higher frequency ranges, which might be in conjunction with maintained attentional processes enhanced through alpha and beta ranges (Tallon-Baudry 2004, Salari, Buchel et al. 2012).

In conclusion, this study examined the neural correlates underlying superior performance in a perceptual simultaneity task in ASD. It was demonstrated that oscillatory synchrony in the gamma range in response to the task was altered in ASD. Visual apparent simultaneity in ASD was associated with an early 20-40 ms increase in 70-80 Hz right frontal evoked gamma phase locking followed by a 50-80 ms reduction in occipital 50-80 Hz evoked gamma phase-locking compared with the TD group. These responses were specific to the ASD group as demonstrated by strong correlations between severity scores of the ADOS-G RSI domain and both right frontal and occipital phase locking. Thus, perceptual binding of visual events mediated through frontal and occipital gamma oscillatory synchrony changes in ASD might support behavioural recognition of apparent simultaneity thereby accounting for superior task performance compared with TDs.

Chapter 9 Final discussion and concluding remarks

This thesis extends our knowledge of primary sensory areas in autism spectrum disorders. It also addresses the high incidence of epileptiform activity in autism individuals directly through the investigation of the neuropathology of epileptogenic areas (PiC, hippocampus) in patients with autism, epilepsy or both and indirectly through the investigation of gamma oscillations used as a proxy for inhibition in individuals with high-functioning autism and Asperger's (Buzsaki and Wang 2012). Pilot studies on *in vitro* hippocampal rodent neuronal cultures and the human post-mortem hippocampus were included as building blocks for larger-scale studies on limbic areas and memory in autism and epilepsy. Finally, qualitative analysis of the olfactory tubercle was undertaken in autism and epilepsy.

Neuropathological findings of primary olfactory cortex are in support of existing theories on neuroinflammatory processes that may be involved in autism pathogenesis (Vargas, Nascimbene et al. 2005, Edmonson, Ziats et al. 2014). Consistent with Rubenstein's model of altered cortical E/I in autism (Rubenstein and Merzenich 2003), astroglia may be key in modifying paleocortical excitability in the piriform early in life. In cases where individuals suffered from severe intellectual disabilities and had a diagnosis of autism co-morbid with epilepsy, gliosis early in life may have disrupted olfactory connectivity. This may happen through reactive astrogliosis specifically which leads to the creation of a glial scar usually beneficial to isolate the site of a lesion. This however has consequences on neurite growth, axonal regeneration and synaptic remodelling (Giaume, Kirchhoff et al. 2007). Astroglia also remove 80% of synaptic glutamate through glutamate transporters (Excitatory amino acid transporter (EAAT1 and EAAT2) modulated by gap junction proteins and can therefore protect against glutamate-induced excitotoxicity (Pannasch, Freche et al.

2014). They regulate the uptake of extracellular potassium released by neurons, are pivotal in buffering the extraneuronal space and may have a direct effect on altering the excitability of the milieu (Phelps and Korneva 2008) and sometimes the normal wiring of neurons in the cortical network.

If astroglial cells had mutated expressions of specific molecular markers, dramatic structural changes would be seen in cortical matter such as in Alexander disease where mutated GFAP expression results in major structural changes (Zeidan-Chulia, Salmina et al. 2014). This would suggest a primary role for these cells in neuropathology and may result in the possible development of epileptogenicity. As neuronal populations were spared in autism in this study, gliosis could be a secondary response. It remains however unclear what type of insult glial cells are reacting to early in life in autism.

The usual prevalence of epilepsy drops with age in individuals with cerebral palsy and intellectual disability without ASD (Silver and Rapin 2012). This is quite interesting because the prevalence of epilepsy increases in ASD with age suggesting a possible degenerative mechanism that may be reflected by increased glial cell densities in epileptogenic areas such as the piriform cortex as shown in this study (Tuchman, Cuccaro et al. 2010).

Whether changes in glia directly underlie olfactory impairments in autism remains unclear. Changes in the cytoarchitecture associated with differences in the perception of olfactory experience have been documented in patients with temporal lobe epilepsy. In these patients, histologic diagnosis showed gliosis in mesial temporal regions (Chen, Shih et al. 2003). The collection of olfactory scores for example would benefit future neuropathological studies, which could provide insight into whether cytoarchitectural changes directly underlie olfactory impairments in autism.

The restricted presence of patterns of corpora amylacea in the olfactory tubercle warrants further investigation in autism and epilepsy. The high neuronal and non-neuronal cell turnover in the striatum could be the reason why low levels of corpora amylacea may be seen in the tubercle (Ernst, Alkass et al. 2014). To date, there is very little evidence on the neuropathology of the tubercle in humans. Perhaps to relate neuropathological processes in the tubercle to social behaviour, investigating oxytocin receptor distribution may provide a good example. Experiments on animal models of social bonding (prairie-vole) have demonstrated that increased densities of oxytocin receptors in the nucleus accumbens area compared with non-monogamaous species were associated with social attachment and partner bonding (Young, Lim et al. 2001). Dysfunctions of the reward system circuitry, which the tubercle is part of, have been reported in autism spectrum disorders (Dichter, Damiano et al. 2012). Post-mortem studies on human autism brains have shown reduced oxytocin-receptor expression in the ventral striatum (Damiano, Aloi et al. 2014) and the piriform cortex (Liu, Pappas et al. 2005). Oxytocin administration exogenously improves social communication in adults and children with autism (Hollander, Bartz et al. 2007, Guastella, Einfeld et al. 2010). Additionally, ventral striatal responses in autism are reduced in tasks of social reward versus non-social reward (Scott-Van Zeeland, Dapretto et al. 2010). Therefore, investigating these receptors may provide a more direct link between the clinical symptoms and the underlying neuropathology.

Results from neuropathological studies largely support the high incidence of sensory anomalies in autism in the domain of olfaction and contribute to a growing body of literature indicating a widely distributed neuropathology of autism including primary sensory regions (Marco, Hinkley et al. 2011). Although this offers a challenge to previous hypotheses, which have emphasized some higher cognitive functions in

heteromodal associative cortex (Casanova, Buxhoeveden et al. 2002, Casanova, Buxhoeveden et al. 2003), it may present an opportunity for the development of tests in early life, which investigate basic sensory processing.

Investigating the oscillatory properties of firing cell assemblies in response to sensory stimuli extended the neuropathology work to another primary sensory area in autism in living subjects. Since the binding-by-synchrony proposal by Wolf Singer, which stipulated that the temporal organization of neuronal activity through gamma oscillatory synchrony was more important than connectivity, the perceptual binding of visual objects as coherent wholes implicating oscillatory synchrony in the gamma range between large cortical areas remained central in helping resolve the binding problem (Gray, Konig et al. 1989, Tallon-Baudry 2009). Gamma synchrony could be specific to cortical areas engaged in a particular task (Vidal, Chaumon et al. 2006) and was also shown to relate the binding problem to synaptic plasticity through spike-dependent-timing plasticity, whereby neuronal connectivity is strengthened through spike-timing at the length of a gamma cycle (Buzsaki 2006). With autism being termed a 'disconnectivity syndrome' with impairments in local and long-range synchronization in the gamma-band (Uhlhaas and Singer 2007), the discovery of characteristic neural synchrony patterns of the autism brain may provide potential biomarkers for these disorders and extend our understanding of the clinical phenotype. Disturbances of gamma synchrony in autism have been already described to be different compared to the neurotypical population in a wide variety of tasks (Grice, Spratling et al. 2001, Brown, Gruber et al. 2005, Wright, Alderson-Day et al. 2012). However, whether these changes are specific to autism remains a matter of debate. More importantly, the behavioural advantages and superior task performance in autism associated with atypicalities in gamma oscillations contributes to the

ongoing debate on whether impairments or alternative cognitive strategies should be adopted instead to describe these differences.

The current neurophysiological study added to the body of literature on neural synchrony changes in the gamma range in autism in a new task involving time perception. The behavioural findings contribute largely to the body of literature on heightened sensory and perceptual differences in the autism population in the visual domain (Marco, Hinkley et al. 2011). The enhanced temporal resolution in autism is in support of weak central coherence theory (Shah and Frith 1983), which might explain why autism individuals performed better in the short condition and also slightly worse in the longer condition. Consistently with this theory, when the resolution of the temporal appearance of the visual bars decreased (the long condition), local processing conferring a better behavioural outcome might have been lost. The superiority of autism individuals in visual tasks such as visual search (Hessels, Hooge et al. 2014) has been linked to 'load theory' positing that at high perceptual loads, individuals with autism maintain superiority in performance (Lavie, Hirst et al. 2004, Remington, Swettenham et al. 2009). In a similar fashion, as the task became more difficult with higher temporal loads (SHORT condition), individuals with autism performed better and as the temporal load dropped (LONG condition), individuals started making more errors.

At the level of the neurophysiological response, it is only perceptual binding in the gamma range at high temporal resolutions that predicted symptom severity suggesting a more characteristic response in autism in this paradigm. New results from the LONG condition corroborated the notion that the gamma effects seen at early latency in the SHORT condition are specific to ASD pathology and are not easily explained in terms of altered task performance. The loss of the temporal resolution in the LONG

condition also demonstrated gamma activity confined to certain frequencies compared with the TDs. Importantly, the gamma response did not always predict the behavioural outcome in ASD. This may be due to altered connectivity between the occipital areas and the frontal areas: although the primary visual response in the gamma range was consistent with what we predicted, it might not always be relayed to the executive regions.

To link neuronal synchrony in the gamma range to its cellular components, evidence has accumulated that parvalbumin GABA-ergic interneurons in the neocortex drive these oscillations (Sohal, Zhang et al. 2009). In visual cortex in particular, layers 2/3 contain most of the parvalbumin interneurons (Helm, Akgul et al. 2013) and gamma rhythms are consistently recorded from layer IV (Hu, Gan et al. 2014). Studies on post-mortem human and animal brains consistently report changes in GABA-ergic parvalbumin positive interneurons in visual cortex (Gogolla, Leblanc et al. 2009, Allegra, Genovesi et al. 2014) and other areas of the brain (Lawrence, Kemper et al. 2010, Marin 2012) early in development, postnatally and in adult life. These changes in the parvalbumin system have been associated with behavioural symptoms (Saunders, Tatard-Leitman et al. 2013). Because of the link between gamma and the parvalbumin system, alterations in gamma neural synchrony have been linked with the imbalance in the E/I ratio (Snijders, Milivojevic et al. 2013). With respect to the current study, one way to investigate the parvalbumin system would have been to sample visual cortex from IQ and age-matched post-mortem brains of consenting autism donors to determine associations between structure and function. Determining the density of parvalbumin neurons as well as examining their morphologies in layers two and three of the visual cortex might provide more clues about possible associations with gamma and the relationship with excitation and inhibition. Methods

to investigate the relationship between gamma and the E/I balance consisted of combined magnetic resonance spectroscopy studies to measure extra-synaptic levels of inhibitory and excitatory metabolites in conjunction with gamma data obtained using MEG or EEG recordings (Muthukumaraswamy, Edden et al. 2009) although a recent study has demonstrated no associations between GABA levels and the gamma response (Cousijn, Haegens et al. 2014). The best way to demonstrate associations between gamma and GABA would be to use positron emission tomography to radioactively bind cell surface GABA receptors and quantify them subsequent to collecting MEG data to extract gamma oscillations following a sensory paradigm. However, this method is not cost effective at the moment and has not been implemented in any study to the author's knowledge.

Associations with symptom severity in the social and stereotypical behaviours domain in visual perception (gamma) and olfaction (the piriform) are in line with sensory atypicalities underlying autism symptomatology as demonstrated by association studies between hyper-responsiveness and stereotypical and non-social behaviour (Riby, Janes et al. 2013, Robertson, Kravitz et al. 2013). Both the gamma and piriform studies extend these sensory atypicalities with potential implications on the roles of the piriform in particular as associative cortex linking the frontal and temporal areas (Gottfried 2010).

Finally, an autoimmune aetiology of autism has been previously suggested by several studies (Vincent, Deacon et al. 2002, Dalton, Deacon et al. 2003). The authors reported that maternal antibodies from mothers' sera whose children (at least one child) had a neurodevelopmental disorder bound Purkinje cell neurons *in vitro* suggesting a possible immune-mediated process. When the sera were injected in pregnant mice, the offspring phenotype had features of autism. With the discovery of

more autoantibodies to cell surface receptors (Irani, Gelfand et al. 2014), the shift of focus towards temporal and frontal regions in autism away from the cerebellum (Voineagu, Wang et al. 2011) and the glial perspective in autism pathogenesis (Zeidan-Chulia, Salmina et al. 2014), *in vitro* hippocampal neurons and astrocyte cultures optimized in this thesis would be very useful cultures to test the effects of autoantibody binding from larger cohorts of maternal serum samples and to test animal models for a clinical phenotype.

Limitations and future work

These studies have some limitations. Ideally, MEG and post-mortem studies from the same sensory modality would provide a great way to examine structure and function in autism. This was not possible in this study. The main limitation of post-mortem studies on human tissue in general is the difficulty of obtaining adequate samples. This compromises statistical power and makes it challenging to draw strong conclusions, particularly with the heterogeneity in clinical phenotypes in autism in particular. Very recently, the brain bank for autism and related developmental research (BBA) was formed under the umbrella of the Oxford Brain Bank (formerly the Thomas Willis Oxford Brain Collection (TWOBC)) in Oxford, UK, which organizes the collection and storage of post-mortem tissue from consenting ASD individuals prior to their death. With this resource, in addition to the autism tissue program and the NICHD and Harvard brain banks in the USA, it was possible to sample a larger number of ASD cases than many previous studies.

Another challenge was matching cases for ID or IQ and comorbidity to truly account for effects based on a specific cognitive phenotype. However, it is hoped that detailed reporting and diagnosis are improving with time. Another limitation of this study is

the contribution of the type of glial cell to the overall increased densities using immunolabeling. Although the reported associations demonstrate a role for astroglia in autism, it would be useful to demonstrate specifically which population of reactive astroglia is affected (GFAP or other) as well as investigate the involvement of other cells in the process such as microglia and macrophages. Finally, it would be interesting to consider the subdivisions of the PiC: aPiC and pPiC regions, and assess them separately due to the hypothesized differences in function. This also largely depends on tissue availability.

In the MEG study, responses were correlated with the same behavioural outcome. It was not possible to use electrophysiological data from the SHORT condition associated with a non-simultaneous behavioural outcome mainly because of much fewer epochs in the TD group available for comparison with the ASD group. Similarly, LONG condition MEG epochs with a 'simultaneous' behavioural outcome would have been useful to examine the neurophysiological response between TD and ASD with the incorrect answer, but these were difficult to obtain due to their paucity as a result of the nature of the task. Due to time constraints, gamma power has not been addressed in this thesis. Also, there were not enough structural MRI scans to perform adequate source localization analyses to determine the neural generators of the observed responses. This constituted another limitation of the study. Future work would be first to examine apparent simultaneity data correlated with the true behavioural outcome (asynchronous) despite the limitations in epoch numbers. Gamma band power might give clues about local processing mechanisms and therefore, another possibility for future work would be to clean the contaminated data in order to analyse and correlate power results with phase results. Finally, adequate

source localization using model MRIs and obtained structural MRIs from the subjects should make it possible to determine the neural generators of the observed responses.

In conclusion, autism spectrum disorders (including broader phenotypes) affect as many as 1% of children in the United Kingdom (Roth and Rezaie 2011). These studies extend our knowledge of these disorders and provide a unique combination of methods to address the complexity of the clinical phenotype. This combination of MEG and post-mortem studies is not yet common and can be a useful approach to examine both the complex functional electrophysiology and the fine anatomy and microstructure in the brain. This may provide a platform for association studies that would help us relate structure to function. This thesis investigated the neuropathology and neurophysiology of autism spectrum disorders and the co-morbidity with epilepsy. Olfactory and visual differences in autism were placed in the context of existing theories on sensory and perceptual anomalies. In the visual domain, individuals with autism show anomalies in face processing (Bailey, Braeutigam et al. 2005) and other visual atypicalities, which might relate to the weak central coherence theory of recognising better individual parts rather than a whole. This may be due to an imbalance between E/I at a cortical level. Similarly, just as in the visual domain, the olfactory domain affected in autism may stem from an imbalance between E/I in the epileptogenic piriform. Enhanced temporal resolutions in a perceptual simultaneity paradigm may also support an imbalance between E/I in the visual areas demonstrated through changes in gamma oscillatory synchrony. Future studies should focus on providing more evidence on whether gamma synchrony in visual areas and olfactory identification testing could constitute biomarkers of autism hence paving the way for early diagnosis.

Appendix

Appendix A

Nissl-substance staining protocol

Reagents

95% Ethanol

70% Ethanol

Differentiation solution: 2 drops glacial acetic acid in 95% ethanol

Cresyl Violet Acetate 0.1% in Acetate Buffer-Filtered

Working solution:

Add 200 µl of 10% acetic acid to 25 mL of 0.1% cresyl-violet in distilled water solution and mix. Filter.

Protocol

1. De-wax sections in histoclear (2 or 3 changes of 5min each)
2. Rehydrate in alcohol (100%x2), 3min each.
3. Stain in 0.1% Cresyl Violet for 1-3 min.
4. Quick rinse in tap water to remove excess stain.
5. Wash in 70% ethanol.
6. Immerse sections for 2min in Differentiation solution – check staining on microscope.
7. Dehydrate through 2x3min changes of absolute ethanol.
8. Clear in histoclear x2 and mount in DPX solution (Sigma-Aldrich).
9. Allow drying in the fume hood.

Appendix B

Normality of stereological measurements

The values below represent the Shapiro statistic for all groupings to assess normality of cell density measurements. All p-values > 0.05 suggesting that density measurements per group, layer and cell type as well as across groups per layer are normally distributed.

Table B: Shapiro-Wilk statistic for normality of data

Across Groups				
Layer	CellType	Shapiro W Statistic	p-value	
"2"	"PCD"	0.97	0.47	
"2"	"NPCD"	0.98	0.76	
"2"	"GCD"	0.95	0.11	
"2"	"NCD"	0.97	0.49	
"3"	"PCD"	0.97	0.41	
"3"	"NPCD"	0.97	0.43	
"3"	"GCD"	0.96	0.18	
"3"	"NCD"	0.96	0.22	
Layer	Diagnosis	CellType	Shapiro W Statistic	p-value
"2"	"ASD"	"PCD"	0.98	0.94
"2"	"ASD"	"NPCD"	0.96	0.91
"2"	"ASD"	"GCD"	0.89	0.13
"2"	"ASD"	"NCD"	0.98	0.93
"2"	"ASD + E	"PCD"	0.85	0.17
"2"	"ASD + E	"NPCD"	0.91	0.46
"2"	"ASD + E	"GCD"	0.96	0.86
"2"	"ASD + E	"NCD"	0.86	0.19
"2"	"E"	"PCD"	0.91	0.28
"2"	"E"	"NPCD"	0.99	0.99
"2"	"E"	"GCD"	0.90	0.19
"2"	"E"	"NCD"	0.89	0.12
"2"	"TD"	"PCD"	0.93	0.45
"2"	"TD"	"NPCD"	0.96	0.80
"2"	"TD"	"GCD"	0.94	0.56
"2"	"TD"	"NCD"	0.94	0.56
"3"	"ASD"	"PCD"	0.94	0.49
"3"	"ASD"	"NPCD"	0.91	0.24
"3"	"ASD"	"GCD"	0.97	0.91
"3"	"ASD"	"NCD"	0.96	0.77
"3"	"ASD + E	"PCD"	0.94	0.69
"3"	"ASD + E	"NPCD"	0.94	0.69
"3"	"ASD + E	"GCD"	0.89	0.33
"3"	"ASD + E	"NCD"	0.90	0.37
"3"	"E"	"PCD"	0.94	0.51
"3"	"E"	"NPCD"	0.96	0.72
"3"	"E"	"GCD"	0.91	0.26
"3"	"E"	"NCD"	0.96	0.79
"3"	"TD"	"PCD"	0.88	0.11
"3"	"TD"	"NPCD"	0.89	0.14
"3"	"TD"	"GCD"	0.88	0.10
"3"	"TD"	"NCD"	0.94	0.50

Appendix C

Homogeneity of variance between stereological measurements

The values below represent the Brown-Forsythe statistic for all groupings to assess homogeneity of variance between cell density measurements. All p-values > 0.05 suggesting homogeneous variances between groups per layer and cell-type.

Table C: Brown-Forsythe statistic for homoscedasticity

Layer	Group1	Group2	CellType	Brown-Forsythe statistic	Brown-Forsythe p-value
2	ASD	"ASD + E"	"PCD"	4.67	0.05
2	ASD	"ASD + E"	"NPCD"	1.75	0.21
2	ASD	"ASD + E"	"GCD"	0.08	0.78
2	ASD	"ASD + E"	"NCD"	2.58	0.13
2	ASD	"E"	"PCD"	2.78	0.11
2	ASD	"E"	"NPCD"	0.08	0.78
2	ASD	"E"	"GCD"	1.54	0.23
2	ASD	"E"	"NCD"	1.51	0.23
2	ASD	"TD"	"PCD"	0.27	0.61
2	ASD	"TD"	"NPCD"	0.92	0.35
2	ASD	"TD"	"GCD"	0.39	0.54
2	ASD	"TD"	"NCD"	0.08	0.78
2	ASD + E	"E"	"PCD"	0.08	0.78
2	ASD + E	"E"	"NPCD"	1.09	0.31
2	ASD + E	"E"	"GCD"	0.83	0.38
2	ASD + E	"E"	"NCD"	0.07	0.81
2	ASD + E	"TD"	"PCD"	2.01	0.18
2	ASD + E	"TD"	"NPCD"	0.25	0.63
2	ASD + E	"TD"	"GCD"	0.07	0.79
2	ASD + E	"TD"	"NCD"	1.51	0.24
2	E	"TD"	"PCD"	1.29	0.27
2	E	"TD"	"NPCD"	0.43	0.52
2	E	"TD"	"GCD"	0.85	0.37
2	E	"TD"	"NCD"	0.91	0.35
3	ASD	"ASD + E"	"PCD"	0.06	0.81
3	ASD	"ASD + E"	"NPCD"	0.89	0.36
3	ASD	"ASD + E"	"GCD"	1.97	0.18
3	ASD	"ASD + E"	"NCD"	0.33	0.58
3	ASD	"E"	"PCD"	0.07	0.79
3	ASD	"E"	"NPCD"	0.75	0.41
3	ASD	"E"	"GCD"	2.68	0.12
3	ASD	"E"	"NCD"	0.004	0.95
3	ASD	"TD"	"PCD"	0.48	0.51
3	ASD	"TD"	"NPCD"	0.71	0.41
3	ASD	"TD"	"GCD"	0.42	0.53
3	ASD	"TD"	"NCD"	0.28	0.61
3	ASD + E	"E"	"PCD"	0.32	0.58
3	ASD + E	"E"	"NPCD"	0.01	0.92
3	ASD + E	"E"	"GCD"	0.001	0.98
3	ASD + E	"E"	"NCD"	0.25	0.62

Appendix D

Poisson distribution measurements

The values below are the p-values arising from groupings of cell counts that should follow a Poisson distribution to apply the Gundersen and Jensen CE for counts. In 6 groupings, the general CE formula was applied and not the Gundersen one as distributions followed not a Poisson trend ($p<0.05$).

Table D: p-values for Poisson distribution

Layer	Group	CellType	Chi-square statistic	df	p-value
"2"	"ASD"	"PCD"	6.91	18	0.99
"2"	"ASD + E"	"NPCD"	4.91	31	0.18
"2"	"E"	"GCD"	10.67	17	0.87
"2"	"TD"	"NCD"	9.28	22	0.99
"3"	"ASD"	"PCD"	3.43	15	0.99
"3"	"ASD + E"	"NPCD"	3.21	3	0.36
"3"	"E"	"GCD"	7.71	13	0.86
"3"	"TD"	"NCD"	10.78	19	0.93
"2"	"E"	"PCD"	14.38	17	0.64
"2"	**"E"**	**"NPCD"**	**12.73**	**3**	**0.005**
"2"	"E"	"GCD"	6.35	10	0.79
"2"	"E"	"NCD"	14.2	20	0.82
"2"	"TD"	"PCD"	9.24	20	0.98
"2"	"TD"	"NPCD"	6.49	3	0.09
"2"	"TD"	"GCD"	5.27	11	0.92
"2"	"TD"	"NCD"	7.98	23	0.99
"3"	"ASD"	"PCD"	10.73	6	0.1
"3"	**"ASD"**	**"NPCD"**	**17.3**	**2**	**0.00018**
"3"	"ASD"	"GCD"	12.49	20	0.9
"3"	"ASD"	"NCD"	10.45	8	0.23
"3"	"ASD + E"	"PCD"	5.09	4	0.28
"3"	"ASD + E"	"NPCD"	1.63	1	0.21
"3"	"ASD + E"	"GCD"	6.15	16	0.99
"3"	"ASD + E"	"NCD"	10.98	6	0.09
"3"	**"E"**	**"PCD"**	**14.64**	**4**	**0.005**
"3"	**"E"**	**"NPCD"**	**11.93**	**2**	**0.003**
"3"	"E"	"GCD"	7.06	18	0.99
"3"	"E"	"NCD"	2.55	6	0.87
"3"	**"TD"**	**"PCD"**	**15.61**	**6**	**0.02**
"3"	**"TD"**	**"NPCD"**	**9.39**	**2**	**0.009**
"3"	"TD"	"GCD"	11.9	18	0.85
"3"	"TD"	"NCD"	10.04	8	0.26

Appendix E

Example of variation in cell counts in 4 cases

To determine the usage of alpha smoothness value (12 or 240) to apply the Gundersen equation, pyramidal cell counts, non-pyramidal cell counts and glial cell counts over 62 counting frames were taken from 4 control cases. An alpha level of 240 suggests variation of less than 2SD across counts whilst an alpha of 12 suggests higher variation. Mean counts and standard deviations (SD) were plotted against counting frame to show mean variation in counts from section to section. The diagram below is used for illustration. Generally, mean counts varied by less than 2SD over each counting frame in these 4 cases. Alpha smoothness factor applied in this study was 240 in agreement with guidelines provided by West et al (2012).

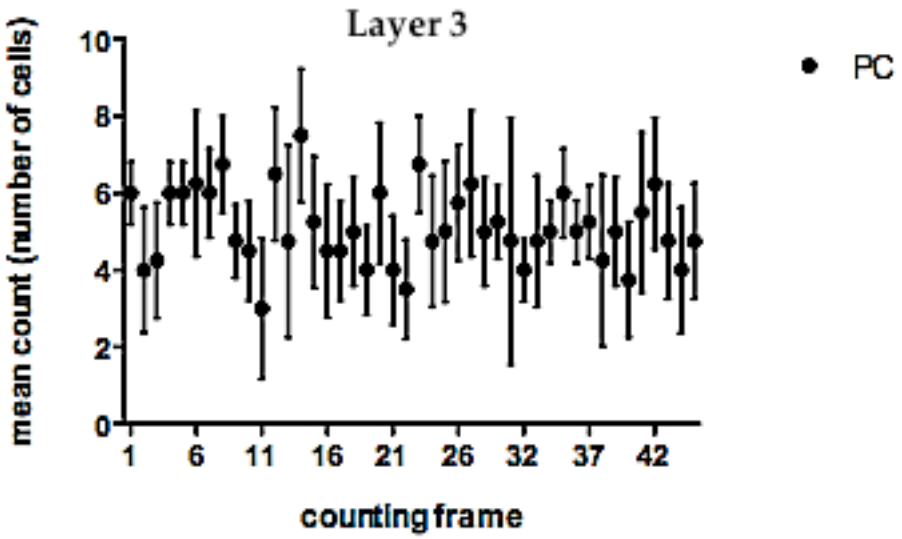


Figure 1 Smoothness of data. This figure shows mean pyramidal cell (PC) counts per frame over 45 counting frames of 4 cases.

Appendix F

Variability of density measurements with z-height

Table F: Variation of cell densities at z= 20 µm and z=12 µm

Case No.	PCD			GCD			NPCD		
	z=20 µm	z=12 µm	CV (%)	z=20 µm	z=12 µm	CV (%)	z=20 µm	z=12 µm	CV (%)
1	121980.37	114195.65	4.66	77956.27	76195.92	1.61	27255.64	26675.45	1.52
2	81391.03	85795.78	3.72	39873.69	37278.24	4.76	21902.37	25811.59	11.59
3	100068.37	95060.34	3.62	46799.22	43046.15	5.91	17205.69	17826.06	2.50
4	92861.29	83631.27	7.39	56455.51	64093.71	8.96	25664.53	25056.33	1.70

To prove that density values do not vary by more than 10% from the utilized z-value in this study (20 µm), a proof of principle study was undertaken with 4 cases. Cell densities were measured with z=12 µm in both layers (II and III) and compared with values obtained with z=20 µm. Three tables are shown for layer II demonstrating a general variation of less than 12% between measurements at different z-values.

Appendix G

Coefficient of error measurements per case on cell counts

CE measurements on counts with smoothness factor α=240 using the Gundersen and Jensen equation.

Table G: Coefficient of error per individual case in cell counts

case	group	layer	PC_CE	NPC_CE	GC_CE	NC_CE
4	ASD	2	0.05	0.09	0.05	0.04
6	ASD	2	0.05	0.11	0.07	0.05
8	ASD	2	0.05	0.10	0.06	0.05
10	ASD	2	0.05	0.09	0.05	0.04
12	ASD	2	0.04	0.09	0.06	0.04
15	ASD	2	0.05	0.12	0.06	0.05
28	ASD	2	0.05	0.09	0.06	0.05
30	ASD	2	0.04	0.08	0.04	0.04
32	ASD	2	0.05	0.10	0.05	0.05
34	ASD	2	0.05	0.09	0.05	0.04
36	ASD	2	0.05	0.10	0.06	0.04
1	ASD + E	2	0.05	0.09	0.06	0.04
3	ASD + E	2	0.05	0.11	0.06	0.05
22	ASD + E	2	0.05	0.11	0.06	0.05
38	ASD + E	2	0.05	0.10	0.05	0.05
39	ASD + E	2	0.06	0.09	0.06	0.05
40	ASD + E	2	0.06	0.09	0.06	0.05
9	E	2	0.05	0.10	0.08	0.05
11	E	2	0.04	0.10	0.06	0.04
16	E	2	0.05	0.10	0.06	0.04
17	E	2	0.05	0.10	0.06	0.04
19	E	2	0.04	0.10	0.06	0.04
21	E	2	0.04	0.11	0.06	0.04
23	E	2	0.05	0.12	0.08	0.04
24	E	2	0.05	0.12	0.08	0.05
26	E	2	0.06	0.10	0.07	0.05
27	E	2	0.07	0.12	0.05	0.06
31	E	2	0.05	0.09	0.06	0.04
2	TD	2	0.05	0.09	0.08	0.05
5	TD	2	0.05	0.10	0.06	0.05
7	TD	2	0.05	0.11	0.06	0.05
13	TD	2	0.04	0.10	0.06	0.04
14	TD	2	0.05	0.11	0.07	0.05
18	TD	2	0.04	0.11	0.06	0.04
20	TD	2	0.04	0.12	0.06	0.04
25	TD	2	0.05	0.09	0.08	0.04
29	TD	2	0.05	0.09	0.05	0.05
33	TD	2	0.05	0.11	0.05	0.05
35	TD	2	0.05	0.09	0.05	0.04
4	ASD	3	0.08	0.10	0.04	0.06
6	ASD	3	0.07	0.10	0.04	0.06
8	ASD	3	0.09	0.12	0.04	0.07
10	ASD	3	0.06	0.10	0.04	0.05
12	ASD	3	0.07	0.10	0.04	0.06

15	ASD	3	0.09	0.12	0.04	0.07
28	ASD	3	0.08	0.12	0.05	0.07
30	ASD	3	0.07	0.10	0.04	0.06
32	ASD	3	0.08	0.11	0.04	0.07
34	ASD	3	0.08	0.10	0.04	0.06
36	ASD	3	0.08	0.12	0.04	0.07
1	ASD + E	3	0.08	0.11	0.04	0.06
3	ASD + E	3	0.07	0.10	0.05	0.06
22	ASD + E	3	0.09	0.12	0.05	0.07
38	ASD + E	3	0.08	0.13	0.04	0.07
39	ASD + E	3	0.09	0.14	0.05	0.08
40	ASD + E	3	0.09	0.11	0.05	0.07
9	E	3	0.09	0.12	0.05	0.07
11	E	3	0.07	0.12	0.04	0.06
16	E	3	0.08	0.10	0.04	0.06
17	E	3	0.08	0.11	0.05	0.07
19	E	3	0.10	0.12	0.04	0.08
21	E	3	0.08	0.10	0.04	0.06
23	E	3	0.08	0.10	0.05	0.06
24	E	3	0.08	0.12	0.05	0.07
26	E	3	0.08	0.12	0.06	0.07
27	E	3	0.08	0.13	0.04	0.07
31	E	3	0.07	0.11	0.05	0.06
2	TD	3	0.08	0.12	0.05	0.07
5	TD	3	0.08	0.11	0.05	0.07
7	TD	3	0.09	0.12	0.05	0.07
13	TD	3	0.07	0.10	0.04	0.06
14	TD	3	0.09	0.11	0.04	0.07
18	TD	3	0.09	0.11	0.04	0.07
20	TD	3	0.08	0.10	0.04	0.06
25	TD	3	0.07	0.09	0.04	0.06
29	TD	3	0.08	0.11	0.04	0.06
33	TD	3	0.08	0.12	0.05	0.07
35	TD	3	0.06	0.10	0.04	0.05

Appendix H

Coefficient of error measurements per case on cell densities

The values below represent the individual CE values per layer per case on density measurements of different cell types.

Table H: Coefficient of error per case in cell densities

case	group	layer	PCD_CE	NPCD_CE	GCD_CE	NCD_CE
2	TD	2	0.02	0.05	0.06	0.01
5	TD	2	0.08	0.05	0.06	0.07
7	TD	2	0.06	0.08	0.06	0.04
13	TD	2	0.04	0.10	0.03	0.05
14	TD	2	0.06	0.05	0.09	0.06
18	TD	2	0.07	0.09	0.03	0.07
20	TD	2	0.02	0.10	0.04	0.02
25	TD	2	0.06	0.08	0.02	0.06
29	TD	2	0.03	0.06	0.06	0.02
33	TD	2	0.05	0.06	0.04	0.05
35	TD	2	0.08	0.10	0.08	0.08
4	ASD	2	0.10	0.08	0.04	0.09
6	ASD	2	0.04	0.12	0.10	0.04
8	ASD	2	0.05	0.07	0.06	0.05
10	ASD	2	0.06	0.07	0.05	0.06
12	ASD	2	0.04	0.08	0.02	0.04
15	ASD	2	0.07	0.15	0.05	0.07
28	ASD	2	0.07	0.05	0.02	0.06
30	ASD	2	0.02	0.08	0.05	0.03
32	ASD	2	0.09	0.14	0.04	0.09
34	ASD	2	0.04	0.06	0.04	0.04
36	ASD	2	0.09	0.06	0.05	0.08
9	E	2	0.03	0.03	0.02	0.03
11	E	2	0.07	0.04	0.07	0.05
16	E	2	0.05	0.04	0.05	0.05
17	E	2	0.05	0.05	0.06	0.05
19	E	2	0.05	0.09	0.10	0.04
21	E	2	0.04	0.12	0.05	0.04
23	E	2	0.06	0.08	0.09	0.05
24	E	2	0.04	0.11	0.04	0.03
26	E	2	0.03	0.08	0.04	0.02
27	E	2	0.03	0.04	0.03	0.02
31	E	2	0.06	0.03	0.04	0.05
1	ASD + E	2	0.04	0.08	0.04	0.04
3	ASD + E	2	0.07	0.09	0.04	0.06
22	ASD + E	2	0.03	0.07	0.05	0.02
38	ASD + E	2	0.08	0.06	0.05	0.06
39	ASD + E	2	0.04	0.09	0.03	0.05
40	ASD + E	2	0.06	0.09	0.03	0.06
2	TD	3	0.05	0.02	0.02	0.03
5	TD	3	0.07	0.07	0.05	0.06
7	TD	3	0.11	0.08	0.04	0.08
13	TD	3	0.06	0.05	0.03	0.05

14	TD	3	0.11	0.14	0.08	0.09
18	TD	3	0.08	0.06	0.08	0.04
20	TD	3	0.07	0.09	0.07	0.06
25	TD	3	0.06	0.09	0.07	0.07
29	TD	3	0.08	0.07	0.06	0.06
33	TD	3	0.06	0.07	0.09	0.05
35	TD	3	0.05	0.05	0.08	0.03
4	ASD	3	0.07	0.06	0.04	0.05
6	ASD	3	0.06	0.08	0.05	0.06
8	ASD	3	0.08	0.08	0.06	0.08
10	ASD	3	0.03	0.05	0.05	0.03
12	ASD	3	0.06	0.10	0.06	0.06
15	ASD	3	0.09	0.10	0.05	0.07
28	ASD	3	0.07	0.09	0.06	0.07
30	ASD	3	0.07	0.09	0.05	0.09
32	ASD	3	0.03	0.10	0.06	0.05
34	ASD	3	0.07	0.10	0.05	0.06
36	ASD	3	0.06	0.06	0.05	0.05
9	E	3	0.06	0.05	0.03	0.04
11	E	3	0.04	0.08	0.04	0.03
16	E	3	0.10	0.10	0.03	0.09
17	E	3	0.11	0.07	0.04	0.08
19	E	3	0.08	0.06	0.04	0.07
21	E	3	0.06	0.07	0.07	0.03
23	E	3	0.05	0.12	0.07	0.08
24	E	3	0.09	0.11	0.09	0.09
26	E	3	0.11	0.05	0.06	0.07
27	E	3	0.08	0.08	0.06	0.05
31	E	3	0.08	0.07	0.12	0.06
1	ASD + E	3	0.03	0.02	0.03	0.02
3	ASD + E	3	0.06	0.07	0.03	0.06
22	ASD + E	3	0.08	0.09	0.05	0.08
38	ASD + E	3	0.11	0.13	0.04	0.07
39	ASD + E	3	0.03	0.12	0.07	0.09
40	ASD + E	3	0.04	0.05	0.06	0.04

Appendix I

Linear regression

Density ~ (cell type + layer + diagnosis + brain-weight + gender + hemisphere + post-mortem interval + age)^2

Significant model: *Density ~ (cell type + layer + diagnosis + brain-weight + age + cell-type: group + cell-type: layer + group: brain-weight + group: age)*

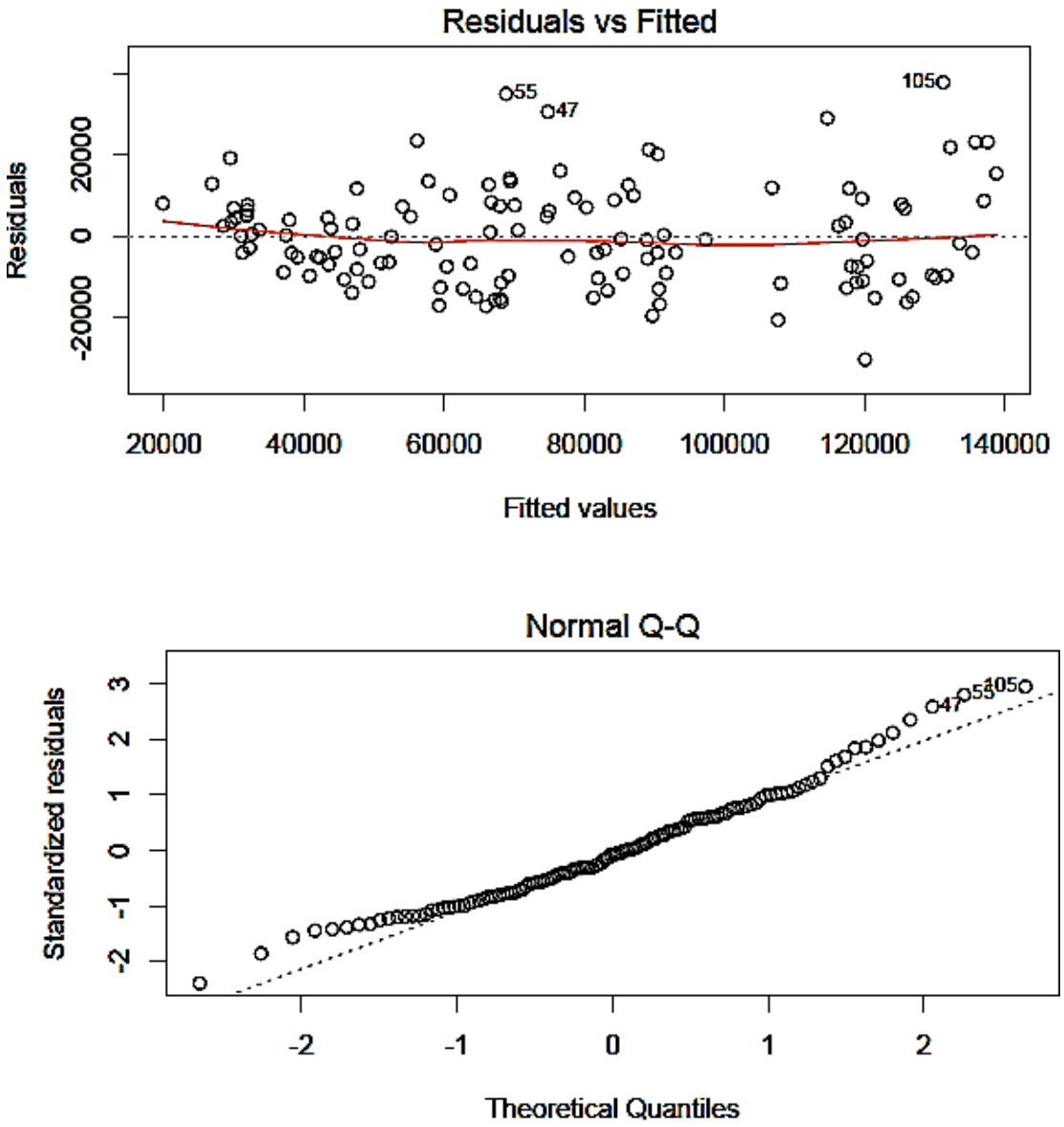


Figure 2 QQ plots and goodness of fit regression lines. This shows in top figure the residual versus fitted data according to the linear model above. This model showed a

high coefficient of determination. Bottom figure shows the normality qq-plot of the data. R^2=0.87.

Final model coefficients and verifications

Residual standard error: 13320 on 108 degrees of freedom							
(20 observations deleted due to missingness)							
Multiple R-squared: 0.8796		Adjusted R-squared: 0.8606					
F-statistic: 46.4 on 17 and 108 DF, p-value: < 2.2e-16				ASD NC Layer2		ASD GC Layer2	
Coefficients	Estimate	Pr(>|t|)		plug in values	estimated value	plug in values	estimated value
(Intercept)	1.34E+04	0.426882		1	1.34E+04	1	1.34E+04
CellTypeNC	2.72E+05	< 2e-16	***	1	2.72E+05	0	0.00E+00
groupASD + E	-7.07E+03	0.773635		0	0.00E+00	0	0.00E+00
groupE	6.14E+04	0.031388	*	0	0.00E+00	0	0.00E+00
groupTD	3.04E+04	0.542765		0	0.00E+00	0	0.00E+00
layer	2.25E+04	7.15E-10	***	0	0.00E+00	0	0.00E+00
BW..g.	8.42E+00	0.30844		1486.4	1.25E+04	1486.4	1.25E+04
Age..yrs.	-8.42E+01	0.592249		29.36364	-2.47E+03	29.36364	-2.47E+03
CellTypeNC:groupASD + E	6.17E+02	0.937765		0	0.00E+00	0	0.00E+00
CellTypeNC:groupE	2.00E+04	0.000976	***	0	0.00E+00	0	0.00E+00
CellTypeNC:groupTD	2.19E+04	0.001156	**	0	0.00E+00	0	0.00E+00
CellTypeNC:layer	-1.10E+05	< 2e-16	***	0	0.00E+00	0	0.00E+00
groupASD + E:BW..g.	2.41E+01	0.115851		0	0.00E+00	0	0.00E+00
groupE:BW..g.	-5.28E+01	0.005548	**	0	0.00E+00	0	0.00E+00
groupTD:BW..g.	-2.73E+01	0.379944		0	0.00E+00	0	0.00E+00
groupASD + E:Age..yrs.	-8.87E+02	0.021448	*	0	0.00E+00	0	0.00E+00
groupE:Age..yrs.	1.97E+02	0.328114		0	0.00E+00	0	0.00E+00
groupTD:Age..yrs.	-3.17E+02	0.249546		0	0.00E+00	0	0.00E+00
					2.95E+05		2.34E+04

Table I Coefficients obtained from regression analyses. This shows the values of the coefficients obtained from the model. On the right, two randomly selected verifications were made on ASD, Layer II, pyramidal cell density to obtain the mean pyramidal cell densities predicted by the model.

	Actual		
		ASD Layer II	
		GCD	73062.66
		NCD	115545.79
		Delta	42483.13
NC estimate	Model Predicted	ASD Layer II	
271700		GCD	23446.042
		NCD	295146.04
		Delta	271700

Table J Difference between mode-predicted value and real value. Predicted mean value was compared with the actual measured value and the difference was much larger than expected suggesting that the model does not predict the actual data.

ANOVA with significant interactions from the model

Anova						
Analysis of Variance Table						
Response: Density						
	Df	Sum Sq	Mean Sq	F value	Pr(>F)	
CellType	1	1.63E+09	1.63E+09	9.2089	0.0030177	**
group	3	1.76E+09	5.87E+08	3.3109	0.0228496	*
layer	1	3.21E+10	3.21E+10	181.1984	< 2.2e-16	***
BW..g.	1	2.50E+08	2.50E+08	1.4101	0.2376478	
Age..yrs.	1	2.16E+08	2.16E+08	1.2161	0.2725881	
CellType:group	3	3.28E+09	1.09E+09	6.157	0.0006649	***
CellType:layer	1	9.66E+10	9.66E+10	544.8059	< 2.2e-16	***
group:BW..g.	3	2.04E+09	6.80E+08	3.8364	0.0118003	*
group:Age..yrs.	3	1.96E+09	6.53E+08	3.6796	0.0143689	*
Residuals	108	1.92E+10	1.77E+08			
Signif. codes:	0 '***'	0.001 '**'	0.01 '*'	.05 '.'	0.1 ' '	

Table K Multivariate ANOVA results from linear regression. This table shows the multivariate ANOVA obtained from the above model.

Appendix J

MEG helmet

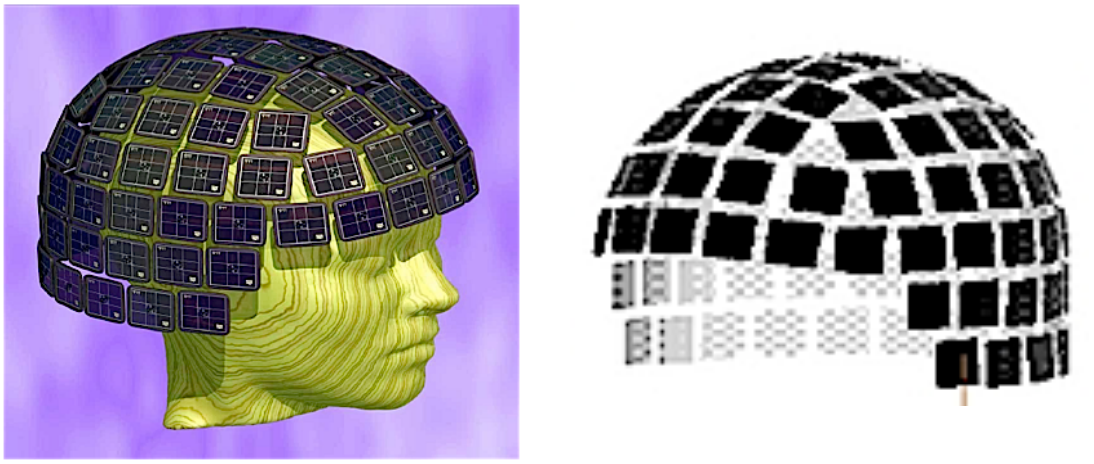


Figure 3 MEG helmet design. This figure shows the helmet-shaped Elekta Neuromag MEG sensors covering the whole head (left). This has been referred to in chapter 7. The helmet (right) consists of 306 sensors formed of 102 units of two orthogonal planar gradiometers and one magnetometer that pick up the magnetic fields of the brain. These photos are courtesy of Elekta Neuromag.

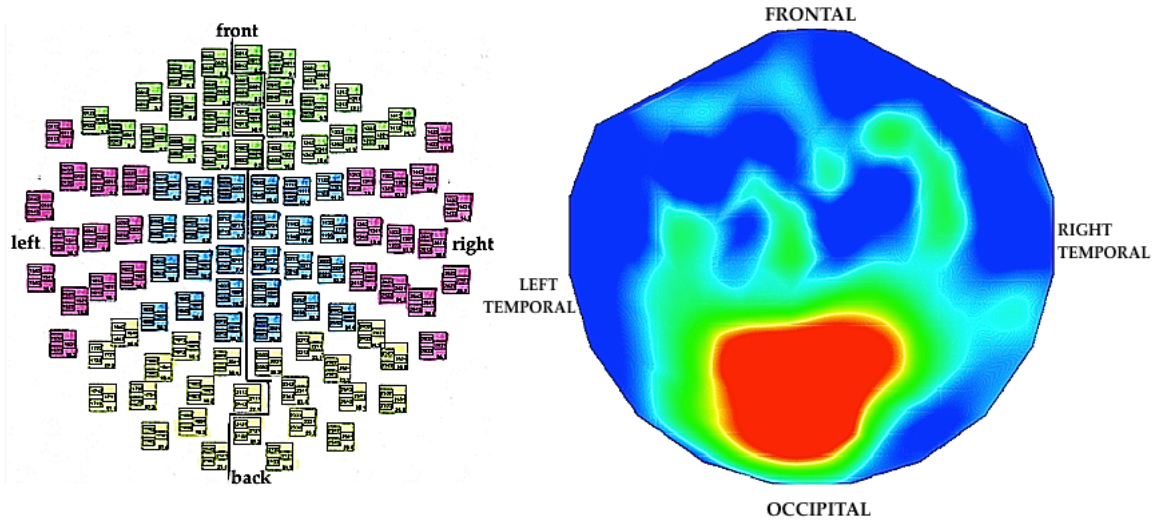


Figure 4 MEG helmet in 2D plane. This figure shows the helmet flattened into a plane with groups of sensors (left) corresponding to different cortical locations (green

is frontal; pink is temporal; blue is central and yellow is occipital). Right figure shows a cortical phase-locking map flattened into sensor space.

Appendix K

Autism diagnostic interview schedule-Generic (ADOS-G)

The ADOS-G is a semi-structured, standardized play and activities-based diagnostic assessment of ASD and other PDDs focussing on impairments in three behavioural domains:

1) communication
2) social interaction
3) play/imaginative use of materials and repetitive behaviour

This tool is based on the ADI-R. The main difference is that it is done with the affected individual whereas the ADI-R is done with caretaker/parent.

Diagnostic algorithms summarize ratings for social behaviour, communication and restricted and repetitive behaviours in accordance with the DSM-IV and ICD-10 diagnostic criteria and according to diagnostic thresholds that are different for different PDDs.

Bibliography

Abel, T. J., A. O. Hebb, C. D. Keene, D. E. Born and D. L. Silbergeld (2010). "Parahippocampal corpora amylacea: case report." Neurosurgery **66**(6): E1206-1207.

Ahlfors, S. P., J. Han, J. W. Belliveau and M. S. Hamalainen (2010). "Sensitivity of MEG and EEG to source orientation." Brain Topogr **23**(3): 227-232.

Allegra, M., S. Genovesi, M. Maggia, M. C. Cenni, G. Zunino, P. Sgado, M. Caleo and Y. Bozzi (2014). "Altered GABAergic markers, increased binocularity and reduced plasticity in the visual cortex of Engrailed-2 knockout mice." Front Cell Neurosci **8**: 163.

Allely, C. S., C. Gillberg and P. Wilson (2013). "Neurobiological abnormalities in the first few years of life in individuals later diagnosed with Autistic Spectrum Disorder: A review of recent data." Behav Neurol.

Amaral, D. G., C. M. Schumann and C. W. Nordahl (2008). "Neuroanatomy of autism." Trends Neurosci **31**(3): 137-145.

American Psychiatric Association Task Force on DSM-IV (2000). Diagnostic and statistical manual of mental disorders : DSM-IV-TR. Washington, DC, American Psychiatric Association.

Andree, C. and R. Sedivy (2005). "Discovery of a letter from Rokitansky to Virchow about subependymal corpora amylacea." Virchows Arch **446**(2): 177-180.

Angelidou, A., S. Asadi, K. D. Alysandratos, A. Karagkouni, S. Kourembanas and T. C. Theoharides (2012). "Perinatal stress, brain inflammation and risk of autism-review and proposal." BMC Pediatr **12**: 89.

Bailey, A., P. Luthert, A. Dean, B. Harding, I. Janota, M. Montgomery, M. Rutter and P. Lantos (1998). "A clinicopathological study of autism." Brain **121 (Pt 5)**: 889-905.

Bailey, A. J., S. Braeutigam, V. Jousmaki and S. J. Swithenby (2005). "Abnormal activation of face processing systems at early and intermediate latency in individuals with autism spectrum disorder: a magnetoencephalographic study." Eur J Neurosci **21**(9): 2575-2585.

Baird, G., E. Simonoff, A. Pickles, S. Chandler, T. Loucas, D. Meldrum and T. Charman (2006). "Prevalence of disorders of the autism spectrum in a population cohort of children in South Thames: the Special Needs and Autism Project (SNAP)." Lancet **368**(9531): 210-215.

Baker, J. P. (2013). "Autism at 70--redrawing the boundaries." N Engl J Med **369**(12): 1089-1091.

Baranek, G. T. (1999). "Autism during infancy: a retrospective video analysis of sensory-motor and social behaviors at 9-12 months of age." J Autism Dev Disord **29**(3): 213-224.

Baron-Cohen, S., T. Jolliffe, C. Mortimore and M. Robertson (1997). "Another advanced test of theory of mind: evidence from very high functioning adults with autism or asperger syndrome." J Child Psychol Psychiatry **38**(7): 813-822.

Bartos, M., I. Vida and P. Jonas (2007). "Synaptic mechanisms of synchronized gamma oscillations in inhibitory interneuron networks." Nat Rev Neurosci **8**(1): 45-56.

Baruth, J. M., M. F. Casanova, A. El-Baz, T. Horrell, G. Mathai, L. Sears and E. Sokhadze (2010). "Low-Frequency Repetitive Transcranial Magnetic Stimulation (rTMS) Modulates Evoked-Gamma Frequency Oscillations in Autism Spectrum Disorder (ASD)." J Neurother **14**(3): 179-194.

Beattie, M. S., G. E. Hermann, R. C. Rogers and J. C. Bresnahan (2002). "Cell death in models of spinal cord injury." Prog Brain Res **137**: 37-47.

Beeton, C. and K. G. Chandy (2005). "Potassium channels, memory T cells, and multiple sclerosis." Neuroscientist **11**(6): 550-562.

Bekkers, J. M. and N. Suzuki (2013). "Neurons and circuits for odor processing in the piriform cortex." Trends Neurosci **36**(7): 429-438.

Ben-Sasson, A., L. Hen, R. Fluss, S. A. Cermak, B. Engel-Yeger and E. Gal (2009). "A meta-analysis of sensory modulation symptoms in individuals with autism spectrum disorders." J Autism Dev Disord **39**(1): 1-11.

Benarroch, E. E. (2009). "Potassium channels: brief overview and implications in epilepsy." Neurology **72**(7): 664-669.

Bender, R. A. and T. Z. Baram (2007). "Epileptogenesis in the developing brain: what can we learn from animal models?" Epilepsia **48 Suppl 5**: 2-6.

Benes, F. M. and N. Lange (2001). "Two-dimensional versus three-dimensional cell counting: a practical perspective." Trends Neurosci **24**(1): 11-17.

Bennetto, L., E. S. Kuschner and S. L. Hyman (2007). "Olfaction and taste processing in autism." Biol Psychiatry **62**(9): 1015-1021.

Bennetto, L., B. F. Pennington and S. J. Rogers (1996). "Intact and impaired memory functions in autism." Child Dev **67**(4): 1816-1835.

Berg, P. and M. Scherg (1994). "A multiple source approach to the correction of eye artifacts." Electroencephalogr Clin Neurophysiol **90**(3): 229-241.

Billstedt, E., I. C. Gillberg and C. Gillberg (2005). "Autism after adolescence: population-based 13- to 22-year follow-up study of 120 individuals with autism diagnosed in childhood." J Autism Dev Disord **35**(3): 351-360.

bioscience, M. (2013). "http://www.stereology.info/."

Bolton, P. F., I. Carcani-Rathwell, J. Hutton, S. Goode, P. Howlin and M. Rutter "Epilepsy in autism: features and correlates." Br J Psychiatry **198**: 289-294.

Braeutigam, S. (2013). "Magnetoencephalography: Fundamentals and Established and Emerging Clinical Applications in Radiology." ISRN Radiology **2013**: 18.

Braeutigam, S., A. J. Bailey and S. J. Swithenby (2001). "Phase-locked gamma band responses to semantic violation stimuli." Brain Res Cogn Brain Res **10**(3): 365-377.

Braeutigam, S., S. P. Rose, S. J. Swithenby and T. Ambler (2004). "The distributed neuronal systems supporting choice-making in real-life situations: differences between men and women when choosing groceries detected using magnetoencephalography." Eur J Neurosci **20**(1): 293-302.

Braeutigam, S., S. J. Swithenby and A. J. Bailey (2008). "Contextual integration the unusual way: a magnetoencephalographic study of responses to semantic violation in individuals with autism spectrum disorders." Eur J Neurosci **27**(4): 1026-1036.

Brang, D. and V. S. Ramachandran (2010). "Olfactory bulb dysgenesis, mirror neuron system dysfunction, and autonomic dysregulation as the neural basis for autism." Med Hypotheses **74**(5): 919-921.

Braunschweig, D., P. Ashwood, P. Krakowiak, I. Hertz-Picciotto, R. Hansen, L. A. Croen, I. N. Pessah and J. Van de Water (2008). "Autism: maternally derived antibodies specific for fetal brain proteins." Neurotoxicology **29**(2): 226-231.

Brodmann, K. (1909). Vergleichende Lokalisationslehre der Großhirnrinde in ihren Principien dargestellt auf Grund des Zellenbaues Leipzig Barth.

Brown, C., T. Gruber, J. Boucher, G. Rippon and J. Brock (2005). "Gamma abnormalities during perception of illusory figures in autism." Cortex **41**(3): 364-376.

Brugha, T. S., S. McManus, J. Bankart, F. Scott, S. Purdon, J. Smith, P. Bebbington, R. Jenkins and H. Meltzer (2011). "Epidemiology of autism spectrum disorders in adults in the community in England." Arch Gen Psychiatry **68**(5): 459-465.

Buhl, E. H., G. Tamas and A. Fisahn (1998). "Cholinergic activation and tonic excitation induce persistent gamma oscillations in mouse somatosensory cortex in vitro." J Physiol **513 (Pt 1)**: 117-126.

Burack, J. A. (2001). The development of autism : perspectives from theory and research. Mahwah, N.J. ; London, Lawrence Erlbaum.

Burton, A., J. H. Conway and S. T. Holgate (2000). "Reliability: What is it and why is it measured?" Physiotherapy **2**(86): 94-99.

Buxbaum, J. D. and S. Baron-Cohen (2013). "DSM-5: the debate continues." Mol Autism **4**(1): 11.

Buzsaki, G. (2006). Rhythms of the brain. Oxford, Oxford University Press.

Buzsaki, G. and X. J. Wang (2012). "Mechanisms of gamma oscillations." Annu Rev Neurosci **35**: 203-225.

Cajal, R. y. (1955). Histologie du système nerveux de l'homme et des vertébrés Paris.

Canolty, R. T., E. Edwards, S. S. Dalal, M. Soltani, S. S. Nagarajan, H. E. Kirsch, M. S. Berger, N. M. Barbaro and R. T. Knight (2006). "High gamma power is phase-locked to theta oscillations in human neocortex." Science **313**(5793): 1626-1628.

Cao, F., A. Yin, G. Wen, A. M. Sheikh, Z. Tauqeer, M. Malik, A. Nagori, M. Schirripa, F. Schirripa, G. Merz, W. T. Brown and X. Li (2012). "Alteration of astrocytes and Wnt/beta-catenin signaling in the frontal cortex of autistic subjects." J Neuroinflammation **9**(1): 223.

Cardin, J. A., L. A. Palmer and D. Contreras (2005). "Stimulus-dependent gamma (30-50 Hz) oscillations in simple and complex fast rhythmic bursting cells in primary visual cortex." J Neurosci **25**(22): 5339-5350.

Carl, C., A. Acik, P. Konig, A. K. Engel and J. F. Hipp (2012). "The saccadic spike artifact in MEG." Neuroimage **59**(2): 1657-1667.

Carod, F. J., J. M. Prats, C. Garaizar and E. Zuazo (1995). "[Clinical-radiological evaluation of infantile autism and epileptic syndromes associated with autism]." Rev Neurol **23**(124): 1203-1207.

Caron, M. J., L. Mottron, C. Berthiaume and M. Dawson (2006). "Cognitive mechanisms, specificity and neural underpinnings of visuospatial peaks in autism." Brain **129**(Pt 7): 1789-1802.

Caronna, E. B., J. M. Milunsky and H. Tager-Flusberg (2008). "Autism spectrum disorders: clinical and research frontiers." Arch Dis Child **93**(6): 518-523.

Carrette, E., X. De Tiege, M. Op De Beeck, V. De Herdt, A. Meurs, B. Legros, R. Raedt, K. Deblaere, D. Van Roost, M. Bourguignon, S. Goldman, P. Boon, P. Van Bogaert and K. Vonck (2011). "Magnetoencephalography in epilepsy patients carrying a vagus nerve stimulator." Epilepsy Res **93**(1): 44-52.

Carvajal-Gonzalez, A., M. I. Leite, P. Waters, M. Woodhall, E. Coutinho, B. Balint, B. Lang, P. Pettingill, A. Carr, U. M. Sheerin, R. Press, M. P. Lunn, M. Lim, P. Maddison, H. M. Meinck, W. Vandenberghe and A. Vincent (2014). "Glycine receptor antibodies in PERM and related syndromes: characteristics, clinical features and outcomes." Brain **137**(Pt 8): 2178-2192.

Casanova, M. F., D. Buxhoeveden and J. Gomez (2003). "Disruption in the inhibitory architecture of the cell minicolumn: implications for autism." Neuroscientist **9**(6): 496-507.

Casanova, M. F., D. P. Buxhoeveden and C. Brown (2002). "Clinical and macroscopic correlates of minicolumnar pathology in autism." J Child Neurol **17**(9): 692-695.

Casanova, M. F., D. P. Buxhoeveden, A. E. Switala and E. Roy (2002). "Minicolumnar pathology in autism." Neurology **58**(3): 428-432.

Cavanagh, J. B. (1999). "Corpora-amylacea and the family of polyglucosan diseases." Brain Res Brain Res Rev **29**(2-3): 265-295.

Charman, T. (1997). "The relationship between joint attention and pretend play in autism." Dev Psychopathol **9**(1): 1-16.

Chaumon, M., V. Drouet and C. Tallon-Baudry (2008). "Unconscious associative memory affects visual processing before 100 ms." J Vis **8**(3): 10 11-10.

Chaumon, M., D. Schwartz and C. Tallon-Baudry (2009). "Unconscious learning versus visual perception: dissociable roles for gamma oscillations revealed in MEG." J Cogn Neurosci **21**(12): 2287-2299.

Chen, C., Y. H. Shih, D. J. Yen, J. F. Lirng, Y. C. Guo, H. Y. Yu and C. H. Yiu (2003). "Olfactory auras in patients with temporal lobe epilepsy." Epilepsia **44**(2): 257-260.

Chez, M. G., M. Chang, V. Krasne, C. Coughlan, M. Kominsky and A. Schwartz (2006). "Frequency of epileptiform EEG abnormalities in a sequential screening of

autistic patients with no known clinical epilepsy from 1996 to 2005." Epilepsy Behav **8**(1): 267-271.

Constantino, J. N., S. A. Davis, R. D. Todd, M. K. Schindler, M. M. Gross, S. L. Brophy, L. M. Metzger, C. S. Shoushtari, R. Splinter and W. Reich (2003). "Validation of a brief quantitative measure of autistic traits: comparison of the social responsiveness scale with the autism diagnostic interview-revised." J Autism Dev Disord **33**(4): 427-433.

Constantino, J. N. and C. P. Gruber (2005). Social Responsiveness Scale (SRS), Western Psychological Services, Los Angeles, California.

Constantino, J. N., Y. Zhang, T. Frazier, A. M. Abbacchi and P. Law (2010). "Sibling recurrence and the genetic epidemiology of autism." Am J Psychiatry **167**(11): 1349-1356.

Constantino, J. N. G., C. P. (2012). Social Responsiveness Scale-2 (SRS-2), Western Psychological Services, Los Angeles, California.

Cornew, L., T. P. Roberts, L. Blaskey and J. C. Edgar (2012). "Resting-state oscillatory activity in autism spectrum disorders." J Autism Dev Disord **42**(9): 1884-1894.

Courchesne, E. (2002). "Abnormal early brain development in autism." Mol Psychiatry **7 Suppl 2**: S21-23.

Courchesne, E., R. Carper and N. Akshoomoff (2003). "Evidence of brain overgrowth in the first year of life in autism." JAMA **290**(3): 337-344.

Courchesne, E., P. R. Mouton, M. E. Calhoun, K. Semendeferi, C. Ahrens-Barbeau, M. J. Hallet, C. C. Barnes and K. Pierce (2011). "Neuron number and size in prefrontal cortex of children with autism." JAMA **306**(18): 2001-2010.

Courchesne, E. and K. Pierce (2005). "Brain overgrowth in autism during a critical time in development: implications for frontal pyramidal neuron and interneuron development and connectivity." Int J Dev Neurosci **23**(2-3): 153-170.

Cousijn, H., S. Haegens, G. Wallis, J. Near, M. G. Stokes, P. J. Harrison and A. C. Nobre (2014). "Resting GABA and glutamate concentrations do not predict visual gamma frequency or amplitude." Proc Natl Acad Sci U S A **111**(25): 9301-9306.

Crosby, E. C. and T. Humphrey (1941). "Studies of the vertebrate telencephalon. II. The nuclear pattern of the anterior olfactory nucleus, tuberculum olfactorium and the amygdaloid complex in adult man." Journal of Comparative Neurology **74**(2): 309-352.

Dakin, S. and U. Frith (2005). "Vagaries of visual perception in autism." Neuron **48**(3): 497-507.

Dalton, P., R. Deacon, A. Blamire, M. Pike, I. McKinlay, J. Stein, P. Styles and A. Vincent (2003). "Maternal neuronal antibodies associated with autism and a language disorder." Ann Neurol **53**(4): 533-537.

Damiano, C. R., J. Aloi, K. Dunlap, C. J. Burrus, M. G. Mosner, R. V. Kozink, R. E. McLaurin, O. A. Mullette-Gillman, R. M. Carter, S. A. Huettel, F. J. McClernon, A. Ashley-Koch and G. S. Dichter (2014). "Association between the oxytocin receptor (OXTR) gene and mesolimbic responses to rewards." Mol Autism **5**(1): 7.

Danielsson, S., I. C. Gillberg, E. Billstedt, C. Gillberg and I. Olsson (2005). "Epilepsy in young adults with autism: a prospective population-based follow-up study of 120 individuals diagnosed in childhood." Epilepsia **46**(6): 918-923.

Davies, D. C., N. Horwood, S. L. Isaacs and D. M. Mann (1992). "The effect of age and Alzheimer's disease on pyramidal neuron density in the individual fields of the hippocampal formation." Acta Neuropathol **83**(5): 510-517.

DeStefano, F. and R. T. Chen (2001). "Autism and measles-mumps-rubella vaccination: controversy laid to rest?" CNS Drugs **15**(11): 831-837.

Diamond, B., P. T. Huerta, P. Mina-Osorio, C. Kowal and B. T. Volpe (2009). "Losing your nerves? Maybe it's the antibodies." Nat Rev Immunol **9**(6): 449-456.

Dichter, G. S., C. A. Damiano and J. A. Allen (2012). "Reward circuitry dysfunction in psychiatric and neurodevelopmental disorders and genetic syndromes: animal models and clinical findings." J Neurodev Disord **4**(1): 19.

Dudova, I., J. Vodicka, M. Havlovicova, Z. Sedlacek, T. Urbanek and M. Hrdlicka (2011). "Odor detection threshold, but not odor identification, is impaired in children with autism." Eur Child Adolesc Psychiatry **20**(7): 333-340.

Duvernoy, H. M., F. Cattin, P.-Y. Risold and SpringerLink (Online service) (2013). The Human Hippocampus Functional Anatomy, Vascularization and Serial Sections with MRI. Berlin, Heidelberg, Springer Berlin Heidelberg : Imprint: Springer,**:** VIII, 237 p. 133 illus., 213 illus. in color.

Ebert, U., P. Wlaz and W. Loscher (2000). "High susceptibility of the anterior and posterior piriform cortex to induction of convulsions by bicuculline." Eur J Neurosci **12**(12): 4195-4205.

Economo, C. and S. Parker (1929). The cytoarchitectonics of the human cerebral cortex. London, Humphrey Milford, Oxford University Press.

Economo, C. and L. C. Triarhou (2009). Cellular structure of the human cerebral cortex. Basel ; London, Karger.

Edalatmanesh, M. A., H. Nikfarjam, F. Vafaee and M. Moghadas (2013). "Increased hippocampal cell density and enhanced spatial memory in the valproic acid rat model of autism." Brain Res **1526**: 15-25.

Edmonson, C., M. N. Ziats and O. M. Rennert (2014). "Altered glial marker expression in autistic post-mortem prefrontal cortex and cerebellum." Mol Autism **5**(1): 3.

Eidt, S., E. J. Kendall and A. Obenaus (2004). "Neuronal and glial cell populations in the piriform cortex distinguished by using an approximation of q-space imaging after status epilepticus." AJNR Am J Neuroradiol **25**(7): 1225-1233.

Elliott, M. A., Z. Shi and F. Surer (2007). "The effects of subthreshold synchrony on the perception of simultaneity." Psychol Res **71**(6): 687-693.

Engel, J., Jr. and E. International League Against (2001). "A proposed diagnostic scheme for people with epileptic seizures and with epilepsy: report of the ILAE Task Force on Classification and Terminology." Epilepsia **42**(6): 796-803.

Ernst, A., K. Alkass, S. Bernard, M. Salehpour, S. Perl, J. Tisdale, G. Possnert, H. Druid and J. Frisen (2014). "Neurogenesis in the striatum of the adult human brain." Cell **156**(5): 1072-1083.

Esiri, M. M. and D. R. Oppenheimer (1996). Oppenheimer's diagnostic neuropathology : a practical manual. Oxford, Blackwell Science.

Etchepareborda, M. C., A. Diaz-Lucero, M. J. Pascuale, L. Abad-Mas and R. Ruiz-Andres (2007). "[Asperger's syndrome, little teachers: special skills]." Rev Neurol **44 Suppl 2**: S43-47.

Fallon, J. H., J. N. Riley, J. C. Sipe and R. Y. Moore (1978). "The islands of Calleja: organization and connections." J Comp Neurol **181**(2): 375-395.

Falter, C. M., S. Braeutigam, R. Nathan, S. Carrington and A. J. Bailey (2013). "Enhanced access to early visual processing of perceptual simultaneity in autism spectrum disorders." J Autism Dev Disord **43**(8): 1857-1866.

Falter, C. M., M. A. Elliott and A. J. Bailey (2012). "Enhanced visual temporal resolution in autism spectrum disorders." PLoS One **7**(3): e32774.

Fatemi, S. H., A. R. Halt, G. Realmuto, J. Earle, D. A. Kist, P. Thuras and A. Merz (2002). "Purkinje cell size is reduced in cerebellum of patients with autism." Cell Mol Neurobiol **22**(2): 171-175.

Field, A. P., Z. Field and J. Miles (2012). Discovering statistics using R. London, SAGE.

Freichel, C., H. Potschka, U. Ebert, C. Brandt and W. Loscher (2006). "Acute changes in the neuronal expression of GABA and glutamate decarboxylase isoforms in the rat piriform cortex following status epilepticus." Neuroscience **141**(4): 2177-2194.

Fries, P., P. R. Roelfsema, A. K. Engel, P. Konig and W. Singer (1997). "Synchronization of oscillatory responses in visual cortex correlates with perception in interocular rivalry." Proc Natl Acad Sci U S A **94**(23): 12699-12704.

Fujikawa, D. G., H. H. Itabashi, A. Wu and S. S. Shinmei (2000). "Status epilepticus-induced neuronal loss in humans without systemic complications or epilepsy." Epilepsia **41**(8): 981-991.

Gadad, B. S., L. Hewitson, K. A. Young and D. C. German (2013). "Neuropathology and Animal Models of Autism: Genetic and Environmental Factors." Autism Res Treat **2013**: 731935.

Gaetz, W., L. Bloy, D. J. Wang, R. G. Port, L. Blaskey, S. E. Levy and T. P. Roberts (2013). "GABA estimation in the brains of children on the autism spectrum: Measurement precision and regional cortical variation." Neuroimage.

Galle, S. A., V. Courchesne, L. Mottron and J. Frasnelli (2013). "Olfaction in the autism spectrum." Perception **42**(3): 341-355.

Garman, R. H. (2011). "Histology of the central nervous system." Toxicol Pathol **39**(1): 22-35.

Garnero, L., S. Baillet, G. Marin, B. Renault, C. Guerin and G. Meunier (1999). "Introducing priors in the EEG/MEG inverse problem." Electroencephalogr Clin Neurophysiol Suppl **50**: 183-189.

Gastaut, H., Lammers, H.J. (1961). Anatomie du Rhinencéphale Les grandes activités du rhinencéphale'. Paris, Masson et Cie.

Gati, I. and L. Leel-Ossy (2001). "Heat shock protein 60 in corpora amylacea." Pathol Oncol Res **7**(2): 140-144.

Giaume, C., F. Kirchhoff, C. Matute, A. Reichenbach and A. Verkhratsky (2007). "Glia: the fulcrum of brain diseases." Cell Death Differ **14**(7): 1324-1335.

Gilchrist, A., J. Green, A. Cox, D. Burton, M. Rutter and A. Le Couteur (2001). "Development and current functioning in adolescents with Asperger syndrome: a comparative study." J Child Psychol Psychiatry **42**(2): 227-240.

Giles, D. C. (2013). "'DSM-V is taking away our identity': The reaction of the online community to the proposed changes in the diagnosis of Asperger's disorder." Health (London).

Gogolla, N., J. J. Leblanc, K. B. Quast, T. C. Sudhof, M. Fagiolini and T. K. Hensch (2009). "Common circuit defect of excitatory-inhibitory balance in mouse models of autism." J Neurodev Disord **1**(2): 172-181.

Gottfried, J. A. (2010). "Central mechanisms of odour object perception." Nat Rev Neurosci **11**(9): 628-641.

Gottfried, J. A., R. Deichmann, J. S. Winston and R. J. Dolan (2002). "Functional heterogeneity in human olfactory cortex: an event-related functional magnetic resonance imaging study." J Neurosci **22**(24): 10819-10828.

Gottfried, J. A., J. O'Doherty and R. J. Dolan (2002). "Appetitive and aversive olfactory learning in humans studied using event-related functional magnetic resonance imaging." J Neurosci **22**(24): 10829-10837.

Gottfried, J. A., A. P. Smith, M. D. Rugg and R. J. Dolan (2004). "Remembrance of odors past: human olfactory cortex in cross-modal recognition memory." Neuron **42**(4): 687-695.

Gray, C. M., P. Konig, A. K. Engel and W. Singer (1989). "Oscillatory responses in cat visual cortex exhibit inter-columnar synchronization which reflects global stimulus properties." Nature **338**(6213): 334-337.

Grice, S. J., M. W. Spratling, A. Karmiloff-Smith, H. Halit, G. Csibra, M. de Haan and M. H. Johnson (2001). "Disordered visual processing and oscillatory brain activity in autism and Williams syndrome." Neuroreport **12**(12): 2697-2700.

Grutzner, C., P. J. Uhlhaas, E. Genc, A. Kohler, W. Singer and M. Wibral (2010). "Neuroelectromagnetic correlates of perceptual closure processes." J Neurosci **30**(24): 8342-8352.

Grzadzinski, R., M. Huerta and C. Lord (2013). "DSM-5 and autism spectrum disorders (ASDs): an opportunity for identifying ASD subtypes." Mol Autism **4**(1): 12.

Guastella, A. J., S. L. Einfeld, K. M. Gray, N. J. Rinehart, B. J. Tonge, T. J. Lambert and I. B. Hickie (2010). "Intranasal oxytocin improves emotion recognition for youth with autism spectrum disorders." Biol Psychiatry **67**(7): 692-694.

Gundersen, H. J. and E. B. Jensen (1987). "The efficiency of systematic sampling in stereology and its prediction." J Microsc **147**(Pt 3): 229-263.

Hansen, P. C., M. L. Kringelbach and R. Salmelin (2010). MEG an introduction to methods. New York, Oxford University Press**:** xii, 436 p.

Happe, F. and U. Frith (2006). "The weak coherence account: detail-focused cognitive style in autism spectrum disorders." J Autism Dev Disord **36**(1): 5-25.

Harada, M., M. M. Taki, A. Nose, H. Kubo, K. Mori, H. Nishitani and T. Matsuda (2011). "Non-invasive evaluation of the GABAergic/glutamatergic system in autistic patients observed by MEGA-editing proton MR spectroscopy using a clinical 3 tesla instrument." J Autism Dev Disord **41**(4): 447-454.

Helm, J., G. Akgul and L. P. Wollmuth (2013). "Subgroups of parvalbumin-expressing interneurons in layers 2/3 of the visual cortex." J Neurophysiol **109**(6): 1600-1613.

Herbert, M. R. (2011). "SHANK3, the synapse, and autism." N Engl J Med **365**(2): 173-175.

Hessels, R. S., I. T. Hooge, T. M. Snijders and C. Kemner (2014). "Is there a limit to the superiority of individuals with ASD in visual search?" J Autism Dev Disord **44**(2): 443-451.

Highley, J. R., M. A. Walker, M. M. Esiri, T. J. Crow and P. J. Harrison (2002). "Asymmetry of the uncinate fasciculus: a post-mortem study of normal subjects and patients with schizophrenia." Cereb Cortex **12**(11): 1218-1224.

Hollander, E., J. Bartz, W. Chaplin, A. Phillips, J. Sumner, L. Soorya, E. Anagnostou and S. Wasserman (2007). "Oxytocin increases retention of social cognition in autism." Biol Psychiatry **61**(4): 498-503.

Howard, J. D., J. Plailly, M. Grueschow, J. D. Haynes and J. A. Gottfried (2009). "Odor quality coding and categorization in human posterior piriform cortex." Nat Neurosci **12**(7): 932-938.

Hoyaux, D., C. Decaestecker, C. W. Heizmann, T. Vogl, B. W. Schafer, I. Salmon, R. Kiss and R. Pochet (2000). "S100 proteins in Corpora amylacea from normal human brain." Brain Res **867**(1-2): 280-288.

Hsieh, Y. C. and A. C. Puche (2013). "Development of the Islands of Calleja." Brain Res **1490**: 52-60.

Hu, H., J. Gan and P. Jonas (2014). "Interneurons. Fast-spiking, parvalbumin(+) GABAergic interneurons: from cellular design to microcircuit function." Science **345**(6196): 1255263.

Hussman, J. P. (2001). "Suppressed GABAergic inhibition as a common factor in suspected etiologies of autism." J Autism Dev Disord **31**(2): 247-248.

Ikemoto, S. (2007). "Dopamine reward circuitry: two projection systems from the ventral midbrain to the nucleus accumbens-olfactory tubercle complex." Brain Res Rev **56**(1): 27-78.

Iossifov, I., M. Ronemus, D. Levy, Z. Wang, I. Hakker, J. Rosenbaum, B. Yamrom, Y. H. Lee, G. Narzisi, A. Leotta, J. Kendall, E. Grabowska, B. Ma, S. Marks, L. Rodgers, A. Stepansky, J. Troge, P. Andrews, M. Bekritsky, K. Pradhan, E. Ghiban, M. Kramer, J. Parla, R. Demeter, L. L. Fulton, R. S. Fulton, V. J. Magrini, K. Ye, J. C. Darnell, R. B. Darnell, E. R. Mardis, R. K. Wilson, M. C. Schatz, W. R. McCombie and M. Wigler (2012). "De novo gene disruptions in children on the autistic spectrum." Neuron **74**(2): 285-299.

Irani, S. R., K. Bera, P. Waters, L. Zuliani, S. Maxwell, M. S. Zandi, M. A. Friese, I. Galea, D. M. Kullmann, D. Beeson, B. Lang, C. G. Bien and A. Vincent (2010). "N-methyl-D-aspartate antibody encephalitis: temporal progression of clinical and

paraclinical observations in a predominantly non-paraneoplastic disorder of both sexes." Brain **133**(Pt 6): 1655-1667.

Irani, S. R., J. M. Gelfand, A. Al-Diwani and A. Vincent (2014). "Cell-surface central nervous system autoantibodies: Clinical relevance and emerging paradigms." Ann Neurol **76**(2): 168-184.

Jackson, J. D. (1963). Classical electrodynamics. New York,, Wiley.

Jacot-Descombes, S., N. Uppal, B. Wicinski, M. Santos, J. Schmeidler, P. Giannakopoulos, H. Heinsen, C. Schmitz and P. R. Hof (2012). "Decreased pyramidal neuron size in Brodmann areas 44 and 45 in patients with autism." Acta Neuropathol **124**(1): 67-79.

Jagadeesh, B., C. M. Gray and D. Ferster (1992). "Visually evoked oscillations of membrane potential in cells of cat visual cortex." Science **257**(5069): 552-554.

Jaspar, H. H. and J. J. Prick (1968). "[Morphology and histochemistry of the corpora amylacea]." Ned Tijdschr Geneeskd **112**(24): 1153-1156.

Johnson, D. M., K. R. Illig, M. Behan and L. B. Haberly (2000). "New features of connectivity in piriform cortex visualized by intracellular injection of pyramidal cells suggest that "primary" olfactory cortex functions like "association" cortex in other sensory systems." J Neurosci **20**(18): 6974-6982.

Jones, E. V., D. Cook and K. K. Murai (2012). "A neuron-astrocyte co-culture system to investigate astrocyte-secreted factors in mouse neuronal development." Methods Mol Biol **814**: 341-352.

Jung, J., J. Hudry, P. Ryvlin, J. P. Royet, O. Bertrand and J. P. Lachaux (2006). "Functional significance of olfactory-induced oscillations in the human amygdala." Cereb Cortex **16**(1): 1-8.

Kaech, S. and G. Banker (2006). "Culturing hippocampal neurons." Nat Protoc **1**(5): 2406-2415.

Kanner, L. (1968). "Autistic disturbances of affective contact." Acta Paedopsychiatr **35**(4): 100-136.

Kawamura, T., T. Morioka, S. Nishio, K. Fukui and M. Fukui (2002). "Temporal lobe epilepsy and corpora amylacea in the hippocampus: clinicopathologic correlation." Neurol Res **24**(6): 563-569.

Kawashima, T., T. Adachi, Y. Tokunaga, A. Furuta, S. O. Suzuki, K. Doh-ura and T. Iwaki (1999). "Immunohistochemical analysis in a case of idiopathic Lennox-Gastaut syndrome." Clin Neuropathol **18**(6): 286-292.

Keller, J. N. (2006). "Age-related neuropathology, cognitive decline, and Alzheimer's disease." Ageing Res Rev **5**(1): 1-13.

Kemper, T. L. and M. Bauman (1998). "Neuropathology of infantile autism." J Neuropathol Exp Neurol **57**(7): 645-652.

Kemper, T. L. and M. L. Bauman (1993). "The contribution of neuropathologic studies to the understanding of autism." Neurol Clin **11**(1): 175-187.

Kern, J. K., M. H. Trivedi, B. D. Grannemann, C. R. Garver, D. G. Johnson, A. A. Andrews, J. S. Savla, J. A. Mehta and J. L. Schroeder (2007). "Sensory correlations in autism." Autism **11**(2): 123-134.

Khan, S., A. Gramfort, N. R. Shetty, M. G. Kitzbichler, S. Ganesan, J. M. Moran, S. M. Lee, J. D. Gabrieli, H. B. Tager-Flusberg, R. M. Joseph, M. R. Herbert, M. S. Hamalainen and T. Kenet (2013). "Local and long-range functional connectivity is reduced in concert in autism spectrum disorders." Proc Natl Acad Sci U S A **110**(8): 3107-3112.

Kikuchi, M., K. Shitamichi, Y. Yoshimura, S. Ueno, H. Hiraishi, T. Hirosawa, T. Munesue, H. Nakatani, T. Tsubokawa, Y. Haruta, M. Oi, Y. Niida, G. B. Remijn, T. Takahashi, M. Suzuki, H. Higashida and Y. Minabe (2013). "Altered brain connectivity in 3-to 7-year-old children with autism spectrum disorder." Neuroimage Clin **2**: 394-401.

Koob, G. F. (1996). "Hedonic valence, dopamine and motivation." Mol Psychiatry **1**(3): 186-189.

Lai, A. Y., R. D. Swayze, A. El-Husseini and C. Song (2006). "Interleukin-1 beta modulates AMPA receptor expression and phosphorylation in hippocampal neurons." J Neuroimmunol **175**(1-2): 97-106.

Lancaster, E. and J. Dalmau (2012). "Neuronal autoantigens--pathogenesis, associated disorders and antibody testing." Nat Rev Neurol **8**(7): 380-390.

Lancaster, E., M. Lai, X. Peng, E. Hughes, R. Constantinescu, J. Raizer, D. Friedman, M. B. Skeen, W. Grisold, A. Kimura, K. Ohta, T. Iizuka, M. Guzman, F. Graus, S. J. Moss, R. Balice-Gordon and J. Dalmau (2010). "Antibodies to the GABA(B) receptor in limbic encephalitis with seizures: case series and characterisation of the antigen." Lancet Neurol **9**(1): 67-76.

Lanuza, E., A. Novejarque, J. Martinez-Ricos, J. Martinez-Hernandez, C. Agustin-Pavon and F. Martinez-Garcia (2008). "Sexual pheromones and the evolution of the reward system of the brain: the chemosensory function of the amygdala." Brain Res Bull **75**(2-4): 460-466.

Laufs, H. (2012). "Functional imaging of seizures and epilepsy: evolution from zones to networks." Curr Opin Neurol **25**(2): 194-200.

Laufs, H., M. P. Richardson, A. Salek-Haddadi, C. Vollmar, J. S. Duncan, K. Gale, L. Lemieux, W. Loscher and M. J. Koepp (2011). "Converging PET and fMRI evidence for a common area involved in human focal epilepsies." Neurology **77**(9): 904-910.

Laurence, J. A. and S. H. Fatemi (2005). "Glial fibrillary acidic protein is elevated in superior frontal, parietal and cerebellar cortices of autistic subjects." Cerebellum **4**(3): 206-210.

Lavie, N., A. Hirst, J. W. de Fockert and E. Viding (2004). "Load theory of selective attention and cognitive control." J Exp Psychol Gen **133**(3): 339-354.

Lawrence, Y. A., T. L. Kemper, M. L. Bauman and G. J. Blatt (2010). "Parvalbumin-, calbindin-, and calretinin-immunoreactive hippocampal interneuron density in autism." Acta Neurol Scand **121**(2): 99-108.

Leekam, S. R., C. Nieto, S. J. Libby, L. Wing and J. Gould (2007). "Describing the sensory abnormalities of children and adults with autism." J Autism Dev Disord **37**(5): 894-910.

Lewine, J. D., R. Andrews, M. Chez, A. A. Patil, O. Devinsky, M. Smith, A. Kanner, J. T. Davis, M. Funke, G. Jones, B. Chong, S. Provencal, M. Weisend, R. R. Lee and W. W. Orrison, Jr. (1999). "Magnetoencephalographic patterns of epileptiform activity in children with regressive autism spectrum disorders." Pediatrics **104**(3 Pt 1): 405-418.

Liu, W., G. D. Pappas and C. S. Carter (2005). "Oxytocin receptors in brain cortical regions are reduced in haploinsufficient (+/-) reeler mice." Neurol Res **27**(4): 339-345.

LLC, L. A. N. S. (2008). from http://www.lanl.gov/quarterly/q_spring03/meg_helmet_measurements.shtml.

Lord, C., S. Risi, L. Lambrecht, E. H. Cook, Jr., B. L. Leventhal, P. C. DiLavore, A. Pickles and M. Rutter (2000). "The autism diagnostic observation schedule-generic: a standard measure of social and communication deficits associated with the spectrum of autism." J Autism Dev Disord **30**(3): 205-223.

Lord, C., M. Rutter and A. Le Couteur (1994). "Autism Diagnostic Interview-Revised: a revised version of a diagnostic interview for caregivers of individuals with possible pervasive developmental disorders." J Autism Dev Disord **24**(5): 659-685.

Loscher, W. and U. Ebert (1996). "The role of the piriform cortex in kindling." Prog Neurobiol **50**(5-6): 427-481.

Loscher, W., H. Lehmann and U. Ebert (1998). "Differences in the distribution of GABA- and GAD-immunoreactive neurons in the anterior and posterior piriform cortex of rats." Brain Res **800**(1): 21-31.

Love, B. C., J. N. Rouder and E. J. Wisniewski (1999). "A structural account of global and local processing." Cogn Psychol **38**(2): 291-316.

Lushchekina, E. A., E. D. Podreznaia, V. S. Lushchekin and V. B. Strelets (2010). "[Comparative EEG study in normal and autistic children]." Zh Vyssh Nerv Deiat Im I P Pavlova **60**(6): 657-666.

Machado, C., M. Estevez, G. Leisman, R. Melillo, R. Rodriguez, P. Defina, A. Hernandez, J. Perez-Nellar, R. Naranjo, M. Chinchilla, N. Garofalo, J. Vargas and C. Beltran (2013). "QEEG Spectral and Coherence Assessment of Autistic Children in Three Different Experimental Conditions." J Autism Dev Disord.

Mack, C. L., C. L. Vanderlugt-Castaneda, K. L. Neville and S. D. Miller (2003). "Microglia are activated to become competent antigen presenting and effector cells in the inflammatory environment of the Theiler's virus model of multiple sclerosis." J Neuroimmunol **144**(1-2): 68-79.

Mai, J. r. K., T. Voss and G. Paxinos (2008). Atlas of the human brain. London, Elsevier/Academic Press.

Marco, E. J., L. B. Hinkley, S. S. Hill and S. S. Nagarajan (2011). "Sensory processing in autism: a review of neurophysiologic findings." Pediatr Res **69**(5 Pt 2): 48R-54R.

Marin, O. (2012). "Interneuron dysfunction in psychiatric disorders." Nat Rev Neurosci **13**(2): 107-120.

Martin, J. E., K. Mather, M. Swash, O. Garofalo, P. N. Leigh and B. H. Anderton (1991). "Heat shock protein expression in corpora amylacea in the central nervous system: clues to their origin." Neuropathol Appl Neurobiol **17**(2): 113-119.

Maxwell, C. R., M. E. Villalobos, R. T. Schultz, B. Herpertz-Dahlmann, K. Konrad and G. Kohls (2013). "Atypical Laterality of Resting Gamma Oscillations in Autism Spectrum Disorders." J Autism Dev Disord.

May, T., W. J. Brewer, N. J. Rinehart, P. G. Enticott, A. V. Brereton and B. J. Tonge (2011). "Differential olfactory identification in children with autism and Asperger's disorder: a comparative and longitudinal study." J Autism Dev Disord **41**(7): 837-847.

McConachie, H., A. Le Couteur and E. Honey (2005). "Can a diagnosis of Asperger syndrome be made in very young children with suspected autism spectrum disorder?" J Autism Dev Disord **35**(2): 167-176.

McFadden, K. L., S. Hepburn, E. Winterrowd, G. L. Schmidt and D. C. Rojas (2012). "Abnormalities in gamma-band responses to language stimuli in first-degree relatives of children with autism spectrum disorder: an MEG study." BMC Psychiatry **12**: 213.

Meme, W., C. F. Calvo, N. Froger, P. Ezan, E. Amigou, A. Koulakoff and C. Giaume (2006). "Proinflammatory cytokines released from microglia inhibit gap junctions in astrocytes: potentiation by beta-amyloid." FASEB J **20**(3): 494-496.

Meyer, G., T. Gonzalez-Hernandez, F. Carrillo-Padilla and R. Ferres-Torres (1989). "Aggregations of granule cells in the basal forebrain (islands of Calleja): Golgi and cytoarchitectonic study in different mammals, including man." J Comp Neurol **284**(3): 405-428.

Miller, L. G., W. R. Galpern, K. Dunlap, C. A. Dinarello and T. J. Turner (1991). "Interleukin-1 augments gamma-aminobutyric acidA receptor function in brain." Mol Pharmacol **39**(2): 105-108.

Miller, P. S. and A. R. Aricescu (2014). "Crystal structure of a human GABAA receptor." Nature **512**(7514): 270-275.

Milne, E., A. Scope, O. Pascalis, D. Buckley and S. Makeig (2009). "Independent component analysis reveals atypical electroencephalographic activity during visual perception in individuals with autism." Biol Psychiatry **65**(1): 22-30.

Monaghan, M. M., J. S. Trimmer and K. J. Rhodes (2001). "Experimental localization of Kv1 family voltage-gated K+ channel alpha and beta subunits in rat hippocampal formation." J Neurosci **21**(16): 5973-5983.

Morgan, J. T., G. Chana, C. A. Pardo, C. Achim, K. Semendeferi, J. Buckwalter, E. Courchesne and I. P. Everall (2010). "Microglial activation and increased microglial density observed in the dorsolateral prefrontal cortex in autism." Biol Psychiatry **68**(4): 368-376.

Mottron, L., M. Dawson, I. Soulieres, B. Hubert and J. Burack (2006). "Enhanced perceptual functioning in autism: an update, and eight principles of autistic perception." J Autism Dev Disord **36**(1): 27-43.

Muhle, R., S. V. Trentacoste and I. Rapin (2004). "The genetics of autism." Pediatrics **113**(5): e472-486.

Munoz-Yunta, J. A., T. Ortiz, M. Palau-Baduell, L. Martin-Munoz, B. Salvado-Salvado, A. Valls-Santasusana, J. Perich-Alsina, I. Cristobal, A. Fernandez, F. Maestu and C. Dursteler (2008). "Magnetoencephalographic pattern of epileptiform activity in children with early-onset autism spectrum disorders." Clin Neurophysiol **119**(3): 626-634.

Munoz-Yunta, J. A., M. Palau-Baduell, B. Salvado-Salvado, A. Valls-Santasusana, N. Rosendo-Moreno, M. Clofent-Torrento and F. Manchado (2008). "[Autism, epilepsy and genetics]." Rev Neurol **46 Suppl 1**: S71-77.

Muthukumaraswamy, S. D., R. A. Edden, D. K. Jones, J. B. Swettenham and K. D. Singh (2009). "Resting GABA concentration predicts peak gamma frequency and fMRI amplitude in response to visual stimulation in humans." Proc Natl Acad Sci U S A **106**(20): 8356-8361.

Muthukumaraswamy, S. D., J. F. Myers, S. J. Wilson, D. J. Nutt, K. Hamandi, A. Lingford-Hughes and K. D. Singh (2013). "Elevating endogenous GABA levels with GAT-1 blockade modulates evoked but not induced responses in human visual cortex." Neuropsychopharmacology **38**(6): 1105-1112.

Muthukumaraswamy, S. D., K. D. Singh, J. B. Swettenham and D. K. Jones "Visual gamma oscillations and evoked responses: variability, repeatability and structural MRI correlates." Neuroimage **49**(4): 3349-3357.

Nam, I. H., D. W. Kim, H. Y. Song, S. Kim, K. S. Lee and Y. H. Lee (2012). "Association of Corpora Amylacea Formation with Astrocytes and Cerebrospinal Fluid in the Aged Human Brain " Korean J Phys Anthropol **25**(4): 177-184.

Nieuwenhuys, R., C. v. Huijzen, J. Voogd and SpringerLink (Online service) (2008). The Human Central Nervous System. Berlin, Heidelberg, Springer Berlin Heidelberg,.

Numis, A. L., P. Major, M. A. Montenegro, D. A. Muzykewicz, M. B. Pulsifer and E. A. Thiele (2011). "Identification of risk factors for autism spectrum disorders in tuberous sclerosis complex." Neurology **76**(11): 981-987.

O'Leary, J. L. (1937). "Structure of the primary olfactory cortex of the mouse." J. comp. Neurol. (67): 1-31.

O'Roak, B. J., L. Vives, S. Girirajan, E. Karakoc, N. Krumm, B. P. Coe, R. Levy, A. Ko, C. Lee, J. D. Smith, E. H. Turner, I. B. Stanaway, B. Vernot, M. Malig, C. Baker, B. Reilly, J. M. Akey, E. Borenstein, M. J. Rieder, D. A. Nickerson, R. Bernier, J. Shendure and E. E. Eichler (2012). "Sporadic autism exomes reveal a highly interconnected protein network of de novo mutations." Nature **485**(7397): 246-250.

Oblak, A. L., D. L. Rosene, T. L. Kemper, M. L. Bauman and G. J. Blatt (2011). "Altered posterior cingulate cortical cyctoarchitecture, but normal density of neurons and interneurons in the posterior cingulate cortex and fusiform gyrus in autism." Autism Res **4**(3): 200-211.

Oostenveld, R., P. Fries, E. Maris and J. M. Schoffelen (2011). "FieldTrip: Open source software for advanced analysis of MEG, EEG, and invasive electrophysiological data." Comput Intell Neurosci **2011**: 156869.

Orekhova, E. V., T. A. Stroganova, G. Nygren, M. M. Tsetlin, I. N. Posikera, C. Gillberg and M. Elam (2007). "Excess of high frequency electroencephalogram oscillations in boys with autism." Biol Psychiatry **62**(9): 1022-1029.

Ota, Y., A. T. Zanetti and R. M. Hallock (2013). "The Role of Astrocytes in the Regulation of Synaptic Plasticity and Memory Formation." Neural Plast **2013**: 185463.

Pannasch, U., D. Freche, G. Dallerac, G. Ghezali, C. Escartin, P. Ezan, M. Cohen-Salmon, K. Benchenane, V. Abudara, A. Dufour, J. H. Lubke, N. Deglon, G. Knott,

D. Holcman and N. Rouach (2014). "Connexin 30 sets synaptic strength by controlling astroglial synapse invasion." Nat Neurosci.

Papadakis, M., G. Hadley, M. Xilouri, L. C. Hoyte, S. Nagel, M. M. McMenamin, G. Tsaknakis, S. M. Watt, C. W. Drakesmith, R. Chen, M. J. Wood, Z. Zhao, B. Kessler, K. Vekrellis and A. M. Buchan (2013). "Tsc1 (hamartin) confers neuroprotection against ischemia by inducing autophagy." Nat Med **19**(3): 351-357.

Parellada, M., M. J. Penzol, L. Pina, C. Moreno, E. Gonzalez-Vioque, G. Zalsman and C. Arango (2013). "The neurobiology of autism spectrum disorders." Eur Psychiatry.

Paxinos, G. (1990). The Human nervous system. San Diego, Academic Press.

Petit-Pedrol, M., T. Armangue, X. Peng, L. Bataller, T. Cellucci, R. Davis, L. McCracken, E. Martinez-Hernandez, W. P. Mason, M. C. Kruer, D. G. Ritacco, W. Grisold, B. F. Meaney, C. Alcala, P. Sillevis-Smitt, M. J. Titulaer, R. Balice-Gordon, F. Graus and J. Dalmau (2014). "Encephalitis with refractory seizures, status epilepticus, and antibodies to the GABAA receptor: a case series, characterisation of the antigen, and analysis of the effects of antibodies." Lancet Neurol **13**(3): 276-286.

Phelps, C. and E. A. Korneva (2008). Cytokines and the brain. Amsterdam ; Oxford, Elsevier.

Pigache, R. M. and SpringerLink (Online service) (1970). The Anatomy of the Paleocortex: A Critical Review. Ergebnisse der Anatomie und Entwicklungsgeschichte / Advances in Anatomy, Embryology and Cell Biology / Revues anatomie et de morphologie expérimentale,. Berlin, Heidelberg, Springer Berlin Heidelberg,**:** 1 online resource.

Plaisted, K., J. Swettenham and L. Rees (1999). "Children with autism show local precedence in a divided attention task and global precedence in a selective attention task." J Child Psychol Psychiatry **40**(5): 733-742.

Plonsey, R. (1982). "The nature of sources of bioelectric and biomagnetic fields." Biophys J **39**(3): 309-312.

Powell, T. P., W. M. Cowan and G. Raisman (1965). "The central olfactory connexions." J Anat **99**(Pt 4): 791-813.

Raymond, G. V., M. L. Bauman and T. L. Kemper (1996). "Hippocampus in autism: a Golgi analysis." Acta Neuropathol **91**(1): 117-119.

Raznahan, A., G. L. Wallace, L. Antezana, D. Greenstein, R. Lenroot, A. Thurm, M. Gozzi, S. Spence, A. Martin, S. E. Swedo and J. N. Giedd (2013). "Compared to what? Early brain overgrowth in autism and the perils of population norms." Biol Psychiatry **74**(8): 563-575.

Remington, A., J. Swettenham, R. Campbell and M. Coleman (2009). "Selective attention and perceptual load in autism spectrum disorder." Psychol Sci **20**(11): 1388-1393.

Riby, D. M., E. Janes and J. Rodgers (2013). "Brief report: exploring the relationship between sensory processing and repetitive behaviours in Williams Syndrome." J Autism Dev Disord **43**(2): 478-482.

Richard, A. E., R. R. Lajiness-O'Neill and S. M. Bowyer (2013). "Impaired prefrontal gamma band synchrony in autism spectrum disorders during gaze cueing." Neuroreport **24**(16): 894-897.

Rippon, G., J. Brock, C. Brown and J. Boucher (2007). "Disordered connectivity in the autistic brain: challenges for the "new psychophysiology"." Int J Psychophysiol **63**(2): 164-172.

Ritvo, E. R., B. J. Freeman, A. Mason-Brothers, A. Mo and A. M. Ritvo (1985). "Concordance for the syndrome of autism in 40 pairs of afflicted twins." Am J Psychiatry **142**(1): 74-77.

Ritvo, E. R., L. B. Jorde, A. Mason-Brothers, B. J. Freeman, C. Pingree, M. B. Jones, W. M. McMahon, P. B. Petersen, W. R. Jenson and A. Mo (1989). "The UCLA-University of Utah epidemiologic survey of autism: recurrence risk estimates and genetic counseling." Am J Psychiatry **146**(8): 1032-1036.

Robertson, C. E., D. J. Kravitz, J. Freyberg, S. Baron-Cohen and C. I. Baker (2013). "Slower rate of binocular rivalry in autism." J Neurosci **33**(43): 16983-16991.

Rodriguez, E., N. George, J. P. Lachaux, J. Martinerie, B. Renault and F. J. Varela (1999). "Perception's shadow: long-distance synchronization of human brain activity." Nature **397**(6718): 430-433.

Roelfsema, P. R., P. Konig, A. K. Engel, R. Sireteanu and W. Singer (1994). "Reduced synchronization in the visual cortex of cats with strabismic amblyopia." Eur J Neurosci **6**(11): 1645-1655.

Rojas, D. C., K. Maharajh, P. Teale and S. J. Rogers (2008). "Reduced neural synchronization of gamma-band MEG oscillations in first-degree relatives of children with autism." BMC Psychiatry **8**: 66.

Rojas, D. C., D. Singel, S. Steinmetz, S. Hepburn and M. S. Brown (2013). "Decreased left perisylvian GABA concentration in children with autism and unaffected siblings." Neuroimage.

Rojas, D. C., P. D. Teale, K. Maharajh, E. Kronberg, K. Youngpeter, L. B. Wilson, A. Wallace and S. Hepburn (2011). "Transient and steady-state auditory gamma-band responses in first-degree relatives of people with autism spectrum disorder." Mol Autism **2**: 11.

Roth, I. and P. Rezaie (2011). Researching the autism spectrum : contemporary perspectives. Cambridge, Cambridge University Press.

Rubenstein, J. L. and M. M. Merzenich (2003). "Model of autism: increased ratio of excitation/inhibition in key neural systems." Genes Brain Behav **2**(5): 255-267.

Rutter, M. (2005). "Incidence of autism spectrum disorders: changes over time and their meaning." Acta Paediatr **94**(1): 2-15.

Rutter, M., A. Bailey and C. Lord (2003). Social Communication Questionnaire (SCQ), Western Psychological Services, Los Angeles, California

Sakai, M., J. Austin and F. Witmer (1968). "Polyglucosans in the systemic deposits of myoclonic epilepsy and in corpora amylacea." Neurology **18**(3): 298.

Salari, N., C. Buchel and M. Rose (2012). "Functional dissociation of ongoing oscillatory brain states." PLoS One **7**(5): e38090.

Saunders, J. A., V. M. Tatard-Leitman, J. Suh, E. N. Billingslea, T. P. Roberts and S. J. Siegel (2013). "Knockout of NMDA receptors in parvalbumin interneurons recreates autism-like phenotypes." Autism Res **6**(2): 69-77.

Saxena, V., S. Ramdas, C. R. Ochoa, D. Wallace, P. Bhide and I. Kohane (2012). "Structural, genetic, and functional signatures of disordered neuro-immunological development in autism spectrum disorder." PLoS One **7**(12): e48835.

Schaaf, R. C., S. Toth-Cohen, S. L. Johnson, G. Outten and T. W. Benevides (2011). "The everyday routines of families of children with autism: examining the impact of sensory processing difficulties on the family." Autism **15**(3): 373-389.

Schafers, M. and L. Sorkin (2008). "Effect of cytokines on neuronal excitability." Neurosci Lett **437**(3): 188-193.

Schecklmann, M., C. Schwenck, R. Taurines, C. Freitag, A. Warnke, M. Gerlach and M. Romanos (2013). "A systematic review on olfaction in child and adolescent psychiatric disorders." J Neural Transm **120**(1): 121-130.

Schipper, H. M., W. Song, H. Zukor, J. R. Hascalovici and D. Zeligman (2009). "Heme oxygenase-1 and neurodegeneration: expanding frontiers of engagement." J Neurochem **110**(2): 469-485.

Schumann, C. M. and D. G. Amaral (2006). "Stereological analysis of amygdala neuron number in autism." J Neurosci **26**(29): 7674-7679.

Schwartz, E. S., J. C. Edgar, W. C. Gaetz and T. P. Roberts (2010). "Magnetoencephalography." Pediatr Radiol **40**(1): 50-58.

Scott-Van Zeeland, A. A., M. Dapretto, D. G. Ghahremani, R. A. Poldrack and S. Y. Bookheimer (2010). "Reward processing in autism." Autism Res **3**(2): 53-67.

Sedley, W. and M. O. Cunningham (2013). "Do cortical gamma oscillations promote or suppress perception? An under-asked question with an over-assumed answer." Front Hum Neurosci **7**: 595.

Selmaj, K., Z. Pawlowska, A. Walczak, W. Koziolkiewicz, C. S. Raine and C. S. Cierniewski (2008). "Corpora amylacea from multiple sclerosis brain tissue consists of aggregated neuronal cells." Acta Biochim Pol **55**(1): 43-49.

Shah, A. and U. Frith (1983). "An islet of ability in autistic children: a research note." J Child Psychol Psychiatry **24**(4): 613-620.

Sheikhani, A., H. Behnam, M. R. Mohammadi, M. Noroozian and M. Mohammadi (2012). "Detection of abnormalities for diagnosing of children with autism disorders using of quantitative electroencephalography analysis." J Med Syst **36**(2): 957-963.

Sigel, E. and M. E. Steinmann (2012). "Structure, function, and modulation of GABA(A) receptors." J Biol Chem **287**(48): 40224-40231.

Silver, W. G. and I. Rapin (2012). "Neurobiological basis of autism." Pediatr Clin North Am **59**(1): 45-61, x.

Singer, W. (2001). "Consciousness and the binding problem." Ann N Y Acad Sci **929**: 123-146.

Singhrao, S. K., J. W. Neal and G. R. Newman (1993). "Corpora amylacea could be an indicator of neurodegeneration." Neuropathol Appl Neurobiol **19**(3): 269-276.

Singhrao, S. K., J. W. Neal, S. J. Piddlesden and G. R. Newman (1994). "New immunocytochemical evidence for a neuronal/oligodendroglial origin for corpora amylacea." Neuropathol Appl Neurobiol **20**(1): 66-73.

Snijders, T. M., B. Milivojevic and C. Kemner (2013). "Atypical excitation-inhibition balance in autism captured by the gamma response to contextual modulation." Neuroimage Clin **3**: 65-72.

Software, M. (2003). Inquisit 3. Seattle, WA.

Sohal, V. S., F. Zhang, O. Yizhar and K. Deisseroth (2009). "Parvalbumin neurons and gamma rhythms enhance cortical circuit performance." Nature **459**(7247): 698-702.

Spencer, M. D., R. J. Holt, L. R. Chura, A. J. Calder, J. Suckling, E. T. Bullmore and S. Baron-Cohen (2012). "Atypical activation during the Embedded Figures Task as a functional magnetic resonance imaging endophenotype of autism." Brain **135**(Pt 11): 3469-3480.

Steffenburg, S., C. Gillberg and U. Steffenburg (1996). "Psychiatric disorders in children and adolescents with mental retardation and active epilepsy." Arch Neurol **53**(9): 904-912.

Stellwagen, D., E. C. Beattie, J. Y. Seo and R. C. Malenka (2005). "Differential regulation of AMPA receptor and GABA receptor trafficking by tumor necrosis factor-alpha." J Neurosci **25**(12): 3219-3228.

Strauss, K. A., E. G. Puffenberger, M. J. Huentelman, S. Gottlieb, S. E. Dobrin, J. M. Parod, D. A. Stephan and D. H. Morton (2006). "Recessive symptomatic focal epilepsy and mutant contactin-associated protein-like 2." N Engl J Med **354**(13): 1370-1377.

Stroganova, T. A., E. V. Orekhova, A. O. Prokofyev, M. M. Tsetlin, V. V. Gratchev, A. A. Morozov and Y. V. Obukhov (2012). "High-frequency oscillatory response to illusory contour in typically developing boys and boys with autism spectrum disorders." Cortex **48**(6): 701-717.

Sun, L., C. Grutzner, S. Bolte, M. Wibral, T. Tozman, S. Schlitt, F. Poustka, W. Singer, C. M. Freitag and P. J. Uhlhaas (2012). "Impaired gamma-band activity during perceptual organization in adults with autism spectrum disorders: evidence for dysfunctional network activity in frontal-posterior cortices." J Neurosci **32**(28): 9563-9573.

Suzuki, K., G. Sugihara, Y. Ouchi, K. Nakamura, M. Futatsubashi, K. Takebayashi, Y. Yoshihara, K. Omata, K. Matsumoto, K. J. Tsuchiya, Y. Iwata, M. Tsujii, T. Sugiyama and N. Mori (2013). "Microglial activation in young adults with autism spectrum disorder." JAMA Psychiatry **70**(1): 49-58.

Suzuki, N. and J. M. Bekkers (2007). "Inhibitory interneurons in the piriform cortex." Clin Exp Pharmacol Physiol **34**(10): 1064-1069.

Suzuki, N., J. M. Bekkers and 1 (2010). "Inhibitory neurons in the anterior piriform cortex of the mouse: classification using molecular markers." J Comp Neurol **518**(10): 1670-1687.

Suzuki, N., J. M. Bekkers and 2 (2010). "Distinctive classes of GABAergic interneurons provide layer-specific phasic inhibition in the anterior piriform cortex." Cereb Cortex **20**(12): 2971-2984.

Suzuki, Y., H. D. Critchley, A. Rowe, P. Howlin and D. G. Murphy (2003). "Impaired olfactory identification in Asperger's syndrome." J Neuropsychiatry Clin Neurosci **15**(1): 105-107.

Talbot, K., N. J. Woolf and L. L. Butcher (1988). "Feline islands of Calleja complex: I. Cytoarchitectural organization and comparative anatomy." J Comp Neurol **275**(4): 553-579.

Tallon-Baudry, C. (2003). "Oscillatory synchrony and human visual cognition." J Physiol Paris **97**(2-3): 355-363.

Tallon-Baudry, C. (2004). "Attention and awareness in synchrony." Trends Cogn Sci **8**(12): 523-525.

Tallon-Baudry, C. (2009). "The roles of gamma-band oscillatory synchrony in human visual cognition." Front Biosci (Landmark Ed) **14**: 321-332.

Tallon-Baudry, C. and O. Bertrand (1999). "Oscillatory gamma activity in humans and its role in object representation." Trends Cogn Sci **3**(4): 151-162.

Tallon-Baudry, C., O. Bertrand, C. Delpuech and J. Permier (1997). "Oscillatory gamma-band (30-70 Hz) activity induced by a visual search task in humans." J Neurosci **17**(2): 722-734.

Tallon-Baudry, C., O. Bertrand, M. A. Henaff, J. Isnard and C. Fischer (2005). "Attention modulates gamma-band oscillations differently in the human lateral occipital cortex and fusiform gyrus." Cereb Cortex **15**(5): 654-662.

Tallon-Baudry, C., O. Bertrand, C. Wienbruch, B. Ross and C. Pantev (1997). "Combined EEG and MEG recordings of visual 40 Hz responses to illusory triangles in human." Neuroreport **8**(5): 1103-1107.

Taylor, M. J., E. J. Donner and E. W. Pang (2012). "fMRI and MEG in the study of typical and atypical cognitive development." Neurophysiol Clin **42**(1-2): 19-25.

Terry, R. D., R. DeTeresa and L. A. Hansen (1987). "Neocortical cell counts in normal human adult aging." Ann Neurol **21**(6): 530-539.

Tetreault, N. A., A. Y. Hakeem, S. Jiang, B. A. Williams, E. Allman, B. J. Wold and J. M. Allman (2012). "Microglia in the cerebral cortex in autism." J Autism Dev Disord **42**(12): 2569-2584.

Thom, M. (2014). "Review: Hippocampal sclerosis in epilepsy: a neuropathology review." Neuropathol Appl Neurobiol **40**(5): 520-543.

Traub, R. D. and M. A. Whittington (2010). Cortical oscillations in health and disease. New York, Oxford University Press.

Tuchman, R., M. Cuccaro and M. Alessandri (2010). "Autism and epilepsy: historical perspective." Brain Dev **32**(9): 709-718.

Tuchman, R. and I. Rapin (2006). Autism : a neurological disorder of early brain development. London, MacKeith Press for the International Child Neurology Association.

Ubeda-Banon, I., A. Novejarque, A. Mohedano-Moriano, P. Pro-Sistiaga, C. de la Rosa-Prieto, R. Insausti, F. Martinez-Garcia, E. Lanuza and A. Martinez-Marcos (2007). "Projections from the posterolateral olfactory amygdala to the ventral striatum: neural basis for reinforcing properties of chemical stimuli." BMC Neurosci **8**: 103.

Uhlhaas, P. J., G. Pipa, B. Lima, L. Melloni, S. Neuenschwander, D. Nikolic and W. Singer (2009). "Neural synchrony in cortical networks: history, concept and current status." Front Integr Neurosci **3**: 17.

Uhlhaas, P. J., F. Roux, W. Singer, C. Haenschel, R. Sireteanu and E. Rodriguez (2009). "The development of neural synchrony reflects late maturation and restructuring of functional networks in humans." Proc Natl Acad Sci U S A **106**(24): 9866-9871.

Uhlhaas, P. J. and W. Singer (2007). "What do disturbances in neural synchrony tell us about autism?" Biol Psychiatry **62**(3): 190-191.

Valicenti-McDermott, M., K. McVicar, I. Rapin, B. K. Wershil, H. Cohen and S. Shinnar (2006). "Frequency of gastrointestinal symptoms in children with autistic spectrum disorders and association with family history of autoimmune disease." J Dev Behav Pediatr **27**(2 Suppl): S128-136.

van Kooten, I. A., S. J. Palmen, P. von Cappeln, H. W. Steinbusch, H. Korr, H. Heinsen, P. R. Hof, H. van Engeland and C. Schmitz (2008). "Neurons in the fusiform gyrus are fewer and smaller in autism." Brain **131**(Pt 4): 987-999.

Vargas, D. L., C. Nascimbene, C. Krishnan, A. W. Zimmerman and C. A. Pardo (2005). "Neuroglial activation and neuroinflammation in the brain of patients with autism." Ann Neurol **57**(1): 67-81.

Vereyken, E. J., H. Bajova, S. Chow, P. N. de Graan and D. L. Gruol (2007). "Chronic interleukin-6 alters the level of synaptic proteins in hippocampus in culture and in vivo." Eur J Neurosci **25**(12): 3605-3616.

Vezzani, A., T. Ravizza, S. Balosso and E. Aronica (2008). "Glia as a source of cytokines: implications for neuronal excitability and survival." Epilepsia **49 Suppl 2**: 24-32.

Vidal, J. R., M. Chaumon, J. K. O'Regan and C. Tallon-Baudry (2006). "Visual grouping and the focusing of attention induce gamma-band oscillations at different frequencies in human magnetoencephalogram signals." J Cogn Neurosci **18**(11): 1850-1862.

Vincent, A., C. G. Bien, S. R. Irani and P. Waters (2011). "Autoantibodies associated with diseases of the CNS: new developments and future challenges." Lancet Neurol **10**(8): 759-772.

Vincent, A., R. Deacon, P. Dalton, C. Salmond, A. M. Blamire, S. Pendlebury, H. Johansen-Berg, B. Rajogopalan, P. Styles and J. Stein (2002). "Maternal antibody-mediated dyslexia? Evidence for a pathogenic serum factor in a mother of two dyslexic children shown by transfer to mice using behavioural studies and magnetic resonance spectroscopy." J Neuroimmunol **130**(1-2): 243-247.

Voineagu, I., X. Wang, P. Johnston, J. K. Lowe, Y. Tian, S. Horvath, J. Mill, R. M. Cantor, B. J. Blencowe and D. H. Geschwind (2011). "Transcriptomic analysis of autistic brain reveals convergent molecular pathology." Nature **474**(7351): 380-384.

von Bartheld, C. (2002). "Counting particles in tissue sections: choices of methods and importance of calibration to minimize biases." Histol Histopathol **17**(2): 639-648.

von Bartheld, C. S. (2012). "Distribution of Particles in the Z-axis of Tissue Sections: Relevance for Counting Methods." Neuroquantology **10**(1): 66-75.

Vrba, J. and S. E. Robinson (2001). "Signal processing in magnetoencephalography." Methods **25**(2): 249-271.

Wacker, M. and H. Witte (2013). "Time-frequency techniques in biomedical signal analysis. a tutorial review of similarities and differences." Methods Inf Med **52**(4): 279-296.

Walker, M. A., J. R. Highley, M. M. Esiri, B. McDonald, H. C. Roberts, S. P. Evans and T. J. Crow (2002). "Estimated neuronal populations and volumes of the hippocampus and its subfields in schizophrenia." Am J Psychiatry **159**(5): 821-828.

Wang, C., Y. You, D. Qi, X. Zhou, L. Wang, S. Wei, Z. Zhang, W. Huang, Z. Liu, F. Liu, L. Ma and Z. Yang (2014). "Human and monkey striatal interneurons are derived from the medial ganglionic eminence but not from the adult subventricular zone." J Neurosci **34**(33): 10906-10923.

Ward, T. S., G. D. Rosen and C. S. von Bartheld (2008). "Optical disector counting in cryosections and vibratome sections underestimates particle numbers: effects of tissue quality." Microsc Res Tech **71**(1): 60-68.

Wechsler, D. (1999). Wechsler abbrievated scale of intelligence (WASI), Pearson.

Wegiel, J., N. C. Schanen, E. H. Cook, M. Sigman, W. T. Brown, I. Kuchna, K. Nowicki, J. Wegiel, H. Imaki, S. Y. Ma, E. Marchi, T. Wierzba-Bobrowicz, A. Chauhan, V. Chauhan, I. L. Cohen, E. London, M. Flory, B. Lach and T. Wisniewski (2012). "Differences between the pattern of developmental abnormalities in autism associated with duplications 15q11.2-q13 and idiopathic autism." J Neuropathol Exp Neurol **71**(5): 382-397.

Weintraub, K. (2011). "The prevalence puzzle: Autism counts." Nature **479**(7371): 22-24.

Wendel, K., O. Vaisanen, J. Malmivuo, N. G. Gencer, B. Vanrumste, P. Durka, R. Magjarevic, S. Supek, M. L. Pascu, H. Fontenelle and R. Grave de Peralta Menendez (2009). "EEG/MEG source imaging: methods, challenges, and open issues." Comput Intell Neurosci: 656092.

Wesson, D. W. and D. A. Wilson (2011). "Sniffing out the contributions of the olfactory tubercle to the sense of smell: hedonics, sensory integration, and more?" Neurosci Biobehav Rev **35**(3): 655-668.

West, M. J. (2012). "The precision of estimates in stereological analyses." Cold Spring Harb Protoc **2012**(9): 937-949.

West, M. J. (2013). "Optimizing the sampling scheme for a stereological study: how many individuals, sections, and probes should be used." Cold Spring Harb Protoc **2013**(6): 521-532.

West, S. E. and R. L. Doty (1995). "Influence of epilepsy and temporal lobe resection on olfactory function." Epilepsia **36**(6): 531-542.

Whitney, E. R., T. L. Kemper, M. L. Bauman, D. L. Rosene and G. J. Blatt (2008). "Cerebellar Purkinje cells are reduced in a subpopulation of autistic brains: a stereological experiment using calbindin-D28k." Cerebellum **7**(3): 406-416.

Whittington, M. A., H. C. Doheny, R. D. Traub, F. E. LeBeau and E. H. Buhl (2001). "Differential expression of synaptic and nonsynaptic mechanisms underlying stimulus-induced gamma oscillations in vitro." J Neurosci **21**(5): 1727-1738.

Wilhelmus, M. M., R. Verhaar, J. G. Bol, A. M. van Dam, J. J. Hoozemans, A. J. Rozemuller and B. Drukarch (2011). "Novel role of transglutaminase 1 in corpora amylacea formation?" Neurobiol Aging **32**(5): 845-856.

Wilson, T. W., D. C. Rojas, M. L. Reite, P. D. Teale and S. J. Rogers (2007). "Children and adolescents with autism exhibit reduced MEG steady-state gamma responses." Biol Psychiatry **62**(3): 192-197.

World Health Organization. and ebrary Inc. (1992). The ICD-10 classification of mental and behavioural disorders clinical descriptions and diagnostic guidelines. Geneva, World Health Organization,**:** xii, 362 p.

Wright, B., B. Alderson-Day, G. Prendergast, S. Bennett, J. Jordan, C. Whitton, A. Gouws, N. Jones, R. Attur, H. Tomlinson and G. Green (2012). "Gamma activation in young people with autism spectrum disorders and typically-developing controls when viewing emotions on faces." PLoS One **7**(7): e41326.

Young, A. M., E. Campbell, S. Lynch, J. Suckling and S. J. Powis (2011). "Aberrant NF-kappaB expression in autism spectrum condition: a mechanism for neuroinflammation." Front Psychiatry **2**: 27.

Young, L. J., M. M. Lim, B. Gingrich and T. R. Insel (2001). "Cellular mechanisms of social attachment." Horm Behav **40**(2): 133-138.

Zeidan-Chulia, F., A. B. Salmina, N. A. Malinovskaya, M. Noda, A. Verkhratsky and J. C. Moreira (2014). "The glial perspective of autism spectrum disorders." Neurosci Biobehav Rev **38**: 160-172.

Zelano, C., J. Montag, B. Johnson, R. Khan and N. Sobel (2007). "Dissociated representations of irritation and valence in human primary olfactory cortex." J Neurophysiol **97**(3): 1969-1976.

Zelikowsky, M., S. Bissiere, T. A. Hast, R. Z. Bennett, A. Abdipranoto, B. Vissel and M. S. Fanselow (2013). "Prefrontal microcircuit underlies contextual learning after hippocampal loss." Proc Natl Acad Sci U S A **110**(24): 9938-9943.

Zerbo, O., Y. Qian, C. Yoshida, J. K. Grether, J. Van de Water and L. A. Croen (2013). "Maternal Infection During Pregnancy and Autism Spectrum Disorders." J Autism Dev Disord.